CUKUROVA UNIVERSITY

INSTITUTE OF NATURAL AND APPLIED SCIENCES

PhD THESIS

Investigation of Flow Characteristics and Heat Transfer Performance in Heat Exchangers with Magnetic Field Effect

Sergen TÜMSE

Mechanical Engineering Department

June, 2023

CUKUROVA UNIVERSITY

INSTITUTE OF NATURAL AND APPLIED SCIENCES

PhD THESIS APPROVAL

Investigation of Flow Characteristics and Heat Transfer Performance in Heat Exchangers with Magnetic Field Effect

---

Sergen TÜMSE

Mechanical Engineering Department

This Doctorate Thesis was evaluated by the following Jury Members on 14/06/2023 and was approved by unanimity.

Jury : Prof. Dr. Beşir ŞAHİN (Advisor) ……

: Prof. Dr. Hüseyin AKILLI ……

: Prof. Dr. Mehmet BİLGİLİ ……

: Assoc.Prof. Dr. Fırat EKİNCİ ……

: Asst. Prof. Dr. Tural TUNAY ……

This Thesis was written in the Department of Mechanical Engineering, Institute of Natural and Applied Sciences.
Thesis Number:

Prof. Dr. Sadık DİNÇER
Director
Institute of Natural and Applied Sciences

This thesis was supported by the Scientific Research Office of Çukurova University
Project ID: FDK-2021-13879.

CONTENTS

CUKUROVA UNIVERSITY
INSTITUTE OF NATURAL AND APPLIED SCIENCES

PhD THESIS

Investigation of Flow Characteristics and Heat Transfer Performance in Heat Exchangers with Magnetic Field Effect

Sergen TÜMSE

Advisor: Prof. Dr. Beşir ŞAHİN
2nd Advisor: Assoc. Prof. Dr. Göktürk Memduh ÖZKAN

Department of MechanicalEngineering

ABSTRACT

In the first part of the thesis, the hydrothermal flow and entropy generation properties of ferrofluid (water and Fe_3O_4) on a cylindrical body in the rectangular channel subjected to the non-uniform magnetic field going through current-carrying wires are numerically explored. The effect of various parameters, such as ferroparticle volume fraction, Φ the strength of the non-uniform magnetic field, *Ha*, and Reynolds number, *Re* on the flow characteristics, and forced convection heat transfer is investigated using finite-volume based Ansys Fluent 20. Obtained results demonstrate that the applied magnetic field shortens the length of recirculating wake downstream of the cylinder at *Re*=25 and makes unsteady flow with alternate vortex shedding as a time-independent steady flow for Hartmann numbers greater than, *Ha*≥6 at *Re*=100. At *Re*=50, the total drag coefficient, C_D gets higher by almost 20% when *Ha* increases from *Ha*=0 to *Ha*=6 and subsequently grows by 61% at *Ha*=10. The findings show that the average Nusselt number, Nu_{avg} demonstrates monotonic behavior with the *Ha* and it augments when the strength of the non-uniform magnetic field increases. The Nu_{avg} improvement is in the vicinity of 11.71% at *Ha*=10 and 23.26% at *Ha*=18 for *Re*=25. The maximum value of entropy generation, S_L reduces when the non-uniform magnetic field is applied. Moreover, increasing the Hartmann number, *Ha* influences the high levels region of entropy production by relatively extending this zone towards the downstream of the channel and covering more area around the cylinder. According to the outcomes of numerical simulation, there is an increase in Nu_{avg} with 3.98% and 3.88% for *Ha*=2 and 18 respectively when the ferroparticle volume fraction rises from Φ=0% to Φ=4% at *Re*=25. Finally, the optimum thermal performance criterion, ζ is obtained at *Re*=150 for *Ha*=0 and Φ=4%.

In the second part of the thesis, the hydrothermal and entropy generation characteristics of nanofluid (water and CuO) in a rectangular grooved channel exposed to a uniform magnetic field in a transverse direction are numerically investigated. The influence of different parameters, such as volume fraction of nanoparticles, Φ Hartmann number, Ha indicating the intensity of the uniform magnetic field, and Reynolds numbers, *Re* on the flow behaviors and forced convection heat transfer is explored using finite-volume based Ansys Fluent 20. The acquired outcomes demonstrated that applying a uniform magnetic field in a rectangular grooved channel causes major variations in the streamline patterns and reduces the extent of the recirculation zone in rectangular grooves at both *Re*=250 and 1250. But the required Hartmann number, *Ha* for the beginning of recirculation region suppression increases with the rise in Reynolds numbers, from *Re*=250 to *Re*=1250. The Lorentz force resulting from the uniform magnetic field attenuates the velocity of nanofluid flow at the center of the channel and considering constant mass flow throughout the channel, the flow velocity remarkably augments near the heated walls. This situation increases the velocity gradient and temperature gradient near the hot walls and heat exchange between hot walls and nanofluid flow improves. According to the results of the numerical simulation, the average Nusselt number, Nu_{avg} augmentation is in the vicinity of 9.08% for *Ha*=8 and 30.42% for *Ha*=24 at *Re*=250 and 0.087% for *Ha*=8 and 21.13% for *Ha*=24 at *Re*=1250 compared to the absence of uniform magnetic field application case, *Ha*=0.

Keywords: Confined cylinder, Entropy generation, Forced convection, Hartmann number, Non-uniform magnetic field, Nusselt number, Rectangular grooved channel, Uniform magnetic field

ÇUKUROVA ÜNİVERSİTESİ
FEN BİLİMLERİ ENSTİTÜSÜ

DOKTORA TEZİ

Manyetik Alan Etkisiyle Isı Eşanjörlerinde Akış Karakteristiklerinin ve Isı Transferi Performansının İncelenmesi

Sergen TÜMSE

Danışman: Prof. Dr. Beşir ŞAHİN
2. Danışman: Doç. Dr. Göktürk Memduh ÖZKAN

Makine Mühendisliği Anabilim Dalı

ÖZ

Tezin ilk bölümünde, akım taşıyan tellerden geçen uniform olmayan bir manyetik alana maruz kalan, dikdörtgensel bir kapalı kanal içerisindeki silindirik bir cismin çevresinde akan bir ferroakışkanın (su ve Fe_3O_4) hidrotermal ve entropi üretimi özellikleri sayısal olarak incelenmiştir. Ferropartikül hacimsel oranı, Φ uniform olmayan manyetik alan şiddeti, Ha ve Reynolds sayısı, Re gibi çeşitli parametrelerin akış karakteristikleri ve zorlanmış taşınım ile ısı transferi üzerindeki etkisi sonlu hacim tabanlı Ansys Fluent 20 kullanılarak araştırılmıştır. Elde edilen sonuçlar, uygulanan manyetik alanın, Re=25'te silindirin arkasında oluşan ölü akış bölgesinin uzunluğunu kısalttığını ve Re=100'de $Ha\geq$6'dan büyük Hartmann sayıları için periyodik girdap kopmalarından oluşan daimi olmayan akışı, daimi bir akış haline getirdiğini göstermektedir. Re=50'de toplam sürükleme katsayısı, C_D Ha=0'dan Ha=6'ya yükseldiğinde yaklaşık %20 artmıştır ve ardından Ha=10 değerinde %61 artmıştır. Sonuçlar, ortalama Nusselt sayısının, Nu_{avg} Hartmann sayısı ile monoton davranış gösterdiğini ve uniform olmayan manyetik alan şiddeti arttıkça ortalama Nusselt sayısının artığını göstermektedir. Nu_{avg} iyileştirmesi, Re=25 için Ha=10'da %11,71 ve Ha=18'de %23,26 civarındadır. Entropi üretiminin, S_L maksimum değeri uniform olmayan manyetik alan uygulandığında azalmaktadır. Ayrıca artan Hartmann sayısı, Ha silindir etrafında oluşan yüksek entropi değerine sahip bölgelerin boyutunu etkilemektedir. Sayısal simulasyon sonuçlarına göre, Re=25'te ferropartikül hacimsel oranı Φ=%0'dan Φ=%4'e yükseldiğinde Nu_{avg}'da Ha=2 ve 18 için sırasıyla %3,98 ve %3,88 lik bir artış vardır. Son olarak, optimum termal performans kriteri, ξ Re=150'de Ha=0 ve Φ=%4 değerlerinde elde edilmiştir.

Tezin ikinci bölümünde, üniform manyetik alana maruz bırakılan dikdörtgen oluklu bir kanaldaki nanoakışkanın (su ve CuO) hidrotermal ve entropi üretimiz özellikleri sayısal olarak incelenmiştir. Nanopartiküllerin hacimsel oranı, Φ üniform manyetik alan şiddetini gösteren Hartmann sayısı, Ha ve Reynolds sayısı, Re farklı parametrelerin akış karakteristikleri ve zorlanmış taşınım ile ısı transferi üzerindeki etkisi, sonlu hacim tabanlı Anys Fluent 20 kullanılarak araştırılmıştır. Elde edilen sonuçlar, dikdörtgen oluklu kanalda üniform manyetik alan uygulamasının akım çizgilerinin dağılımı üzerinde büyük değişimlere neden olduğunu ve hem Re=250 hem Re=1250'de oluklar içerisinde oluşan resirkülasyon bölgesinin boyutunu azalttığını göstermiştir. Ancak, oluklar içerisinde oluşan resirkülasyon bölgesini baskılama başlangıcı için gerekli Hartmann sayısı, Ha Re=250'den Re=1250'ye yükselmesiyle artmıştır. Üniform manyetik alandan kaynaklı Lorentz kuvveti, kanalın merkezindeki nanoakışkan akışın hızını azaltır ve kanal boyunca sabit kütle düşünüldüğünde, akış hızı ısıtılmış duvarların yakınında önemli ölçüde artar. Bu durum sıcak duvarların yakınında hız gradyanını ve sıcaklık gradyanını arttırır ve sıcak duvarlar ile nanoakışkan akışı arasındaki ısı alışverişini iyileştirir. Nümerik simülasyon sonuçlarına göre, ortalama Nusselt sayısı, Nu_{avg} artışı manyetik alan uygulanmama durumu ile karşılaştırıldığında, Ha=0 Re=250'de Ha=8 için 9,08%, Ha=24 için 30,42%, Re=1250'de Ha=8 için 0,087%, Ha=24 için 21,13% olarak gözlemlenmiştir.

Anahtar Kelimeler: Entropi üretimi, Dikdörtgen oluklu kanal, Hartmann sayısı, Nusselt sayısı, Sınırlandırılmış silindir, Üniform manyetik alan, Üniform olmayan manyetik alan, Zorlanmış taşınım

EXTENDED ABSTRACT

In the first section of the thesis, the flow, heat transfer, and entropy production characteristics of a ferrofluid with a mixture of water and Fe_3O_4 over a confined cylinder under the non-uniform magnetic field effect are numerically investigated. After the industrial revolution, energy has become an essential requirement for human life. However, the efficiency of energy generation, utilization, and conversion processes has become more crucial because of the restricted sources, prices, ambient conditions, and growing requests with time. The quick increment in the universal market is the main inspiration for investigations on the efficiency of energy-including operations. Investigations aimed at increasing energy efficiency are within the extent of several various disciplines. However, attempts to enhance heat transfer have the main influence on energy efficiency from the generation stage to the end-user consumption stage because most of these operations include heat transfer in one way or another. The fluid flow on a circular cylindrical body is a widespread circumstance in great quantities of engineering practices. The occurrence of separated flow, wake region, and estimation of heat transfer from the circular cylindrical body has been extensively investigated for a long while since their essential importance in flow characteristics and practical significance in the field of heat transfer and aerodynamic applications. The flow on a circular body mainly depends on the Reynolds number independent of the confined or unconfined domain. If the fluid over the cylinder flows in an unconfined domain, the Reynolds number is the individual parameter. When the Reynolds number gets higher, the flow around the cylinder turns into firstly unstable case, later three-dimensional instability modes (Williamson, 1996). For the Reynolds number smaller than $Re \leq 46$, the flow structure on the cylinder is time-independent and the wake region includes two-counter rotating symmetric vortices with respect to the cylinder axis appended to the rear side of the cylinder. The periodic vortex shedding occurs from alternating sides of the cylinder which is also known as Karman vortex street, if the Reynolds number is bigger than $Re>46$. This flow phenomenon proceeds up to the Reynolds number, $Re=180$, beyond which three-dimensional flow occurs around the cylinder. The investigation of flow structure around the cylindrical body in a rectangular channel has an extensive application area such as heat exchangers, off-shore marines and heat sinks for electronic components. The structure and stability of fluid flow around the confined cylinder significantly alter from the fluid flow structure of an unconfined cylinder. Magnetic fields act as external body forces on the fluid flow. The flow control by magnetic forces is achieved by operating a magnetic field on electrically conductive liquids. In this active flow control technique, the flow control can be utilized to gain a greater flow mixing. Furthermore, the aim of the flow control is to remove the circumstances that can inversely impact heat transfer such as flow separation. Magnetic forces are more influential at low Reynolds numbers and natural convection states in which the influence of momentum forces is very weak. In the first part of the thesis, the effect of various parameters, such as ferroparticle

volume fraction, Φ the strength of the non-uniform magnetic field, *Ha*, and Reynolds number, *Re* on the flow characteristics, and forced convection heat transfer is investigated using finite-volume based Ansys Fluent 20. The results demonstrated that when the non-uniform magnetic field passing current carrying wires with *Ha*=2 is applied, the recirculation bubble length in the domain of the wake downstream of the cylinder is reduced. This recirculation region gradually weakens both longitudinally and laterally by strengthening the non-uniform magnetic field intensity from *Ha*=2 to *Ha*=6. However, if the *Ha* further increased to a value *Ha*=10, the flow separation is suppressed, and the recirculation bubble like the wake region completely disappears. By intensifying the non-uniform magnetic field strength, the unsteady attitude of the flow field diminishes, and the time-independent flow is created. It was detected that the total drag coefficient, C_D gets higher with the applied non-uniform magnetic field going through current-carrying wires for all examined Reynolds numbers, *Re*=25, 50, 100 and 150. Obtained results demonstrate that in steady flow cases at *Re*= 25 and 50, the Nu_{avg} shows monotonic behavior with *Ha* and it enhances as the strength of the non-uniform magnetic field intensifies. Generally, the outcomes revealed that the maximum value of entropy generation grows significantly with increasing *Re* and relatively decreases with augmenting both *Ha* and Φ.

In the second part of the thesis, the hydrothermal and entropy generation characteristics of nanofluid (water and CuO) in a rectangular grooved channel exposed to the uniform magnetic field in a transverse direction are numerically investigated. In passive techniques, heat transfer improvement is acquired by changing the shape of the surface or employing fluid additives. The purpose of the surface modification is to increase the surface area in which heat transfer takes place and to improve the convective heat transfer by growing the fluid mixing. Furthermore, the improvement of energy transfer is acquired by adding extended fins or baffles because of the increment in turbulence level within the flow domain. The most important drawback of the passive techniques which grow heat transfer rate is that they also cause the pressure drop to be increased. This pressure drop due to the surface modification leads to a rise in the required pumping power. So that reason, scientists have investigated optimum geometry configuration that supplies greater heat transfer improvement with lower pumping power. The area of expertise which investigates the structure and attitude of electrically conductive fluids in the existence of magnetic field defined magnetohydrodynamic (MHD) is a crucial scientific branch for a broad range of engineering applications such as microelectronic device cooling, turbulence control, liquid metal cooling, crystal growth, nuclear reactor cooling, heat and mass transfer control and so forth. A high number of studies have explored the influence of magnetic fields on convective heat transfer in corrugated or similar channels. In the second part of the thesis, the hydrothermal and entropy generation characteristics of nanofluid (water and CuO) in a rectangular grooved channel exposed to the uniform magnetic field in a transverse direction are numerically investigated. Obtained results demonstrated that applying a uniform magnetic field with different intensities induces major

changes in the streamline patterns. When the Hartmann number, *Ha* increases from *Ha*=0 towards *Ha*=24 progressively the extent of the recirculation region in the rectangular grooves diminishes. The velocity gradient near walls gets higher by increasing the Hartmann number, *Ha* so the extent of vortices close to the walls diminishes at both Reynolds numbers, *Re*=250 and 1250. Because the Lorentz force resulting from the magnetic field reduces the flow velocity at the center of the channel and with regarding constant mass flow throughout the channel, the flow velocity substantially enhances near the hot walls. This situation grows the velocity gradient and temperature gradient near the hot walls and heat exchange between heated walls and nanofluid flow enhances. It can be seen that when the Hartmann number progressively increases from *Ha*=0 towards *Ha*=24, the thermal boundary layer in the rectangular grooves gets thinner at both Reynolds numbers, *Re*=250 and 1250. Furthermore, the applied uniform magnetic field in a transverse direction makes the temperature gradient in the vicinity of heated walls to increase. According to the results, the average Nusselt number, Nu_{avg} augments by increasing uniform magnetic field intensity. Including CuO nanoparticles into the water with volume fractions, Φ=3% and 5% makes the Nu_{avg} to be augmented for all examined *Ha* at *Re*=250. It is apparent in the figures, the Nu_L is enhanced when the uniform magnetic field is applied and its intensity gets higher along the rectangular grooved channel at both Reynolds numbers, *Re*=250 and 1250. When the Hartmann number progressively increases from *Ha*=0 towards *Ha*=24, the Nu_L is distributed with greater values along the grooved channel.

GENİŞLETİLMİŞ ÖZET

Tezin birinci bölümünde su ve Fe_3O_4 karışımından oluşan bir ferroakışkanın kapalı bir silindir etrafında üniform olmayan manyetik alan etkisi altında akı, ısı transferi ve entropi üretim özellikleri sayısal olarak incelenmiştir. Sanayi devriminden sonra enerji, insan yaşamı için vazgeçilmez bir ihtiyaç haline gelmiştir. Ancak kısıtlı kaynaklar, fiyatlar, ortam koşulları ve zamanla artan talepler nedeniyle enerji üretimi, kullanımı ve enerji dönüşüm süreçlerinin verimliliği daha da önemli hale gelmiştir. Evrensel pazardaki hızlı enerji talebi artışı, enerji verimliliğine ilişkin araştırmalar için ilham kaynağı olmuştur. Enerji verimliliğinin arttırılmasına yönelik araştırmalar birçok farklı disiplinin kapsamı içindedir. Bununla birlikte, ısı transferini arttırmaya yönelik girişimler, üretim aşamasından kullanıcı tüketim aşamasına kadar enerji verimliliği üzerinde ana etkiye sahiptir, çünkü bu işlemler bir şekilde ısı transferini içermektedir. Dairesel silindirik bir cisim üzerindeki akışkan akışı, mühendislik uygulamalarında yaygın olarak görülen bir durumdur. Silindir yüzeyinden akış ayrılması, ölü akış bölgesi ve silindir ile akışkan arasındaki ısı transferi, akışkanlar meaniği, ısı transferi ve aerodinamik alanlarındaki pratik önemi nedeniyle uzun bir süredir kapsamlı bir şekilde araştırılmaktadır. Dairesel kesitli bir silindir etrafındaki akış, silindirin kanal içerisinde veya serbest akış bölgesinde olmasına bakılmaksızın esas olarak Reynolds sayısına bağlıdır. Akışkan silindir üzerinde serbest bir akış bölgesinde akıyorsa, Reynolds sayısı akış karakteristiğini etkileyen tek parametredir. Reynolds sayısı yükseldiğinde, silindir etrafındaki akış önce kararsız duruma, daha sonra üç boyutlu kararsızlık moduna dönüşür (Williamson, 1996). $Re \leq 46$'dan küçük Reynolds sayısı için, silindir üzerindeki akış yapısı zamandan bağımsızdır ve silindir arka kısmındaki ölü akış bölgesi, silindir eksenine göre simetrik ters yönde dönen iki çevrintiden oluşmaktadır. Eğer Reynolds sayısı, $Re > 46$'dan büyük ise silindirin alt ve üst yüzeylerinden periyodik olarak kopan Karman girdapları oluşur. Bu akış olayı, Reynolds sayısı, $Re = 180$'e kadar devam eder ve daha büyük Reynolds sayıları için silindir etrafında üç boyutlu akış oluşur. Kapalı bir kanaldaki silindirik cisim etrafındaki akış yapısının araştırılması, ısı eşanjörleri, açık deniz gemileri, elektronik bileşenlerde yer alan ısı emicileri gibi geniş bir uygulama alanına sahiptir. Kapalı bir silindir etrafındaki akışın yapısı ve kararlılığı, serbest akış bölgesinde yer alan silindirin etrafındaki akışın yapısından önemli ölçüde farklıdır. Manyetik alan, akışkan akışı üzerinde dış cisim kuvveti olarak davranır. Manyetik kuvvetler ile akış kontrolü, elektriksel olarak iletken akışkanlara bir manyetik alan uygulanmasıyla sağlanır. Bu aktif akış kontrol tekniğinde, akış kontrolü daha fazla akış karışımı elde etmek için kullanılabilir. Ayrıca akış kontrolünün amacı, akış ayrılması gibi ısı transferini olumsuz yönde etkileyebilecek durumları ortadan kaldırmaktır. Momentum kuvvetlerinin etkisinin çok zayıf olduğu düşük Reynolds sayılarında ve doğan taşınım durumlarında manyetik kuvvetler daha etkilidir. Tezin birinci bölümünde, ferropartikül hacimsel oranı, Φ üniform olmayan manyetik alan şiddeti, Ha ve Reynolds sayısı, Re gibi çeşitli parametrelerin akış karakteristikleri ve zorlanmış

taşınım ile ısı transferi üzerindeki etkisi sonlu hacim tabanlı Anys Fluent 20 kullanılarak araştırılmıştır. Sonuçlar akım taşıyan tellerden geçen üniform olmayan manyetik alan *Ha*=2 şiddeti ile uygulandığında, silindirin akış yönündeki ölü akış bölgesinde oluşan resirkülasyon bölgesinin azaldığını göstermiştir. Bu resirkülasyon bölgesi, üniform olmayan manyetik alan şiddeti *Ha*=2'den *Ha*=6'ya arttırıldığında hem uzunlamasına hem de yanal olarak zayıflamıştır. Ancak, üniform olmayan manyetik alan şiddeti *Ha*=10 değerine daha da yükselirse, akış ayrılması bastırılır ve resirkülasyon bölgesi tamamen ortadan kalkar. Üniform olmayan manyetik alan şiddeti arttıkça, daimi olmayan akış yapısı ortadan kalkar ve zamandan bağımsız daimi bir akış yapısı oluşur. İncelenen tüm Reynolds sayıları için *Re*=25, 50, 100 ve 150, akım taşıyan teller vasıtasıyla uygulanan üniform olmayan manyetik alan şiddeti arttıkça toplam sürükleme katsayısının, C_D arttığı tespit edilmiştir. Elde edilen sonuçlar, *Re*=25 ve 50'de oluşan daimi akış durumlarında ortalama Nusselt sayısının, Nu_{avg} Hartmann sayısı, *Ha* ile monoton davranış gösterdiğini ve uniform olmayan manyetik alan şiddeti arttıkça Nu_{avg}'in arttığını göstermektedir. Genel olarak sonuçlar, entropi üretiminin maksimum değerinin artan Reynolds sayısı, *Re* ile önemli ölçüde arttığını ve hem *Ha* hem de Φ arttıkça nispeten azaldığını ortaya koymuştur.

Tezin ikinci bölümünde, üniform manyetik alan uygulanan bir dikdörtgen oluklu kanaldaki nanoakışkanın (su ve CuO) hidrotermal ve entropi üretim özellikleri sayısal olarak incelenmiştir. Pasif akış kontrol tekniklerinde, ısı transferi yüzeyinin şekli değiştirilerek veya akışkana çeşitli katkı maddeleri eklenerek ısı transferi iyileştirmesi sağlanır. Yüzey modifikasyonunun amacı, ısı transferinin gerçekleştiği yüzey alanını arttırmak ve akışkan karışımını arttırarak taşınım ile ısı transferini iyileştirmektedir. Ayrıca, uzatılmış kanatçıklar ve bölmeler eklenerek türbülans seviyesindeki artış nedeniyle enerji transferinde iyileşme meydana gelir. Isı transferini arttıran pasif tekniklerin en önemli dezavantajı ise basınç kaybının da artmasına neden olmalarıdır. Yüzey modifikasyonundan kaynaklanan bu basınç kaybı gerekli pompalama gücünde bir artışa yol açar. Bu nedenle bilim adamları düşük pompalama gücü ile daha fazla ısı transferi iyileştirmesi sağlayan optimum geometri konfigürasyonu araştırmaktadır. Manyetohidrodinamik (MHD) olarak tanımlanan manyetik alanın varlığında elektriği ileten akışkanların yapısını ve davranışlarını araştıran uzmanlık alanı, mikroelektronik cihaz soğutması, türbülans kontrolü, sıvı metal soğutması, kristal büyümesi, nükleer reaktör soğutması, ısı ve kütle transferi kontrolü gibi çok çeşitli mühendislik alanlarında uygulanan çok önemli bir bilim dalıdır. Çok sayıda çalışma, oluklu veya benzer kanallarda manyetik alan uygulamasının konvektif ısı transferi üzerindeki etkisini araştırmıştır. Tezin ikinci bölümünde, üniform manyetik alan uygulanan bir dikdörtgen oluklu kanaldaki nanoakışkanın (su ve CuO) hidrotermal ve entropi üretim özellikleri sayısal olarak incelenmiştir. Elde edilen sonuçlar, farklı şiddetlerde manyetik alan uygulanmasının dikdörtgen oluklu kanal içerisindeki akım çizgilerinde büyük değişikliklere neden olduğunu göstermiştir. Hartmann sayısı, *Ha*=0'dan *Ha*=24'e doğru kademeli olarak arttığında dikdörgen oluklardaki resirkülasyon bölgesinin boyutu küçülür. Isıtılan duvarların yakınındaki hız gradyanı Hartmann

sayısı, Ha arttıkça artar ve bu nedenle duvarlara yakın girdapların boyut, *Re*=250 ve 1250 değerlerinde azalır. Çünkü manyetik alan uygulanması sonucu oluşan Lorentz kuvveti, kanalın merkezinde akış hızını azaltır ve kanal boyunca sabit kütle akışı dikkate alındığında akış hızı ısıtılan duvarların yakın bölgesinde önemli ölçüde artar. Bu durum, sıcak duvarların yakınında hız ve sıcaklık gradyanını büyütür ve ısıtılmış duvarlar ile nanoakışkan akışı arasındaki ısı transferini arttırır. Hartmann sayısı, *Ha*=0'dan Ha=24'e doğru kademeli olarak arttırıldığında dikdörtgne oluklardaki termal sınır tabakanın *Re*=250 ve 1250 değerleri için inceldiği görülmektedir. Ayrıca uygulanan üniform manyetik alan, ısıtılan duvarların çevresindeki sıcaklık gradyanının artmasına neden olur. Elde edilen sonuçlara göre, ortalama Nusselt sayısı, Nu_{avg} üniform manyetik alan şiddetinin artmasıyla beraber artmaktadır. CuO nanoparçacıklarının suya Φ=%3 ve %5 hacimsel oranlarıyla ilave edilmesi, *Re*=250'de incelenen tüm Hartmann sayıları için ortalama Nusselt sayısının, Nu_{avg} artmasını sağlar. Şekillerde açıkça görüldüğü gibi, yerel Nusselt sayısı, Nu_L dikdörtgen oluklu kanal boyunca üniform manyetik uygulanmasıyla beraber *Re*=250 ve 1250 değerleri için artmaktadır. Hartmann sayısı, *Ha*=0'dan *Ha*=24'e doğru kademeli olarak arttığında NuL oluklu kanal boyunca daha büyük değerlere sahip olur.

ACKNOWLEDGEMENTS

I would like to thank my supervisor Prof. Dr. Beşir ŞAHİN who continuously supported and guided my thesis work. I would like to express my gratitude to my co-advisor Assoc. Prof. Dr. Göktürk Memduh ÖZKAN for his support and encouragement. Also, I would like to thank Prof. Dr. Hüseyin AKILLI for his support and encouragement as the Head of the Mechanical Engineering Department.

I would like to thank Assist. Prof. Dr. Harun ZONTUL, Dr. Hudhaifa Hamzah, and PhD student Fouad SARIĞIGÜZEL for their invaluable assistance during my studies.

I would like to express my special thanks to my wife, Tuğçe TÜMSE who was with me during my Ph.D. studies, sharing my sadness and joy, and giving me strength with her presence and mentorship.

I sincerely thank Assist. Prof. Dr. Nazım KURTULMUŞ, Assist. Prof. Dr. Tural TUNAY, and PhD student Mohammed ALHASSAN for their help during my journey. My sincere thanks go to my dearest family for their great patience and support during my PhD study.

I express my deepest gratitude, especially to my wife Tuğçe TÜMSE and to all family members who have continuously encouraged me along the way to my Ph.D. studies.

Lastly, I am grateful to the Çukurova University Scientific Research Project Office for their financial support under contract no: FDK-2021-13879.

Thank you so much to everyone who shared this journey with me.

LIST OF TABLES

LIST OF FIGURES

1. INTRODUCTION

After the industrial revolution, energy has become an essential requirement for human life. However, the efficiency of energy generation, utilization, and conversion processes has become more crucial because of the restricted sources, prices, ambient conditions, and growing requests with time. The U.S. Energy Information Administration (2020) stated that the energy request of the world will grow by approximately 50% by 2050. The quick increment in the universal market is the main inspiration for investigations on the efficiency of energy-including operations. Investigations aimed at increasing energy efficiency are within the extent of several various disciplines. However, attempts to enhance heat transfer have the main influence on energy efficiency from the generation stage to the end-user consumption stage because most of these operations include heat transfer in one way or another.

About 77 percent of world electricity generation in 2018 comprises operations that convert thermal energy into electrical energy (International Energy Agency, 2020). Thermal energy is a source that can be utilized directly in the chemical, manufacturing, and food sectors, as well as in electricity production. It is also a recoverable source in extreme heat industries such as cement and metal generation. Furthermore, the electrical consumption of house devices such as air conditioning and refrigerator is directly associated with their capability to transfer heat between source and sink. The working performance and efficiency of microprocessors are influenced by the temperature of these processors, thus they require to be cooled to use them with high performance and efficiency. As mentioned in all examples above, heat exchangers play a fundamental role and they are very effective in determining the overall efficiency and working performance of the thermal systems. As a result, improving the efficiency and thermal performance of heat exchangers is a topic that draws the attention of scientists and engineers for a long while. The flow control methods enhancing the heat transfer efficiency are composed of three essential methods which are the passive flow control method, active flow control method, and compound flow control method.

The categorization is made concerning whether additional energy is necessitated or not. If a heat transfer improvement is obtained without using extra energy than pumping power, the technique is defined as a passive heat transfer enhancement method. However, if the external energy is used for heat transfer enhancement, the technique is defined active heat transfer enhancement method. Furthermore, sometimes, active and passive techniques are employed at the same time, and the combination of these techniques is called as compound heat transfer enhancement method.

1.1. Passive Heat Transfer Enhancement Methods

In passive techniques, heat transfer improvement is acquired by changing the shape of the surface or employing fluid additives. The purpose of the surface modification is to increase the

surface area in which heat transfer takes place and to improve the convective heat transfer by growing the fluid mixing. Fig.1 demonstrates the many types of compact heat changers with different surface modifications. The most common instances of passive methods are adding obstacles (Al-Kouz et al., 2018; Siavashi et al., 2018), swirl generators (Jafari et al., 2017), rough surfaces (A. Albojamal et al., 2017; H. Hamzah et al., 2020), porous structures (Feng et al., 2020; P. Hu and Li, 2020), coiled tubes (Janssen and Hoogendoorn, 1978; Naphon and Wongwises, 2006), change cross-section or flow direction (Darr et al., 2016), using rectangular grooved surfaces (Tokgoz et al., 2017; Zontul et al., 2021), using sinusoidal grooved surfaces (Kurtulmus et al., 2020; Hamzah et al., 2022) and so forth. The surface modification improves the mixing of the flow between the core flow region and the thermal boundary layer near the surface, causing a high thermal transmission rate. Furthermore, the improvement of energy transfer is acquired by adding extended fins or baffles because of the increment in turbulence level within the flow domain. The most important drawback of the passive techniques which grow heat transfer rate is that they also cause the pressure drop to be increased. This pressure drop due to the surface modification leads to a rise in the required pumping power. So that reason, scientists have investigated optimum geometry configuration that supplies greater heat transfer improvement with lower pumping power.

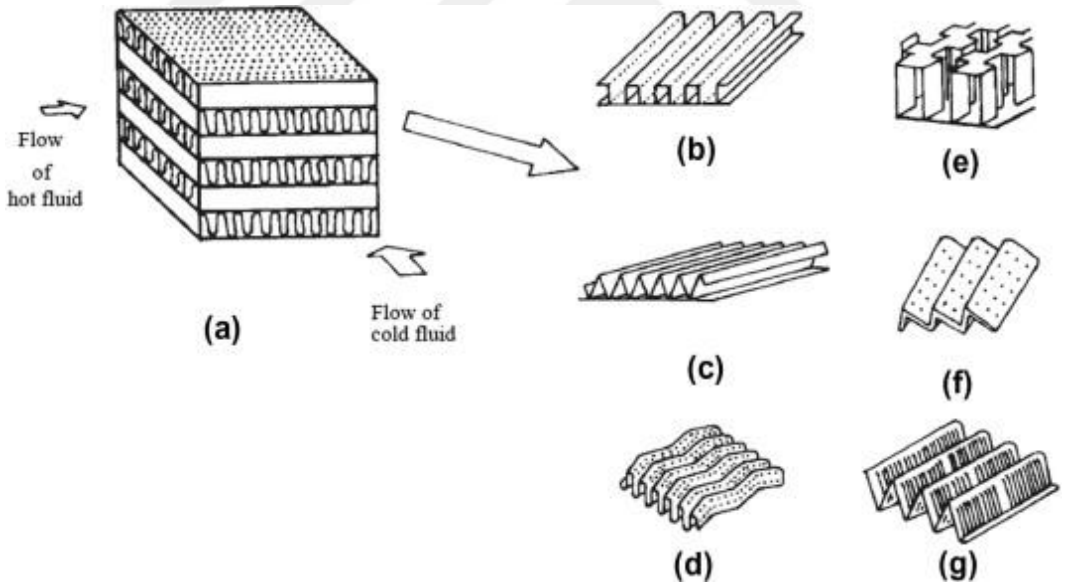

Figure 1.1. (a) Plate-fin heat exchanger and its surface geometries, (b) plain rectangular fins, (c) plain triangular fins, (d) wavy fins, (e) offset strip fins, (f) perforated fins, and (g) louvered fins (Kotcioglu, 1998).

Several kinds of heat exchange systems provide diverse levels of thermal performance; their main role is to transfer heat at a low financial expense. The performance of heat exchangers can further be improved by raising the thermal conductivity of the base fluid. This can be achieved by inserting solid materials which have high thermal conductivity into the working fluid. The employment of nano-sized solid materials in the base fluid is a common technique to improve the

thermal efficiency of heat exchangers for a long while. However, there are not many application areas where the solid particles are added into the base fluid in practice since the employment of these particles has some drawbacks such as sedimentation, clogging, and corrosion. Progress in nanotechnology science makes it possible to fabricate solid particles in nanometer size so clogging and sedimentation issues have become less significant and the employment of fluid additives as a heat transfer enhancement attracts the interest of scientists and manufacturers. Nanotechnology is gradually thought of as an applicable strategy to remove energy storage dangers in the last two decades. In this respect, scientists have been effectively following several techniques in which nanotechnology can substantially enhance the performance of heat exchangers. Thus, improvements in nanotechnology in heat transfer applications demonstrated that the suspension of nano-sized particles (generally smaller than 100 nm) in a working fluid provides to produce a stable mixture describes as nanofluids.

Nanofluid is an encouraging method for whole systems including heat transfer fluid and is further the key for the high efficient heat transfer applications because of the subsequent features:

. The wide heat transfer area between working fluid and nano-sized solid particles and therefore substantially enhances the nanofluid's thermal capacity.

. The great suspension stability with common Brownian motion of nanoparticle.

. The great optical features than the base fluid and therefore appear poor emission and effective absorption in solar systems.

. Many types containing metallic or non-metallic nanoparticles can be suspended in working fluids to constitute nanofluids.

. Adaptable properties like viscosity, density, thermal conductivity, and surface wettability by altering the solid volume fraction of nanoparticles to set for different heat transfer applications.

. Usually, nanofluids possess higher thermal conductivity, density, and viscosity compared to base fluids. However, the thermal expansion coefficient and specific heat are lower than the base fluid. These situations provide higher heat transfer efficiency together with a higher pressure drop of thermal systems.

. Nano-sized particles can remain dispersed in base fluids for an extended period compared to micro-sized particles.

. Reducing erosion and clogging problems compared to micro-sized solid particles thus suitable for use in microchannels.

The use of nanofluids has made an excellent improvement in the heat transfer rate for several engineering processes such as reactor-heat exchangers (Fan et al., 2008), cooling and heating equipment (Kulkarni et al., 2009), solar collectors (Taylor et al., 2011), solar stills (Gnanadason et al., 2012), energy storage tank (Thirugnanasambandam et al., 2010), refrigerator equipments (Bi et al., 2008), engine cooling system (Bai et al., 2008), automobile radiator (Zafar Said et al., 2019), hydraulic braking system (Popa et al., 2010), cooling of automatic transmission

(Tzeng et al., 2005), microelectronic structures (Tsai et al., 2004), magnetic sealing (Kim and Kim, 2003), optical filters (Philip et al., 2003), medical applications (Jalal et al., 2010), nuclear reactors (Boungiorno et al., 2008), plasma charging arc system (Kao et al., 2007), the lubricating mechanism (J. Zhou et al., 2000), grinding process of cast iron (Shen et al., 2008) and so forth. For more comprehensive knowledge of nanofluid applications, examine the subsequent references (Devendiran and Amirtham, 2016; Saidur et al., 2011).

As seen the employment of nanofluids provides a remarkable improvement in heat transfer, but this situation does not mean they supply heat transfer enhancement without any cost. The inserting of nano-sized solid particles into the base fluid grows the shear stress which increases the pumping power requirement. As a result, attention must be taken during the determination of nanoparticle volume fraction in the working fluid (Gosselin and Da Silva, 2004). Figures 1.2 and 1.3 demonstrate various types of working fluids and nano-sized solid particles, which are generally employed by scientists during the comparison of nanofluids. Hwang et al. (2006) revealed that the thermal conductivity improvement of nanofluids including CuO nanoparticles suspended in distilled water and ethylene glycol are 3% and 9%, respectively. Sivakumar et al. (2016) experimentally investigated forced convection heat transfer of CuO-water and Al_2O_3-water nanofluid, separately in the microchannel heat sink. According to the authors, the employment of nano-sized solid particles considerably augments the heat transfer efficiency of the working fluid. Moreover, obtained experimental results demonstrate that CuO-water nanofluid has a greater forced convection thermal coefficient than Al_2O_3-water nanofluid. Wang et al. (2006) have theoretically explored the effect of particle dimension and temperature on the specific heat of CuO nanoparticles. The main observation from their study is that the suggested theoretical model is coherent with corresponding experimental results. In the investigation of Saeedinia et al. (2012), it was revealed that the reducing specific heat value of CuO-oil nanofluid with volume fraction of solid particles Φ=2% at a temperature of 40 ºC is up to 22%. As revealed by Hanley et al. (2011), the specific heat values of Al_2O_3-water, CuO-water, and SiO_2-water nanofluids with particle diameters, d_p=50,30 and 32 nm, respectively augment with increasing the temperature of the nanofluid. Albojamal et al. (2017) carried out a numerical investigation on the prediction of the thermal transmission of Al_2O_3-water and CuO-water nanofluids in a channel with wavy walls. According to the obtained results, the transmission rate enhances by 20% compared to the single use of working fluid. But this enhancement is accompanied by an increment in pressure drop values. Bahiraei (2016) investigated the effect of CuO-water nanofluid use for volume fraction within the range of $0.3 \leq \Phi \leq 3\%$ on the laminar heat transfer performance in a straight tube at Re=1350. They found that the highest variation of local heat transfer coefficient with the corresponding experimental results is observed by 2 % with the discrete phase model and 10% with the single-phase model. Nada et al. (2010) carried out heat transfer improvement investigations utilizing Al_2O_3-water and CuO-water nanofluids in a heated enclosure. The mean Nusselt number,

Nu_{avg} deteriorates as the nanoparticles volume fraction, Φ was higher than 5%. Mousavi et al. (2016) carried out 2D numerical simulations to discover the impact of the applied non-uniform magnetic field on the heat transfer characteristics of a nanofluid (mixing of water and 4% Fe_3O_4) in a sinusoidal channel. According to the acquired findings, the applied non-uniform magnetic field raises the possibility of eddy generation in the cavities and thus improves the heat transfer by more than 200% in a close region where the magnetic field is applied at a small Reynolds number, *Re*=50. In the numerical study of Ghasemian et al. (2015), laminar forced convection heat transfer of a ferrofluid with a mixture of water and Fe_3O_4 in the existence of constant and alternating magnetic fields is investigated. According to them, while a constant magnetic field enhances the heat transfer mechanism by 16.48% at *Re*=25, this enhancement grows up to 27.72% when the alternating magnetic field is applied with the same magnetic field strength at magnetic field frequency, *f*=4 Hz. Sheikholeslami and Vajravelu (2017) investigated the flow and heat transfer characteristics of Fe_3O_4-water nanofluid with a non-uniform magnetic field. The simulations demonstrate that the increase in the magnitude of Lorentz forces augments the heat transfer rate and induces the vortex core to be moved downward direction.

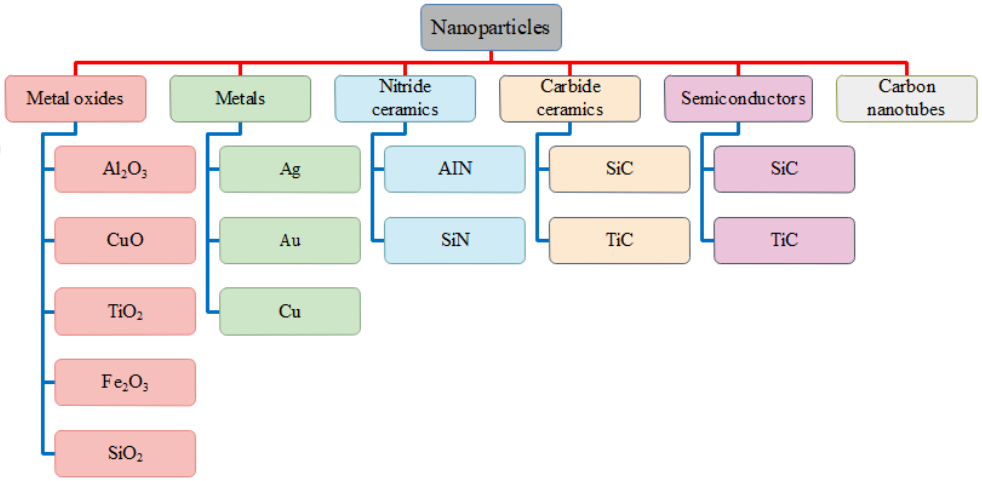

Figure 1.2. Various kinds of nanofluids.

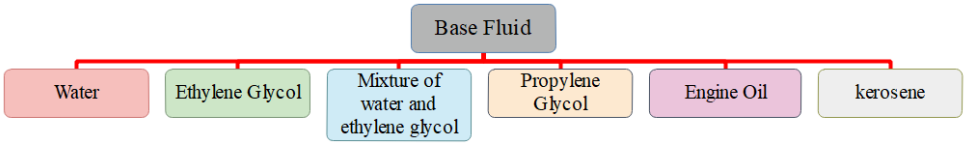

Figure 1.3. Various kinds of base fluids.

1.2. Active Heat Transfer Enhancement Methods

The active flow control method needs external power input to supply heat transfer augmentation. It supplies greater flow mixing and heat transfer improvement. These techniques can

be further aggressive compared to passive techniques in terms of flow mixing and disturbance. The most popular active heat transfer improvement techniques employed in investigations are as follows;

Mechanical Aid: Increasing heat transfer by mechanical aids is based either on the motion of the heat transfer surface or the motion/rotation of other objects near the heat transfer surface. Rotating cylinders in close regions of the heat transfer surface or cooled rotating tubes are very familiar examples of this technique.

Pulsating Flow: Periodic change of the flow velocity with time is a situation that substantially influences flow mixing. The pulsation frequency and amplitude are two essential factors in the heat transfer enhancement level. Furthermore, the flow velocity variation with time can be in sine waveform or square waveform. Pulsating flow is more influential in improving heat transfer as it is employed together with corrugated surfaces than flat surfaces.

Acoustic Waves: Acoustic waves improve heat transfer in two manners: they generate acoustically induced streams and create acoustic cavitation. Acoustically induced stream is just influential at low Reynolds numbers and natural convection. In acoustic cavitation, bubble bursting generates a disturbance in the flow and improves the flow mixing. But this technique also induces the erosion of surfaces.

Synthetic Jets: Synthetic jets are produced by absorbing surrounding the fluid in the flow field and ejecting it from the compact cavity.

Magnetic Fields: Magnetic fields act as external body forces on the fluid flow. The flow control by magnetic forces is achieved by operating a magnetic field to electrically conductive liquids. In this active flow control technique, the flow control can be utilized to gain a greater flow mixing. Furthermore, the aim of the flow control is to remove the circumstances that can inversely impact heat transfer such as flow separation. Magnetic forces are more influential at low Reynolds numbers and natural convection states in which the influence of momentum forces is very weak.

Magnetohydrodynamics (MHD) flows are carried out in extensive engineering and industrial applications such as in the field of materials science, flow meters, metallurgical processes, and casting that comprise the interaction of conducting fluid with an external magnetic field. Another effective application of MHD flow is the cooling circuits of fast fission reactors and self-cooled blankets of fusion reactors as stated by Morley et al. (2000). The MHD flow problems are attractive and demanding due to the combination of Maxwell equation with common hydrodynamics of the flow and then Lorentz force in the hydrodynamic momentum equation submitted a variety of nonlinearities.

1.2.1. Magnetic Field Effect on a Confined Cylinder

The research of conducting fluid flow on a confined cylinder located in a straight channel with the impact of the magnetic field attracts much practical attention (Kanaris et al., 2013). The

nanofluid flows in the closed channels with the existence of a magnetic field play an essential role in extensive engineering and industrial applications such as the stirring of melts in the metallurgical industry and cooling of liquid metal blankets in fusion reactors. Placing the circular cylinder in a channel can cause the occurrence of vortices and augment thermal performance favoring these processes (Lahjomri et al., 1993; Mutschke et al., 2001; Dousset and Pothérat, 2008; Hussam et al., 2011). Thus, understanding the augmentation of heat transfer by induced vortices or suppression of instabilities in the fluid flow can supply beneficial information of practical significance. The effect of the magnetic field may contribute or hamper the convective heat transfer depending on its magnitude and direction. Mostly, heat transfer augmentation arises from forcing the flow to interact with wake flow regions and heat transfer deterioration which occurs because of suppression of flow instabilities, increasing the size of the wake region or slowing down the flow velocity components in critical regions. Therefore, the application direction and magnitude of the magnetic field should be wisely chosen. There are several studies in the literature about the influence of uniform magnetic field in streamwise or transverse directions on the hydrothermal features of a confined cylinder such as Selimefendigil and Oztop (2018), Sekhar et al. (2007), Nikelham et al. (2022), Dousset and Potherat (2008). The major outcome of these investigations is that the shed of vortices from the alternate sides of the cylinder in the wake region gets weaker and beyond, if the strength of the magnetic field surpasses the critical value, the unsteady flow structure turns into a steady one. The major outcome of these investigations is that the shed of vortices from the alternate sides of the cylinder in the wake region gets weaker and beyond, if the strength of the magnetic field surpasses the critical value, the unsteady flow structure turns into a steady one. Udyakumar et al. (2016) revealed that the drag coefficient, C_D augments by 37% if the magnetic field is imposed parallel to the fluid flow and it substantially grows by 390% if the magnetic field is imposed perpendicularly to the fluid flow at Re=40 and lower strengths of the applied magnetic field. According to Tassone et al. (2018), due to the increment of the mass flow rate under an applied magnetic field, the mean Nusselt number is detected to enhance by Ha and this increment is nearly 20% for the Hartmann number of Ha=50. Sheikholeslami et al. (2014) numerically investigated the thermal and flow characteristics of Al_2O_3-water nanofluid in a square cavity in the existence of a magnetic field utilizing the lattice Boltzmann technique. According to the authors, the heat transfer enhancement gets higher by increasing the Hartmann number, Ha except the Rayleigh number, Ra=10^4. Furthermore, they stated that the Nusselt number, Nu augments with an increasing volume concentration of nanofluid and Rayleigh number, Ra.

1.3. Compound Heat Transfer Enhancement Methods

Combining passive and active flow control techniques yields better outcomes in improving heat transfer efficiency. Since they are simpler to apply, passive techniques are more favored. However, their heat transfer improvement capability is restrained. For instance, in corrugated

channels, the surfaces of corrugations are weak positions for heat transfer because of the low flow velocity. Utilizing an active flow control technique enables the interaction between the high flow velocity region and corrugations surface area thus the weakness of corrugated channels is eliminated and heat transfer efficiency is improved compared to the single employment of the passive method.

1.3.1. Magnetic Field Effect on Corrugated Channels

The area of expertise which investigates the structure and attitude of electrically conductive fluids in the existence of magnetic field defined magnetohydrodynamic (MHD) is a crucial scientific branch for a broad range of engineering applications such as microelectronic device cooling, turbulence control, liquid metal cooling, crystal growth, nuclear reactor cooling, heat and mass transfer control and so forth. A high number of studies have explored the influence of magnetic fields on convective heat transfer in corrugated or similar channels.

Aminfar et al. (2013) conducted numerical research on the impact of the nonuniform magnetic field of hydrothermal characteristics of a Fe_3O_4-water ferrofluid in a corrugated channel. Obtained results show that the applied magnetic field with a negative gradient enhances heat transfer performance and coefficient together with reducing wall temperature. According to the authors, the recirculation region in corrugations disappears with the applied non-uniform magnetic field. Sachica et al. (2020) carried out unsteady numerical simulations to observe the influence of Al_2O_3-water nanofluid on the mixed convection with the magnetohydrodynamic flow in a vertical channel. According to them, the vorticity characteristics, heat transfer rate, and amount of irreversibility during the entropy production are highly influenced by the intensity of the applied magnetic field and volume concentration of the nanofluid, Φ. In the investigation of Blischchik et al. (2021), the influence of magnetohydrodynamic (MHD) laminar duct flow including finite conductivity of surrounding walls, turbulent duct flow, a shallow 2D multi-phase cavity, and finally a rising bubble in the liquid metal was analyzed. According to their results, when the intensity of magnetic induction increases, the length of the recirculation bubble attenuates, and much more uniform flow occurs. Mei et al. (2019) conducted an experimental investigation to explore the hydrothermal performance of Fe_3O_4-water nanofluid in a corrugated tube with various magnetic field strengths. According to the presented results, the Nusselt number, Nu_{avg} enhances with increasing magnetic induction intensity and volume fraction of nano-sized solid particles, Φ in the base fluid. Gurdal et al. (2021) studied the influence of the external magnetic field on the hydrothermal characteristics of a dimpled tube. The 3D visual of the studied geometry, magnetic field application, and boundary conditions are demonstrated in Figure 1.4. The findings showed that the convection heat transfer augments due to the corruption of the boundary layer as a result of dimpled fin induced flow area narrowing. According to the authors, the maximum thermal

performance factor acquired under magnetic field intensity, *Ha*=75, the volume fraction of solid particles, *Φ*=0.025 and pitch ratio, *P/d*=7.5

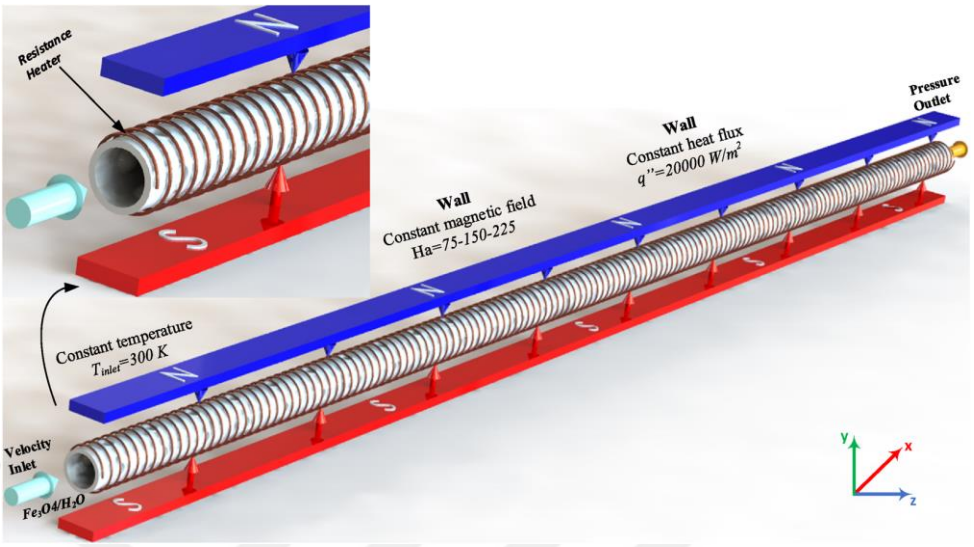

Figure 1.4. Nanofluid flow in the dimpled tube with the influence of the magnetic field (Gurdal et al., 2021).

2. LITERATURE SURVEY

2.1. Preliminary Studies About Effect of Uniform Magnetic Field on Hydrothermal Characteristics of Nanofluid Flows over Cylindrical Bodies

The fluid flow on a circular cylindrical body is widespread in great quantities of engineering practices. The occurrence of separated flow, wake region, and estimation of heat transfer from the circular cylindrical body has been extensively investigated for a long while since their essential importance in flow characteristics and practical significance in the field of heat transfer and aerodynamic applications.

The flow on a circular body mainly depends on the Reynolds number independent of the confined or unconfined domain. If the fluid over the cylinder flows in an unconfined domain, the Reynolds number is the individual parameter. When the Reynolds number gets higher, the flow around the cylinder turns into the firstly instable case, later three-dimensional instability modes (Williamson,1996). For Reynolds numbers smaller than $Re \leq 46$, the flow structure on the cylinder is time-independent and the wake region includes two-counter rotating symmetric vortices with respect to the cylinder axis appended to the rear side of the cylinder. The periodic vortex shedding occurs from alternating sides of the cylinder which is also known as Karman vortex street, if Reynolds numbers are bigger than $Re > 46$. This flow phenomenon proceeds up to the Reynolds number, $Re = 180$, beyond which three-dimensional flow occurs around the cylinder. For detailed information please refer to Williamson (1996) and Zdravkovich (2009).

The investigation of flow structure around the cylindrical body in a rectangular channel has an extensive application area such as heat exchangers, off-shore marines, and heat sinks for electronic components. Having such significant practices, the confined flow around bluff bodies has been the topic of extensive investigations from the past to the present (Prasad et al., 2011; Paramane and Sharma, 2009; Sahin and Owens, 2004).

The structure and stability of fluid flow around the confined cylinder significantly alter from the fluid flow structure of an unconfined cylinder. The influence of confinement characteristics, stability of flow, and flow parameters such as Nusselt numbers, Nu lift, C_L and drag coefficients, C_D have been studied by Coutaanceau and Bouard, 1977; Chen et al., 1995; Behr et al., 1995; Anagnostopoulos et al., 1996; Zovatto and Pedrizzetti, 2001; Khan et al., 2004; Chakraborty et al., 2004; Sahin and Owens, 2004; Cliffe and Tavener, 2004; Mettu et al., 2006). The blockage ratio, β which is the proportion of the diameter of the cylinder, D to the width of the channel, is an extra control parameter for the flow structure around the confined cylinder compared to the unconfined one. Because of the extra dissipation at the walls of the confined channel, the transition from time-independent to time-dependent flow is postponed and takes place at a higher Reynolds number, Re than the Reynolds number, Re that the steady flow turns into unsteady flow in unconfined flow.

Magnetohydrodynamics (MHD) flows are carried out in extensive engineering and industrial applications such as in the field of materials science, flow meters, metallurgical processes, and casting that comprises the interaction of conducting fluid with the external magnetic field. Another effective application of MHD flow is the cooling circuits of fast fission reactors and self-cooled blankets of fusion reactors as stated by Morley et al. (2000). The magnetohydrodynamic (MHD) flow problems are attracting and demanding due to the combination of Maxwell's equation with common hydrodynamics of the flow and then Lorentz force in the hydrodynamic momentum equation submitted a variety of nonlinearities. In the existence of topologically complex boundaries, amazing flow phenomena may occur as improvement or repression of the stability of the flow (Müller and Büller, 2001), the occurrence of secondary flow, and increased or decreased heat transfer rates (Moreau, 1990). A classical instance is the employment of the cylindrical obstacle to improve heat transfer performance and cause the occurrence of vortices that has been studied numerically (Mück et al., 2000; Mutschke et al., 1997; Sekhar et al., 2017; Mutschke et al., 1998; Dousset and Potherat, 2008) and experimentally (Papailiou, 1985; Kolesnikov and Tsinober, 1976; Lahjomri et al., 1993). The major outcome from these investigations is that the shed of vortices from the alternate sides of the cylinder in the wake region gets weaker and beyond if the magnitude of the magnetic field surpasses the critical value, the unsteady flow structure turns into a steady one.

Sommeria and Moreau (1982) demonstrated that the velocity components normal to the direction of the magnetic field are distributed by the dissipation of intense joule heating with the exception of in the Hartmann layer where the turbulent fluctuations are poorly absorbed. Frank et al. (2001) experimentally studied the effect of Hartmann numbers within the range of $50 \leq Ha \leq 1200$, on the wake region of the cylinder in a rectangular channel for Reynolds numbers of $100 \leq Re \leq 10000$. The employed Hartmann numbers correspond to Stuart numbers within the range of $10 \leq N \leq 576$. The blockage ratio, β which is the ratio of cylinder diameter to the channel height, was adjusted to $\beta = 0.1$. One of the most important outcomes of this study is the existence of linear dependence between the critical Reynolds number, *Re* and the Hartmann number, *Ha* at which the shed of unsteady vortices begins. They revealed that the vortical energy dissipation induces a continuous reduction of the magnitude of vorticities in the direction of free-stream flow. Muck et al. (2000) numerically investigated three-dimensional liquid-metal flows on a square cylinder in a rectangular channel. In this study, the Hartmann number was changed within the range of $0 \leq Ha \leq 85$ corresponding to Stuart numbers of $0 \leq N \leq 36$ at two constant Reynolds numbers, $Re = 200$ and 250. It was stated that the acquired results are in good agreement with the study of Frank et al. (2001). Kim and Lee (2000) performed research on the impact of the local electromagnetic force on the flow characteristics of a circular cylinder. This force was locally applied on the various locations of the cylinder surface. Also, they conducted experimental studies to validate numerical studies. The numerical results revealed that the applied Lorentz force causes the separation point to move

rearward direction and decreases the drag force on the cylinder. The Lorentz force greater than the critical value hinders the periodic vortex shedding phenomena and reduces the length of the wake region, drastically, ending up with just a little separation bubble. But for a negative Lorentz force, the width of the wake region enlarges, and flow physics described for positive Lorentz forces reverse. Furthermore, the positive Lorentz force, $LF>0$ causes the separation point to move the rearward side of the cylinder drastically but the negative Lorentz force, $LF<0$ quickens the flow separation. Bramley (1975) investigated the time-independent 2D-incompressible MHD flow over a circular cylinder with imposed magnetic field in parallel to the mainstream flow by employing numerical and analytical methods. He revealed that the applied magnetic field enables the flow to remain attached to the cylinder surface for a larger time and in some cases, the flow did not separate from the surface of the cylinder up to the stagnation point on the rear side of the cylinder. Josserand et al. (1993) investigated the influence of an aligned magnetic field in the liquid metal flow on a circular cylinder and discovered that the applied magnetic field can decrease the drag coefficient, C_D on the cylinder and if this applied magnetic field is sufficiently high, it suppresses the Karman vortex street in the wake of the cylinder. In the experimental investigation of Uda et al. (2001), it was pointed out by examining temperature fluctuations that the applied magnetic field in a transverse direction worsens the heat transfer rate in an annular channel. Mutschke et al. (1998) conducted an investigation into the control of cylinder wake induced instabilities in the conductive fluid flow past a circular cylinder through the application of external magnetic fields. The direction of the external magnetic field has caused the occurrence of many different flow configurations and thus the various transition flow regions. The two-dimensional flow can be stabilized and the vortex shedding can be suppressed by means of strong magnetic fields. The extent of recirculation length and separation angle reduces with an increase in the intensity of the applied magnetic field. Furthermore, the increasing magnitude of the external magnetic field may cause the time-dependent flow turns into a steady flow with a lower drag coefficient, C_D. According to them, at a critical value of the interaction parameter, N the Strouhal frequency, f of vortex street changed by the magnetic field reduces just weakly by increasing the Stuart number, N till the occurrence of steady flow. Although the flow is three-dimensional and unstable in the pure hydrodynamic flow, $N=0$ the extent of three-dimensional instability diminishes even at a weak magnetic field, $N=0.05$.

Dousset and Potherat (2008) numerically investigated the influence of the strong magnetic field applied parallel through the cylinder axis on the 2-D liquid metal flow in a square channel. The blockage ratio was kept constant as $\beta=0.25$ with Hartmann numbers in the range of $0\leq Ha\leq 2160$, for Reynolds numbers smaller than 6000, $Re\leq 6000$. This study demonstrated that the linear friction term which is proportional to the ratio of the Reynolds number, Re to the Hartmann number, Ha is a very effective parameter for the control of the transition of the flow region. Moreover, it has been stated that the 2D vortex street breakdown takes place at the Reynolds number of $Re=5000$. Midya et al. (2003) explored the impact of magnetohydrodynamics on the

incompressible viscous flow in a channel including restriction. According to them, the applied magnetic field in the transverse direction decreased the extent of the separated flow region in the flow direction downstream of the constriction and if this applied magnetic field in the transverse direction is sufficiently large, the flow separation can be eliminated. They revealed that when the intensity of the applied magnetic field gets higher, the wall shear stress increases. Sekhar et al. (2006) conducted an investigation into the influence of an inclined magnetic field in the laminar flow over a cylinder and discovered that the applied magnetic field in a parallel direction with flow decreases the length of the wake region. Sekhar et al. (2007) presented a study about the influence of an aligned magnetic field on the time-independent incompressible viscous flow past to the circular cylinder. According to them, the downstream base pressure is more influenced than the upstream base pressure with the applied magnetic field. Rashidi et al. (2015) observed the effect of the magnetic field applied both in streamwise and transverse directions on the flow and thermal characteristics of a porous obstacle. They revealed that the magnetic field applied in the transverse direction is more effective on the flow and heat transfer parameters than in the streamwise direction. Yu et al. (2013) numerically investigated the free conductive flow of conductive fluid in a rectangular cavity exposed to the uniform magnetic field in various directions. According to them, the direction of the applied magnetic field is also effective in heat transfer parameters as well as the intensity of the applied magnetic field. In the numerical investigation of Ishak et al. (2008) which is related to the effect of applied magnetic field on the flow and heat transfer properties in the region outside of a stretching cylinder, the value of the skin friction coefficient is found to grow by increasing the intensity of the magnetic field. In this study, the Laplace transfer method was utilized. Cuevas et al. (2006) have demonstrated that for a constant Reynolds number, *Re* the augmentation of the Hartmann number, *Ha* strengths, the breaking of fluid in the region of high magnetic field causing the occurrence of a quasi-stagnant zone either in the near cylinder wake or in the magnetic obstacle.

In the study of Yoon et al. (2004) the Stuart number, *N* which is described as the proportion of electromagnetic forces to inertial forces, was altered between $0 \leq N \leq 10$ for the Prandtl numbers of 0.02, 0.7 and 7 corresponding liquid metal, air and water respectively at two different Reynolds numbers, $Re=100$ and 200. They revealed that when the severity of applied magnetic fields raises, the shed of vortices in the wake region gets weaker. Moreover, they stated that the oscillation amplitude of the lift coefficient, C_L attenuates with increasing severity of magnetic fields. If the interaction parameter, *N* which depends on the Reynolds number, *Re* is higher than the critical value, the flow field around the cylinder becomes time-independent. Furthermore, the flow and thermal parameters on the circular cylinder such as the drag coefficient, C_D the lift coefficient, C_L and the Nusselt number, *Nu* alters with an increase or decrease in the Stuart number, *N*. The oscillation amplitude of flow and thermal parameters reduces with increasing Stuart parameter, *N* in the region where $N<N_{cr}$, eventuate in reducing the lift coefficient, C_L and the Strouhal number,

St. Moreover, the separation point moves toward the rear side of the cylinder and the width of the wake region which gets narrower with a raising of the Strouhal number, *St* within the region $N>N_{cr}$. The wall vorticity throughout the cylinder surface which is very effective on the values of time-averaged Nusselt numbers, Nu_{avg} pressure, C_P and drag coefficients, C_D reduces in the neighboring of the front stagnation point and gets higher in flow direction by increasing Stuart numbers, *N* within the region of $N>N_{cr}$. Rashidi et al. (2015) employed a 2D numerical simulation related to time-dependent MHD flow past a square cylinder located in a rectangular channel. In this investigation, the time-dependent Navier-Stokes equations were solved by using the finite volume method (FVM). The numerical simulations were carried out for Reynolds numbers within the range of $1\leq Re\leq 250$, and Stuart numbers, $0\leq N\leq 10$. The impact of the magnetic field applied in a streamwise direction on the separated flow zone and vortex shedding was handled comprehensively for the Reynolds and Stuart numbers stated above. Moreover, new empirical equations were proposed for the Stuart number and length of the wake region. To be able to handle the effect of the magnetic field with the channel confinement, numerical simulations were also performed on a square cylinder in an unbounded flow region. According to Rashidi et al. (2015), a linear decrease in the Strouhal number, *St* was happened by increasing the Stuart number, *N*. This decrease is about 80% for the Stuart numbers, $N=0.14$. Besides, the increase of the Stuart number, *N* changes the flow pattern from unsteady to a time-independent one. They claimed that the critical Stuart number, N_{cr} that changes unsteady flow structure with steady one increases by increasing the Reynolds number, *Re*. Singha et al. (2006) simulated the 2D laminar flow of an electrically conducted fluid over a square cylinder located centrally in a rectangular channel exposed to the magnetic field in a transverse direction to investigate the impact of a magnetic field on the shed of vortices in varying Reynolds numbers changing from 50 to 250. According to them, the extent of the separated flow zone in a steady flow around a cylinder reduces when the intensity of the applied magnetic field grows. The applied magnetic field in a transverse direction is observed to have remarkable impacts on the characteristics of flow structure with slight augmentation of the Strouhal number, *St* and a substantial attenuation of the lift coefficient, C_L amplitude, demonstrating a decrease in the vortex shedding strength. Furthermore, they observed that the periodic shed of vortices at higher Reynolds numbers can be entirely suppressed and the unsteady flow patterns can be turned into steady ones if the severity of the applied magnetic field is sufficiently strong. However, the required intensity of the applied magnetic field to convert the unsteady flow as a steady one depends mainly on the Reynolds number, *Re* and there is a direct proportion between the required magnetic field strength and the Reynolds number, *Re* for the transition of flow pattern. The increase in the Hartmann number reduces the length of wake in time-independent flow. With the increase in Hartmann number, *Ha* while a slight amount of reduction in the drag coefficient, C_D was observed in the unsteady flow region, it remarkably increased in a steady flow regime. Finally, it was concluded that the fluid flows past the cylinder at a low Reynolds number is less susceptible to the change of

the Strouhal number, *St* per unit variation of the Hartmann number, *Ha*. The investigation of the free conductive flow of electrically conducting fluid emphasized that the applied magnetic field in radial direction influences the structures of streamlines as well as thermal boundary thickness with increasing patterns (Ashorynejad et al., 2013). Sathiyamoorrthy and Chamkha (2010) investigated the impact of magnetic field direction on the conductive heat transfer in the square cavity. According to them, a nonlinear reduction of the mean Nusselt number, Nu_{avg} under imposed magnetic field which is consistent with the study of Teamah (2008). Udyakumar et al. (2016) studied the impact of a magnetic field on the 2D laminar, incompressible flow of conducting fluid past a circular cylinder under mixed convection heat transfer. The numerical simulations for flow and thermal characteristics are performed at a low Reynolds number, *Re* and the impact of the applied magnetic field on flow and thermal fields is examined. They stated that while there are two symmetrical vortex structures with respect to the axis of the cylinder in forced convection, the symmetrical flow structures disrupt mixed convection heat transfer without an applied magnetic field. But the imposed magnetic field enhances the symmetrical structure of the flow in mixed convection. According to them, the non-monotone increase in the total drag coefficient happens by increasing the Prandtl number. Furthermore, whereas the monotone in the mean Nusselt number, Nu_{avg} was detected by increasing the Prandtl, *Pr* and Richardson numbers, *Ri* the applied magnetic field induced non-monotone behavior of the mean Nusselt number, Nu_{avg}. They pointed out that the imposed magnetic field is beneficial in terms of suppressing flow separation and controlling heat convection. The inclined structure of streamlines in mixed convection reorients to the more symmetrical one with respect to cylinder axis by the applied magnetic field. A deterioration of absolute vorticity values in the cylinder surface with an applied magnetic field causes degradation of heat transfer. They finalized the study with the sentence that the applied magnetic field is a well-active control flow control technique for the controlling of large mixed convection of 2D laminar incompressible flow of conducting fluid. Figure 2.1 demonstrates the effect of the magnetic field on the streamline and isotherm contours around the cylinder at Re=40 for the forced convection case, Ri=0. According to Figure 2.1, the flow separation on the cylinder surface is not completely removed despite the magnetic field strength, N=4. The length of the recirculation bubble and separation angle reduces quickly for initially applied lower magnetic field strength up to N=2. But, further augmentation of magnetic field strength does not provide flow suppression.

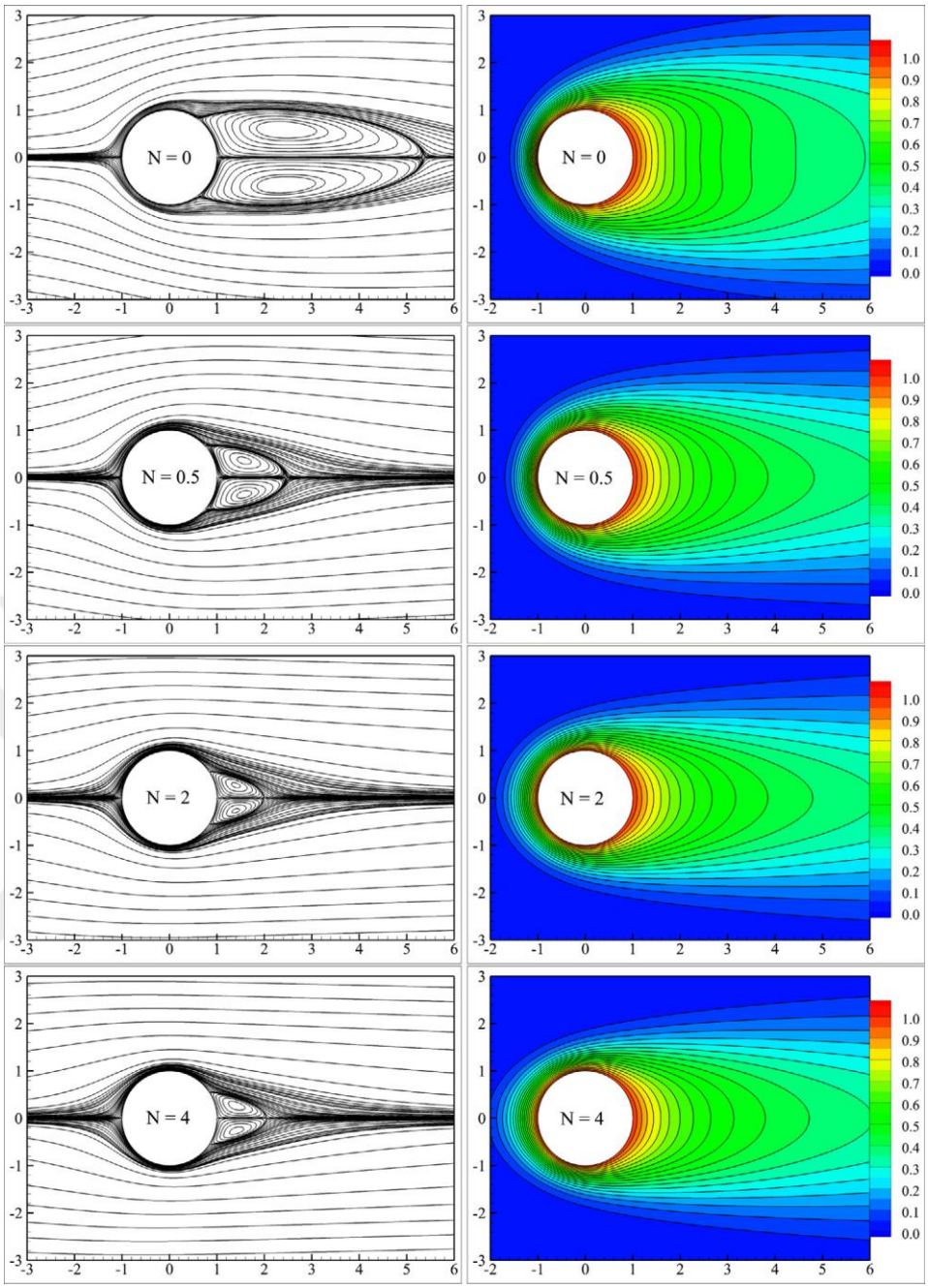

Figure 2.1. The effect of the magnetic field on the streamline and isotherm contours around the cylinder at *Re*=40 for forced convection case, *Ri*=0 (Udyakumar et al., 2016).

The immersed boundary method is an effective numerical simulation technique for analyzing simply hydrodynamic flows in flow domains of complex geometries. Soon Grigoriadis et al. (2009) suggested an expanding model of immersed boundary method that takes into account electromagnetic effects close to the non-conducting boundaries in MHD flows. Grigoriadis et al. (2010) used this extended immersed boundary method to investigate the effect of an applied magnetic field on flow and heat transfer characteristics of the magnetohydrodynamic flow of a conducting fluid past a circular cylinder. The comprehensive investigations, including 2D and 3D flows, the time-independent and dependent flow patterns with the value of Stuart numbers ranging

from N=0 to N=5 were conducted by using the highly accurate numerical scheme. The drag coefficient, C_D and recirculation length vary non-monotonically in both two and three-dimensional flows under a magnetic field in a streamwise direction. They stated that the drag coefficient, C_D was observed as lower under the applied magnetic field compared to the simple hydrodynamic flows. In the time-independent flow region, the drag coefficient was observed to change with respect to $\sqrt{(N_x+c)}$ where N_x is the magnitude of the applied magnetic field in a streamwise direction and c is a constant value. When the magnetic field is applied in a transverse direction, the vortex is suppressed more strongly compared to the streamwise magnetic field. Grigoriadis et al. (2010) dependent the drag attenuation under weak magnetic fields on the pressure force distribution near the cylinder. They determined the maximum values of streamwise and transverse interaction parameters, N_x=0.14 and N_z=0.07, respectively which the periodic shed of vortices was maintained. Tassone et al. (2018) numerically investigated flow characteristics on a heating cylinder which electrically insulated under an applied magnetic field in a transverse direction. The three-dimensional flow domain was simulated at Reynolds numbers, Re=20 and 40, for the inclination angle of the magnetic field $0° \leq \Upsilon \leq 32°$ and for the Hartmann numbers of $0 \leq Ha \leq 50$. It was observed that the applied magnetic field suppresses the wake of the cylinder. The heat transfer was observed to augment with increasing the Hartmann number, Ha and inclination angle, Υ. Moreover, pressure drag, as well as heat transfer in the channel, was detected to change non-monotonically by increasing the inclination angle, Υ of the applied magnetic field. According to the authors, the mass flow rate flowing through the sub-channel under cylindrical objects augments linearly by applied magnetic field strength. This augmentation is about between 3 and 5 times compared to the case of purely hydrodynamic flow. Due to the increment of this mass flow rate under the applied magnetic field, the mean Nusselt number is detected to increase by the Hartmann number. This increment is nearly 20% for the Hartmann number of Ha=50. Vimala et al. (2016) investigated the function of a magnetic Reynolds number, Re in magnetohydrodynamic forced convective heat transfer of a circular cylinder under an applied magnetic field by using a high-order compact scheme associated with the multigrid method. According to them, the average Nusselt number reduces up to the interaction parameter of $N \leq 1$ and later grows by further augmentation of the interaction parameter. It was also observed that the relatively weak intensity of applied magnetic fields can influentially control the flow of fluids with higher electrical conductivity. According to the authors, the average Nusselt number, Nu_{avg} gets lower with Alfven and magnetic Reynolds numbers, Re_m which is consistent with experimental studies findings. The implementation of Lorentz force in the fluid flow can be separated into situations. One of them which is extensively employed is the quasi-static approximation. It is known as the low magnetic Reynolds number approximation ($Re_m << 1$) which the induced magnetic field is disregarded for very small Re_m. In quasi-static approximation, the magnetic field turns out to be stationary thus a large number of non-linearities that occur because of Ohms Law can be removed.

Arjun and Rakesh (2020) carried out a nodal spectral element method based on the Eulerian-mixture model to investigate forced convective heat transfer and flow hydrodynamics under an applied magnetic field in a rectangular channel. In this study, various parameters were handled and the correlation between them was investigated such as the Reynolds number, *Re* volume fraction of nanoparticles, Φ the intensity of the applied magnetic field, *Ha* and Nusselt numbers, *Nu*. Nusselt numbers, *Nu* were observed to increase with Reynolds numbers, *Re* blockage ratio, *BR* which is the ratio of the cylinder diameter, *D* to the channel height, *H* and volume fraction of nanoparticles, Φ and Hartmann numbers up to the *Ha*=20. Nusselt numbers, *Nu* grow for the Hartmann numbers within the range of $0 \leq Ha \leq 20$ with a substantial increase up to the Hartmann numbers, *Ha*=10, and a moderate increase for Hartmann numbers from *Ha*=10 to *Ha*=20. The important outcome of this study is that the applied magnetic field controls the flow past a circular cylinder, alters the structure of vortical flow in cylinder wake, attenuates the average drag, and the fluctuations of lift coefficient, and postpones the main flow separation which is effective in reducing of drag coefficient, C_D and lift fluctuations. The Nusselt number, *Nu* augmentation was detected by increasing the nanoparticle volume fraction, Φ Reynolds numbers, *Re,* and cylinder diameter, *D* at a constant channel height, *H* while a reduction of the Nusselt number, *Nu* was noticed with the increase in the Hartmann number, *Ha* after a critical value. The Nusselt number, *Nu* augments by 163% when the gap ratio is 1, cylinder diameter, $D=0.4H$, and the Hartmann number is *Ha*=20 at the Reynolds number *Re*=3500 with 10*D* displacement of the cylinder diameter in a downstream direction. According to them, the vortices become strengthened by the increase in the Reynolds number, *Re* and they become weakened with the augmentation of the Hartmann number after *Ha*=20. Moreover, the size of the vortex reduces with the increase in Hartmann number after *Ha*=20. Figure 2.2 demonstrates the vorticity and temperature contours at *Re*=3500 the cylinder diameter, $D=0.4H$ for the Hartmann number, *Ha*=0. According to the obtained results, a double-row vortex street is observable in the downstream region of the cylinder wake. The interaction of negative vortices that shed from the wall boundary layer and upper shear wall occurs on the cylinder. Figure 2.3 shows the vorticity and temperature contours at *Re*=3500 cylinder diameter, $D=0.4H$ for the Hartmann number, *Ha*=10. This figure reveals that there is a strong interaction between the top cold wall Shercliff layer and the cylinder wake.

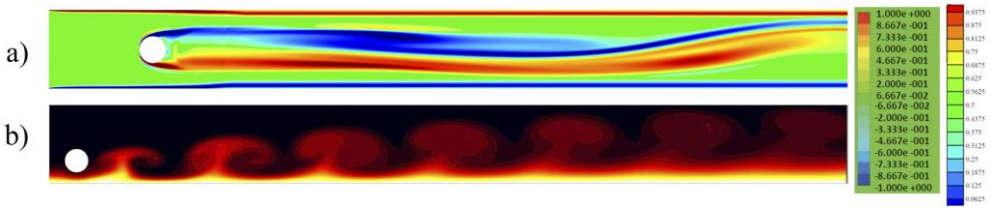

Figure 2.2. The vorticity and temperature contours at *Re*=3500 cylinder diameter, $D=0.4H$ for the Hartmann number, *Ha*=0 (Arjun and Rakesh, 2020).

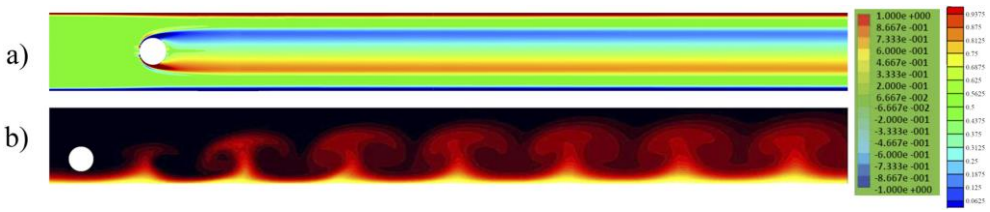

Figure 2.3. The vorticity and temperature contours at Re=3500 cylinder diameter, D=0.4H for the Hartmann number, Ha=10 (Arjun and Rakesh, 2020).

Ghosh et al. (2018) explored the full magnetohydrodynamic flow, which includes the effect of the magnetic Reynolds number, Re_m in constant quasi-static approximation around a circular cylinder regarding the magnetic field penetration inside the cylinder. According to Ghosh et al. (2018), the inwards bending of magnetic streamlines by the augmentation of the magnetic Reynolds number, Re_m while the magnetic streamlines flatten by increasing the Stuart number, N. The contours of vorticity become denser by increasing the Stuart number, N or the kinematic Reynolds number. But when the interaction parameter, N increases beyond the contours of vorticity contracts close to the center of the cylinder which shifted toward the flow direction for greater values of the magnetic Reynolds number, Re_m. The applied magnetic field grows the radial and transverse velocity gradient through the cylinder surface whereas the impact of fluid conductivity is just the contrary. Ying and Hulin (2007) numerically investigated magnetohydrodynamic flow past a circular cylinder at various Reynolds and Hartmann numbers. According to them, the applied magnetic field could not just alter the flow pattern around the cylinder, it also suppresses the turbulent viscosity and renewal of the surface which diminish the heat transfer characteristics. They emphasized that the higher turbulent intensity and interaction of surface and cylinder wake were detected at higher Reynolds numbers compared to lower ones under the same magnitude of applied magnetic fields. According to them, with an increase in Reynolds number, the effect of the applied magnetic field on flow and thermal pattern around the cylinder weakens and Lorentz force contour gets less dense. Chatterjee et al. (2013) conducted a 2D numerical simulation on forced convective heat transfer and magnetohydrodynamic flow past a square cylinder in a rectangular channel at weak Hartmann, Ha, and Reynolds numbers, Re. The streamwise and transverse magnetic fields were applied at Hartmann numbers within the range of $0 \leq Ha \leq 15$, for Reynolds numbers, Re between 10 and 60, at various Prandtl numbers, Pr=0.02, 0.71, and 7. The blockage ratio, β was kept constant at β=0.25 throughout the simulation. As well as the channel wall, the magnetic field provides extra stability to the fluid flow as a result of shortening the recirculation length in the rear of the square cylinder by increasing the intensity of the magnetic field at constant Reynolds numbers, Re. While the heat transfer rate enhances reasonably under imposed magnetic field at higher Reynolds numbers, Re it remains nearly the same at lower Reynolds numbers, Re. General the heat transfer augments with an increase in the Reynolds number, Re at a given Hartmann

number, *Ha*. The hydrodynamic instability is noticed to be further prohibited for the applied magnetic field in the transverse direction compared to the streamwise direction. The quicker weakening of recirculating region for the applied magnetic field in the transverse direction compared to the streamwise direction is evidence of the previous sentence. The quicker increase in the drag coefficient, C_D was detected at a relatively smaller Reynolds number, *Re* and this increment is large for the transversely applied magnetic field than in the streamwise direction. While direct proportion between Hartmann, *Ha* and Nusselt numbers, *Nu* were recorded, when the magnetic field is applied in the transverse direction, the change of the Nusselt number, *Nu* with the Hartmann number, *Ha* is not remarkable for the streamwise magnetic field. Furthermore, they emphasized that a stronger magnetic field is required for the suppression of cylinder wake when the shape of the cylinder is square other than circular form.

Hussam and Sheard (2013) studied the impact of a strongly applied magnetic field in the transverse direction on the flow and heat transfer characteristics of an electrically conducting fluid flow past a circular cylinder. In this study, the various Reynolds numbers up to the Re=3000 were handled together with the blockage ratio within the range of $0.1 \leq \beta \leq 0.4$, cylinder position ratio at the fixed Hartmann number, Ha=100. According to them, heat transfer improves by 48% when the cylinder offsets from the centerline of the cylinder wake compared to the centerline placement of the cylinder axis but just a moderate raise of pressure loss is observed due to the centerline displacement. Sivakumar et al. (2015) investigated the impact of an induced magnetic field on the forced convection heat transfer rate of the isothermal cylinder in the existence of an applied magnetic field. According to them, the applied magnetic field diminishes recirculation bubbles and alters the Nusselt number, *Nu*. They pointed out that while the Nusselt number, *Nu* enhances on the upper side of the cylinder, it attenuates in upstream and downstream zones. Magnetic Reynolds number, Re_m was also observed to contribute to the attenuation of the Nusselt number, *Nu*. Furthermore, the influence of the magnetic Reynolds number, Re_m vanishes on a flow of fluid having a low Prandtl number. According to them, the applied magnetic field decelerates the fluid flow. The implementation of a magnetic field brings about an effective decrease in the adverse pressure gradient. Thus, the extent of the separation bubble decreases. Udhayakumar et al. (2016) utilized a type of high numerical scheme in a curvilinear coordinate system to reveal the effect of a magnetic field on the 2D laminar flow of electrically conducted fluid and thermal characteristics on a cylindrical geometry. The numerical simulations were performed for the range of Prandtl numbers $0.065 \leq Pr \leq 7$, Reynolds numbers $10 \leq Re \leq 40$, and Stuart numbers, $0 \leq N \leq 5$. For lower strengths of applied magnetic fields, the drag coefficient augments by 37% if the magnetic field is imposed in the direction parallel to the fluid flow and it substantially grows by 390% if the magnetic field is imposed in the direction perpendicular to the fluid flow at the Reynolds number, Re=40. For higher strengths of the applied magnetic field, the drag coefficient, C_D grows with the proportion of the square root of the Stuart number, *N*. According to the authors, the direction of the

imposed magnetic field impacts the heat transfer characteristics on the cylinder. They emphasized that although the mean Nusselt number, Nu_{avg} attenuates because of the aligned magnetic field, the applied magnetic field in a transverse direction enhances heat transfer parameters. They pointed out that while wake length is not completely suppressed for the magnetic field applied in a streamwise direction, the wake length entirely disappears for any other orientation of the applied magnetic field. It was reported that when the magnetic field inclination angle, Υ is greater than 0, the flow symmetry with respect to the cylinder axis disappears and upward movement of the reattachment point is observed. On the other hand, the downward movement of the reattachment point was detected for negative magnetic field inclination angle, Υ. The drag coefficient, C_D changes as the square root of the Stuart number , N for the Stuart number, N is bigger than or equal to 1. Furthermore, the drag coefficient, C_D goes up monotonically with increasing inclination angle, Υ of the applied magnetic field. The influence of imposed magnetic field on the flow of fluid with a higher Prandtl number is greater than a fluid flow with a lower Prandtl number. Hence mean Nusselt number is detected not to be a monotone function of the imposed magnetic field. The orientation of imposed magnetic field changes the location of maximum heat convection on the surface of the cylinder. Finally, it was concluded that the applied magnetic field in a transverse direction, Υ=90° provides a maximum improvement of heat transfer for a constant intensity of the magnetic field. Figure 2.4 demonstrates the change of an angular Nusselt number on the cylinder surface for the various magnetic field strengths and directions. According to the authors, when a streamwise magnetic field, Υ=0° is employed the single maxima is bifurcated into two smaller maxima and the minimum heat transfer occurs at θ=180º. In the wake region of the cylinder 0º≤θ≤40º, the heat transfer rate is attenuated to approximately 50% of its value for the case of no magnetic field application. Similarly, a 50% heat transfer reduction is detected in the region close to the front stagnation point of the cylinder upon the employment of a proper streamwise magnetic field. In the cylinder surface except the regions mentioned above, heat transfer augmentation is detected with the application of a streamwise magnetic field, Υ=0°.

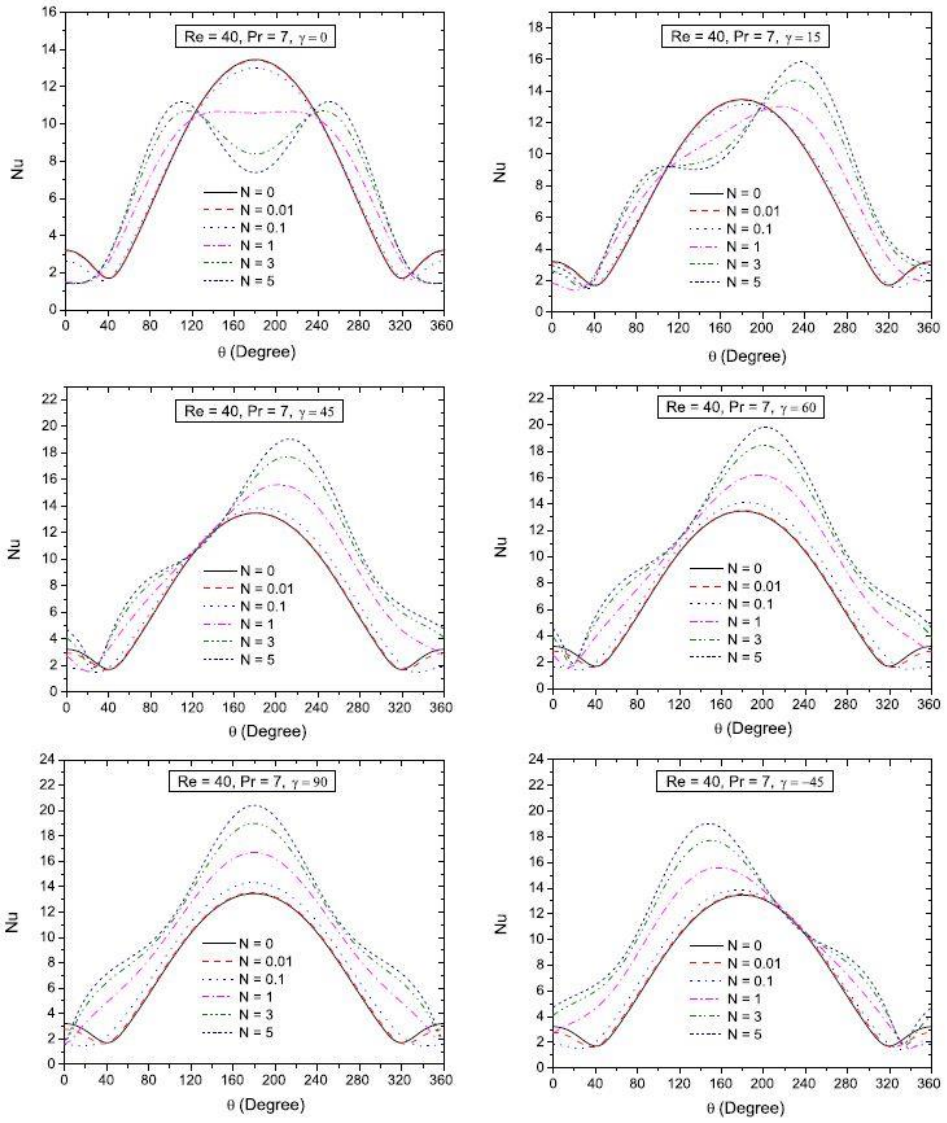

Figure 2.4. The change of angular Nusselt numbers on the cylinder surface for various magnetic field strengths and directions at *Re*=40 (Udyakumar et al., 2016).

According to the study of Krasnov et al. (2012) even at high Reynolds numbers, *Re* the unsteady flow pattern turns into a steady one due to the damping effect of the applied magnetic field if the Hartmann number, *Ha* is sufficiently high. In the study of Dousset and Potherat (2008) which the applied magnetic field aligned with the axis of the cylinder, it was demonstrated that the beginning of the shed of vortices is delayed until greater Reynolds numbers, *Re* at Hartmann numbers greater than 320, *Ha*>320. For a specific Hartmann number, *Ha* a linear relationship between the Hartmann number, *Ha*, and the corresponding critical Reynolds number, *Re* was observed. Rezaie and Norouzi (2018) employed the Lattice Boltzman model to investigate the effect of an applied magnetic field on the flow of a non-newtonian fluid past a circular cylinder confined with the 2D rectangular channel. In this study, the change of the Strouhal number, *St* and the drag coefficient, C_D by the Stuart number, *N* is demonstrated at various power law indexes.

According to them, the magnetic field should be strongly applied to be able to control the shed of vortices in a shear-thinning fluid. They emphasized that the extent of the wake region downstream of the cylinder weakens when the Stuart number, N grows for both Newtonian and non-Newtonian fluids in the time-independent flow region at Re=50. The linear increase in the drag coefficient, C_D was detected when the intensity of the applied magnetic field enhances at various power law indexes and time-independent flow regions. When the Reynolds number was set to Re=250 in the time-dependent flow region, the linear reduction of the Strouhal number, St was recognized with the increase in the Stuart number, N. Moreover, the amplitude of drag, C_D and lift coefficients, C_L attenuates as the magnitude of the applied magnetic field gets reduced. They pointed out that contrary to the steady flow region, in the unsteady flow region, the mean drag coefficient reduces with the increase in applied magnetic field strength. When the Stuart number, N continues to increase beyond a certain value, the unsteady flow behavior turns into a steady one. Shahri and Nezhad (2017) investigated the MHD flow and heat transfer characteristics of a liquid metal flow past a square obstacle in a channel by employing a quasi two dimensional model which is known as SM82 equations. The influences of Hartmann, Ha and Reynolds numbers, Re and blockage ratio on the length of wake region, mean Nusselt number, Nu_{avg} and iso-contours were discussed. When the Hartmann number grows to, Ha=1200 the shed of vortices entirely vanishes and the time-dependent flow structure turns into a steady one. According to them, the increase in blockage ratio usually increases the Strouhal number which may increase or decrease with the change of Reynolds numbers, Re, and Hartmann numbers, Ha. The mean Nusselt number, Nu_{avg} worsens when the Hartmann number goes up from Ha=300 to Ha=1200. At fixed Hartmann numbers, Ha the mean Nusselt number substantially increases when the blockage ratio is increased from β=0.1 to β=0.4. The intensity of mixing of hot and cold fluids enhances with the increase in heat transfer rate by decreasing Hartmann number, Ha, and increase in blockage ratio. Kanaris et al. (2013) performed three-dimensional numerical simulations about MHD flow over a confined circular cylinder under various magnetic field strengths. This simulation was performed for Reynolds numbers within the range of $0 \leq Re \leq 5000$ and for Hartmann numbers within the range of $0 \leq Ha \leq 1120$. In this study, a non-monotone attitude of a critical Reynolds number, Re for the beginning of the shed of vortices in accordance with the Hartmann number, Ha has been demonstrated. A linear dependency between the critical Reynolds number, Re and Hartmann number, Ha was discovered for the Hartmann number, Ha greater than 80, Ha>80. They revealed that for a high Reynolds number, Re=5000 even at a greater value of Stuart numbers, N i.e. up to 16, inertia effects close to the wake region, demonstrate a substantial role in the occurrence and movement of vorticities. For the Hartmann number, Ha=320 which corresponds to the interaction parameter of nearly 1, N=1, inertial forces give rise to the formation of instabilities that break up the energy into small scales, at last decreasing the energy of vortex shedding. Figure 2.5 (a) displays the critical Reynolds number, Re_{cr} for the beginning of the vortex shedding as a function of the Hartmann number, Ha. In this

figure, the lower end of the bar demonstrates the numerical simulation with the greatest Reynolds number, *Re* in which the flow is steady, whereas, the upper end of the bar demonstrates the simulation with the smallest Reynolds number, *Re* in which the flow is time-dependent. According to observed results, the critical Reynolds number, Re_{cr} increases with increasing Hartmann number, *Ha*. In Figure 2.5 (b), one can observe that the required Hartmann number, Ha that turns the unsteady flow with periodic vortex shedding into time-independent flow gets higher with increasing Reynolds number, *Re*.

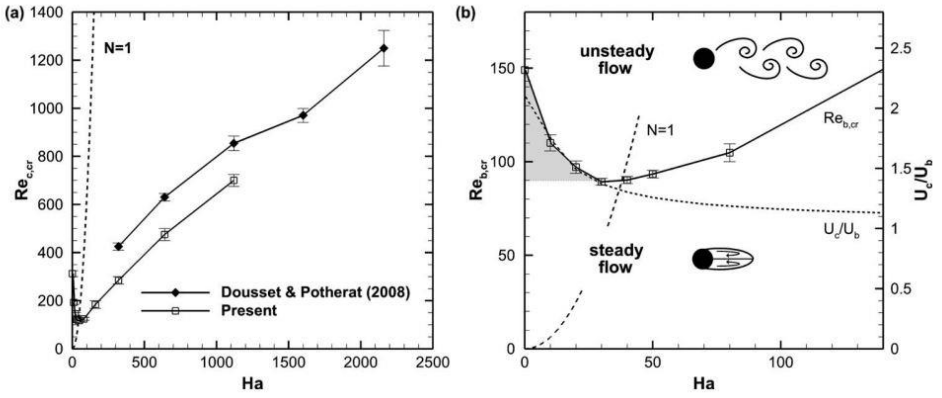

Figure 2.5. (a) The effect of magnetic field strength on the critical Reynolds number, Re_{cr} for the beginning of the vortex shedding (b) Enlarged demonstration in the region of the low Hartmann number, *Ha* (Kanaris et al., 2003).

Singha and Sinhamahapatra (2011) simulated a conducting fluid flow around a circular cylinder located on a rectangular channel exposed to a magnetic field in a transverse direction to investigate the impact of a magnetic field on the shed of vortices at Reynolds numbers within the range of $50 \leq Re \leq 250$. They revealed that the applied magnetic field in a transverse direction substantially decreases the time-dependent amplitude of the lift coefficient, C_L remarking an attenuation of vortex shedding strength. It was reported that the periodic shed of vortices at greater Reynolds numbers, *Re* can be entirely eliminated if an adequately strong magnetic field is applied. The intensity of the magnetic field required to eliminate vortex shedding augments with increasing Reynolds numbers, *Re*. According to their simulation, the width of the wake region on the rear side of the cylinder decreases when the magnitude of the applied magnetic field increases. The drag coefficient, C_D was observed to substantially increase in the time-independent flow field whereas it was found to slightly attenuate in the time-dependent flow field. For example, the time-averaged drag coefficient decreases by 4% when the Hartmann number alters from $Ha=0$ to $Ha=2.5$ whereas it increases by 48% when the Hartmann number alters from 0 to 6.5. According to them, the drag coefficient goes up more quickly at greater Hartmann numbers. Figures 2.6 (a-g) demonstrate the instantaneous vorticity contours at various Hartmann numbers, H_m for $Re=250$. According to Figure 2.6 (a-g), the flow remains time-dependent for the Hartmann number, $H_m \leq 50$ and turns into a steady state for the Hartmann number within the range of $5 \leq H_m \leq 5.5$.

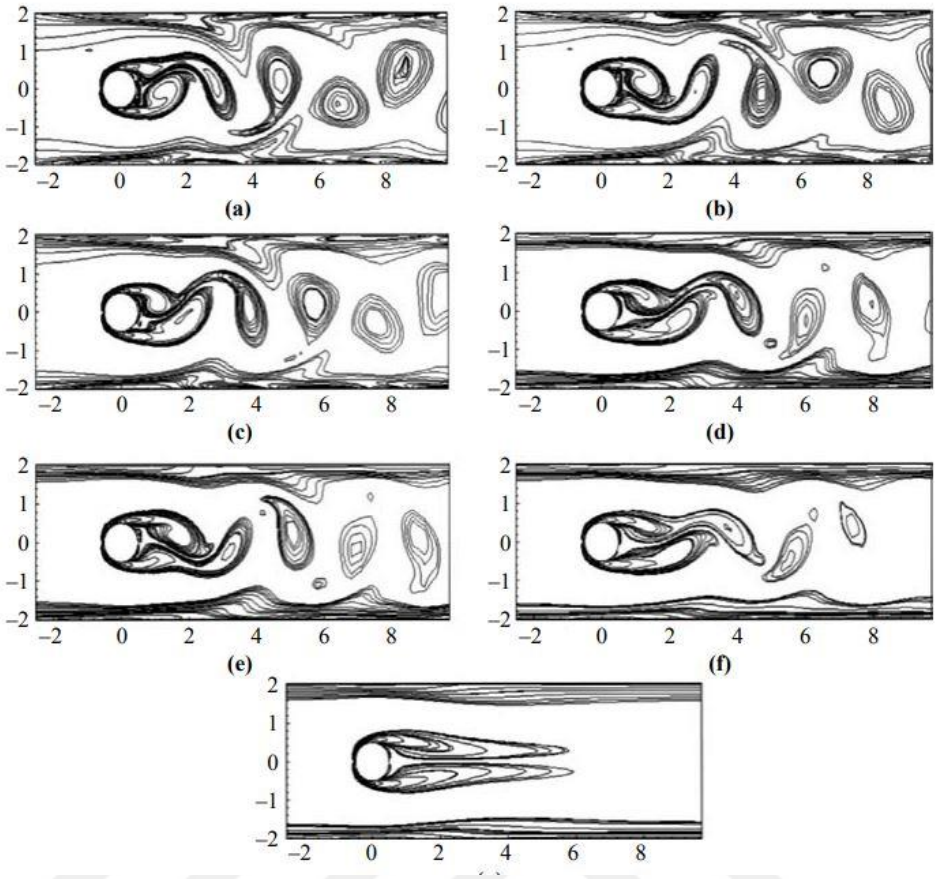

Figure 2.6. The effect of transverse magnetic field on the instantaneous vorticity contours around the cylinder at a) H_m = 0, b) H_m = 1.0, c) H_m = 2.0 d) H_m = 3.0, e) H_m = 4.0, f) H_m = 5.0, g) H_m = 5.5 (Singha and Sinhamahapatra, 2011)

Bovand et al. (2015) studied the influences of Stuart, *N* Darcy, *Da* and Reynolds numbers, *Re* on the flow characteristics of a 2D porous cylinder by employing the finite volume method (FVM). The conclusions demonstrated that the critical Stuart number, *N* which the shed of vortices suppressed reduces by growing Darcy numbers, *Da*. According to them, the Stuart number, *N* in which the cylinder wake disappeared gets higher by the augmentation of the Reynolds number, *Re* independent of the porosity of the cylinder. They revealed that the width of the cylinder wake reduces by raising the Darcy number, *Da* and the unsteady flow pattern distribution becomes a time-independent flow pattern by increasing the Darcy number, *Da*. The impact of the magnetic field intensity on the time history of the drag coefficient, C_D is represented in Figure 2.7. This figure reveals that for lower magnetic field intensities, $N<0.22$, the drag coefficient, C_D attenuates. The fluctuations of drag coefficient, C_D are diminished with the applied magnetic field and the diagrams have a monotonic behavior. Furthermore, for strong magnetic field strengths such as $N=5$, the drag coefficient, C_D grows. It is reported that the drag coefficient, C_D of a solid cylinder is higher than a porous cylinder.

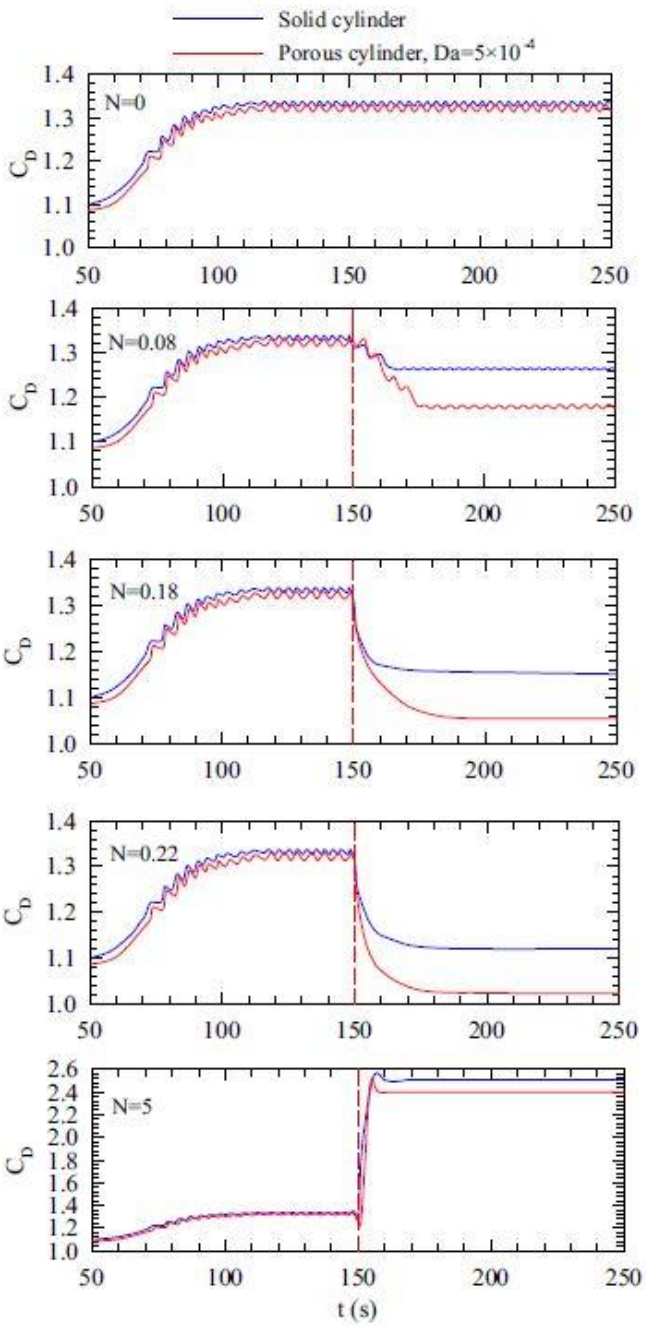

Figure 2.7. The time history of drag coefficient, C_D at various Stuart numbers, N for solid and porous cylinders (Bovand et al., 2015).

Rashidi and Esfahani (2015) aimed to demonstrate the impact of the applied magnetic field in a transverse direction and channel wall confinement on flow characteristics and forced convective heat transfer on a square cylinder. The numerical solutions were carried at a fixed Prandtl number, Pr=0.71, and for Reynolds numbers, Re within the range of 1 and 250 for interaction parameters, N within the range of 0 and 10. The acquired outcomes demonstrated that the presence of channel walls reduces the impact of the applied magnetic field on the heat transfer parameters such as the Nusselt number, Nu. According to them, the boundary layer thickness grows

and the rate of convective heat transfer attenuates by increasing interaction parameters. The reduction of the average Nusselt number, Nu_{avg} is about 12.5% for interaction parameters within the range of $0.001<N<10$ at Reynolds number, $Re=100$. The influences of the applied magnetic field were found to be negligible in the time-independent flow field. Figure 2.8 presents Iso-Lorentz force contours superimposed on isotherm contours for various Stuart numbers, $N=0$, 0.15, 5, and 8 at $Re=100$. In this figure, while the solid line represents the force in the y direction, the dashed line presents the force in opposite direction. As seen in this figure, the flow pattern changes its distribution from an unsteady state to a steady state by increasing the Stuart number, N. There is no Lorentz force when the Stuart number is zero, $N=0$. It is detected that the Lorentz force direction alters continuously for a small Stuart number, i.e., $N=0.15$, where the flow structure is still time-dependent with a periodic vortex shedding mechanism. When the Stuart number is increased $N=5$ or 8, the Lorentz force becomes symmetric with respect to the centerline since the flow pattern becomes time-independent with a symmetric form by applying a strong magnetic field. According to Figure 2.8, the Lorentz force at a high Stuart number, $N=5$ is positive at the upper part of the centerline ($x=0$) and is negative at the lower part of the centerline for the upstream of the obstacle. On the other hand, the reverse behavior is detected for downstream of the obstacle. This situation occurs because of the different velocity component directions of these zones.

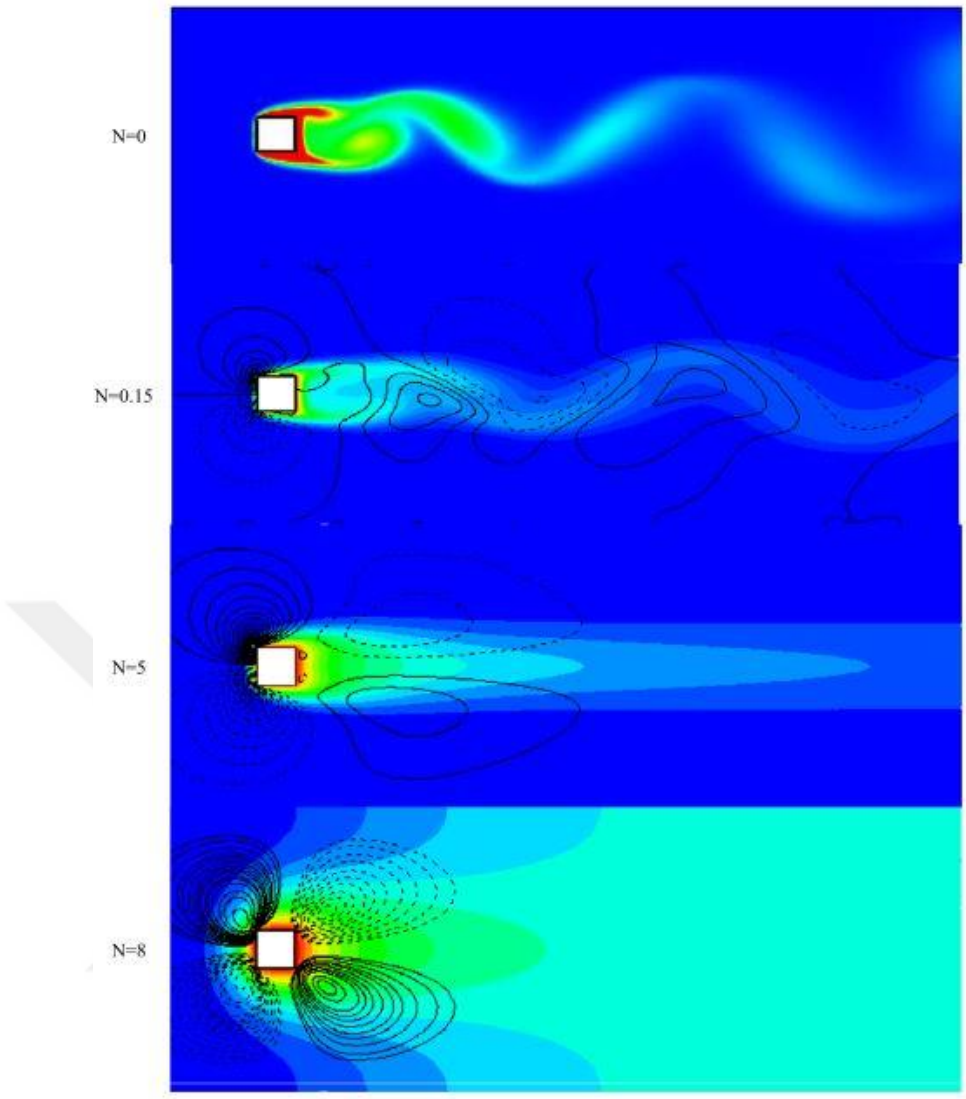

Figure 2.8. Iso-Lorentz force contours together with isotherm contours for various Stuart numbers, *N*=0, 0.15, 5 and 8 at *Re*=100 (Rashidi et al., 2015).

2.2. Preliminary Studies About Effect of Non-Uniform Magnetic Field on Hydrothermal Characteristics of Nanofluid Flow in Various Kinds of Heat Transfer Channels

Larimi et al. (2016) studied hydro-thermal behaviors of a ferrofluid, with a mixture of water and Fe_3O_4, in a ribbed channel subjected to many non-uniform transverse magnetic fields going through current-carrying wires perpendicularly positioned in the flow and between ribs. They revealed that the applied non-uniform magnetic field is very effective in increasing the Nusselt number, *Nu* in the channel, moreover, the maximum and minimum local Nusselt numbers, Nu_L in the rib region enhance with the increase in the intensity of the non-uniform magnetic field. According to them, the non-uniform magnetic field causes the skin friction coefficient to be increased particularly in the situation in which all magnetic wires are positioned on only one side of the channel. Sheikholeslami et al. (2015) investigated forced convection heat transfer in a lid-driven semi-annulus enclosure filled with a ferrofluid in the existence of a non-uniform magnetic

field. They revealed that while the Nusselt number enhances by increasing the Reynolds number, *Re,* and ferroparticle volume fraction, Φ it attenuates with the augmentation of the Hartmann number, *Ha*. In the investigation of Sheikholeslami and Vajravelu (2017), the impact of a variable magnetic field on a ferrofluid (water and Fe_3O_4) flow and thermal characteristics in a cavity is studied. Obtained results showed that the temperature gradient augments with increasing volume fraction of the ferrofluid and it deteriorates when Lorentz forces increase. Furthermore, increasing Lorentz forces induce the heat transfer rate to be augmented and the thermal plume to be diminished. Gerdroodbary et al. (2018) investigated the hydrothermal characteristics of a ferrofluid inside a T-junction in the presence of a non-uniform magnetic field. In this study, the ferrofluid flow inside the T-junction is modeled as a time-independent and single phase with the application of constant heat flux on the channel walls. On the other hand, three wires are used as a non-uniform magnetic field source. According to the authors, the application of a non-uniform magnetic field has caused the average heat transfer to augment by more than 64% and the local heat transfer to enhance by more than 200% in the close region where the magnetic field is applied. They revealed that the non-uniform magnetic field substantially strengthens the skin friction in close regions to the magnetic source. They mainly attributed the skin friction increment to the vorticities formation in the T-junction. Mousavi et al. (2016) numerically investigated the impact of the variable magnetic field on the ferrofluid flow in the sinusoidal two-tube heat exchanger. According to the obtained results, when the strength of the variable magnetic field enhances, the diffusion of the cold boundary layer elevates. Thus, the heat transfer rate and Nusselt number, *Nu* improve and this improvement grows at high *Re* numbers. Aminfar et al. (2013) numerically investigated the impact of the non-uniform transverse magnetic field on the flow and thermal characteristics of a ferrofluid with water and 4% Fe_3O_4 in a vertical rectangular duct. According to the authors, the non-uniform magnetic field generated by an electric current going through a wire improves the Nusselt number, *Nu* and friction factor and it causes the occurrence of a pair of vorticities that augments heat transfer. Obtained results demonstrate that the influence of transverse non-uniform magnetic field on the local Nusselt number, Nu_L attenuates by increasing *Re* number. In the numerical study of Ghasemian et al. (2015) laminar forced convection heat transfer of a ferrofluid with a mixture of water and Fe_3O_4 in the existence of constant and alternating magnetic fields is investigated. According to them, while constant magnetic field enhances the heat transfer mechanism by 16.48% at *Re*=25, this enhancement grows up to 27.72% when the alternating magnetic field is applied with the same magnetic field strength at magnetic field frequency, *f*=4 Hz. The numerical simulations have demonstrated that the heat transfer augmentation due to the applied magnetic field worsens with increasing the Reynolds number, *Re*. It should be noted that the vortices corrupt the thermal boundary layer and this situation provides heat transfer enhancement. This enhancement is more substantial as the magnetic field is settled in the fully developed region. Lee and Kim (2020) studied the impacts of non-uniform magnetic fields on the natural convection heat transfer of a

ferrofluid-filled enclosure. They revealed that the natural convection heat transfer performance of the ferrofluid inside the enclosure is improved with the applied non-uniform magnetic field due to the occurrence of the vorticities in the enclosure to create a recirculation zone. Malgir-Chegini and Amanifard (2019) numerically studied the effects of the non-uniform magnetic field on the hydrodynamic and hydrothermal characteristics of laminar nanofluid flow in the horizontal semi-insulated tube. Numerical simulations demonstrated that the existence of non-uniform magnetic field makes the heat transfer the existence of non-uniform magnetic field makes the heat transfer and pressure drop to be higher than 3.7 and 1.8 times for those obtained in the non-magnetic case at *Re*=500 and *Mn*=5.7e8. Obtained results revealed that the non-uniform magnetic field entirely controls the fluid flow and the entrance length shortens by increasing the intensity of non-uniform magnetic field strength at several *Re* numbers. The location of the wire which is a source of the non-uniform magnetic field has a vital influence on the Nusselt number, *Nu*. Izadi et al. (2019) aimed to numerically search the natural convection heat transfer of a hybrid nanofluid into a porous cavity subjected to a variable magnetic field. According to the authors, at greater Rayleigh numbers, *Ra* a substantial reduction in Nusselt number, *Nu* is detected when the *Ha* number grows, which can be interpreted as the attenuated power of the flow. They revealed that the distortion isothermal lines weaken, they seem in a straighter form when *Ha* number enhances. Hariri et al. (2017) performed a three-dimensional numerical simulation to investigate the impact of a non-uniform magnetic field in the heat transfer of a ferrofluid (water and 0.86% Fe_3O_4) inside a tube. According to them, the existence of a non-uniform magnetic field substantially augments the Nusselt number, *Nu* by more than 300% inside the tube. They revealed that the magnetic field induced by the parallel wire influences the mean velocity of the ferrofluid and constitutes two vigorous eddies inside the tube and these two vigorous eddies are very effective on the heat transfer characteristics of ferrofluid flow inside the tube. Mousavi et al. (2016) conducted a two-dimensional numerical simulation to investigate the influence of a non-uniform magnetic field in the heat transfer of a ferrofluid (water and 4% Fe_3O_4) inside a sinusoidal channel. Obtained results demonstrate that the application of a non-uniform magnetic field enhances the possibility of eddy occurrence inside the cavities and thus augments the heat transfer by higher than 200% in the vicinity of the magnetic field at a low *Re* number, *Re*=50. Furthermore, skin friction is observed to increase by more than 600% with the application of a non-uniform magnetic field inside the sinusoidal channel. According to the results, a large eddy is clearly recognized at low *Re* numbers when the non-uniform magnetic field is employed in the orthogonal direction of the sinusoidal channel. They revealed that the non-uniform magnetic field strengthens the adverse pressure gradient which augments the possibility of the eddy occurrence. Their findings show that the non-uniform magnetic field increases the velocity gradient in the vicinity of the channel wall and thus ends up with an increase in the Nusselt number. Since a large eddy is created in the cavity near the magnetic field application point, the temperature substantially attenuates in this region compared to

the case of no magnetic field application. When the ferrofluid flow velocity gets higher, the influence of the non-uniform magnetic field on the temperature weakens.

2.2.1. Significance and novelty of the current study

Magnetohydrodynamics (MHD) flows are employed in widespread engineering and industrial fields such as materials science, flow meter, metallurgical processes, casting, and cooling circuits of fast fission reactors. Locating a circular cylinder in the rectangular duct can induce vortices and improve heat transfer characteristics in the channel. It is of practical interest to investigate the hydrothermal characteristics of circular cylinders in a rectangular duct under the influence of a homogenous magnetic field. Even though it is possible to find many studies in literature related to the influence of the uniform magnetic field on hydrothermal characteristics, the research on the impacts of the non-uniform magnetic field is extremely restricted. Moreover, there are a few investigations related to the application of non-uniform magnetic field effects on various geometries such as semi-annulus enclosure, T-junction, sinusoidal double pipe heat exchanger, semi-insulated horizontal pipe, sinusoidal channel, and ribbed channel whereas no work has been documented related to the impact of the non-uniform magnetic field on the circular cylinder placed in a rectangular channel. In addition, this work regards the influences of thermal, frictional, and non-uniform magnetic sources on the irreversibility process through the studied channel. The present study becomes the first report on the non-uniform magnetic field effect on the flow and thermal characteristics of a ferrofluid on a confined cylinder with comprehensive analysis including the effects of together *Re*, *Ha,* and *Φ*.

2.3. Preliminary Studies About Effect of Uniform Magnetic Field on Hydrothermal Characteristics of Nanofluid Flow in Various Kinds of Corrugated Heat Transfer Channels

Asadi et al. (2019) studied the influence of the nonuniform magnetic field on the 2D laminar forced convection of heat transfer of a ferrofluid in a channel having sinusoidal corrugated walls. The findings show that the applied negative magnetic gradient augments the average Nusselt number, $Nu_{avg,}$ and also increases the pump work with a higher influence at a smaller Reynolds number, *Re*. In the investigation of Heidary et al. (2017) the hydrothermal characteristics of a channel with wavy walls were studied in the presence of the magnetic field applied in a transverse direction to the mainstream flow. Their computational results showed that the existence of a magnetic field and wavy wall at the same time is not appropriate for heat transfer improvement, any one of these flow control techniques is suitable for heat transfer augmentation. According to the authors, the applied magnetic field highly enhances flow velocity in the vicinity of hot walls and the intensity of vortex attenuates with the Hartmann number, *Ha*. With increasing magnetic field intensity, the velocity gradient grows in the vicinity of channel walls and results in increased friction coefficient and pressure drop. They concluded that the thickness of the thermal boundary

layer reduces by the presence of a magnetic field which enhances the heat transfer rate. Figure 2.9 demonstrates non-dimensional isotherm lines for Hartmann numbers, Ha=0 and 30 at Reynolds numbers, Re=25 and 250 in a wavy corrugated channel. As it is clear in this figure, the thickness of the thermal boundary layer reduces when the magnetic field is applied with Ha=30. Furthermore, when the Reynolds number increases from Re=25 to Re=250, the thermal boundary layer shrinks in size thus isotherm lines gravitate toward the channel walls. This situation makes the temperature gradient in the vicinity of the channel wall to be enhanced, so the Nusselt number, Nu and heat exchange augments. Sachica et al. (2020) carried out unsteady numerical simulations to observe the influence of Al_2O_3-water nanofluid on the mixed convection with the magnetohydrodynamic flow in a vertical channel. According to them, the vortex characteristics, heat transfer rate, and amount of irreversibility during entropy production are highly influenced by the intensity of the applied magnetic field and volume concentration of the nanofluid, Φ. Furthermore, according to their results, the asymmetry of the flow structure is deteriorated and the symmetric flow structure is enhanced with magnetic field application. Furthermore, they stated that the modulation impact of the exerted magnetic field can play a significant part in practical implementations for entropy production minimization. In the investigation of Blischchik et al. (2021) the influence of magnetohydrodynamic (MHD) laminar duct flow including finite conductivity of surrounding walls, turbulent duct flow, a shallow 2D multi-phase cavity, and finally a rising bubble in the liquid metal was analyzed. According to their results, when the intensity of magnetic induction increases, the length of the recirculation bubble attenuates, and much more uniform flow occurs. Mei et al. (2019) conducted an experimental investigation to explore the hydrothermal performance of Fe_3O_4-water nanofluid in a corrugated tube with various magnetic field strengths. According to the presented results, Nusselt number, Nu_{avg} enhances with increasing magnetic induction intensity and volume fraction of nano-sized solid particles, Φ in the base fluid. Nusselt number, Nu_{avg} is improved by 17.6% and 10% with the use of the nanofluid compared to the water in smooth and corrugated tubes, respectively. Furthermore, the simultaneous applications of a nanofluid, magnetic field, and corrugated tube grow heat transfer remarkably at the little expense of increasing the flow resistance.

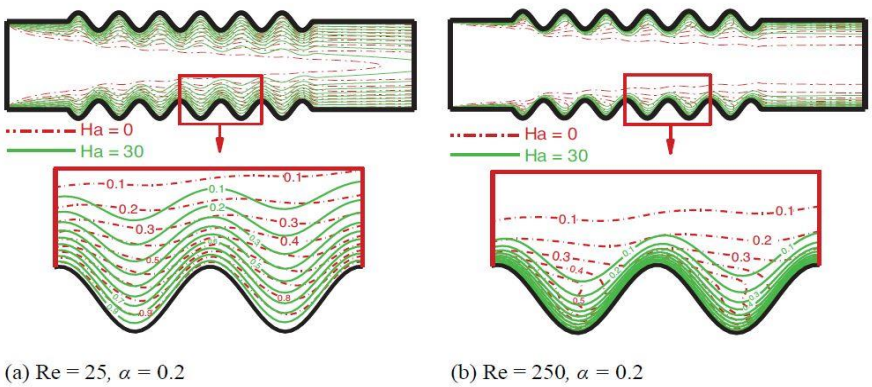

(a) Re = 25, α = 0.2 (b) Re = 250, α = 0.2

Figure 2.9. Non-dimensional isotherm lines for Hartmann numbers, *Ha*=0 and 30 at Reynolds numbers, a) *Re*=25 b) *Re*=250 (Heidary et al., 2017).

Larimi et al. (2016) studied hydro-thermal behaviors of a ferrofluid, with a mixture of water and Fe_3O_4, in a ribbed channel subjected to many non-uniform transverse magnetic fields going through current-carrying wires perpendicularly positioned in the flow and between ribs. They revealed that the applied non-uniform magnetic field is very effective on increasing the Nusselt number in the channel, moreover, the maximum and minimum local Nusselt numbers, Nu_L in the ribbed region enhances with the increase in the intensity of the non-uniform magnetic field. According to them, the non-uniform magnetic field causes the skin friction coefficient to be increased particularly in the situation in which all magnetic wires are positioned on only one side of the channel. Mousavi et al. (2016) numerically investigated the impact of the variable magnetic field on the ferrofluid flow in the sinusoidal two-tube heat exchanger. According to the obtained results, when the strength of the variable magnetic field enhances, the diffusion of the cold boundary layer elevates. Thus, heat transfer rate and Nusselt number, Nu_{avg} improves and this improvement grows at high Reynolds numbers, *Re*. Mehrez et al. (2015) carried out numerical research into the magnetic field effect on the entropy production and heat transfer characteristics of Cu-water nanofluid flow in an open cavity. This work has been performed for a broad variety of solid-particle volume fractions, $0 \leq \Phi \leq 0.06$, Hartmann numbers, $0 \leq Ha \leq 100$, Reynolds numbers, $10 \leq Re \leq 500$, and Richardson numbers, $0.001 \leq Ri \leq 1$ for three magnetic field inclination angles as Υ=0º, 45º and 90º. The findings demonstrate that flow characteristics, temperature distribution, entropy production, and heat transfer rate are profoundly influenced by the existence of the magnetic field. The average Nusselt number, $Nu_{avg,}$ and entropy production which grows by the increment in volume fraction of solid particles, Φ depends primarily on the Hartmann number, *Ha*, and magnetic field inclination angle, Υ. According to the authors, at a magnetic field inclination angle of Υ=45º, the recirculation bubble diminishes with increasing the Hartmann number, *Ha*. Furthermore, the average Nusselt number, $Nu_{avg,}$ and entropy production grow with increasing magnetic field intensity. Rashidi et al. (2016) carried out numerical work on the mixed convection heat transfer of Al_2O_3-water nanofluid flow in a vertical channel having sinusoidal walls. The

hydrothermal characteristics of Al_2O_3-water flow under a magnetic field are examined for Reynolds numbers within the range of $500 \leq Re \leq 1000$, Grasshof number, Gr in the range of $5\times10^4 \leq Gr \leq 10^{6,}$ and three different Hartmann numbers Ha=0, 5 and 10. The main observation from this study is that the mean Nusselt number, Nu_{avg} and Poiseuille number augment with growing the Hartmann number, Ha. Furthermore, obtained results demonstrate that the velocity profile in the channel becomes flatter, and the velocity gradient raises in the vicinity of the wall with a growing Hartmann number, Ha thus the vortices near the wall diminish. Figure 2.10 demonstrates the effect of the magnetic field on the streamline patterns for three Hartmann numbers, Ha=0,5 and 10 at Re=900 and Al_2O_3 nanoparticle volume fraction, Φ=4%. According to this figure, the vortices appear near the channel wall at Ha=0 while these vortices vanish and streamlines become regular by increasing the Hartmann number, Ha.

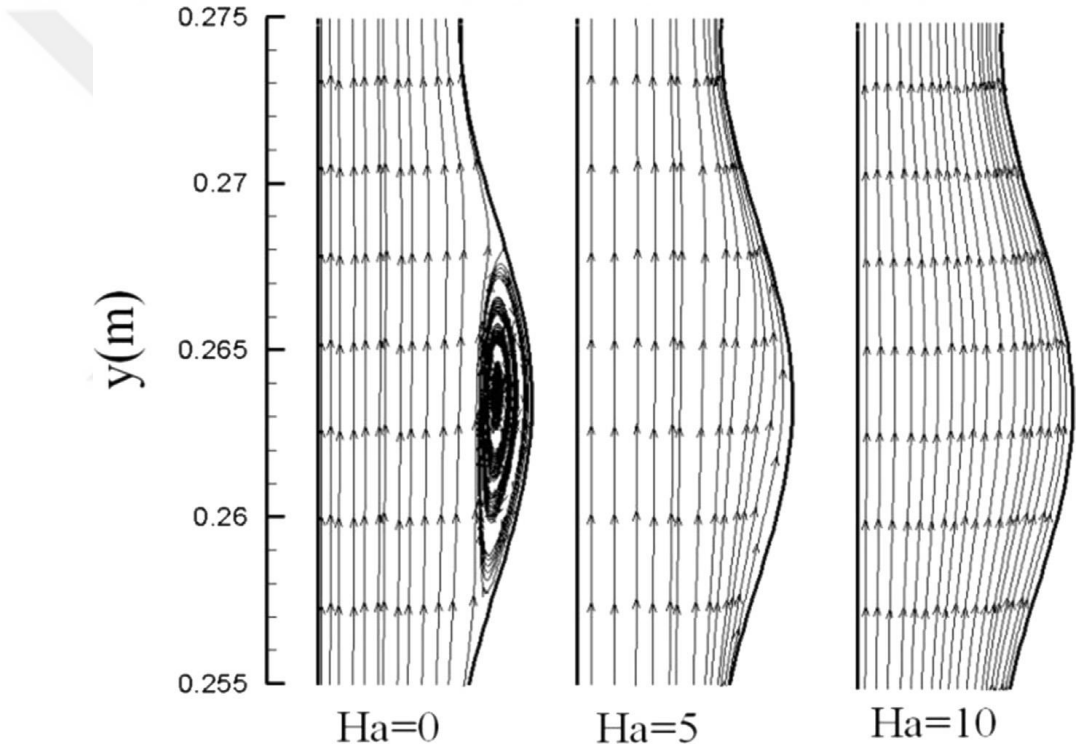

Figure 2.10 The effect of magnetic field on streamline patterns for three Hartmann numbers, Ha=0, 5, and 10 at Re=900 and Φ=4% (Rashidi et al., 2016).

Hussain et al. (2019) developed a numerical study to investigate the effect of the magnetic field on the ferrofluid flow and heat transfer rate in a channel with non-symmetric cavities. The simulations have been performed for governing parameters such as Reynolds numbers in the range of $1 \leq Re \leq 200$, Hartmann numbers in the range of $0 \leq Ha \leq 100$, the volume fractions of the solid particle, Φ in the range of $0 \leq \Phi \leq 0.15$, cavity aspect ratios in the range of $0.2 \leq h/H \leq 1$ and Richardson numbers in the range of $0.01 \leq Ri \leq 10$. They concluded that the heat transfer rate is

diminished when the magnetic field is applied with very high intensity. According to the presented results, the change in volume fraction of nano-sized solid particles, Φ causes little impact on the ferrofluid flow and heat transfer rate, particularly for the lower values of Richardson numbers, *Ri*. Selimefendigil and Oztop (2015) numerically studied the laminar forced convection of Cu-water flow on a backward-facing step at various magnetic field inclination angles, Υ. The hydrothermal characteristics of Cu-water flow under a magnetic field are examined for Reynolds numbers within the range of $20 \leq Re \leq 200$, Hartmann numbers in the range of $0 \leq Ha \leq 50$, and volume fractions of nano-sized solid particles between $0 \leq \Phi \leq 0.04$. According to the results of the article, the average heat transfer improves with increasing Reynolds number, *Re* and this improvement is more visible at greater values of magnetic field inclination angle, Υ. When the Hartmann number, *Ha* for horizontally oriented magnetic field and nanoparticle volume fraction, Φ increase, the local, Nu_L and the average Nusselt number, Nu_{avg} increment is observed. The finding shows that for the magnetic field in a vertical direction, the recirculation zone downstream of the step is suppressed when the magnetic field strength intensifies which ends up with heat transfer improvement. Furthermore, they reported that the entropy production rate gets higher with the increment in the Reynolds number, *Re* the volume fraction of solid particle, Φ, and decrement in the Hartmann number, *Ha* for the magnetic field in a horizontal direction. Figure 2.11 displays the entropy generation ratio with the Hartmann number, *Ha* for various magnetic field inclination angles, Υ. One can observe from this figure that the total entropy generation ratio attenuates for the horizontally oriented magnetic field, Υ=0º which can be attributed to the suppression of convection and slowing down the fluid motion with growing *Ha* values. For the magnetic field inclination angles, Υ=45º and 90º, the entropy generation ratio get higher with increasing *Ha* values.

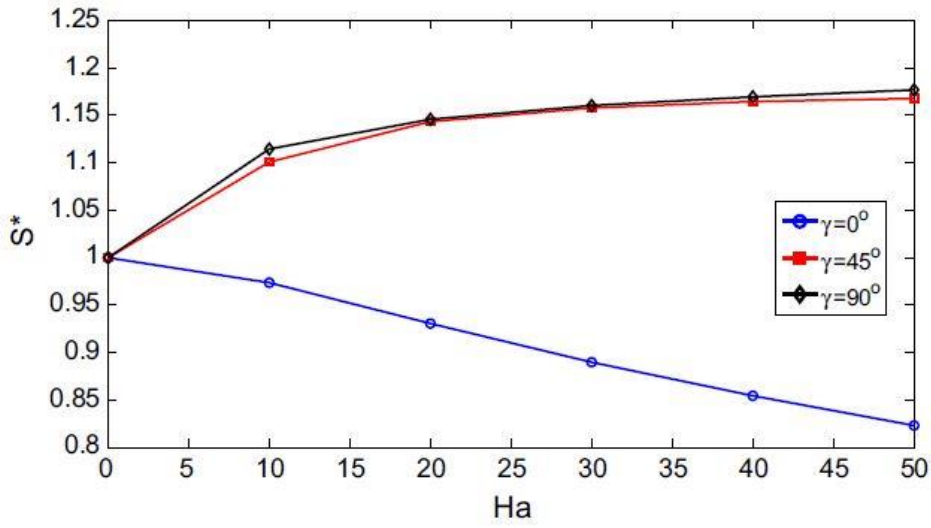

Figure 2.11. The entropy generation ratio with Hartmann number, Ha for various magnetic field inclination angles, Υ (Selimefendigil and Oztop, 2015).

According to Gurdal et al. (2022), the maximum heat transfer improvement was observed for a greater volume fraction of nanoparticles, Φ greater strength of magnetic field intensity, *Ha*, and complicated geometries for the flow in the channel. They stated that the maximum heat transfer augmentation is acquired for the MWCNT-water nanofluid flow with a percentage between 70% and 190%. When the Hartmann number is set to Ha=30 in the Cu-water nanofluid flow, a thermal recovery of 76% is obtained. Ali et al. (2020) conducted research into the effect of the magnetic field on the natural convection in a grooved enclosure including CuO-water nanofluid. They employed the Galerkin finite element technique to resolve governing equations. The simulation is performed for a broad range of parameters such as magnetic field intensity, $10 \leq Ha \leq 100$, the volume fraction of nano-sized solid particles, $0 \leq \Phi \leq 0.05$, and Rayleigh number, $10^3 \leq Ra \leq 10^6$. According to the results of numerical simulation, the average Nusselt number, Nu_{avg} and entropy production grow with increasing Rayleigh numbers, *Ra*, and volume fraction of solid particles, Φ while they attenuate with rising the Hartmann number, *Ha*. Furthermore, the findings show that the proper integration of governing parameters can provide maximum heat transfer efficiency and minimum entropy production. Shaker et al. (2021) developed a numerical study to investigate the influence of the magnetic field on mixed convection heat transfer of a Fe_3O_4-water ferrofluid flow in an open cavity. In this study, the impact of changing different parameters such as Reynolds numbers in the range of $20 \leq Re \leq 600$, magnetic numbers in the range of $0 \leq Mn \leq 5 \times 10^7$ and the location of current carrying wires on the flow structure and the average Nusselt number, Nu_{avg} have been explored. They found out that the applied non-uniform magnetic field alters the flow characteristics and formed new vortices in the ferrofluid flow because of the impact of the Kelvin force. According to the authors, while the average Nusselt number, Nu_{avg} reduces with poor magnetic field strength up to $Mn = 5 \times 10^6$, it substantially augments with the increment in magnetic field strength further. The maximum improvement in the average Nusselt numbers, Nu_{avg} was acquired by 57.07% with the application of the non-uniform magnetic field. In the investigation of Ma et al. (2019), a two-dimensional numerical study is represented to investigate the influence of magnetic field on the convection heat transfer of Ag-MgO/water hybrid nanofluid in a channel including active heaters and coolers. They systematically examine the impacts of different thermal arrangements, *Case 1, 2 and 3* Reynolds numbers in the range of $50 \leq Re \leq 100$, block side lengths in the range of $0.3 \leq h \leq 0.5$ and volume fractions of solid particles in the range of $0 \leq \Phi \leq 0.02$ on the flow characteristics and heat transfer performance. According to acquired outcomes, the maximum value of the local Nusselt number, Nu_L takes place on the junction of the heater and cooler because of the great temperature gradient. Furthermore, they stated that the heat transfer rate is greater at the sharp corner of the heater than that of the sharp corner of the cooler. Their computational results demonstrated that the average Nusselt number, Nu_{avg} or heat transfer rate augments with the increment in the volume fraction of nanoparticles, Φ, and the decrement in the Hartmann number, *Ha*. According to the presented results, when the Hartmann number enhances from Ha=0 to Ha=20

the flow structure alters slowly and the intensity of vorticities diminishes. But when the Hartmann number augments from Ha=20 to Ha=40, the flow structure remarkably alters and the form of vorticities varies from triangular to trapezoidal. Gibanov et al. (2017) numerically investigated the influence of the variable magnetic field on the mixed convection of Fe_3O_4-water ferrofluid flow in a lid-driven cavity. In this study, numerical simulations have been performed for a broad range of magnetic numbers, volume fractions of nanoparticle, Φ and Hartmann number, Ha. According to the authors, the increment in the magnetic number makes the heat transfer rate to be augmented. They revealed that the increasing magnetic number grows the major circulation rate with more main streamlines distortion.

Mousavi et al. (2019) conducted a 3D numerical investigation about the influences of a non-uniform magnetic field on hydrothermal characteristics of Fe_3O_4-water ferrofluid flow in a wavy channel. According to the results of the numerical simulation, the effect of the non-uniform magnetic field on the hydrothermal characteristics in the channel with wavy walls is higher than in the channel with straight walls. They attributed this situation to the diminishing of recirculation bubbles in the sinusoidal cavities of wavy walls by the applied magnetic field. The increment in the magnetic gradient value from 0 to 1.5×10^5 grows the skin friction factors on the bottom and top wavy walls with factors of 1.6 and 11, respectively. Furthermore, the variation in the Nusselt number, Nu on the bottom and top walls reduce by rising the magnetic gradient value. Selimefendigil and Oztop (2019) employed the Galerkin weighted residual finite element technique to investigate the forced convection of pulsating CuO-water nanofluid flow on corrugated parallel plate with the existence of the inclined magnetic field. In this investigation, effects of Reynolds numbers in the range of $100\leq Re\leq500$, Hartmann numbers in the range of $0\leq Ha\leq15$, inclination angles of the magnetic field, Υ between 0º and 90º, corrugation wave number between 1 and 12, corrugation wave height between 0.05h and 0.35h, the volume fraction of CuO particles, Φ between 0 and 0.04, amplitudes of flow pulsation between 0 and 0.9 and Strouhal numbers, St between 0.25 and 2 on the forced convection heat transfer have been examined. Their computational results demonstrated that the magnetic field causes the redistribution of vortices between heated blocks of the corrugated plate and augments the heat transfer rate in time-independent flow as well as pulsating flow. They revealed that when the magnetic field intensity gets higher, the fluid flow slows down and also the size of recirculation bubbles between hot blocks weakens. The average Nusselt number, Nu_{avg} enhances when the Hartmann number, Ha increases for nanofluids at various volume fractions, Φ due to the suppression of vortices between heated blocks. Obtained results demonstrated that the flow symmetry and thermal structures in the channel alter with the magnetic field inclination angle, Υ. The average Nusselt number, Nu_{avg} augments by 25% as the inclination angles of the magnetic field, Υ increases from 0º to 90º. In the investigation of Hussain et al. (2019), the time-dependent MHD forced convection of Fe_3O_4-water ferrofluid

flow in the backward-facing step benchmark has been studied. In this work, broad ranges of governing parameters are reported such as Reynolds numbers in the range of $10 \leq Re \leq 200$, Hartmann number in the range of $0 \leq Ha \leq 100$, the angular velocities of a rotating cylinder in the range of $-75 \leq \Omega \leq 75$, the inclination angles of the magnetic field, Υ between 0º and 90º and volume fractions of Fe_3O_4 particles in the base fluid within the range of $0 \leq \Phi \leq 0.15$. According to the results of the article, the magnetic force reduces the motion of the ferrofluid flow, however, the drag coefficient, C_D grows with applied magnetic forces. The average Nusselt number, Nu_{avg} deteriorates by 53.12% when Hartmann numbers increase from Ha=0 to Ha=100. The findings demonstrated that the heat transfer rate is improved when the inclination angles of the magnetic field, Υ increases from 0º to 90º progressively. Aminfar et al. (2013) conducted numerical research on the impact of the nonuniform magnetic field of hydrothermal characteristics of a Fe_3O_4-water ferrofluid in a corrugated channel. Obtained results show that the applied magnetic field with a negative gradient enhances heat transfer performance and coefficient together with reducing wall temperature. According to the authors, the recirculation region in corrugations disappears with the applied non-uniform magnetic field. Their computational results revealed that the non-uniform magnetic field enhances the flow velocity near the wall of the channel and this situation leads to an increase in the heat transfer coefficient. Furthermore, applying a negative gradient magnetic field grows the local friction factor. Because magnetic field induced flattened velocity profile causes a rise in velocity gradient in the vicinity of walls and thus improvement in the friction factor and heat transfer coefficient. The influence of applying a magnetic field on the streamwise velocity component is demonstrated in Figure 2.12 at Re=100. According to this figure, the applying magnetic field disappears recirculation zones in corrugated surfaces thus the main flow penetrates the corrugated cavities so the flow rate increases in the vicinity of corrugated walls. The other conclusion that can be drawn from Figure 2.12 is that the streamwise velocity in the center of the corrugated channel attenuates with the applied magnetic field due to the effect of the Kelvin force.

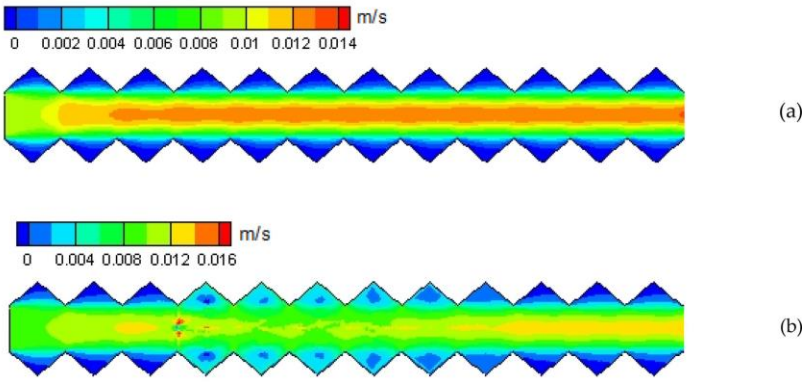

Figure 2.12. The distribution of streamwise velocity component in the corrugated channel for the cases of a) without the magnetic field b) with the magnetic field (Aminfar et al., 2013).

2.3.1. Significance and Novelty of Current Study

Based on the literature survey above and to the best of the authors' knowledge, although it is possible to find a few studies about the magnetic field effect on hydrothermal characteristics in the sinusoidal and trapezoidal corrugated channels, the research on the influences of the magnetic field on the hydrothermal characteristics of the rectangular grooved channel has not been previously published. Furthermore, considering the importance of entropy generation in industrial and engineering applications, this study includes the magnetic field effect on the entropy generation of CuO-water nanofluid flow in the rectangular grooved channel, unlike the existing studies of magnetic field effect on the sinusoidal and trapezoidal corrugated channels. The aim of the current study is to investigate the effect of the uniform magnetic field on the hydrodynamic, thermal, and entropy generation characteristics of a CuO-water nanofluid flow in the rectangular grooved channel. In this context, the effects of the Hartmann number, *Ha* Reynolds number, *Re* and volume fraction of nanoparticle, Φ are discussed.

3. MATERIALS AND METHODS

3.1. Materials and Methods for the Effect of Non-Uniform Magnetic Field on Hydrothermal and Entropy Generation Characteristics of Ferrofluid Flow Around a Confined Cylinder Using Wire Magnetic Sources

3.1.1. Problem Definition and Governing Equations

The problem domain consists of a straight channel and a heated cylinder which is positioned at 12*D* and 18*D* away from the channel inlet and channel outlet, respectively as shown in Figure 3.1. The cylinder is on the central axis of the channel and its diameter is three-tenths of the channel height (i.e. blockage ratio, *BR* = *D/H* = 0.3). Constant wall temperature, θ_h = 1 which is higher than inlet flow temperature, θ_c =0 defined for cylinder however, channel walls are adiabatic. Moreover, a no-slip condition is available for all solid surfaces (u = v = 0). The parabolic velocity profile that is defined by, $u = 6BRy\,(1 - BRy)$ imposed at the channel inlet and pressure at the channel outlet is equal to zero, P = 0.

The schematic representation of the flow domain is demonstrated in Figure 3.1 in which the flow is considered from left to right and φ=180º is taken as the front stagnation point, *F* whereas φ=0º is regarded as the rear stagnation point, *A*. On the other hand, *E* presents the reattachment point while *S* and *P* are the separation points. φ is the angle measured from the rear stagnation point, *A* thus L_s and φ_s define the separation length and separation angle respectively.

The influence of the magnetic field produced by the two wires on the flow is defined by the mathematical expressions (Equations 3.1-3.5) used in the study of Sheikholeslamia and Vajravelu (2017). These expressions allow calculating the influence of magnetic force on the flow as a momentum source which is radially distributed with a decrease in intensity with distance from the epicenter. Variables *a* and *b* in equations represent the *x* and *y* coordinates of the magnetic source epicenters, respectively. The *x* coordinate of each source is the same and it is equal to 13.667*D*. However, the *y* coordinate of the source located near the top wall is 3.667*D* and it is equal to 0.333*D* for the one near the bottom wall. The effect of Joule heating due to magnetic field is not considered in simulations. The constituents of the intensity of the magnetic field, $\overline{H_x}, \overline{H_{xx}}$ and $\overline{H_y}, \overline{H_{yy}}$, the magnetic field strength, $\bar{H}$ and the magnetic field strength at the source (wire), γ are regarded in the subsequent form;

$$\overline{H_x} = \frac{\gamma}{2\pi}\frac{1}{(x-\overline{a_1})^2 + \left(y-\overline{b_1}\right)^2}\left(y-\overline{b_1}\right) \tag{3.1}$$

$$\overline{H_y} = \frac{-\gamma}{2\pi}\frac{1}{(x-\overline{a_1})^2+\left(y-\overline{b_1}\right)^2}(x-\overline{a_1}) \tag{3.2}$$

$$\overline{H_{xx}} = \frac{\gamma}{2\pi}\frac{1}{(x-\overline{a_2})^2+\left(y-\overline{b_2}\right)^2}\left(y-\overline{b_2}\right) \tag{3.3}$$

$$\overline{H_{yy}} = \frac{-\gamma}{2\pi}\frac{1}{(x-\overline{a_2})^2+\left(y-\overline{b_2}\right)^2}(x-\overline{a_2}) \tag{3.4}$$

$$\bar{H} = \sqrt{\bar{H}_x^2+\bar{H}_y^2} = \frac{\gamma}{2\pi}\frac{1}{\sqrt{(x-\bar{a})^2+\left(x-\bar{b}\right)^2}} \tag{3.5}$$

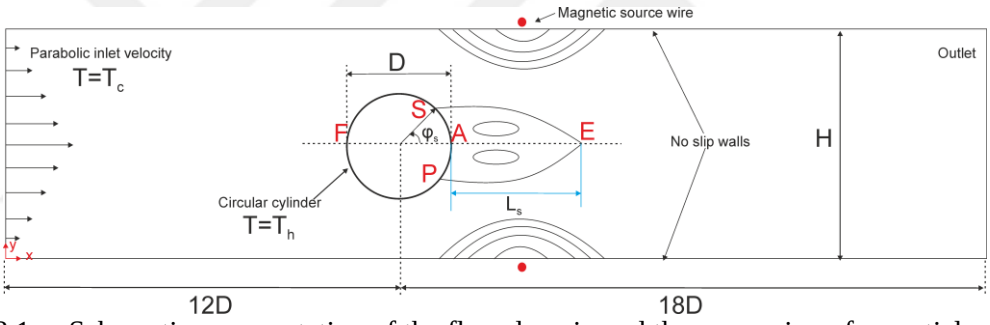

Figure 3.1. Schematic representation of the flow domain and the expression of essential geometry and flow parameters

The flow in the domain is considered laminar and two-dimensional, thermo physical properties of the working fluid are considered constant and the effect of radiation is neglected. Under these conditions the continuity, x-momentum, y-momentum, and energy equations that govern the problem can be respectively demonstrated in the following forms:

$$\frac{\partial \bar{u}}{\partial \bar{x}} + \frac{\partial \bar{v}}{\partial \bar{y}} = 0 \tag{3.6}$$

$$\rho_{nf}\frac{\partial \bar{u}}{\partial \bar{t}} + \rho_{nf}\left(\bar{u}\frac{\partial \bar{u}}{\partial \bar{x}} + \bar{v}\frac{\partial \bar{u}}{\partial \bar{y}}\right) = \frac{-\partial \bar{p}}{\partial \bar{x}} + \mu_{nf}\left(\frac{\partial^2 \bar{u}}{\partial \bar{x}^2} + \frac{\partial^2 \bar{u}}{\partial \bar{y}^2}\right) - \sigma_{nf}\left(\left[B_y^2 + B_{yy}^2\right]\bar{u} - \left[B_x B_y + B_{xx}B_{yy}\right]\bar{v}\right) \tag{3.7}$$

$$\rho_{nf}\frac{\partial \bar{v}}{\partial \bar{t}}+\rho_{nf}\left(\bar{u}\frac{\partial \bar{v}}{\partial \bar{x}}+\bar{v}\frac{\partial \bar{v}}{\partial \bar{y}}\right)=\frac{-\partial \bar{p}}{\partial \bar{x}}+\mu_{nf}\left(\frac{\partial^2 \bar{v}}{\partial \bar{x}^2}+\frac{\partial^2 \bar{v}}{\partial \bar{y}^2}\right)-\sigma_{nf}\left([B_x^2+B_{xx}^2]\bar{v}-\left[B_xB_y+B_{xx}B_{yy}\right]\bar{u}\right) \quad (3.8)$$

$$(\rho Cp)_{nf}\frac{\partial T}{\partial \bar{t}}+(\rho Cp)_{nf}\left(\bar{u}\frac{\partial T}{\partial \bar{x}}+\bar{v}\frac{\partial T}{\partial \bar{y}}\right)=k_{nf}\left(\frac{\partial^2 T}{\partial \bar{x}^2}+\frac{\partial^2 T}{\partial \bar{y}^2}\right) \quad (3.9)$$

In Equations 3.7 and 3.8, the terms of $-\sigma_{nf}\left(\left[B_y^2+B_{yy}^2\right]\bar{u}-\left[B_xB_y+B_{xx}B_{yy}\right]\bar{v}\right)$ and $-\sigma_{nf}\left([B_x^2+B_{xx}^2]\bar{v}-\left[B_xB_y+B_{xx}B_{yy}\right]\bar{u}\right)$, respectively present the Lorentz force per unit volume towards *x* and *y* directions and appear because of the electrical conductivity of the fluid. These two terms are familiar in MHD flow applications.

The equations above are normalized using the following expressions:

$$x=\frac{\bar{x}}{D}, y=\frac{\bar{y}}{D}, u=\frac{\bar{u}}{u_i}, v=\frac{\bar{v}}{u_i}, t=\frac{\bar{t}u_i}{D}, \theta=\frac{T-T_c}{T_h-T_c}, p=\frac{\bar{p}}{\rho_{bf}\,u_i^2}, Pr=\frac{\upsilon_{bf}}{\alpha_{bf}},$$

$$Ha=D\mu_0H_0\sqrt{\frac{\sigma_{bf}}{\mu_{bf}}}, Re=\frac{\rho_{bf}u_iD}{\mu_{bf}}, \left(H,H_x,H_y,H_{xx},H_{yy},\right)=\frac{\left(\bar{H},\bar{H}_x,\bar{H}_y,\bar{H}_{xx},\bar{H}_{yy}\right)}{H_0},$$

$$H_0=\bar{H}(\bar{a},0)=\frac{\gamma}{2\pi|b|}, B_x=\mu_0\bar{H}_x, B_y=\mu_0\bar{H}_y, B_{xx}=\mu_0\bar{H}_{xx}, B_{yy}=\mu_0\bar{H}_{yy} \quad (3.10)$$

In the above equations, while μ_0 denotes the magnetic permeability, B_x, B_y, B_{xx} and B_{yy} are the magnetic inductions.

Normalized forms of governing equations are as subsequent;

$$\frac{\partial u}{\partial x}+\frac{\partial v}{\partial y}=0 \quad (3.11)$$

$$\frac{\partial u}{\partial t}+u\frac{\partial u}{\partial x}+v\frac{\partial u}{\partial y}=-\left(\frac{\rho_{bf}}{\rho_{nf}}\right)\frac{\partial p}{\partial x}+\left(\frac{\upsilon_{nf}}{\upsilon_{bf}}\right)\frac{1}{Re}\left(\frac{\partial^2 u}{\partial x^2}+\frac{\partial^2 u}{\partial y^2}\right)-\left(\frac{\sigma_{nf}}{\sigma_{bf}}\right)\left(\frac{\rho_{bf}}{\rho_{nf}}\right)Ha^2\frac{1}{Re}\left(\left[H_y^2+H_{yy}^2\right]u-\left[H_xH_y+H_{xx}H_{yy}\right]v\right) \quad (3.12)$$

$$\frac{\partial v}{\partial t}+u\frac{\partial v}{\partial x}+v\frac{\partial v}{\partial y}=-\left(\frac{\rho_{bf}}{\rho_{nf}}\right)\frac{\partial p}{\partial y}+\left(\frac{\upsilon_{nf}}{\upsilon_{bf}}\right)\frac{1}{Re}\left(\frac{\partial^2 v}{\partial x^2}+\frac{\partial^2 v}{\partial y^2}\right)-\left(\frac{\sigma_{nf}}{\sigma_{bf}}\right)\left(\frac{\rho_f}{\rho_{nf}}\right)Ha^2\frac{1}{Re}\left([H_x^2+H_{xx}^2]v-\left[H_xH_y+H_{xx}H_{yy}\right]u\right) \quad (3.13)$$

$$\frac{\partial \theta}{\partial t} + u\frac{\partial \theta}{\partial x} + v\frac{\partial \theta}{\partial y} = \left(\frac{\alpha_{nf}}{\alpha_{bf}}\right)\frac{1}{Re\ Pr}\left(\frac{^2\theta}{x^2} + \frac{^2\theta}{y^2}\right) \quad (3.14)$$

In this study, the physical quantity of interest is given by the Nusselt number. This number quantifies the heat transport that takes place between the hot circular cylinder and the working fluid via the cylinder. The local Nusselt number, Nu_L around the heated cylinder is determined in Equation 3.15 as:

$$Nu_L = -\left(\frac{k_{nf}}{k_{bf}}\right)\frac{\partial \theta}{\partial n}\Big|_w \quad (3.15)$$

where n and w indicate the direction perpendicular to the wall and the overall length of the wall cylinder, respectively.

The average Nusselt number, Nu_{avg} is computed by integrating Equation 3.16:

$$Nu_{avg} = \frac{1}{w}\int_0^w Nu_L\, dW \quad (3.16)$$

The total drag coefficient, C_D is calculated by the subsequent Equation 3.17 as:

$$C_D = C_{DP} + C_{DV} = \frac{2F_D}{\rho u^2 D} \quad (3.17)$$

in which C_{DP} and C_{DV} indicate the drag coefficients caused by pressure and viscous forces, respectively, F_D is the drag force acting over the surface of the cylinder. The total drag coefficient, C_D caused by the pressure and viscous forces can be acquired from Equations 3.18 and 3.19:

$$C_{DP} = 2\int_0^1 (p_f - p_r)d_y \quad (3.18)$$

$$C_{DV} = \frac{2}{Re}\int_0^1 \left[\left\{\left(\frac{\partial u}{\partial y}\right)_t + \left(\frac{\partial u}{\partial y}\right)_b\right\}dx + \left\{\left(\frac{\partial u}{\partial x}\right)_f + \left(\frac{\partial u}{\partial x}\right)_r\right\}dy\right] \quad (3.19)$$

The subscripts *f*, *r*, *b* and *t* present the front, rear, bottom, and top surfaces of the cylinder.

Pure water and ferrofluid (Fe_3O_4-water) are used as the working fluid and the effect of two different volume fractions (2% and 4%) are investigated in ferrofluid cases. Ferrofluid is modeled as a single phase, it's thermophysical properties are considered constant and they are calculated as follows:

The density and specific heat of the ferrofluid are given in Equations 3.20 and 3.21, respectively as (Ali et al., 2020):

$$\rho_{nf} = (1 - \Phi)\rho_{bf} + \Phi\rho_{np} \quad (3.20)$$

$$\left(\rho C_p\right)_{nf} = (1-\Phi)\left(\rho C_p\right)_{bf} + \Phi\left(\rho C_p\right)_{np} \quad (3.21)$$

In Equations 3.22 and 3.23, the thermal expansion coefficient and dynamic viscosity of the ferrofluid are expressed as (Selimefendigil and Oztop, 2020):

$$(\rho\beta)_{nf} = (1-\Phi)(\rho\beta)_{bf} + \Phi(\rho\beta)_{np} \quad (3.22)$$

$$\mu_{nf} = \frac{\mu_{bf}}{(1-\Phi)^{2.5}} \quad (3.23)$$

where the subscripts *nf*, *bf*, and *np* represent the nanofluid, base fluid and nanoparticle, respectively.

The thermal conductivity and electrical conductivity of the ferrofluid are mathematically denoted in Equations 3.24 and 3.25 (Kefayati, 2016):

$$\frac{k_{nf}}{k_{bf}} = \frac{(k_{np}+2k_{bf})-2\Phi(k_{bf}-k_{np})}{(k_{np}+2k_{bf})+\Phi(k_{bf}-k_{np})} \quad (3.24)$$

$$\sigma_{nf} = \sigma_{bf}\left(1+\frac{3(\sigma_{np}/\sigma_{bf}-1)\Phi}{(\sigma_{np}/\sigma_{bf}+2)-(\sigma_{np}/\sigma_{bf}-1)\Phi}\right) \quad (3.25)$$

The thermophysical properties of the nanoparticle and pure water are given in Table 3.1.

Table 3.1. Thermophysical properties of pure water and nanoparticles.

	ρ (kg/m^3)	C_p (J/kgK)	k (W/mK)	β (1/K)
Pure Water	998.2	4182	0.6	2.1×10^{-4}
Fe_3O_4	5200	670	6	1.3×10^{-5}

3.1.2. Solution Method

Ansys Fluent 20 (Academic Version) is employed to simulate heat transfer, fluid flow, and entropy production. Momentum source terms in Equations 3.7 and 3.8 which represent the influence of the non-uniform magnetic field are included in the simulations by using the User Defined Functions (UDF) ability of the software. SIMPLE scheme is utilized for pressure velocity coupling and the second order scheme is chosen for interpolation of pressure at cell faces from the cell center value. Moreover, the second-order upwind method is employed for the discretization of convective terms, and temporal discretization is done by the second-order implicit model. The convergence criteria is 10^{-6} for continuity and momentum equations, while it is equal to 10^{-8} for the

energy equation. Additionally, the time step size is used as 0.001 *s* corresponding to the Courant number, *Cr*=0.015 which satisfies the Courant-Lewy-Friedrich (CFL) condition in the smallest cell of the mesh at every time step. The time step size independence has been performed at the largest Reynolds number studied, *Re*=150 before determining the time step size. Various time step sizes have been employed at a constant number of time steps. Afterward, the time step size in which the drag coefficient, $C_{D,}$ and the average Nusselt number, Nu_{avg} do not change is determined, and then it is checked whether this time size satisfies the CFL condition. After it is observed that the CFL condition is met, the same time step size is used in all simulations. On the other hand, in this study, the number of the time step is not constant during simulations. The simulations are continued until the flow is time-periodic, i.e., the amplitude of fluctuations in the drag coefficient, $C_{D,}$ and average Nusselt number, Nu_{avg} becomes constant.

Computational mesh for the flow simulation on a confined cylinder and comprehensive mesh distribution in the close region of the cylinder and channel wall is demonstrated in Figure 3.2. As seen in this Figure, the mesh density is higher near the cylinder and channel wall. Number of elements given in Table 3.2 is tested for mesh independence study and it is seen that 63936 elements provide the best result in terms of computational cost-accuracy balance.

Table 3.2. Results of mesh independence study for *Re* = 100, *BR*= 0.3 and φ = 0.

Element Number	Nusselt Number, Nu_{avg}	Drag Coefficient, C_D
16302	6.5000	3.7120
28416	6.4826	3.1659
63936	6.4701	3.1318
87024	6.4698	3.1295

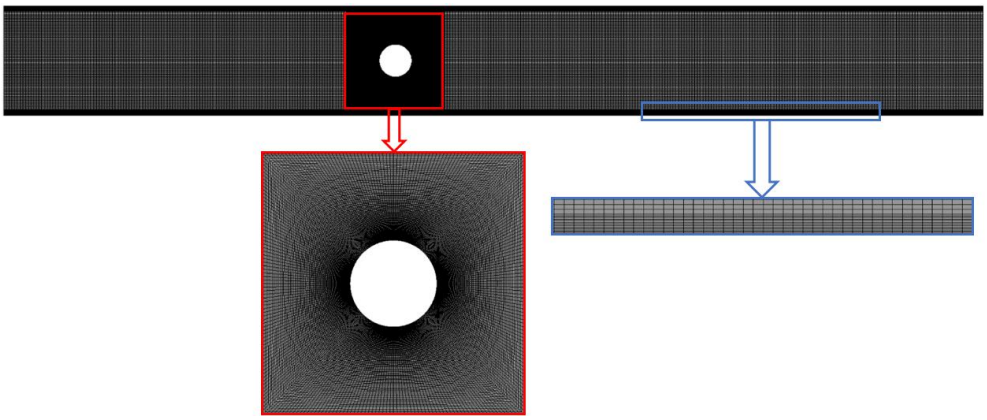

Figure 3.2. Mesh generation for the numerical analysis of fluid flow on a confined cylinder and comprehensive mesh distribution in the close region of the channel wall

The solution procedure presented above is validated by applying it to another heat transfer from a confined cylinder problem which is investigated by Prasad et al. (2011). Two blockage ratios BR = 0.1 and BR = 0.3 are tested and the results are presented in Table 3.3. As the results given in the table indicate the procedure employed in the current study is appropriate to simulate such problem. Moreover, the method used for the simulation of the magnetic field is also validated by testing it on the case presented by Sheikholeslamia and Vajravelu (2017) at Ha=10. The results of this second validation study are shown in Figure 3.3.

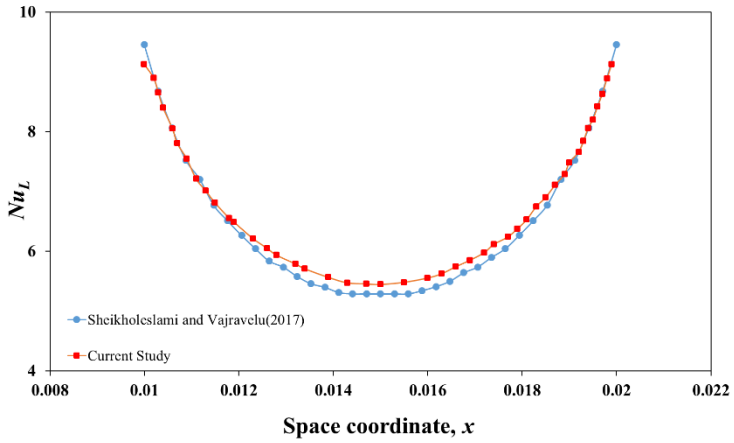

Figure 3.3. The comparison of the local Nusselt number, Nu_L in the case of non-uniform magnetic field application between present results and numerical results of Sheikholeslamia and Vajravelu (2017) at the Rayleigh number, Ra=10^5, and Prandtl number, Pr=6.2 for Ha=10 and nanofluid volume fraction, Φ=4%.

Table 3.3. Results of validation study for the confined cylinder problem.

		Current Study		Prasad et al. (2011)	
		Nu_{avg}	C_D	Nu_{avg}	C_D
BR= 0.1	*Re* = 40	3.88	2.93	3.89	3.03
	Re = 70	5.21	2.85	5.09	2.83
	Re = 100	6.29	2.82	6.25	2.75
BR= 0.3	*Re* = 40	4.24	4.36	4.35	4.35
	Re = 70	5.38	3.47	5.29	3.48
	Re = 100	6.47	3.13	6.46	3.12

3.1.3. Entropy Production

Estimating the production (or generation) of entropy is a promising way for optimizing the thermal performance of engineering systems. All irreversible processes produce entropy. Therefore, estimating the amount of entropy defines the thermal capacity during these processes. For the considered physical problem, the production of entropy within the forced convection flow occurs mainly due to the impacts of thermal transmission and fluid friction. In addition, due to the presence of wire magnetic sources, the production of entropy due to the impact of a magnetic field was also taken into account. The local total entropy generation due to these impacts in dimensional form is expressed in Equation 3.26 as follows:

$$\bar{S}_L = \bar{S}_{L,th} + \bar{S}_{L,fr} + \bar{S}_{L,mag} = \frac{k_{nf}}{T_o^2}\left[\left(\frac{\partial T}{\partial \bar{x}}\right)^2 + \left(\frac{\partial T}{\partial \bar{y}}\right)^2\right] + \frac{\mu_{nf}}{T_o}\left[2\left(\frac{\partial \bar{u}}{\partial \bar{x}}\right)^2 + 2\left(\frac{\partial \bar{v}}{\partial \bar{y}}\right)^2 + \left(\frac{\partial \bar{u}}{\partial \bar{y}} + \frac{\partial \bar{v}}{\partial \bar{x}}\right)^2\right] + \frac{\sigma_{nf}}{T_o}\left(\left[B_y\bar{u} - B_x\bar{v}\right]^2 + \left[B_{yy}\bar{u} - B_{xx}\bar{v}\right]^2\right) \quad (3.26)$$

where $T_o = \frac{T_h + T_c}{2}$

On the right side of Equation 3.26, the first, second, and third terms refer to the irreversibility of thermal transmission, fluid friction, and magnetic field, respectively.

By using the group of dimensionless parameters in Equation 3.10, the non-dimensional form of the local total entropy generation is expressed in Equation 3.27 as follows:

$$s_L = s_{L,th} + s_{L,fr} + s_{L,mag} = \left[\left(\frac{\partial \theta}{\partial x}\right)^2 + \left(\frac{\partial \theta}{\partial y}\right)^2\right] + \left(\frac{\mu_{nf}}{\mu_{bf}}\right)\left(\frac{k_f}{k_{nf}}\right)\chi\left[2\left(\frac{\partial u}{\partial x}\right)^2 + 2\left(\frac{\partial v}{\partial y}\right)^2 + \left(\frac{\partial u}{\partial y} + \frac{\partial v}{\partial x}\right)^2\right] + \left(\frac{\sigma_{nf}}{\sigma_{bf}}\right)\left(\frac{k_f}{k_{nf}}\right)Ha^2\chi\left(\left[H_y u - H_x v\right]^2 + \left[H_{yy}u - H_{xx}v\right]^2\right) \quad (3.27)$$

In Equation 3.28, χ refers to the irreversibility factor, which is the following expression:

$$\chi = \frac{\mu_{bf} T_o}{k_{bf}} \left(\frac{u_i}{\Delta T}\right)^2 \tag{3.28}$$

The average value of the total entropy generation through the studied channel is obtained by integrating Equation 3.29 over the whole flow range:

$$s_{avg} = \frac{\int_A s_L dxdy}{A} \tag{3.29}$$

In addition, the Bejan number defines the impact of thermal entropy on total entropy. The local and average expressions of this number are given in Equations 3.30 and 3.31 as:

$$Be_L = \frac{s_{L,th}}{s_L} \tag{3.30}$$

$$Be_{avg} = \frac{\int_A s_{L,th} dxdy}{\int_A s_L dxdy} \tag{3.31}$$

Furthermore, the criterion of thermal performance, ξ represents the ratio of the average value of the total entropy generation to the average value of the Nusselt number, Nu_{avg}. For the current case study, this criterion is applied to illustrate the thermal characteristics within the considered channel, this gives the percentage of the process with lower reversibility to a higher rate of thermal transmission. Accordingly, it is given in Equation 3.32 as follow:

$$\xi = \frac{s_{avg}}{Nu_{avg}} \tag{3.32}$$

3.2. Materials and Methods for the Effect of Uniform Magnetic Field on Hydrothermal and Entropy Generation Characteristics of Nanofluid Flow in a Rectangular Grooved Channel

3.2.1. Problem Definition and Governing Equations

This study numerically investigates heat transfer and fluid flow through grooved channels under the presence of a uniform magnetic field. The problem domain comprises a channel with a phase angle of 180º having rectangular grooved upper and lower walls as demonstrated in Figure 3.4. The grooved section of the channel includes seven grooves and there are straight sections with 150 mm upstream and 250 mm downstream of it. The height of the channel is equal to H=16 mm. The aspect ratio which is the ratio of the groove depth, l to the channel height, H is used as l/H=0.4.The length of the grooved section is equal to L_g=60 mm and the ratio of the grooved section length, L_g to the straight section length, L_s is used as L_g/L_s=1. Copper oxide (CuO)-water nanofluid is considered as a coolant and its thermophysical properties of it are assumed to be independent of temperature change. The flow is assumed as two-dimensional, additionally, since

the Reynolds number is in the range of 250≤*Re*≤1250, it is accepted as laminar. Equations that govern the problem are given as follows;

Continuity

(3.33)

$$\frac{\partial \bar{u}}{\partial \bar{x}} + \frac{\partial \bar{v}}{\partial \bar{y}} = 0$$

X-momentum

$$\rho_{nf}\left(\frac{\partial \bar{u}}{\partial \bar{t}} + \bar{u}\frac{\partial \bar{u}}{\partial \bar{x}} + \bar{v}\frac{\partial \bar{u}}{\partial \bar{y}}\right) = \frac{-\partial \bar{p}}{\partial \bar{x}} + \mu_{nf}\left(\frac{\partial^2 \bar{u}}{\partial \bar{x}^2} + \frac{\partial^2 \bar{u}}{\partial \bar{y}^2}\right) - \sigma_{nf}B_0^2\,\bar{u} \quad (3.34)$$

Y-momentum

(3.35)

$$\rho_{nf}\left(\frac{\partial \bar{v}}{\partial \bar{t}} + \bar{u}\frac{\partial \bar{v}}{\partial \bar{x}} + \bar{v}\frac{\partial \bar{v}}{\partial \bar{y}}\right) = \frac{-\partial \bar{p}}{\partial \bar{y}} + \mu_{nf}\left(\frac{\partial^2 \bar{v}}{\partial \bar{x}^2} + \frac{\partial^2 \bar{v}}{\partial \bar{y}^2}\right)$$

Energy

$$(\rho Cp\,)_{nf}\left(\frac{\partial T}{\partial \bar{t}} + \bar{u}\frac{\partial T}{\partial \bar{x}} + \bar{v}\frac{\partial T}{\partial \bar{y}}\right) = k_{nf}\left(\frac{\partial^2 T}{\partial \bar{x}^2} + \frac{\partial^2 T}{\partial \bar{y}^2}\right) \quad (3.36)$$

The above equations are normalized by using the following expressions. During the *Re* calculation, twice the channel height, *H* is accepted as a reference length.

$$x = \frac{\bar{x}}{H},\ y = \frac{\bar{y}}{H},\ u = \frac{\bar{u}}{u_i},\ v = \frac{\bar{v}}{v_i},\ t = \frac{\bar{t}u_i}{H},\ \theta = \frac{T-T_c}{T_h-T_c},\ Pr = \frac{\nu_f}{\alpha_f},\ p = \frac{\bar{p}}{\rho_f u_i^2},\ Ha = B_0\sqrt{\frac{\sigma_f}{\mu_f}},Re = \frac{u_i 2H}{\nu_f} \quad (3.37)$$

Therefore, the dimensionless form of governing Equations 3.33-3.36 are as follows;

Continuity

$$\frac{\partial u}{\partial x}+\frac{\partial v}{\partial y}=0 \tag{3.38}$$

X-momentum

$$\frac{\partial u}{\partial t}+u\frac{\partial u}{\partial x}+v\frac{\partial u}{\partial y}=-\frac{\rho_{bf}}{\rho_{nf}}\frac{\partial p}{\partial x}+\frac{\nu_{nf}}{\nu_{bf}}\frac{1}{Re}\left(\frac{\partial^2 u}{\partial x^2}+\frac{\partial^2 u}{\partial y^2}\right)-\left(\frac{\sigma_{nf}}{\sigma_{bf}}\right)\left(\frac{\rho_{bf}}{\rho_{nf}}\right)\frac{Ha^2}{Re}u \tag{3.39}$$

Y-momentum

$$\frac{\partial v}{\partial t}+u\frac{\partial v}{\partial x}+v\frac{\partial v}{\partial y}=-\frac{\rho_{bf}}{\rho_{nf}}\frac{\partial p}{\partial y}+\frac{\nu_{nf}}{\nu_{bf}}\frac{1}{Re}\left(\frac{\partial^2 v}{\partial x^2}+\frac{\partial^2 v}{\partial y^2}\right) \tag{3.40}$$

Energy

$$\frac{\partial \theta}{\partial t}+u\frac{\partial \theta}{\partial x}+v\frac{\partial \theta}{\partial y}=\frac{\alpha_{nf}}{\alpha_{bf}}\frac{1}{RePr}\left(\frac{\partial^2 \theta}{\partial x^2}+\frac{\partial^2 \theta}{\partial y^2}\right) \tag{3.41}$$

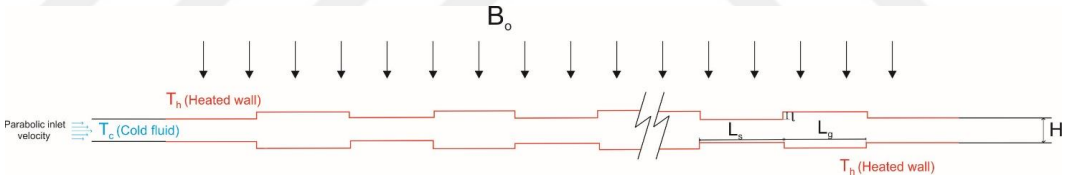

Figure 3.4. Schematic demonstration of the problem domain and the indication of main geometry and flow parameters

As shown in Figure 3.4 the magnetic field is applied in the vertical direction. Therefore, resulting Lorentz forces will occur in the *x*-direction. For this reason, the effect of Lorentz forces on the flow is included in the calculation by adding a source term to the *x*-momentum equation. Hartman number, *Ha* in source term is the ratio of magnetic force to the viscous force. Since the magnetic force is a function of magnetic field intensity, an increased Hartman number, *Ha* represents higher magnetic field strength.

In the current work, the thermal quantity of interest is determined by the Nusselt number. The local Nusselt number, Nu_L along the heated wall of the rectangular corrugated channel can be given as:

$$Nu_L=-\left(\frac{k_{nf}}{k_{bf}}\right)\frac{\partial \theta}{\partial y} \tag{3.42}$$

The average Nusselt number, Nu_{avg} is determined by integrating the above equation (Equation 3.42):

$$Nu_{avg} = \frac{1}{L_w}\int_0^{L_w} Nu_L \, dL \tag{3.43}$$

where L_w represents the length of the rectangular corrugated wall.

3.2.2. Boundary Conditions and Nanofluid Properties

No-slip boundary condition is available for all channel walls (u = v = 0). Constant heat flux is applied on grooved walls but straight channels, located upstream and downstream of the grooved channel, are adiabatic ($\partial\theta/\partial y = 0$). A fully developed velocity profile is defined at the inlet of the channel $u = 6y\,(1-y)$ and pressure at the outlet of the domain is set as zero (P=0). The thermophysical properties of the nanofluid are determined by the equations below. Nanoparticle volume fractions, Φ =0%, 3%, and 5% are tested in simulations. The properties of water and CuO nanoparticles used in the below equations are given in Table 3.4 (Ali et al., 2020; Selimefendigil and Oztop, 2020; Kefayati, 2016).

$$\rho_{nf} = (1-\Phi)\rho_{bf} + \Phi\rho_{np} \tag{3.44}$$

$$\left(\rho C_p\right)_{nf} = (1-\Phi)\left(\rho C_p\right)_{bf} + \Phi\left(\rho C_p\right)_{np} \tag{3.45}$$

$$(\rho\beta)_{nf} = (1-\Phi)(\rho\beta)_{bf} + \Phi(\rho\beta)_{np} \tag{3.46}$$

$$\mu_{nf} = \frac{\mu_{bf}}{(1-\Phi)^{2.5}} \tag{3.47}$$

$$\frac{k_{nf}}{k_{bf}} = \frac{\left(k_{np}+2k_{bf}\right) - 2\Phi\left(k_{bf}-k_{np}\right)}{\left(k_{np}+2k_{bf}\right) + \Phi\left(k_{bf}-k_{np}\right)} \tag{3.48}$$

$$\sigma_{nf} = \sigma_{bf}\left(1 + \frac{3\left(\sigma_{np}/\sigma_{bf}-1\right)\Phi}{\left(\sigma_{np}/\sigma_{bf}+2\right) - \left(\sigma_{np}/\sigma_{bf}-1\right)\Phi}\right) \tag{3.49}$$

Table 3.4. Properties of solid particles and water.

	ρ (kg/m^3)	C_p (J/kgK)	k(W/mK)	σ
Pure Water	998.2	4182	0.6	0.05
CuO	6500	540	18	2.7×10^8

3.2.3. Solution Method

Ansys Fluent 20 (Academic Version) is carried out to simulate fluid flow, heat transfer, and entropy generation. Momentum source terms in Equations 3.34 and 3.35 which express the impact of the uniform magnetic field in the rectangular grooved channel are comprised in simulations by employing the User Defined Functions (UDF) module of Ansys Fluent 20. SIMPLE scheme is used for pressure velocity coupling and the second order scheme is selected for pressure interpolation at cell faces from cell center value. Furthermore, the second-order upwind scheme technique is utilized for convective terms discretization, and temporal discretization is employed with the second-order implicit model. The converge criteria is used as 10^{-8} for the energy equation and 10^{-6} for momentum and continuity equations. Furthermore, the time step size is adjusted as 0.007 *s* which makes the Courant number *Cr*=0.6 providing Courant-Lewy-Friedrich (CFL) condition in the smallest cell of the mesh at every time step. The mesh structure in the rectangular grooved channel and detailed mesh distribution in the rectangular grooves and the close region of channel walls are displayed in Figure 3.5. As it is clear in Figure 3.5, the density of mesh distribution is greater near the upper and lower walls of the channels since velocity and temperature gradients are important in these regions. The element number denoted in Table 3.5 is used for the mesh independence study and it is observed that 147037 elements supply the best outcomes concerning computational cost-accuracy balance.

Table 3.5. Results of mesh independency test

Element Number	Nu_{avg}	f
29044	9.75	0.0681
43566	9.559	0.06815
65350	9.4178	0.06814
98025	9.3246	0.06813
147037	9.2552	0.06813
220556	9.232	0.06813

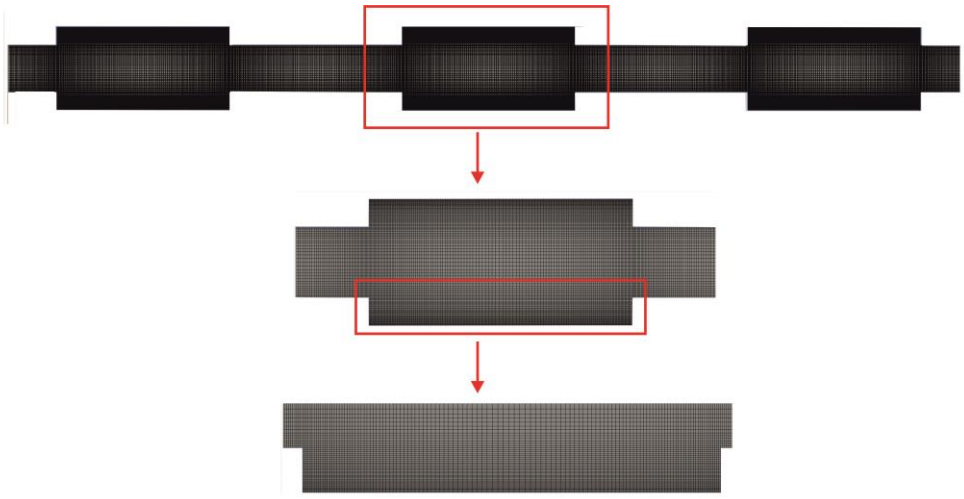

Figure 3.5. Mesh structure for the numerical simulation of fluid flow in a rectangular grooved channel and detailed mesh distribution in the vicinity of channel walls

The solution procedure given above is validated by employing it on another laminar convective heat transfer problem on a similar geometry studied by Wang and Chen (2002). The results shown in Figure 3.6 indicate solution procedures used in the current study are suitable to simulate such a problem. Furthermore, the method employed for the simulation of the uniform magnetic field is also validated by testing it on the problem represented by Ghasemi et al. (2011) at Ha=0 and 30. As seen in Figure 3.7, the perfect agreement is acquired for the local distribution of y velocity and temperature, θ at the middle of the square cavity under a uniform magnetic field.

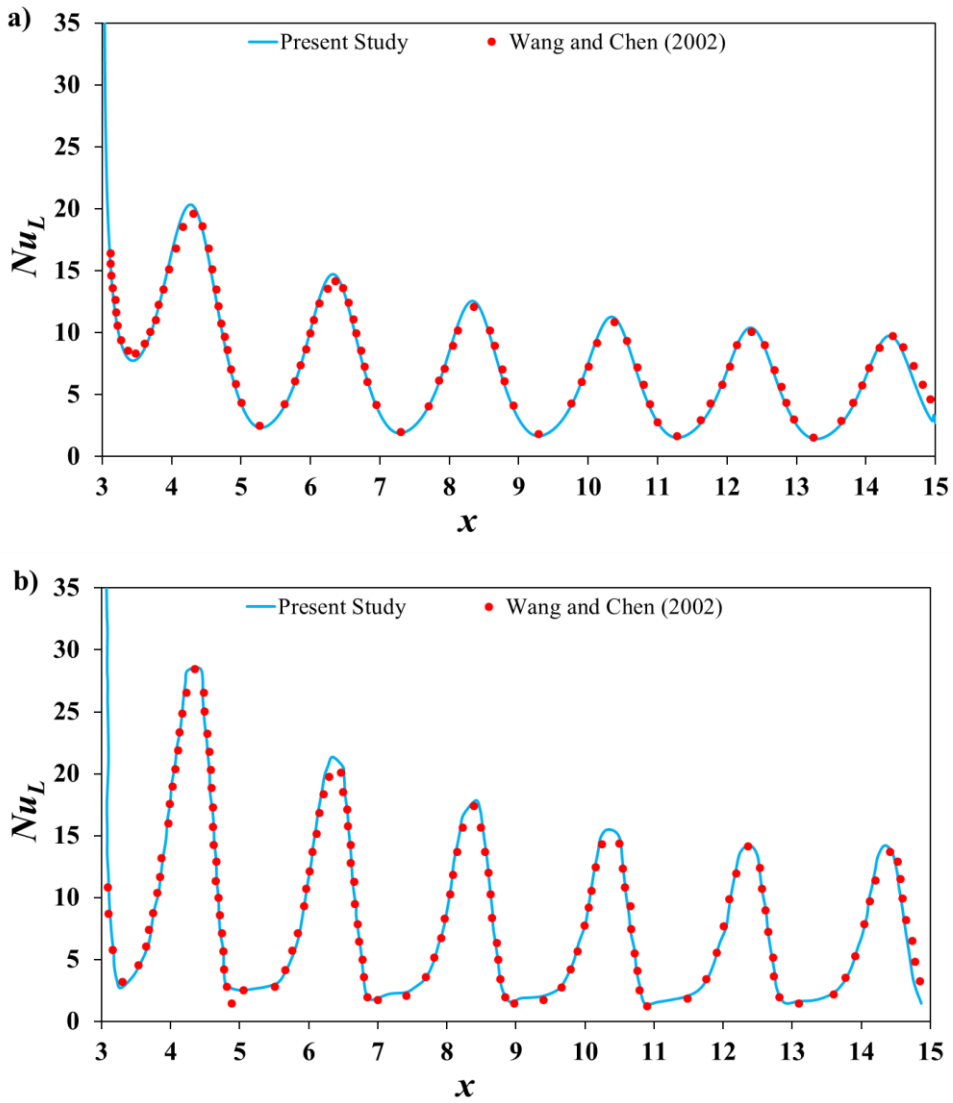

Figure 3.6. The validation study represents the comparison of the local Nusselt number, Nu_L with similar geometry of current work's geometry and the study of Wang and Chen (2002) at Re=500 for a) the ratio of wavy amplitude to the wavelength ratio, α=0.1 b) α=0.2

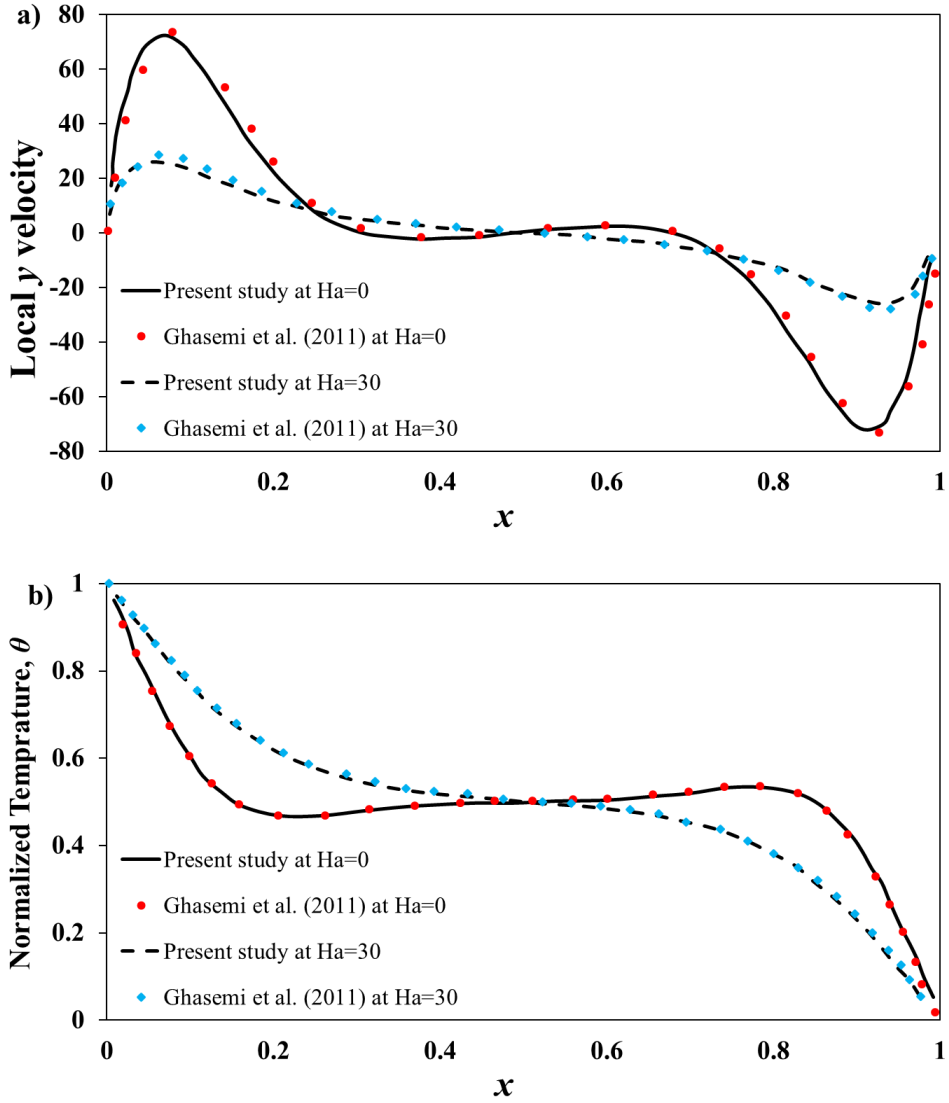

Figure 3.7. The comparison of a) local y velocity distribution b) temperature, θ in the case of uniform magnetic field application between current outcomes and numerical outcomes of Ghasemi et al. (2011) at the middle of the square cavity for Ra=10^5 and Φ=3%

3.2.4. Solution Method

Calculating the generation (or production) of entropy is a beneficial method to optimize the performance of thermal systems. For the present study, the entropy generation due to the forced thermal convection of the nanofluid flow is determined by considering the effects of the thermal, viscous, and applied magnetic sources. Accordingly, the total entropy generation, S_L results from the summation of these effects, which is written in a dimensional form as follows:

$$\bar{s}_L = \bar{s}_{th} + \bar{s}_{vis} + \bar{s}_{mag} = \frac{k_{nf}}{T_o^2}\left[\left(\frac{\partial T}{\partial \bar{x}}\right)^2 + \left(\frac{\partial T}{\partial \bar{y}}\right)^2\right] + \frac{\mu_{nf}}{T_o}\left[2\left(\frac{\partial \bar{u}}{\partial \bar{x}}\right)^2 + 2\left(\frac{\partial \bar{v}}{\partial \bar{y}}\right)^2 + \left(\frac{\partial \bar{u}}{\partial \bar{y}} + \frac{\partial \bar{v}}{\partial \bar{x}}\right)^2\right] + \frac{\sigma_{nf}}{T_o} B_0^2\, \bar{u}^2 \tag{3.50}$$

where $T_o = \frac{T_h+T_c}{2}$

On the right-hand side of the above equation (Equation 3.50), the first, second, and third terms represent the effects of thermal, viscous, and magnetic fields, respectively.

With the help of dimensionless parameters listed in Equation 3.37, the dimensionless form of Equation 3.50 is described as follows:

$$s_L = s_{th} + s_{vis} + s_{mag} = \left[\left(\frac{\partial\theta}{\partial x}\right)^2 + \left(\frac{\partial\theta}{\partial y}\right)^2\right] + \left(\frac{\mu_{nf}}{\mu_{bf}}\right)\left(\frac{k_f}{k_{nf}}\right)\chi\left[2\left(\frac{\partial u}{\partial x}\right)^2 + 2\left(\frac{\partial v}{\partial y}\right)^2 + \left(\frac{\partial u}{\partial y} + \frac{\partial v}{\partial x}\right)^2\right] + \left(\frac{\sigma_{nf}}{\sigma_{bf}}\right)\left(\frac{k_f}{k_{nf}}\right)Ha^2\chi u^2 \quad (3.51)$$

where, χ is an irreversible factor, and its definition is given as below:

$$\chi = \frac{\mu_{bf}T_o}{k_{bf}}\left(\frac{u_i}{\bar{q}L/k_{bf}}\right)^2 \quad (3.52)$$

The average value of the total entropy generation, S_L through the considered channel is obtained by integrating Equation 3.51 over the entire flow domain:

$$S_{avg} = \frac{\int_A s_L dxdy}{A} \quad (3.53)$$

4. RESULTS AND DISCUSSION

4.1. Effect of Non-Uniform Magnetic Field on Hydrothermal and Entropy Generation Characteristics of Ferrofluid Flow Around a Confined Cylinder Using Wire Magnetic Sources

4.1.1. Flow Pattern and Thermal Analysis

Figures 4.1-4.4 demonstrate the variation of streamline patterns around the cylinder with the *Ha* which is an indicator of the influence of the applied non-uniform magnetic field at *Re*=25, 50, 100 and 150, respectively for the ferrofluid volume fraction, Φ=0%. In Figure 4.1, in the lack of the non-uniform magnetic field application, *Ha*=0 the flow structure at *Re*=25 is a steady state with two symmetrical vortices in the closed wake connected to the back surface of the cylindrical object. As inferred from Figure 4.1, when the non-uniform magnetic field passing current-carrying wires with *Ha*=2 is applied, the recirculation bubble length in the domain of the wake downstream of the cylinder is reduced. This recirculation region gradually weakens both longitudinally and laterally by strengthening the non-uniform magnetic field intensity from *Ha*=2 to *Ha*=6. However, if the *Ha* further increased to a value *Ha*=10, the flow separation is suppressed, and the recirculation bubble like the wake region completely disappears. For Hartmann numbers, $Ha \geq 10$, the flow is completely attached to the circular cylinder surface of the cylindrical body and the separated flow and recirculation wake disappears at the back of the cylinder at *Re*=25.

In Figure 4.3, the flow is time-dependent generating a very extended wake with periodic vortex shedding from the upper and lower surfaces of the cylindrical body at *Re*=100 and *Ha*=0. Furthermore, the flow remains unsteady with periodic vortex shedding at *Ha*=2, however, when the *Ha* increased from *Ha*=2 to *Ha*=6, the flow becomes time-independent with a closed wake. The further rise of the *Ha* causes the extent of recirculation wakes to be reduced. But even at *Re*=100 and *Ha*=18, the recirculation bubbles in the closed wake region of the cylinder do not completely disappear unlike in the case of *Re*=25. The physical explanation of the reducing recirculation bubble length and flow pattern change from the unsteady state to a steady state that the Lorentz forces induced by the applied non-uniform magnetic field have a tendency to suppress the vortex diffusion, thus, the recirculation bubble length is reduced, and the shedding of the vortices is weakened. Furthermore, the applied non-uniform magnetic field through current-carrying wires supplies additional stability to the flow and behaves like a damping force that represses any instability in the flow domain.

As seen in Figures 4.1 and 4.3, the applied non-uniform magnetic field induces two symmetrical vortices in the near region of the magnetic field application locations. These two vortices begin to appear at *Ha*=10 for both *Re*=25 and 100. The size of the non-uniform magnetic field induced vortices is larger at *Re*=25 compared to the *Re*=100 since the momentum of the mainstream flow is low at small *Re* and by enhancing the velocity incoming ferrofluid flow, the

extent of the non-uniform magnetic field induced vortices is attenuated because of the large momentum of inflow. The acquired outcomes demonstrated that the applied non-uniform magnetic field enhances the performance of heat transfer rate by forming a pair of vortices in the region close to the current-carrying wires.

Figure 4.5 demonstrates the magnetic field effect on the streamline distribution around the cylinder for *Re*=25, 50, 100, and 150 when the volume fraction of ferrofluid (water and Fe_3O_4) is 4%. In Figure 4.5, when the streamline patterns at *Re*=25 and 100 are carefully examined, it can be said that they are exactly the same as the streamline patterns at Φ=0% ferrofluid (water and Fe_3O_4) volume fraction. So, it can be concluded that the use of ferrofluid in the non-uniform magnetic field application has no clear effect on the streamline distributions around the cylinder. Here, the forming of a pair of vortices in the region close to the current-carrying wire may hinder the sedimentation of the nanoparticles. It should be noted that it is achievable to exactly remove the alternate shedding of vortices at the greater Reynolds number, *Re*=150, and to set time-independent flow if an adequately intense non-uniform magnetic field is applied. The required intensity of the non-uniform magnetic field depends on the *Re* and augments by the *Re*. For example, the unsteady flow patterns change to the steady one at *Re*=100 and *Ha*=6 whereas the flow is still time-dependent at *Re*=150 and *Ha*=6, and it becomes time-independent beyond the rise in the *Ha* such as *Ha*=10.

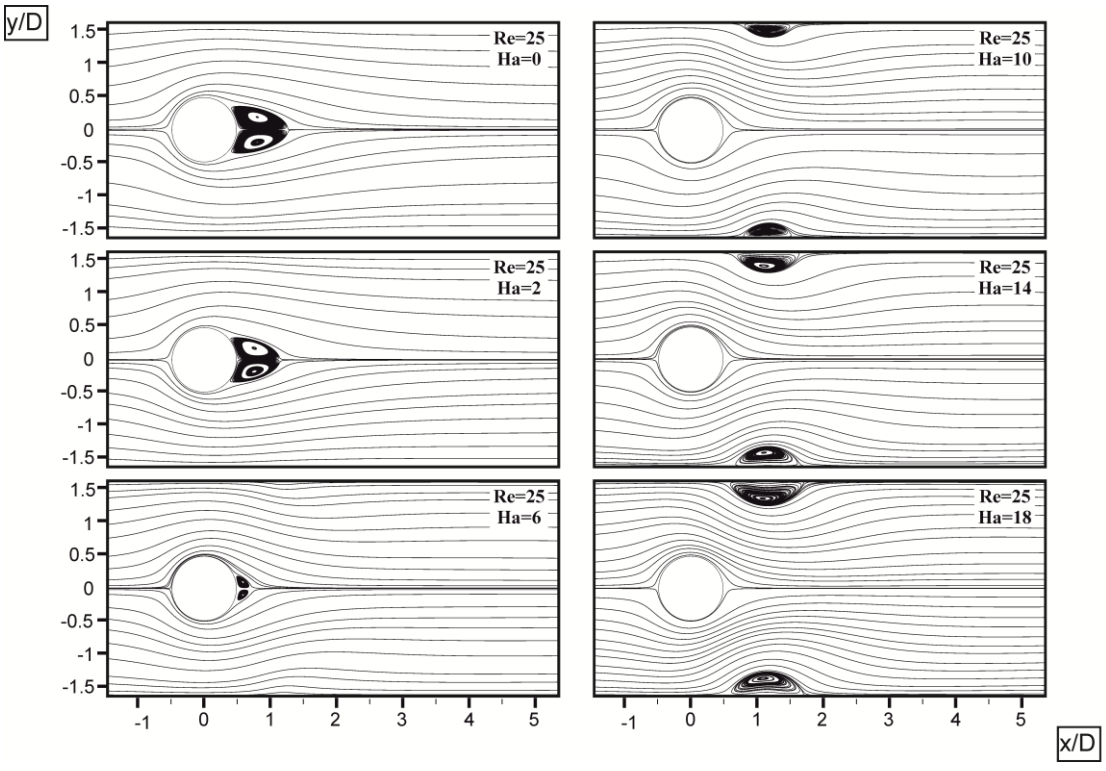

Figure 4.1. The effect of the magnetic field on the boundary layer detachment around the circular cylinder at *Re*=25 and Φ=0%

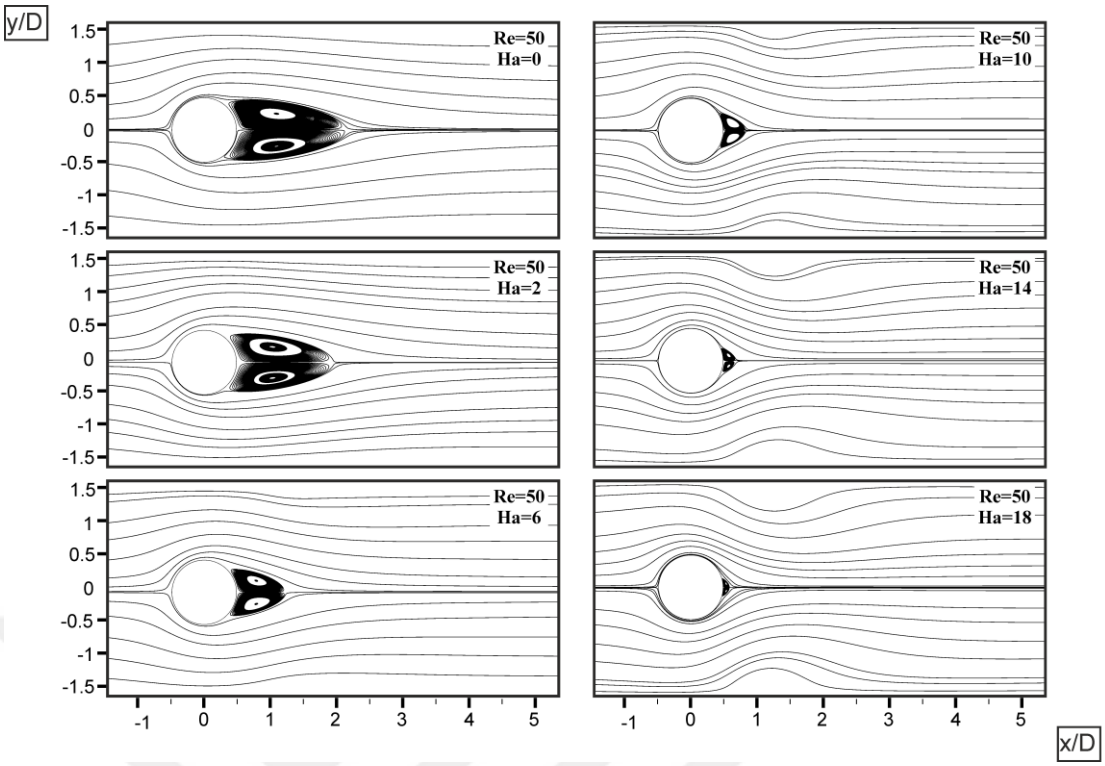

Figure 4.2. The effect of the magnetic field on the boundary layer detachment around the circular cylinder at *Re*=50 and *Φ*=0%

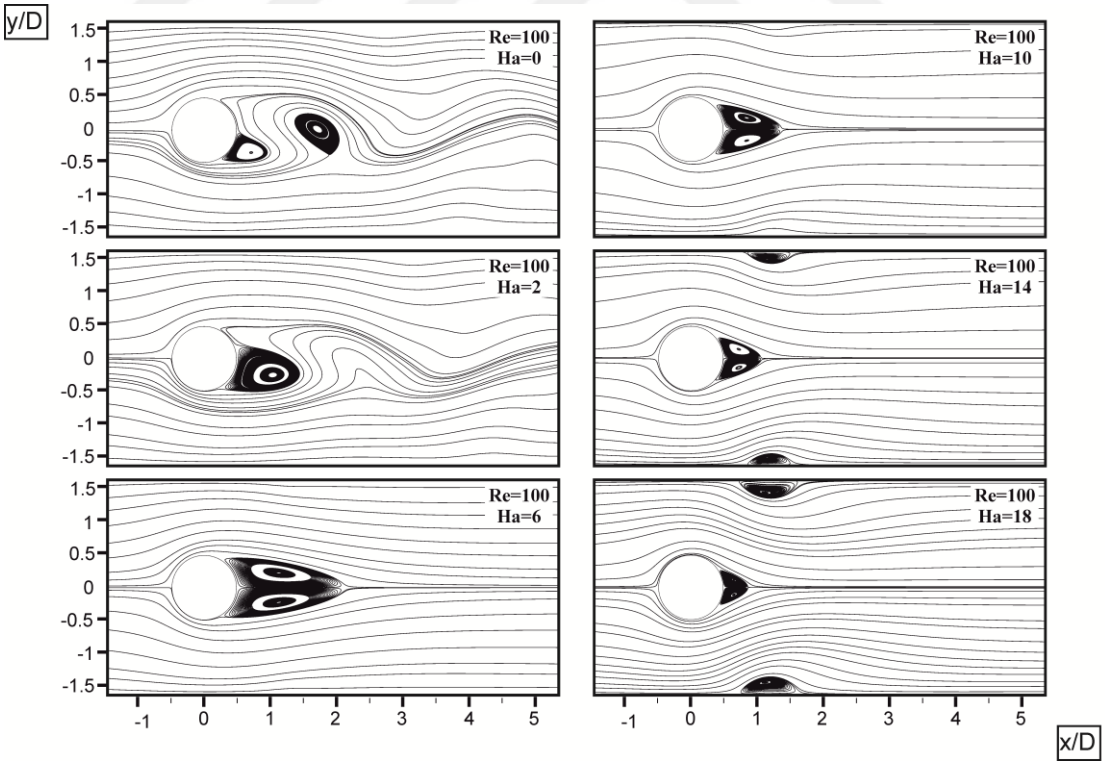

Figure 4.3. The effect of the magnetic field on the boundary layer detachment around the circular cylinder at *Re*=100 and *Φ*=0%

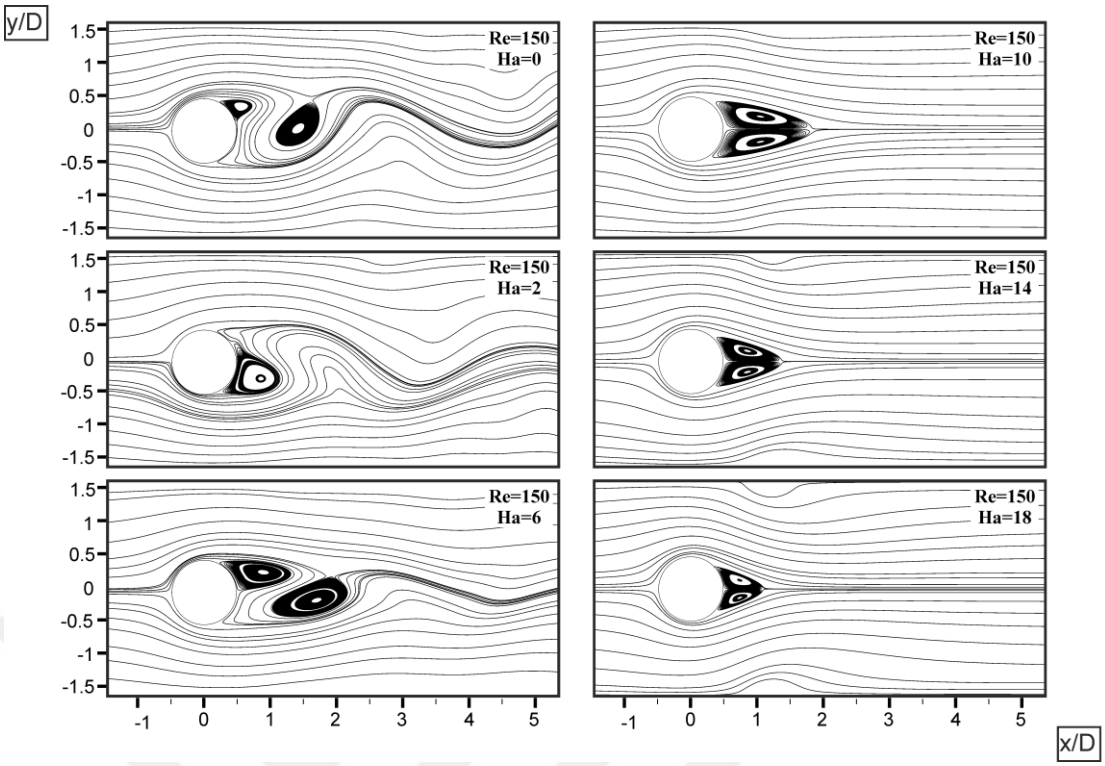

Figure 4.4. The effect of the magnetic field on the boundary layer detachment around the circular cylinder at *Re*=150 and *Φ*=0%

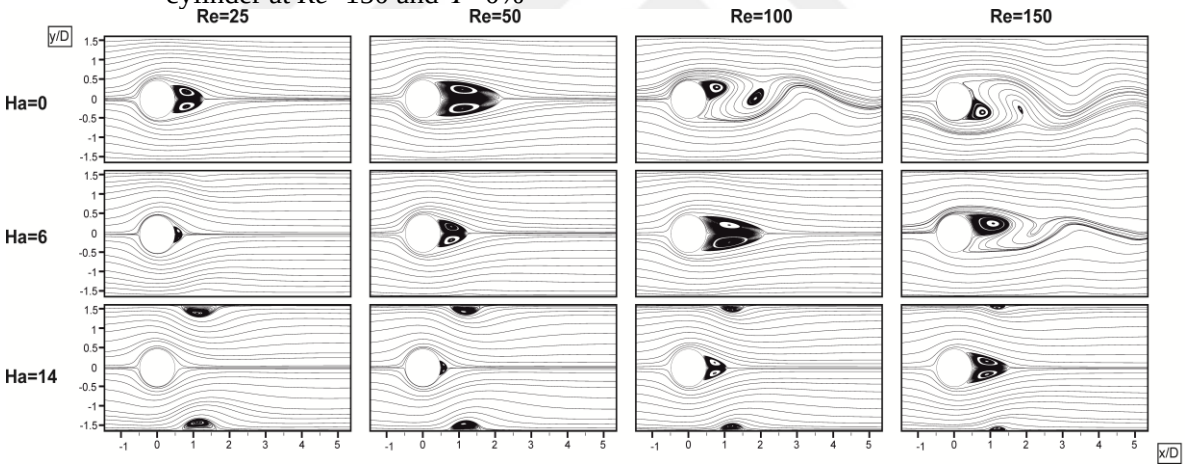

Figure 4.5. The influence of the magnetic field on the boundary layer detachment around the circular cylinder at *Re*=25, 50, 100, and 150 for *Φ* =4%

The change of the normalized separation length, L_s/R (the distance in streamwise direction between the rear stagnation point and reattachment point) with non-uniform magnetic field intensity for different *Re* is demonstrated in Figure 4.6 (a). As seen in Figure 4.6 (a), the normalized separation length, L_s/R reduces with the rise in the *Ha*. In other words, the location of the separation point approaches the rear stagnation point of the cylinder because of the growing squeezing effect with the applied non-uniform magnetic field. This situation can be expressed by the following fact that an applied non-uniform magnetic field in the channel flow of a conducting fluid causes Lorentz forces that suppress the diffusion of vortices thus reduce the wake length. For

example, while the dimensionless separation length, L_s/R was detected as 1.566 and 3.573 at *Re*=25 and 50 for *Ha*=0, it was reduced to the values of 0.4533 and 1.54 for *Ha*=6, 0.12 and 0.346 for *Ha*=14 at *Re*=25 and 50 respectively. While the flow separation and recirculation bubbles are fully suppressed at *Re*=25 and 50 for *Ha*=14 and *Ha*=18, they cannot be fully diminished at *Re*=100 and 150 even at *Ha*=22. So, it can be concluded that the effect of the *Ha* flow characteristics over a confined cylinder attenuates by increasing the *Re* number. Since instabilities in the flow become larger with increasing the *Re* because of the large inertia effect, a stronger non-uniform magnetic field strength is needed to suppress the hydrodynamic instability. Furthermore, when the *Re* augments, the separation length gets higher due to the higher momentum of the conducting fluid flow.

The quantitative variations of separation angle, φ on the cylinder surface with the Hartmann number are displayed in Figure 4.6 (b) for different Reynolds numbers, *Re*=25, 50, 100 and 150. It has been detected that the separation angle, φ lowers when the *Ha* increases. In other words, the separation points on the cylinder surface move through the downstream direction or towards the front stagnation point by increasing the Hartmann number, *Ha* for all *Re*. For instance, when the flow of conducting fluid separates from the cylinder surface at angles of φ= 45º and 56º at *Ha*=0 for *Re*=25 and 50, respectively, it takes place on the location of φ= 27.5º and 46º for *Ha*=6, φ= 2.5º and 23.75º for *Ha*=14 at *Re*=25 and 50, respectively. As seen, the φ is higher at a greater *Re* which means the separation point over the cylinder surface proceeds in the upstream direction due to thinning of the velocity boundary layer thickness at greater *Re*. Furthermore, the φ lessens at a relatively faster rate with applying a non-uniform magnetic field at lower Reynolds numbers, *Re*=25 compared to the higher Reynolds numbers, *Re*=100 and 150. Thus, one can interpret that the application of a non-uniform magnetic field through current-carrying wires is very effective at a lower *Re* and this effectiveness attenuates by increasing Reynolds numbers, *Re*.

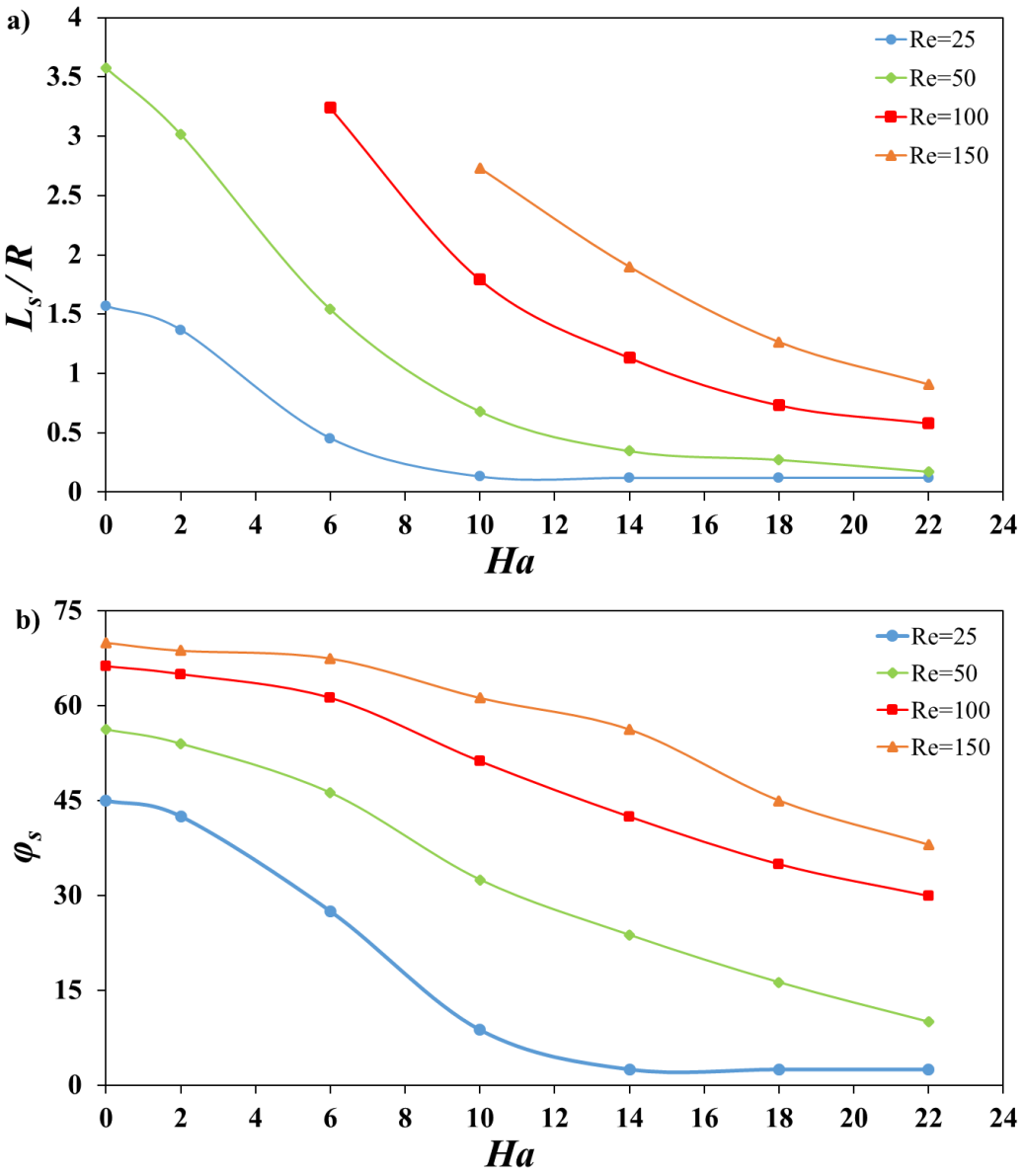

Figure 4.6. The magnetic field effect on the a) dimensionless separation length, L_s/R b) separation angle, φ over the cylinder for Reynolds numbers Re=25, 50, 100, and 150 at ferroparticle volume fraction, Φ=0%

The influence of a non-uniform magnetic field on the vorticity distributions around the confined cylinder at Re=25, 50, 100 and 150 for Φ=0% is demonstrated in Figures 4.7-4.10, respectively. According to Figure 4.7, the structure of vorticity is subjected to a continuous change because of the non-uniform magnetic field passing through a current-carrying wire. With increasing Ha, the vorticity concentration is elongated in a streamwise direction, and the size of these vorticity bubbles gets lower because of the non-uniform magnetic field application. The size of vorticity contracts near the middle of the cylinder when the magnetic field is applied, and the extent of vorticity contraction grows with a further increase in Ha. In other words, the non-uniform magnetic field going through a current-carrying wire causes the wake region downstream of the

cylinder to shrink in size. As demonstrated in Figure 4.7, the maximum value of normalized vorticity strength, $\omega_z D/U_\infty$ augments from the $\omega_z D/U_\infty$=20.68 at *Ha*=0 to the value of $\omega_z D/U_\infty$=22.28 at *Ha*=10 and $\omega_z D/U_\infty$=31.47 by a further rise of the *Ha* to the value of *Ha*=18. In summary, it can be said that there is a corresponding augmentation of heat transfer rate with the application of a magnetic field. Because the improvement in heat transfer can be associated with the increase in the vorticity intensity which is also stated by Arjun and Rakesh (2020).

In Figure 4.9, as one can see, the Karman vortex street forms downstream of the circular cylinder due to the alternate positive and negative vortex shedding from the shear layers on either side of the cylindrical body. The flow is yet unsteady at the *Ha*=2. If the *Ha* is further augmented to the value of *Ha*=6, the ferrofluid flow is stabilized and alters its structure from the unsteady form with the shed of vortices in the wake of the cylinder at *Ha*=0 and *Ha*=2 to the time-independent one along with a symmetrical vorticity distribution according to the cylinder axis. The acquired outcomes demonstrated that the non-uniform magnetic field going through current-carrying wires suppresses and controls the vortex shedding events at the shoulders of the cylinder. By intensifying the non-uniform magnetic field strength, the unsteady attitude of the flow field diminishes, and the time-independent flow is created. The non-uniform magnetic field in a ferrofluid flow generates a resistant force which is called Lorentz force and this force is effective on a fluid carrying a current density in a magnetic field. The Lorentz force is prone to decelerate the movement of the fluid flow and it is an opposing body force that keeps down the shedding of vortices at downstream of the cylindrical body. The level of the flow structure variation under the influence of Lorentz forces becomes stronger when the strength of the non-uniform magnetic field grows. The Lorentz forces withstand the vortical motion, and at last, diminish the vortex shedding mechanism. Thus, one method to eliminate the shedding of vortices downstream of the cylindrical body in a channel is to apply the magnetic field passing through the current-carrying wire. It should be noted that the shed of vortices generates an unsteady periodic force that causes the vibration of the bluff body and may induce structural defects and therefore it is vital to remove or attenuate vortex shedding in some applications. When the *Ha* is further increased from *Ha*=6 to values of *Ha*=10,14 and 18, the vorticity bubbles are progressively less elongated in a streamwise direction with reduced size and narrower region.

In Figure 4.11, the magnetic field influence on the vorticity patterns of the circular cylinder is shown at *Re*=25, 50, 100, and 150, for the ferrofluid volume concentration, Φ=4%. In this figure, one can conclude by looking at the magnetic field effect at *Re*=25 and 100 that increasing the ferrofluid volume concentration from Φ=0% to Φ=4% does not cause any significant effect on the vorticity distributions, structure, and strength around the confined cylinder. Furthermore, it should be reported that the required non-uniform magnetic field strength to convert the unsteady flow case into the steady flow case increases further with increasing Reynolds numbers, *Re* since the flow becomes time-dependent at *Re*=100 and *Ha*=6 and the flow is still unsteady at *Ha*=6 and the flow

pattern alters its structure from the unsteady state to the steady cases when the *Ha* further increases from *Ha*=6 to *Ha*=10 at *Re*=150.

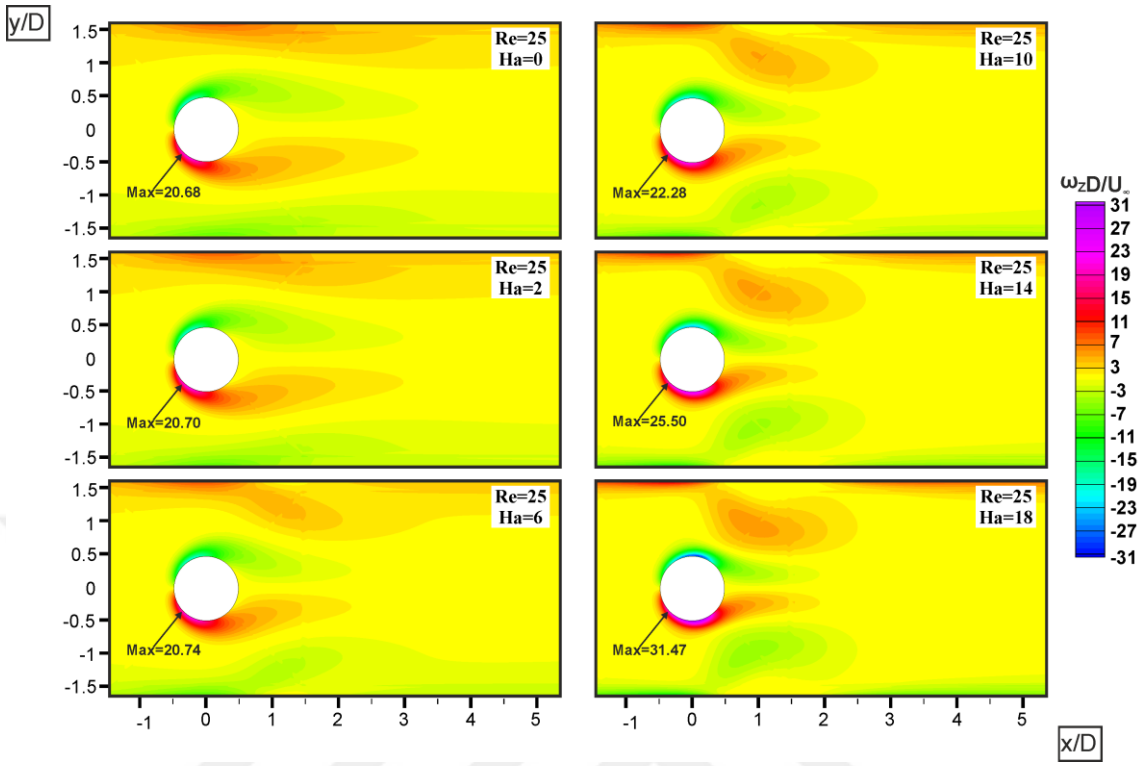

Figure 4.7. The non-uniform magnetic field effect on the vorticity structure around the cylinder at *Re*=25 and Φ =0%

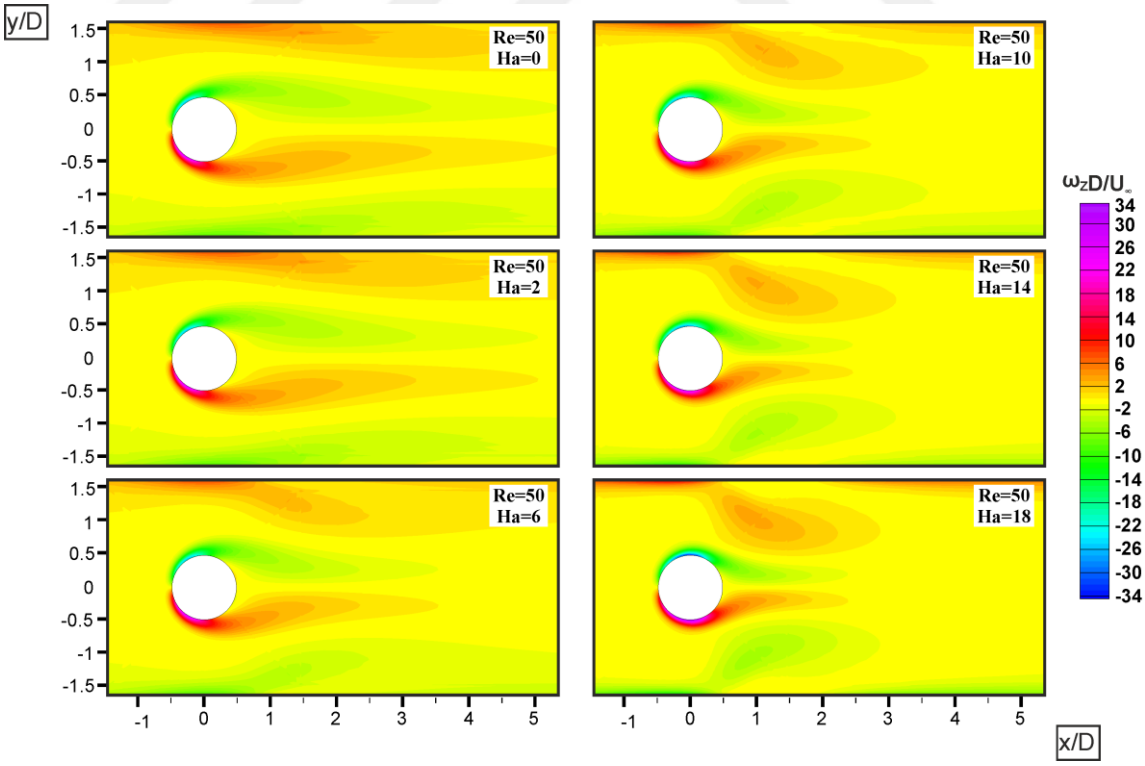

Figure 4.8. The non-uniform magnetic field effect on the vorticity structure around the cylinder at *Re*=50 and Φ =0%

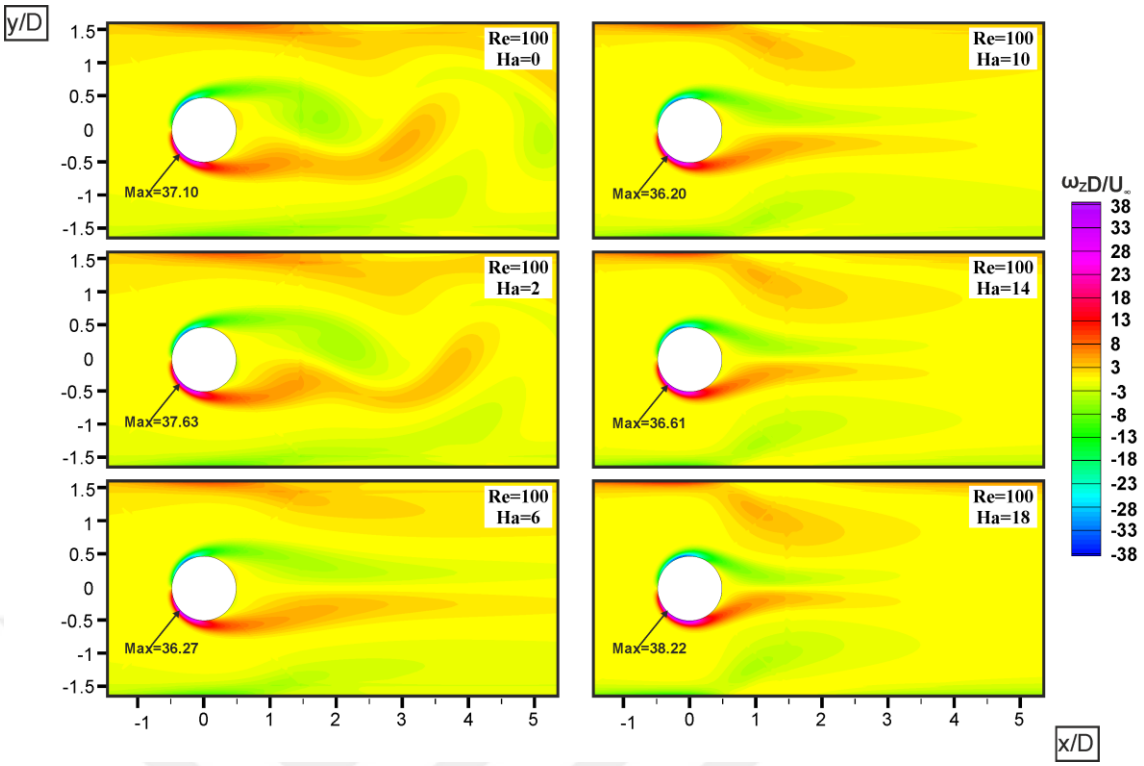

Figure 4.9. The non-uniform magnetic field effect on the vorticity structure around the cylinder at *Re*=100 and Φ =0%

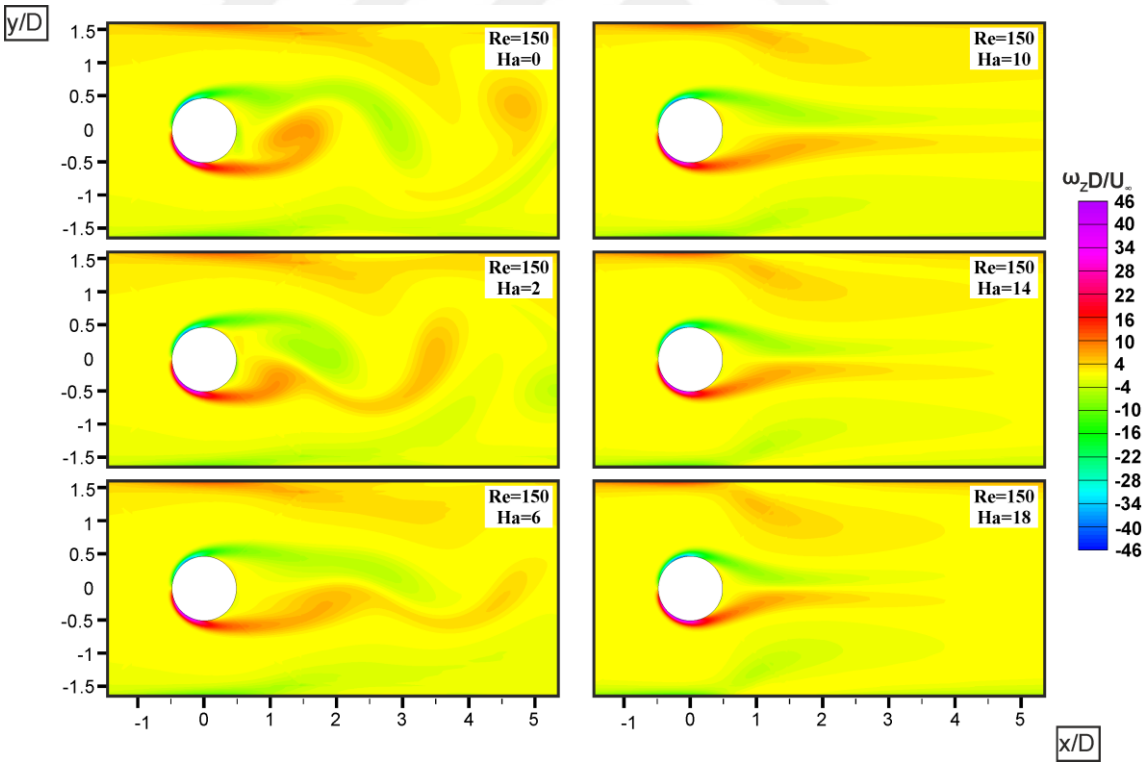

Figure 4.10. The non-uniform magnetic field effect on the vorticity structure around the cylinder at *Re*=150 and Φ =0%

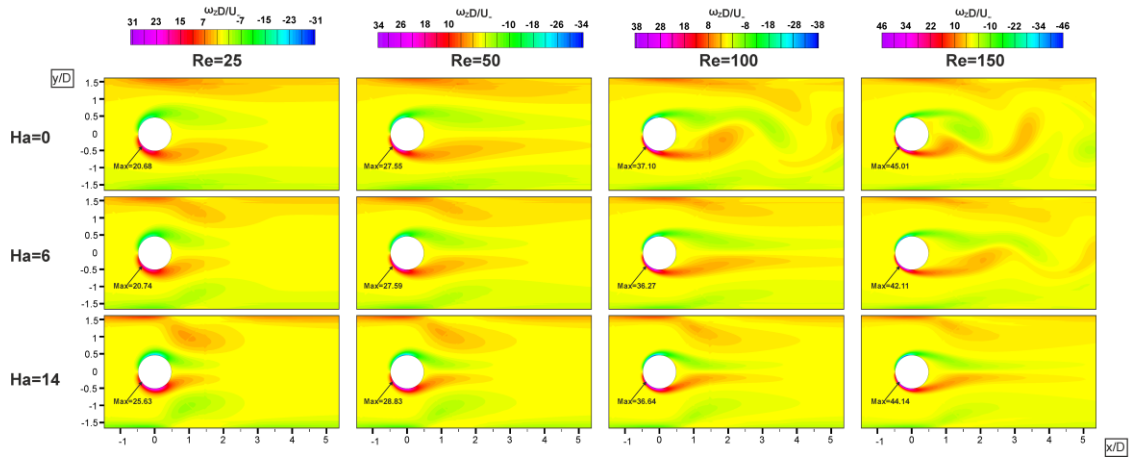

Figure 4.11. The non-uniform magnetic field effect on the vorticity structure around the cylinder at *Re*=25, 50, 100, and 150 for Φ =4%

The variations of C_D with *Re* and *Ha* are demonstrated in Figure 4.12. From Figure 4.12, it was detected that the total drag coefficient, C_D gets higher with the applied non-uniform magnetic field going through current carrying wires for all examined Reynolds numbers, *Re*=25, 50, 100 and 150. For example, at Re=25, when the total drag coefficient, C_D was observed as 5.513 at *Ha*=0, it increases to the values of 7.358 and 15.33 at *Ha*=6 and 14, respectively. In the same way, at *Re*=50, the total C_D increases by almost 20% when *Ha* grows from *Ha*=0 to *Ha*=6 and subsequently increases by 61% at *Ha*=10. As seen, the total C_D gets higher more quickly at greater *Ha*. The increasing trend of total C_D with increasing Hartmann number, *Ha* might be associated with the enhanced value of Lorentz force which acts directly to suppress the mainstream flow velocity constituent. Therefore, an increase in non-uniform magnetic field intensity is always associated with an increasing difference between upstream and downstream pressures, resulting in an increase in total C_D. This increase in the pressure drop because of the substantial rise in pressure on the forward region of the cylinder contributes to the increment of C_{Dp} over the cylindrical body for the time-independent flow which is also stated by Singha and Sinhamahapatra (2011), Rezaie and Norouzi (2018), Singha et al. (2006), Grigoriadis et al. (2010), Sekhar et al. (2006). At *Re*=150, it is detected that the total C_D reduces slightly with the growth of the *Ha* provided that the flow stays time-dependent with a periodic shed of vortices alternately. This slight decline in the total C_D can be interpreted as the diminished vortex shedding that invalidates the influence of augmented pressure drop. However, as soon as the flow turns into a time-independent pattern due to an adequately strong non-uniform magnetic field intensity, the total C_D grows with a beyond increment in the *Ha* because of the augmented pressure drop.

Furthermore, one can observe from Figure 4.12 that the total C_D attenuates with increasing Reynolds numbers, *Re*. Because the greater values of *Re* mean the higher flow velocity, the greater *Re* means the lower viscous drag coefficient, C_D. In addition, it is known that the total C_D for a flow with a larger wake, i.e., at higher *Re*, is lower than the flow with a smaller wake, i.e., at lower *Re*.

Figure 4.13 shows the effect of a non-uniform magnetic field passing through current-carrying wires on overall C_D at *Re*=25 and 100 when volume fractions of ferrofluid are Φ=0%, 2%, and 4%. In Figure 4.13, one can interpret that increasing the volume concentration of the ferrofluid from Φ=0% to Φ=2 % and 4% does not cause any significant effect on the C_D-*Ha* curve for both values of, *Re*=25 and 100. The trend and distribution of the C_D-*Ha* curves are exactly the same for the examined *Re* independent of the ferrofluid volume concentration, Φ.

The influence of the Hartmann number, *Ha* on the variation of drag coefficient, C_D with time is demonstrated in Figure 4.14 for Reynolds numbers, *Re*=25 and 150, and Hartmann numbers, *Ha*=0 and 10. From Figure 4.14 (a) and (b), it is observed that when the Hartmann number increases from *Ha*=0 to *Ha*=10, the drag coefficient, C_D substantially increases. As seen, the flow structure is a steady state at *Re*=25 for both *Ha*=0 and 10, because there is no fluctuation in drag coefficient, C_D with time and it becomes completely constant after a while. However, the time required for the drag coefficient, C_D to be completely constant is lower when the non-uniform magnetic field is applied with *Ha*=10 than no magnetic field application case, *Ha*=0 at *Re*=25. The progress of the drag coefficient, C_D with time at various *Ha* reflects the changes in the flow pattern. As seen in Figure 4.14 (c) and (d), there are remarkable fluctuations in drag coefficient, C_D when no magnetic field is acting on the flow domain of a confined cylinder. This means that the flow pattern is unsteady with a periodic shed of vortices from the upper and lower sides of the cylindrical body. In Figure 4.14 (d), when the Hartmann number is increased from *Ha*=0 to *Ha*=10, the fluctuations in drag coefficient, C_D are eliminated and the flow structure becomes a steady state. Furthermore, when the flow pattern changes from an unsteady state to a steady state, the periodic vortex shedding and asymmetry of flow are diminished as evident from the drag coefficient, C_D history in Figure 4.14 (c) and (d).

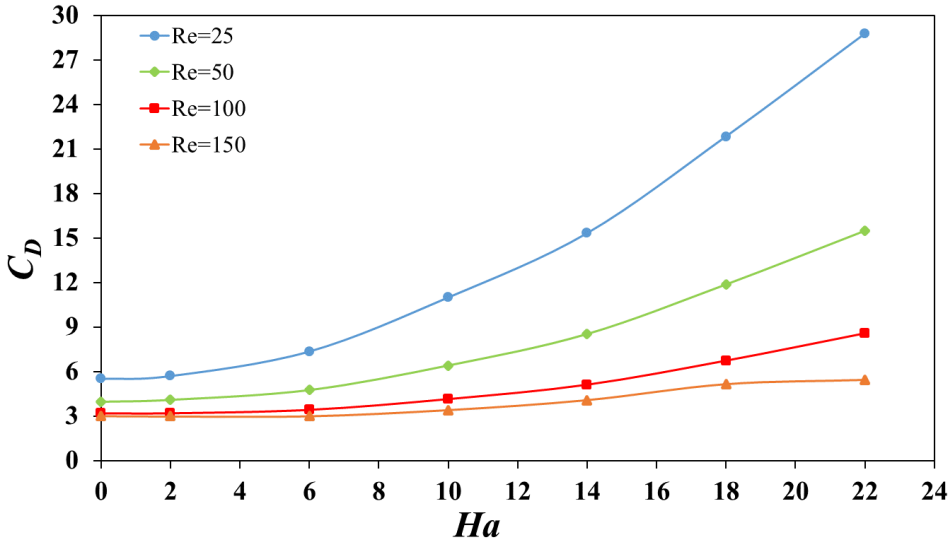

Figure 4.12. The non-uniform magnetic field influence on the C_D of the cylinder at Re=25, 50, 100 and 150 for Φ =0%

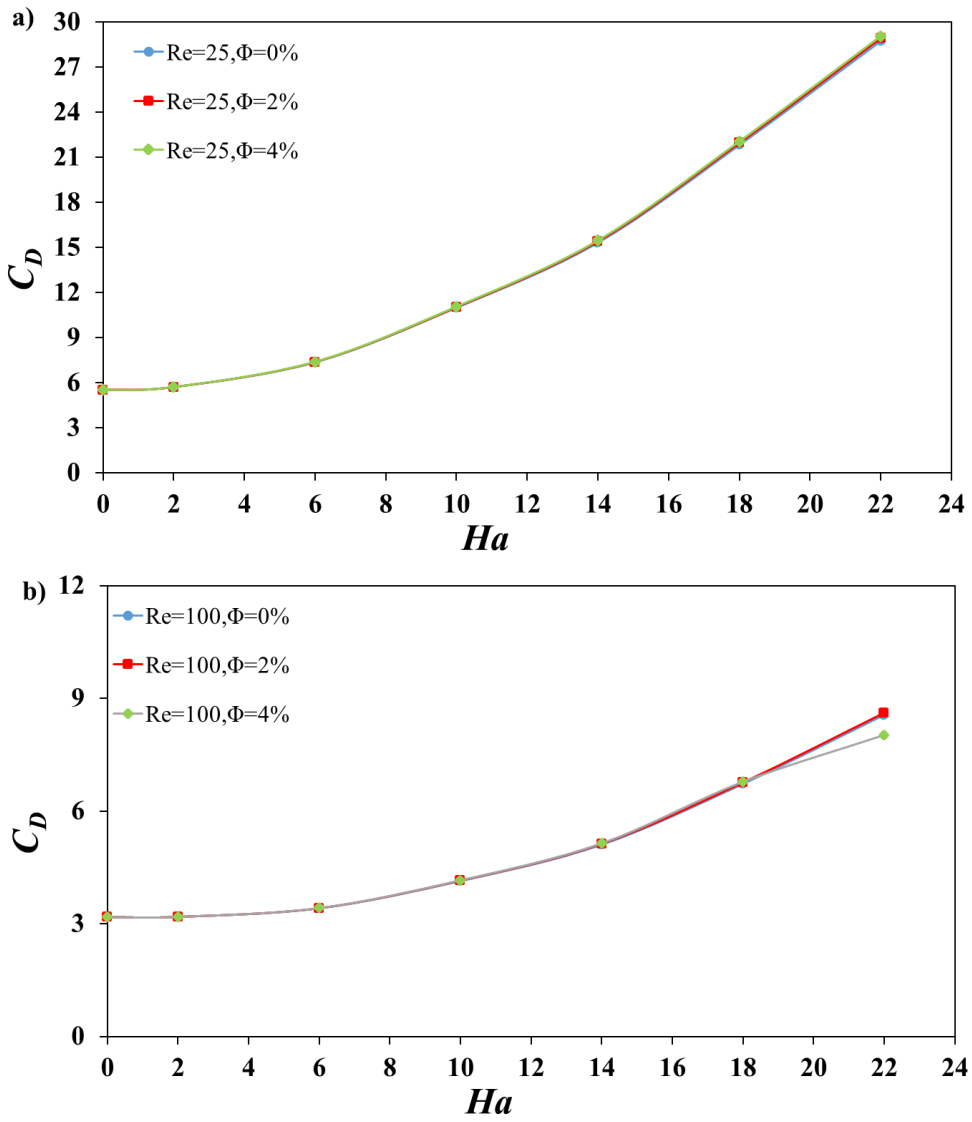

Figure 4.13. The effect Ha and Φ on the C_D of the cylinder at Reynolds numbers a) Re=25 b) Re=100 for Φ =0%, 2% and 4%

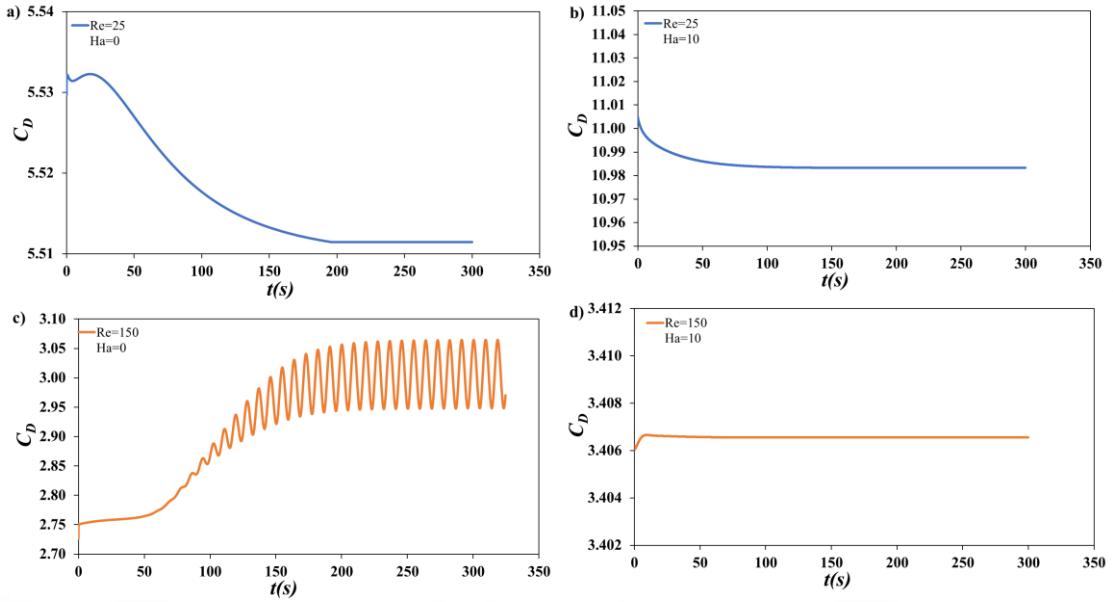

Figure 4.14. Time history of drag coefficient, C_D at *Re*=25 for a) *Ha*=0 b) *Ha*=10 and *Re*=150 for c) *Ha*=0 d) *Ha*=10

4.1.2. Heat Transfer Analysis

The change of isotherm distribution around the circular cylinder with the effect of the non-uniform magnetic field at *Re*=25, 50, 100 and 150 for Φ=0% is demonstrated in Figures 4.15-4.18. The convected heat from the heated circular cylinder is detected by constructing heat contour lines, also referred to as plume formation. As seen in Figure 4.15, the implemented magnetic field going through current-carrying wires alter the plume formation since the extent of the plume formation region gets progressively narrower with the increase in *Ha*. The isotherm lines symmetrically occur with respect to the cylinder axis independent of the non-uniform magnetic field application. Because, at *Re*=25, the flow and thermal structures around the cylindrical body are time-independent. From the isotherm plots, it is observed that when the *Ha* gets higher, the flattened or steeper temperature contours become like a wavefront structure. It is detected that the thermal boundary layer thickness progressively decreases as the *Ha* is gradually increased from *Ha*=0 to *Ha*=18 ending up with the increase in the heat transfer rate around the cylindrical body. Furthermore, the temperature gradient augments with the application of a non-uniform magnetic field since the crowding of isotherm lines gets denser over the surface of the cylinder. The reduced thickness of the thermal boundary layer and growing temperature gradient on the cylinder surface with the magnetic field application lead to an enhanced rate of heat transfer, thus an increase of the average Nusselt number, Nu_{avg} which is also clearly seen in Figure 4.22. Besides, a gathering of isotherms is detected over those regions where the flow separation does not occur and the maximum gathering is observed on the forward face of the cylinder around the front stagnation point according to incoming flow, pointing out the highest Nu_L number at the front stagnation point which is also observed from Figure 4.20 (a).

Figure 4.17 demonstrates the instantaneous isotherm contour for various Hartmann numbers, *Ha*=0, 2, 6, 10, 14 and 18 at *Re*=100 and Φ=0%. One can observe from Figure 4.17 that the isotherm contour is time-dependent at *Ha*=0 and 2 and show shedding phenomena in the wake region of the circular cylinder since the flow structure is unsteady at these values of *Ha*. As *Ha* is further increased from *Ha*=2 to *Ha*=6, the isotherm contour becomes time-independent since the flow is a steady state at *Re*=100 and *Ha*=6. The extent of the plume formation region contracts when the magnetic field intensity progressively augments from *Ha*=6 to *Ha*=18. Moreover, it is apparent that the thickness of the thermal boundary layer marginally gets thinner when the *Ha* is augmented from *Ha*=0 to *Ha*=18.

Another important conclusion that can be drawn from Fig. 4.17 is that the crowding of isotherm lines in the region close to the rear stagnation point between $-60^{o} \leq \varphi \leq 60^{o}$ gets less dense with the increase in the non-uniform magnetic field intensity, from *Ha*=0 towards *Ha*=18. It means the Nu_L attenuates with the rise in *Ha* in the region close to the rear stagnation point $-60^{o} \leq \varphi \leq 60^{o}$ because of the reduced crowding of isotherm lines in this region, which is also expressed in Figure 4.20 (b).

On the other hand, no significant variation is generally observed in the isotherm lines and temperature contours as Φ grows from Φ=0% to Φ=4% which is clear in Figure 4.19. Because the isotherm contours for *Re*=25 and Φ=0% in Figure 4.15 and for *Re*=100 and Φ=0% in Figure 4.17 is nearly the same with *Re*=25 and Φ=4% and *Re*=100 and Φ=4% cases in Figure 4.19.

As seen in Figure 4.19, increasing Reynolds numbers, *Re* result in a decrease in thermal boundary layer thicknesses regardless of whether the non-uniform magnetic field is applied or not. This situation leads to heat transfer enhancement thus the average Nusselt number, Nu_{avg} by the augmentation of *Re* as clearly shown in Figure 4.22. With increasing *Re*, the denser appearance of isotherm lines around the cylinder surface, especially in the rear stagnation point region between $-60 \leq \varphi \leq 60$ specifies the existence of great thermal gradients resulting in higher Nu_L in that zone. The reason for this situation can be explained by considering the fact that at a lower *Re*, heat is transferred overwhelmingly by means of diffusion, while at a greater *Re* the convective heat transfer becomes more dominant which results in a higher temperature gradient.

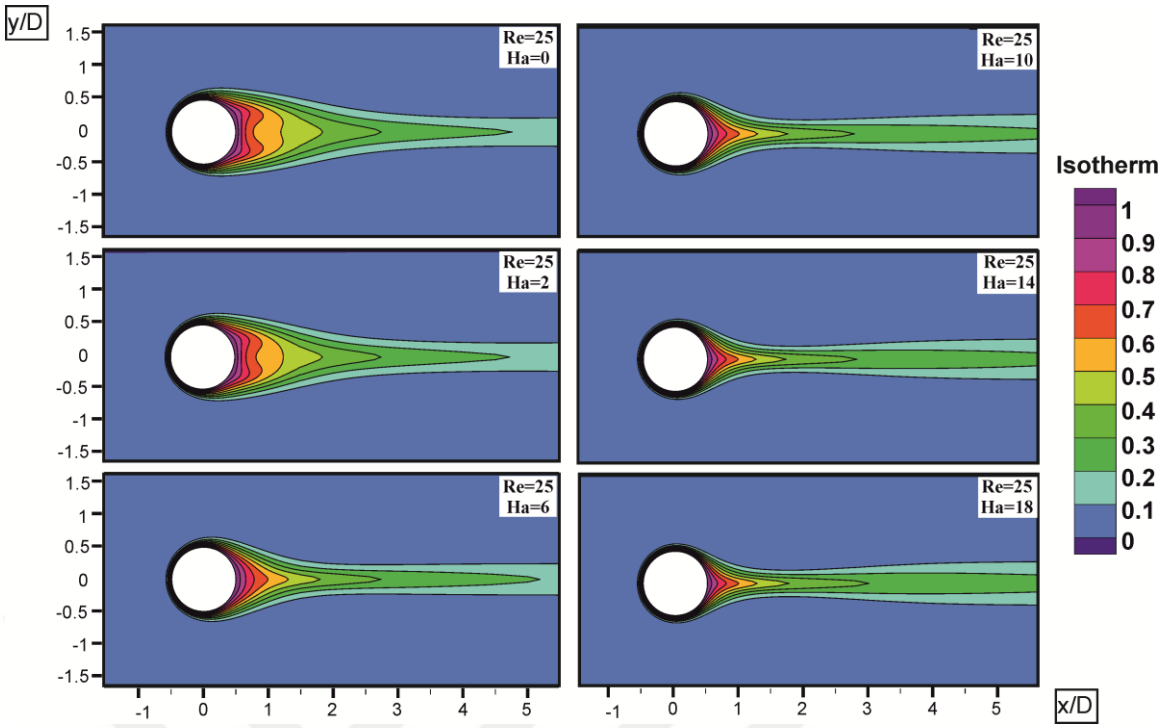

Figure 4.15. The change of isotherm distribution around the cylindrical body with non-uniform magnetic field influence at *Re*=25 and *Φ*=0%

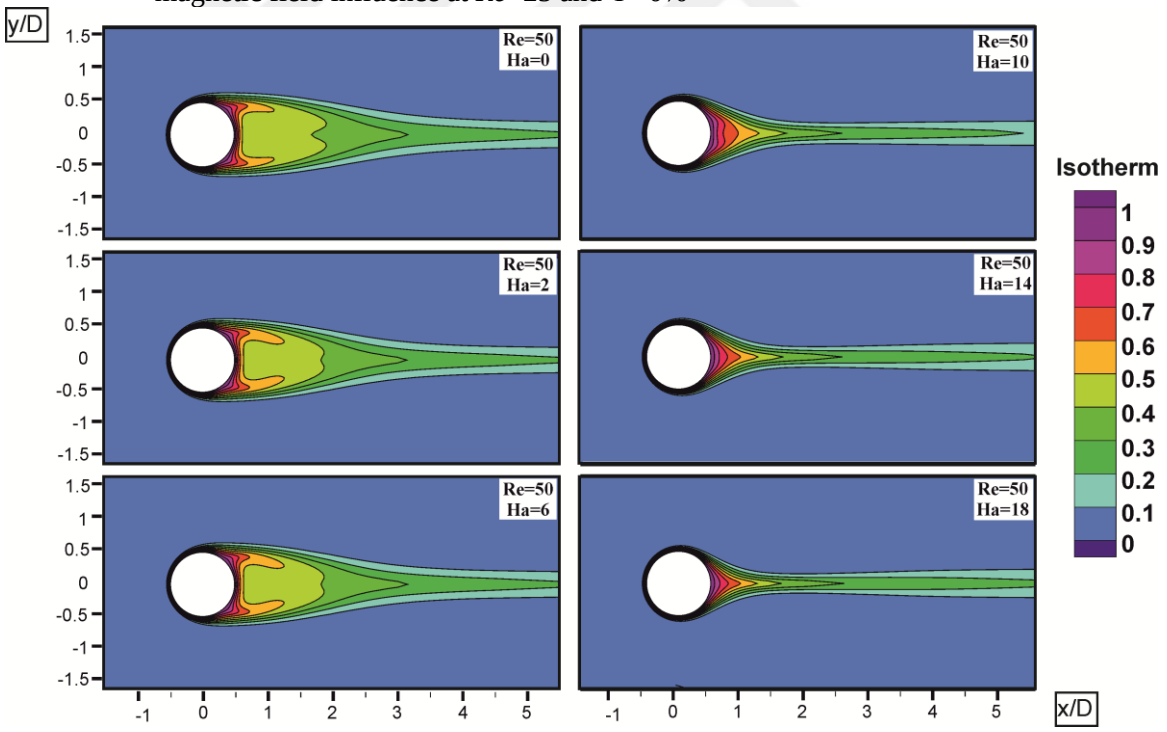

Figure 4.16. The change of isotherm distribution around the cylindrical body with non-uniform magnetic field influence at *Re*=50 and *Φ*=0%

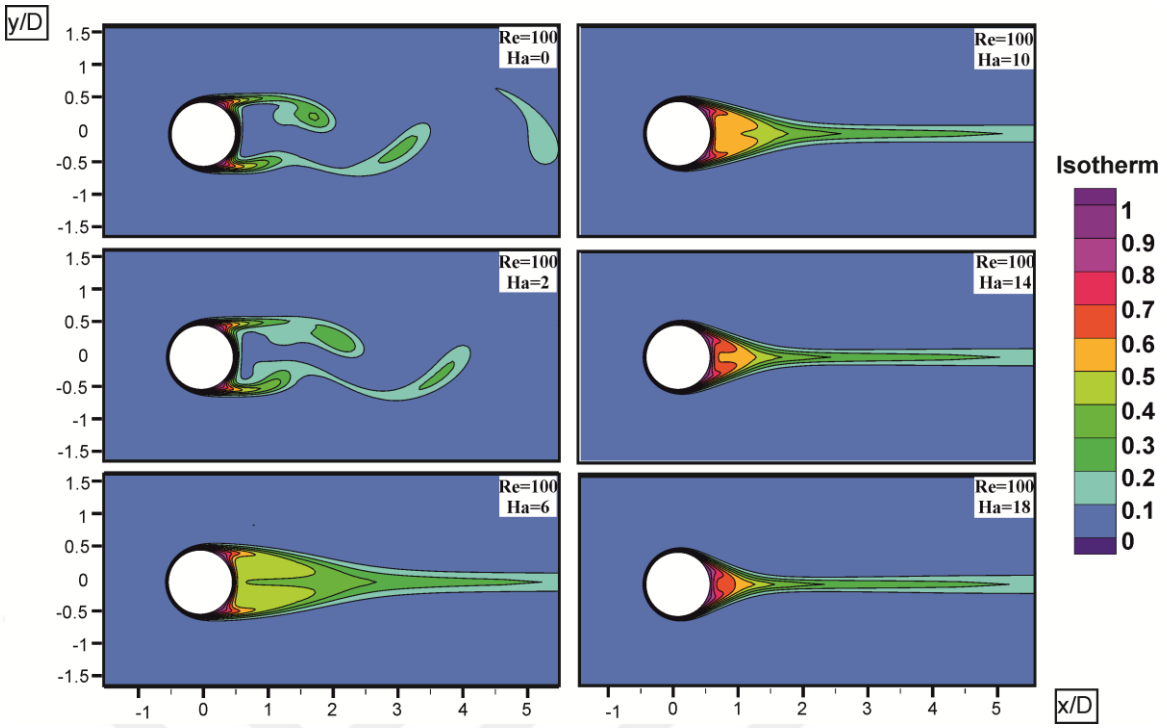

Figure 4.17. The change of isotherm distribution around the cylindrical body with non-uniform magnetic field influence at *Re*=100 and *Φ*=0%

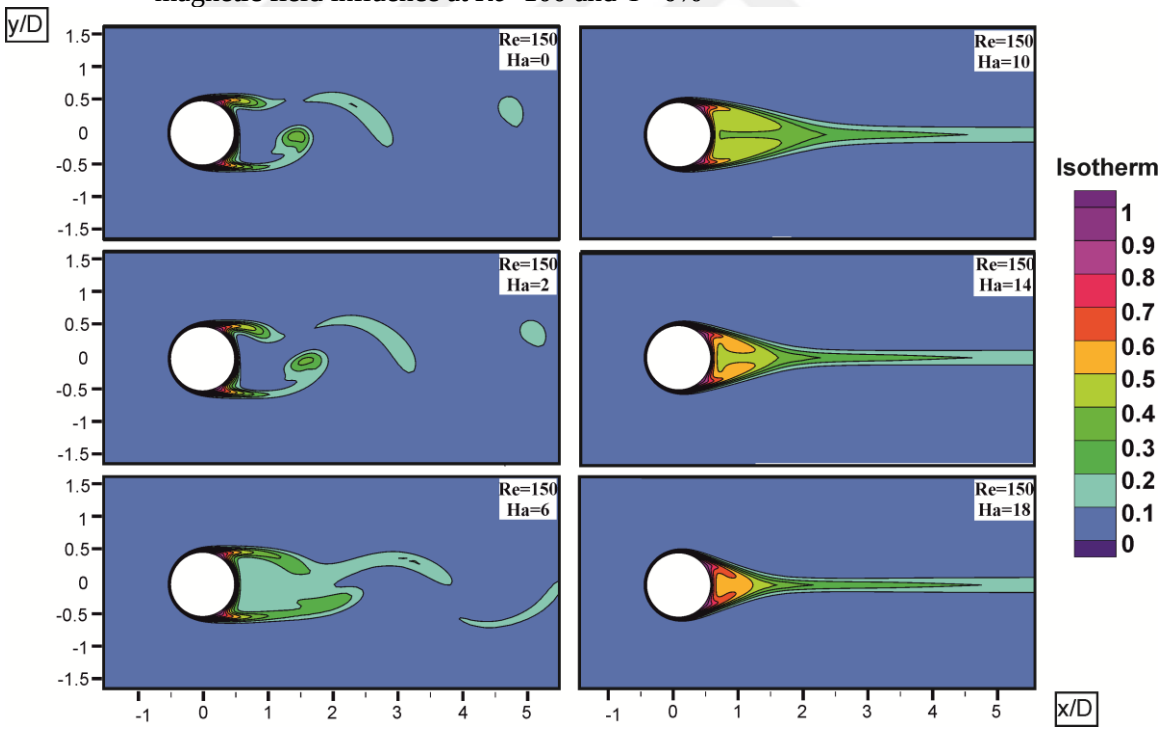

Figure 4.18. The change of isotherm distribution around the cylindrical body with non-uniform magnetic field influence at *Re*=150 and *Φ*=0%

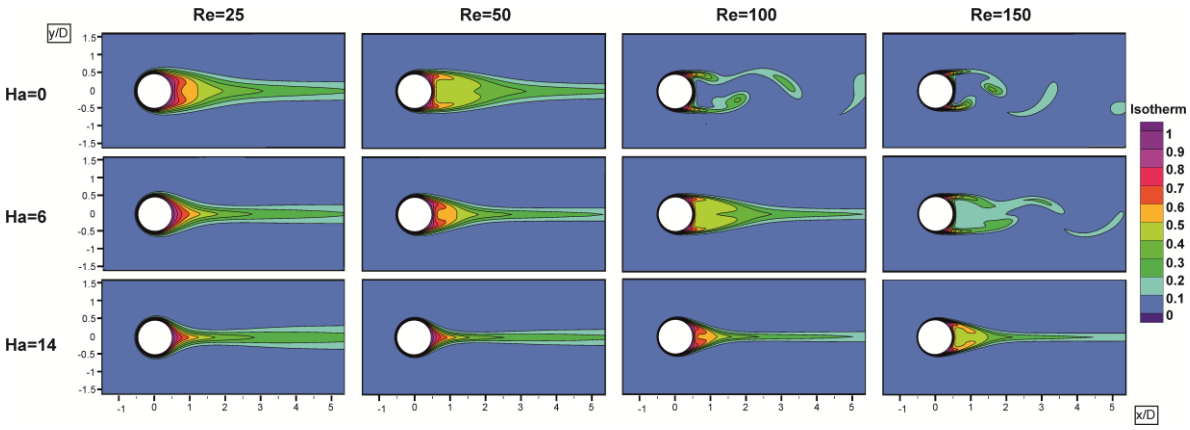

Figure 4.19. The change of isotherm distribution around the cylindrical body with non-uniform magnetic field influence at *Re*=25,50,100 and 150 for Φ=4%

Figure 4.20 (a) demonstrates the local Nusselt number, Nu_L distribution along the cylinder surface for various non-uniform magnetic field strengths, between $0 \leq Ha \leq 22$ at *Re*=25 and Φ=0%. It is apparent in Figure 4.20 (a), the Nu_L distribution along the cylinder surface is symmetric according to the cylinder axis which is demonstrated by the patterns of symmetric streamlines and vorticity distributions at *Re*=25. For the lack of magnetic field, *Ha*=0 one maxima and two equal minima are detected for the Nu_L distribution over the cylinder surface. The maximum $Nu_{L,}$ and thus the maximum heat transfer rate occurs at the front stagnation point of the cylinder (φ=180º) whereas the minimum Nu_L corresponds to the locations of fluid flow separation. Acquired outcomes show that because of the change in fluid velocity distributions with the applied magnetic field, the Nu_L distributions substantially alter over the cylinder surface. Fig. 4.20 (a) depicts that when the magnetic field passes through the current carrying wire is applied, the heat transfer profile on the cylinder surface varies substantially. As the magnetic field is employed and its strength rises from *Ha*=2 to *Ha*=18 gradually, the maximum Nu_L on the cylinder surface is reduced compared to the case of *Ha*=0. For instance, when the *Ha* grows from *Ha*=0 to *Ha*=10, the local Nusselt number deteriorates from Nu_L=14.13 to Nu_L=13.45 which corresponds to a 5% degradation in the heat transfer rate. It is apparent that the maximum Nu_L occurs at the front stagnation point, φ=180º at all values of *Ha* like no applied magnetic field case, *Ha*=0. Because, as already discussed in Figure 4.15, the maximum crowding of isotherm lines takes place on the front stagnation point, φ=180º of the cylinder which means the highest temperature gradient and thus heat transfer on this location. In regions other than around the front stagnation point between $143º \leq \varphi \leq 216º$, there is a *Nu* enhancement with the applied non-uniform magnetic field. Obtained results demonstrate that the *Nu* augments by the non-uniform magnetic field over most regions of the cylinder surface which can be attributed to the decreasing thickness of the thermal boundary layer and growing temperature gradient with the applied magnetic field which is clearly seen in Figure 4.20 (a).

According to Figure 4.20 (b), essentially there are two regions where the rate of heat transfer degrades which are in the region around the wake, $0^o \leq \varphi \leq 40^o$ and the front stagnation point of the cylinder, $130^o \leq \varphi \leq 230^o$ in the existence of the magnetic field, especially for *Ha* greater than 2. It is apparent that the Nu_L is greater in the region of $0^o \leq \varphi \leq 40^o$ at $Ha=0$ and $Ha=2$ since the flow is time-dependent and shows vortex shedding phenomena in the wake region which is clearly seen in Figures 3 and 9. The alternate shed of vortices in the wake region enhances the Nu_L by transferring heat and momentum between the core and wake flow regions. Other than these two regions, the Nu_L enhances by the application of a non-uniform magnetic field over most regions of the cylinder surface. According to the obtained results in Figure 4.20 (b), one maxima and two minima occur on the distribution of Nu_L for all cases independent of non-uniform magnetic field application. The location of maxima takes place on the front stagnation point, $\varphi=180^o$ for all cases while the position of minima corresponds to the location of flow separation and shows that the flow separation point moves in a downstream direction on the cylinder surface with the application of the non-uniform magnetic field. In other words, the non-uniform magnetic field going through current-carrying wires induces delayed flow separation on the cylinder surface.

Figures 4.21 (a), (b), and (c) demonstrates the non-uniform magnetic field impact and ferrofluid volume fraction, $\Phi=0\%$, 2% and 4% on the Nu_L distribution for $Ha=0$, 6 and 14, respectively. It is clear in Fig. 4.21 that the Nu_L distribution on the whole surface of the cylinder augments when ferrofluid volume fraction, Φ increases for all examined *Ha*. For instance, on one hand, the maximum local Nusselt numbers are observed as $Nu_L=14.13$, 13.69 and 13.26 at $Ha=0$, 6 and 14 respectively for $\Phi=0\%$, on the other hand, the Nu_L enhances to the values of $Nu_L=14.65$, 14.19 and 13.74 at $Ha=0$, 6 and 14, respectively for $\Phi=4\%$. According to the results of numerical simulation, it can be said that the Nu_L augments by 3.67% at $Ha=0$, 3.63% at $Ha=6$ and 3.64% at $Ha=14$ when the ferroparticle volume fractions increase from $\Phi=0\%$ to $\Phi=4\%$. The enhancement of Nu_L distribution on the cylinder surface with the increment in the ferrofluid volume fraction, Φ can be attributed to the mixing effect of particles near the cylinder surface, Brownian motion of particles, particle migration, aggregation, and dispersion of particles. Furthermore, Meyer et al. (2013) and Sundar et al. (2012) dependent the nanoparticle induced heat transfer enhancement to the acceleration of energy exchange processes in the fluid due to the chaotic movement of particles.

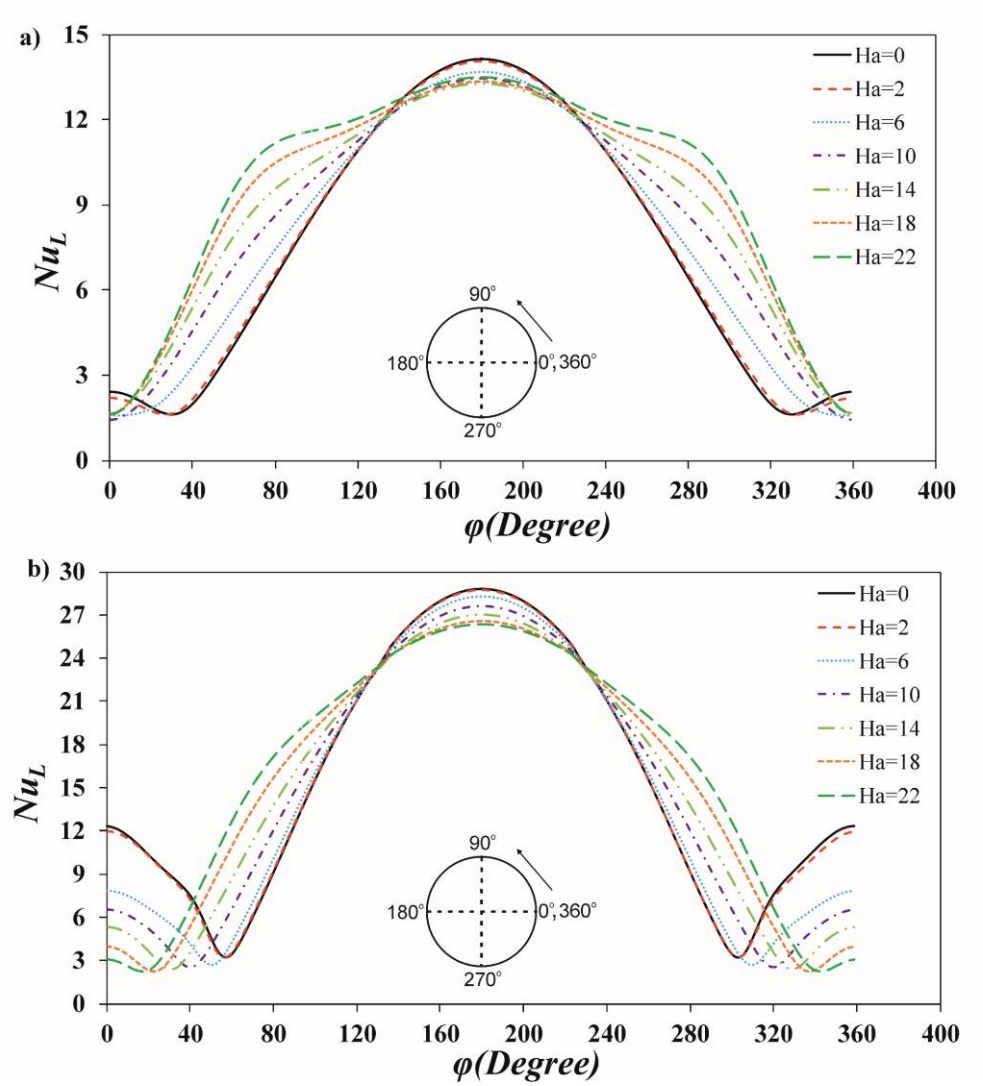

Figure 4.20. The variation of Nu_L on the cylinder surface with the magnetic field effect at Reynolds numbers, a) *Re*=25 b) *Re*=100 for *Φ*=0%

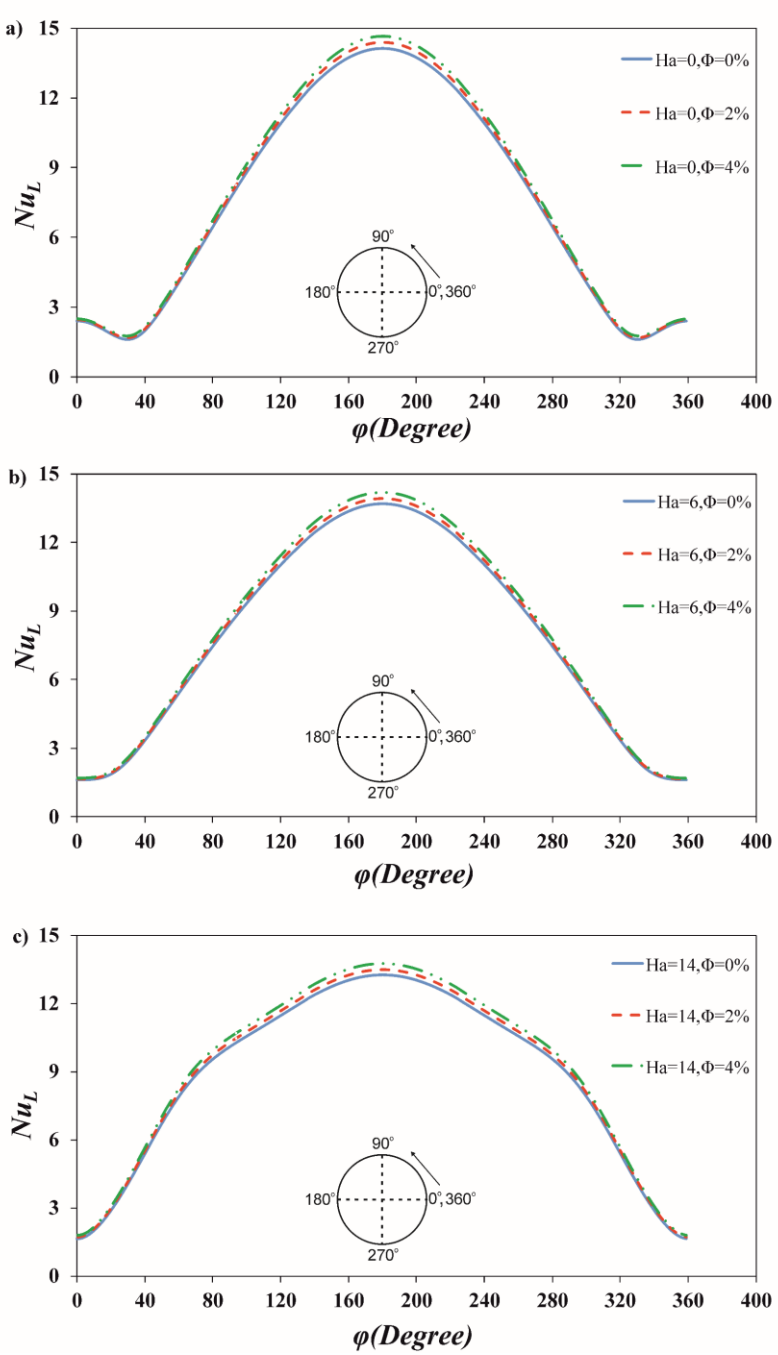

Figure 4.21. The variation of Nu_L on the cylinder surface with the magnetic field effect at Reynolds numbers, a) Re=25 b) Re=100 for Φ=0%

Figure 4.22 demonstrates the variation of Nu_{avg} with the strength of a non-uniform magnetic field at Re=25, 50, 100, and 150 for Φ=0%. On averaging the heat flux, at all points of the cylinder surface, the average Nusselt number, Nu_{avg} is obtained as given in Equation 3.16. The change of Nu_{avg} demonstrates different behavior at different Re and Ha since the flow and temperature fields have different distributions depending on Re and Ha numbers. Obtained results demonstrate that in steady flow cases at Re= 25 and 50, the Nu_{avg} shows monotonic behavior with Ha and it enhances as the strength of the non-uniform magnetic field intensifies. For instance,

when the average Nusselt number is detected as Nu_{avg}= 7.637 for the absence of non-uniform magnetic field, *Ha*=0 it augments to values of Nu_{avg}=8.532 and 9.414 for *Ha*=10 and 18, respectively at *Re*=25. On the other hand, at *Re*=50, while the average Nusselt number is observed as, Nu_{avg}=10.52 at *Ha*=0, there is a marginal increment in heat transfer by observing the average Nusselt number as Nu_{avg}=10.886 and 11.996, respectively when *Ha* is increased from *Ha*=0 to *Ha*=10 then *Ha*=18. According to the results of the numerical simulations for the variation of Nu_{avg} it can be said that the Nu_{avg} enhancement is in the vicinity of 11.71% at *Ha*=10 and 23.26% at *Ha*=18 for *Re*=25, and 3.47% at *Ha*=10 and 13.74% at *Ha*=18 for *Re*=50 compared to the absence of non-uniform magnetic field application. This result can be expressed by considering that the thermal boundary layer thickness gets thinner and the temperature gradient enhances with the magnetic field application at *Re*=25 which is apparent in Figure 4.15. Furthermore, the heat transfer augmentation with the employment of a magnetic field can be dependent on the formation of two-symmetrical vortices in the channel close to the region where the non-uniform magnetic field is employed. In addition, one can infer by analyzing Figure 4.22 that the Nu_{avg} augmentation deteriorates in the time-independent flow region by increasing Reynolds numbers, from *Re*=25 to *Re*=50. According to Figure 4.22, the non-monotonic behavior of Nu_{avg} with the intensity of a non-uniform magnetic field is detected at *Re*=100 and 150. As the Hartman number, *Ha* increases, the degradation of heat transfer is observed up to *Ha*=6, but beyond which there is an increase in the Nu_{avg}. This outcome can be indicated by regarding that the flow structure is time-dependent at *Ha*=0 and 2 for *Re*=100 and at *Ha*=0, 2, and 6 for *Re*=150. The alternate shed of vortices from the upper and lower side of the cylinder in the unsteady flow regime enhances the heat transfer mechanism since these vortices transport mass, heat and momentum in the other points of the flow region. In the time-dependent flow regime, the strength of vortex shedding diminishes with the applied non-uniform magnetic field thus the Nu_{avg} reduces. However, when the flow becomes a steady state, the further increase in Hartmann number, *Ha*>6 makes the Nu_{avg} to be enhanced. The findings show that at *Re*=100 when *Ha* grows from *Ha*=0 to *Ha*=22, the average Nusselt number enhances from Nu_{avg}=15.44 to Nu_{avg}=15.933 which corresponds to 3.2% heat transfer enhancement. Because, as previously explained in Figure 4.20 (b), at *Ha*=22, the decrease of Nu_L in the front stagnation point and wake regions is smaller than the increasing rate of the Nu_L in most regions of the cylinder surface except these two regions compared to *Ha*=0. It should be noted that the employment of a magnetic field does not have a considerable influence on Nu_{avg} at *Re*=100 and 150 compared to *Re*=25 and 50. Because the ferrofluid passes over the wire with a greater velocity and the time that ferrofluid particles are affected by the non-uniform magnetic field is attenuated with the growth of *Re*. According to the obtained results, it is interpreted that the application of low *Re* and high *Ha* enables to achieve a better heat transfer improvement. The results demonstrate that Nu_{avg} enhances as the *Re* number gets higher. For instance, according to Figure 4.22, the average Nusselt number is detected as Nu_{avg}=10.52 and 12.476 at *Re*=50 for *Ha*=0 and 22 respectively, on

the other hand, it is increased to the values of Nu_{avg}=18.69 and 18.42 at *Re*=150 for *Ha*=0 and 22, respectively. So, it percentage increases correspond to 77.66% and 47.64% at *Ha*=0 and 22, respectively, when the Reynolds number increases from *Re*=50 to *Re*=150. It is clear that the application of a non-uniform magnetic field deteriorates the heat transfer augmentation due to an increase in *Re* since the Nu_{avg} considerably enhances at low Reynolds numbers, for example, *Re*=25 and 50, and is not significantly affected at higher *Re*, *Re*=100 and 150 by the application of the non-uniform magnetic field. The improvement in Nu_{avg} due to the rise in *Re* can be related to the higher fluid velocity and rate of convection heat transfer. The convective transport mechanism augments for the higher fluid velocities, especially in the improvement of the local fluid velocity around the cylindrical body. In addition, as depicted before in Figure 4.19, the thickness of the thermal boundary layer gets thinner with increasing *Re* which causes the temperature gradient on the cylinder surface to increase leading the Nu_{avg} to enhance.

In Figure 4.23, as expected, adding Fe_3O_4 nanoparticles into the water with volume fractions, Φ=2% and 4% makes the Nu_{avg} to be enhanced at *Re*=25 and 100 for all considered *Ha*. According to the outcomes of numerical simulation, there is an increase in Nu_{avg} with 3.98% and 3.88% for *Ha*=2 and 18 respectively when Φ increases from Φ=0% to Φ=4% at *Re*=25. The heat transfer augmentation with ferrofluid fraction is also valid at *Re*=100. The Nu_{avg} enhancement with increasing ferrofluid volume fraction, Φ. The Nu_{avg} enhancement with increasing Φ is attributed to the increase in the thermal conductivity, *k* of the working fluid. An increase in *k* of the working fluid results in higher heat transfer from the cylinder surface in the channel and consequent higher heat transfer coefficient, *h* and Nu_{avg}. The increasing rate of the convection heat transfer rate, *h* is greater than the increasing rate of thermal conductivity of the ferrofluid, *k* which enhances the heat transfer mechanism further.

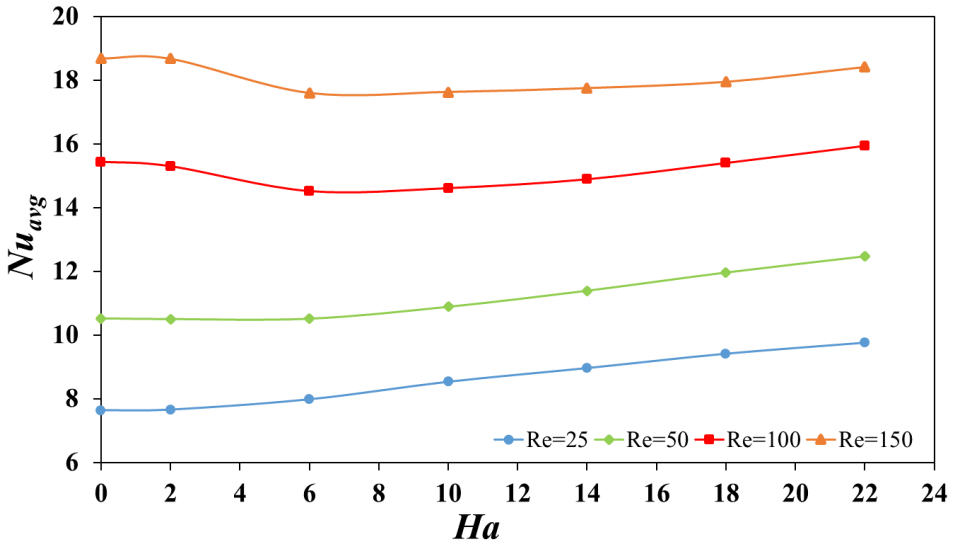

Figure 4.22. The non-uniform magnetic field effect on Nu_{avg} at *Re*=25, 50, 100 and 150 and the for Φ =0%

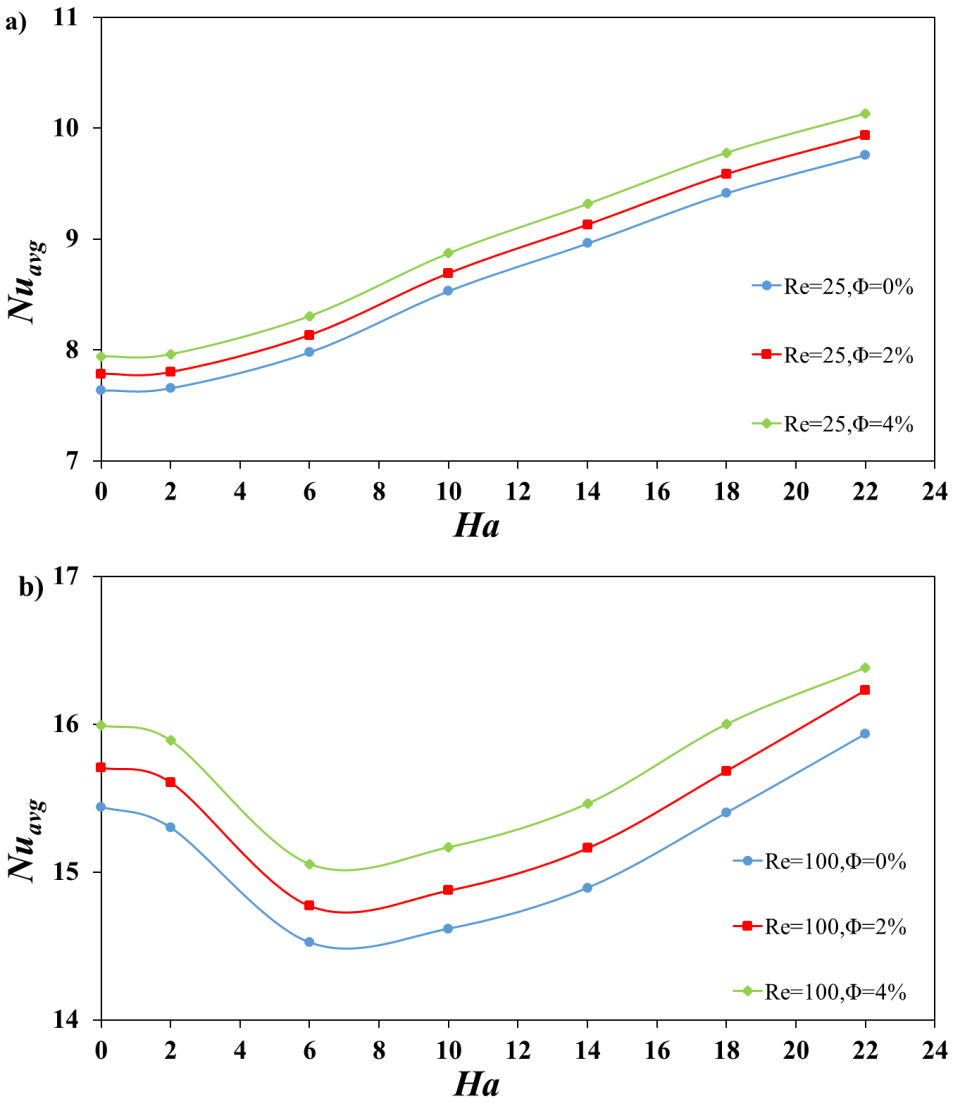

Figure 4.23. The influences of *Ha* and Φ on Nu_{avg} at Reynolds numbers a) *Re*=25 b) *Re*=100 for the ferrofluid volume fractions Φ=0%, 2% and 4%

4.1.3. Entropy Analysis

Figures 4.24-4.27 display the magnetic field effect on the local distribution of the total entropy generation, S_L at Reynolds numbers, *Re*=25, 50, 100 and 150, respectively for Φ=0%. As shown by the contour lines and color scale of data, the high levels of total entropy generation, S_L are concentrated around the stationary heated cylinder with a nearly symmetrical arrangement, while the lower level (almost zero) of blue color covers the remaining regions of the considered channel. The main reason for this distribution is related to the high gradient values of both temperature and velocity around the heated cylinder. In addition, the magnitude of the total entropy generation, S_L is also small on the right-hand side of the cylinder due to the relatively low value of the temperature gradient that formed on this side of the cylinder, as shown in Figures 4.15-4.19. On the contrary, the maximum values of the total entropy generation, S_L are accumulated on the opposite side of the cylinder. The result of these figures exhibits that augmenting *Re* reduces the

thickness of the entropy generation that formed around the cylinder and increases the maximum value of the total entropy generation. However, it can be stated that increasing the Hartmann number, *Ha* affects the high levels zone of entropy generation by relatively extending this zone towards the downstream of the channel and covering more area around the cylinder as well as reducing the maximum value of the total entropy production, S_L.

The maximum value of the local total entropy production is documented in Table 4.1 for various *Ha*, *Re* and Φ. It is apparent in Figures 4.24-4.27 that the maximum value of entropy production is located at the front stagnation point of the heated cylinder. Generally, the outcomes revealed that the maximum value of entropy generation grows significantly with increasing *Re* and relatively decreases with augmenting both *Ha* and Φ. This is due to the distortion of isotherms at the front stagnation point of the cylinder with growing *Re* and accordingly leads to maximum improvement in convective heat transfer at this point (as shown in Figures 4.20 and 4.21) and a maximum value of the temperature gradient. Accordingly, it can be reported that the entropy production relies on the proportional contributions of the studied parameters (i.e., *Re*, *Ha* and Φ) as mentioned above.

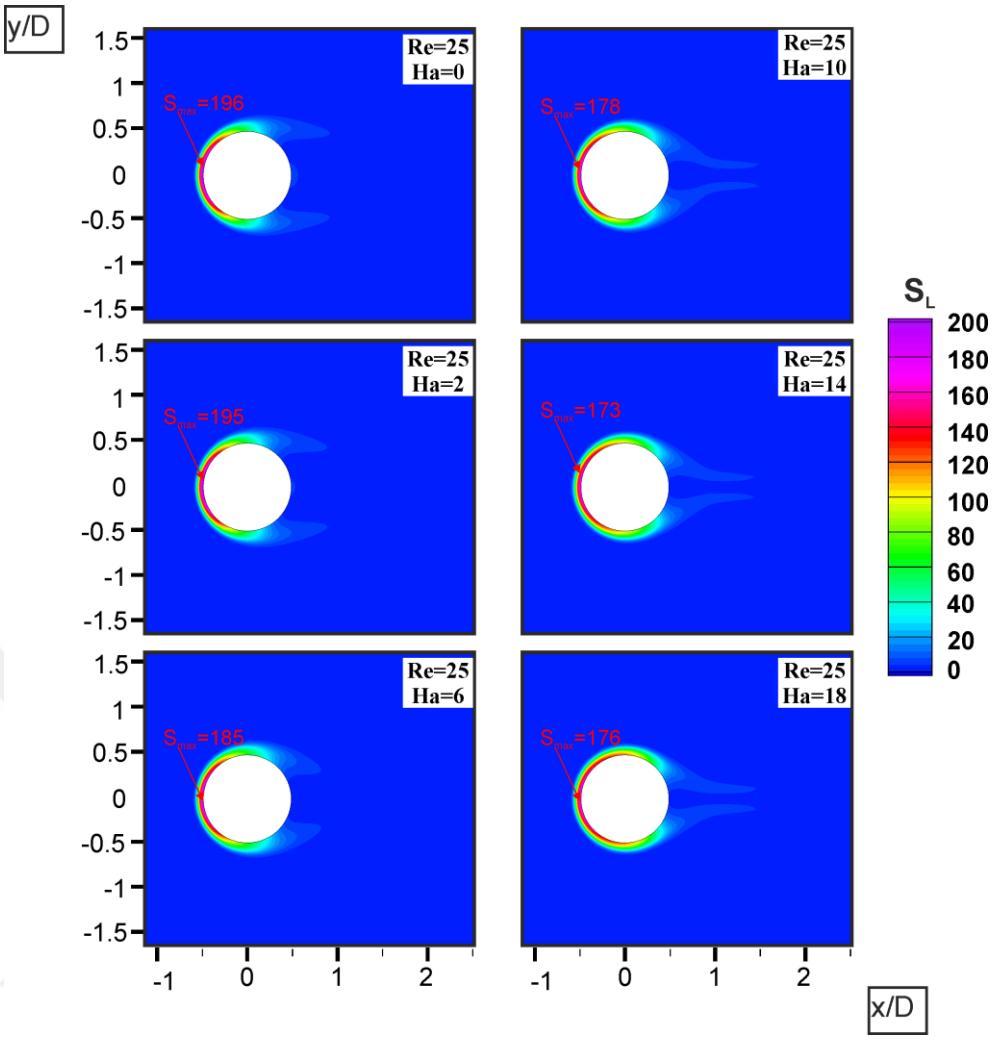

Figure 4.24. The magnetic field effect on the local total entropy generation, S_L at Re=25 for Φ=0%

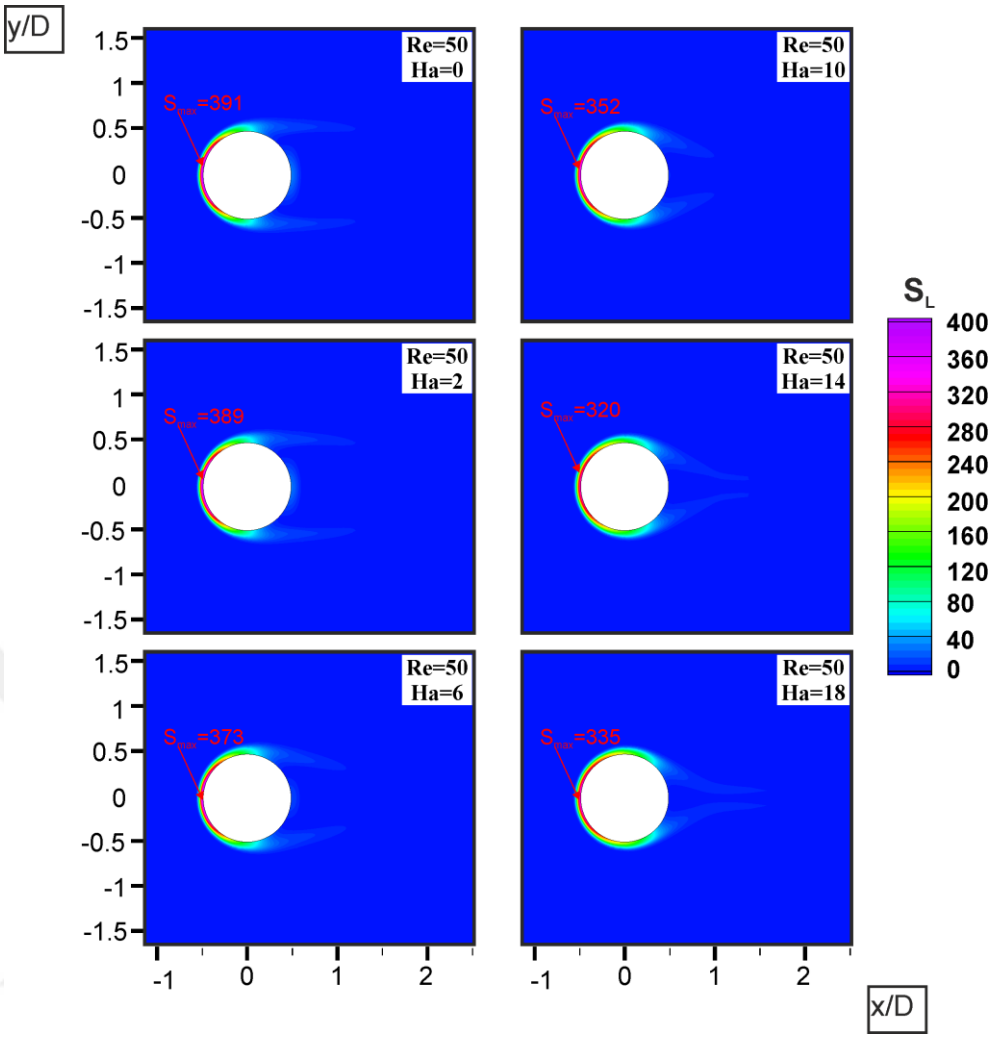

Figure 4.25. The magnetic field effect on the local total entropy generation, S_L at Re=50 for Φ=0%

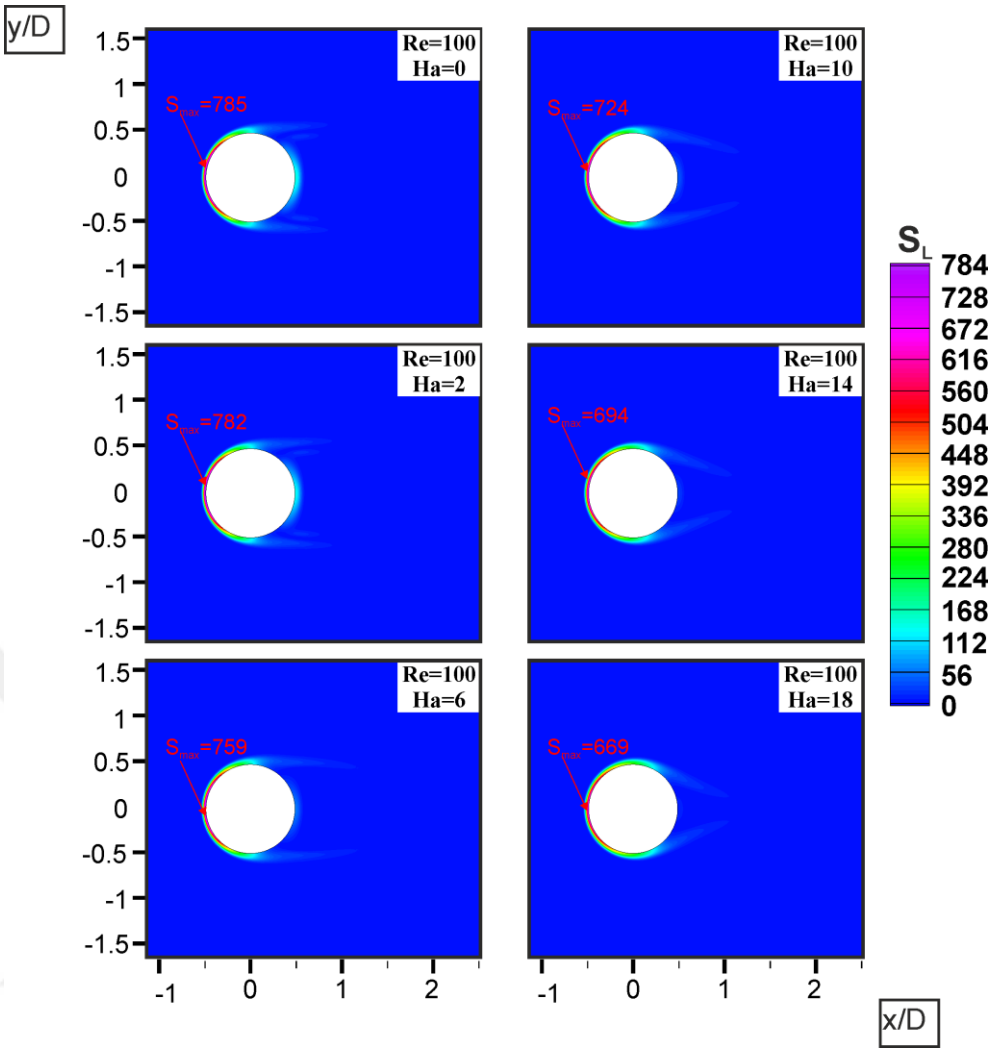

Figure 4.26. The magnetic field effect on the local total entropy generation, S_L at Re=100 for Φ=0%

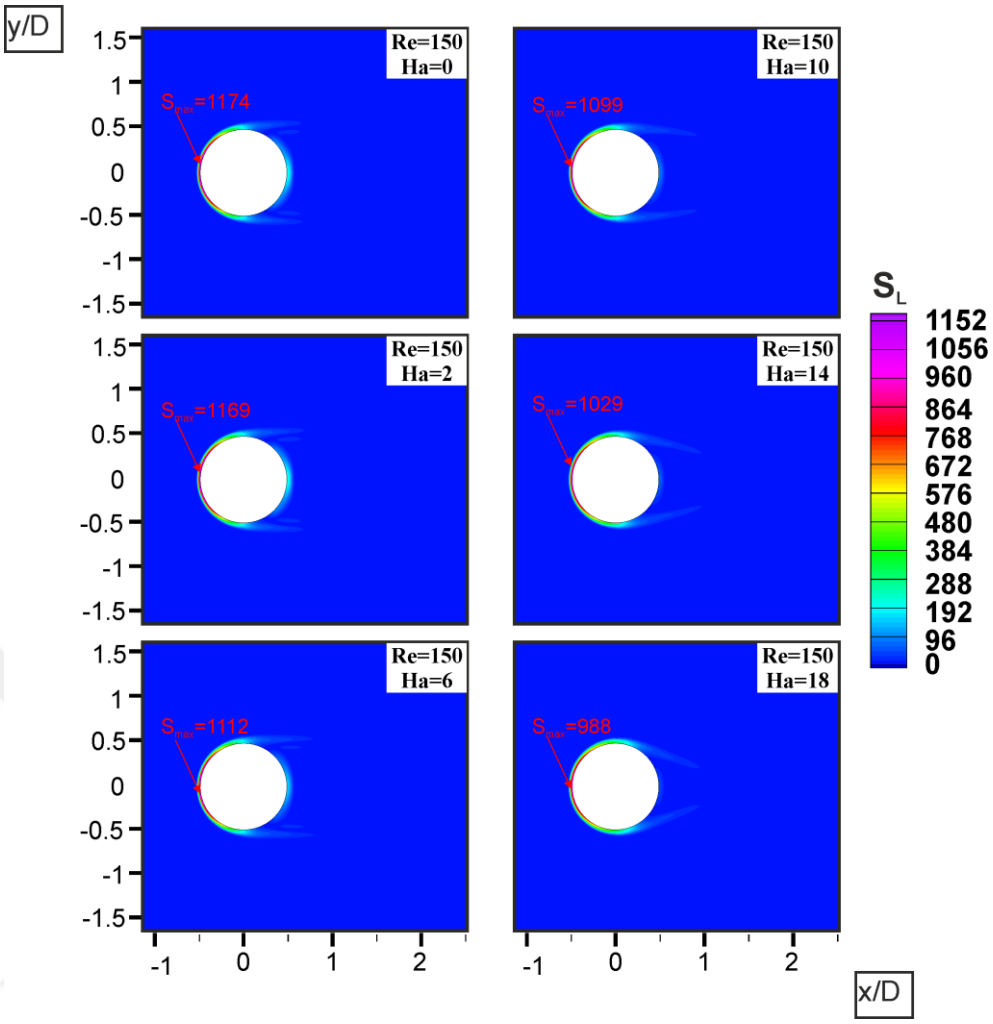

Figure 4.27. The magnetic field effect on the local total entropy generation, S_L at *Re*=150 for Φ=0%

Table 4.1. The influences of magnetic field intensity and ferrofluid volume fraction, Φ on the maximum value of local total entropy generation, S_{max} at *Re*=25, 50, 100, and 150 for Hartmann numbers, *Ha*=0, 6 and 14

	Φ=0%			Φ=2%			Φ=4%		
	Ha=0	Ha=6	Ha=14	Ha=0	Ha=6	Ha=14	Ha=0	Ha=6	Ha=14
Re=25	196	185	173	186	175	164	177	166	156
Re=50	391	373	320	370	352	320	364	342	318
Re=100	785	759	694	743	718	656	706	683	624
Re=150	1174	1112	1029	1115	1084	1005	1045	1019	978

Figures 4.28-4.31 portray the effect of the non-uniform magnetic field on the local distribution of the Bejan number, Be_L at Reynolds numbers, Re=25, 50, 100 and 150, respectively for Φ=0%. As a reminder, from a thermodynamic point of view, the Bejan number represents the percentage of thermal irreversibility to the total irreversibility produced by the flow process. Thus, for $Be_L \geq 0.5$, the thermal entropy dominates the flow and for $Be_L \leq 0.5$ the frictional entropy dominates the flow. As shown, the local Bejan number, Be_L distribution has an almost symmetrical arrangement around the heated cylinder. Note, that thermal irreversibility is the main concept around the cylinder and the zone behind it, which extends along the flow direction of the channel. The reason for this is the increase in the thickness of the thermal boundary layer within this region, as shown in Figures 4.15-4.19. Despite this, frictional irreversibility prevails at the channel inlet and near its walls, where there is a developing flow and there is no heat source. In the absence of a magnetic source, Ha = 0 the change in Re has little impact on the thermal irreversibility zone, while this impact increases relatively as the intensity of the magnetic wire source is increased. For a constant Re, as the Ha raises, the region of significant thermal entropy intensity behind the heated cylinder diminishes, especially for Re=150. This indicates that the wire magnetic source produces low irreversibility and reduces irreversibility due to thermal and frictional impacts by directly affecting both thermal transmission and fluid flow through the channel.

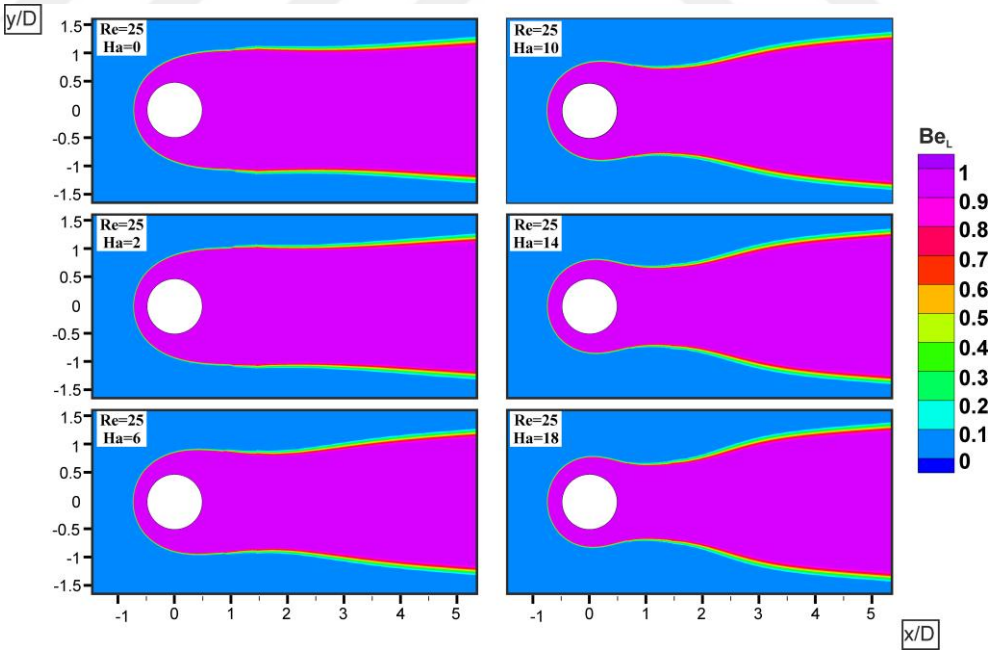

Figure 4.28. The influence of non-uniform magnetic field on the local Bejan number, Be_L at Reynolds numbers, Re=25 for the volume fraction of, Φ =0%

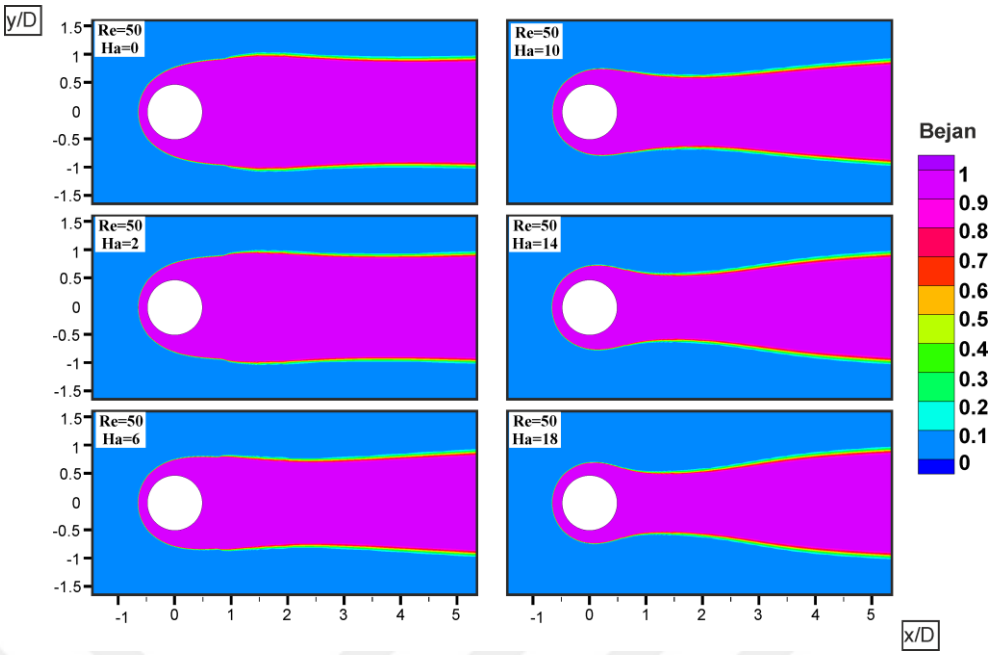

Figure 4.29. The influence of non-uniform magnetic field on the local Bejan number, Be_L at Reynolds numbers, Re=50 for the volume fraction of, Φ =0%

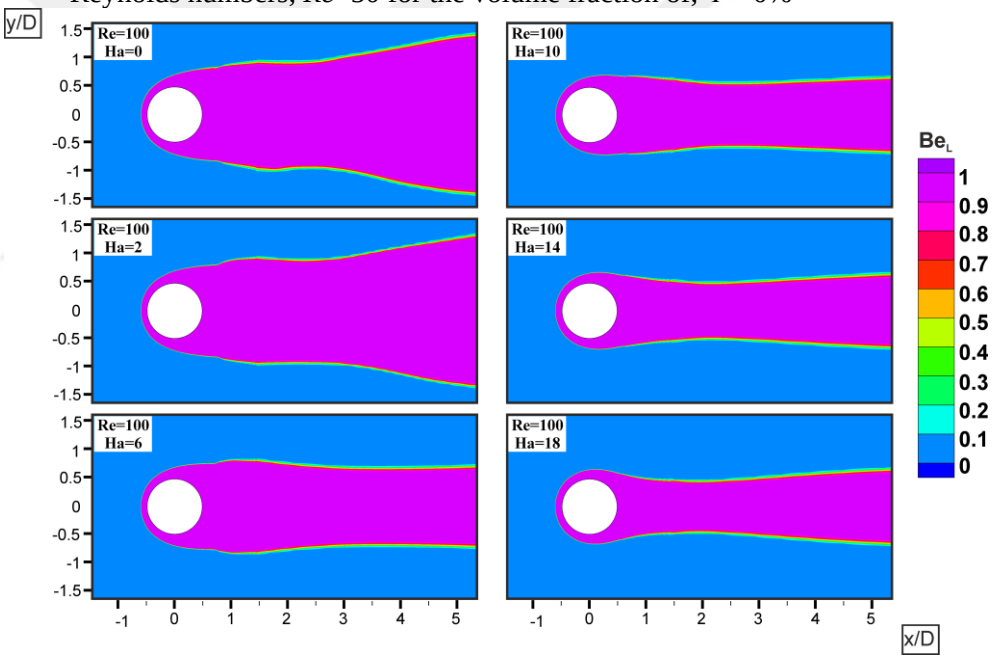

Figure 4.30. The influence of non-uniform magnetic field on the local Bejan number, Be_L at Reynolds numbers, Re=100 for the volume fraction of, Φ =0%

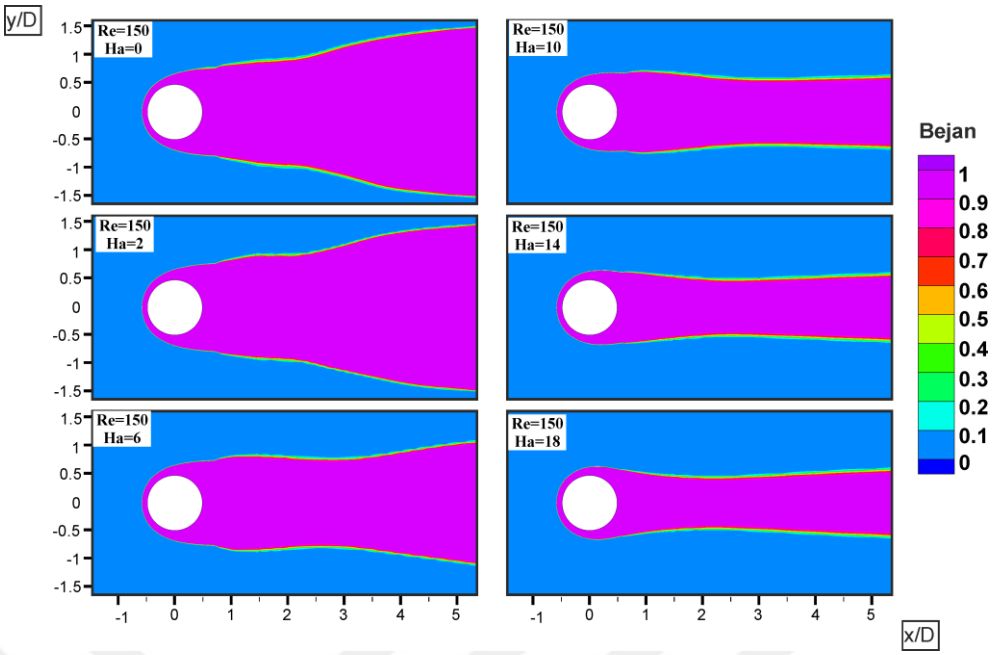

Figure 4.31. The influence of non-uniform magnetic field on the local Bejan number, Be_L at Reynolds numbers, Re=150 for the volume fraction of, Φ =0%

Examination of the quantitative data offered in Figures 4.32 and 4.33 gives valuable details about the energy transport and irreversibility process from the considered physical problem, which is useful from a thermodynamic and design perspective. The findings of related parameters such as total average entropy generation, S_{ave} average Bejan number, Be_{avg} and thermal performance criterion, ξ are presented in Figure 4.32 (a-c), respectively for the considered values of Reynolds, Re and Hartman numbers, Ha for ferrofluid flow at Φ=0%. For a fixed intensity of the magnetic source, Figure 4.32 (a) revealed that the total entropy production, S_L rises significantly with increasing Re. For example, it is noted that the amount of generated entropy increased by almost 84% by changing the Reynolds number from Re=25 to Re=150 at Ha=22. In addition, this increase was approximately 117% when no wire magnet source is present (Ha=0). This is due to the fact that an augmentation in Re induces an increase in velocity gradients within the flow domain of working fluid and, therefore, leads to additional production of frictional entropy. Regarding the change in the value of the magnetic source, it can be noted that there is a slight change in the total entropy production, S_L for a given value of Re. For example, the maximum increment of about 26% was recorded by changing the Hartmann number from Ha=0 to Ha=22 for Re=25. This leads us to the fact that the entropy produced by applying a magnetic field is small compared to the entropy produced by thermal and frictional impacts. This is due to the limitation of the effect of the local magnetic field on the area that lies behind the fixed cylinder and whose intensity is close to the channel walls. This makes sense when the presented figures of the streamline distributions are examined (Figures 4.1-4.5), which show that the application of a magnetic source causes significant changes in these distributions near the channel walls. The curvature of total entropy

generation, S_L has the same trend for *Re*=100 and 150 between *Ha*=0 to *Ha*=22. For these values of the Reynolds number, *Re* it is noted that the slope changes slightly with enhancing the magnetic field strength, while a distinct increase in slope begins for *Ha*>14. The reason for this is due to the fact that the higher strength of the magnetic field has a direct influence on the temperature distribution and subsequently causes an increase in thermal irreversibility. Accordingly, it can be inferred that within the considered range of Reynolds, *Re* and Hartmann numbers, *Ha* the Reynolds number, *Re* has more impact on the generation of the total entropy. It should be noted that for Be_{avg}>0.5, the flow through the channel prevails by thermal irreversibility, while for Be_{avg}<0.5 it means that the flow prevails by viscous reversibility. Figure 4.32 (b) reveals that the behaviors of the average Bejan number, Be_{avg} for low Reynolds numbers of *Re*=25 and *Re*=50 show the same trends along with the corresponding values of *Ha*. For these *Re,* it is observed that the Bejan value is not impacted significantly by changing the strength of the applied magnetic field. Where thermal and frictional irreversibilities remain the main source of entropy production for *Re*=25 and *Re*=50, respectively. This is because the thickness of the thermal boundary layer around the heated cylinder is slightly affected by changing magnetic field strength compared to *Re*=100 and 150. In the absence of an applied magnetic field, *Ha*=0, the thermal impact is a significant cause of irreversibility generation within the flow domain for all values of Reynolds number except *Re*=50. Since Be_{avg}<0.5 for *Re*=50, that denotes the entropy production is predominated by the frictional irreversibility. The deviations in average Bejan number, Be_{avg} with the strength of magnetic source exhibit a unique trend for *Re*=100 and 150. Where there is a sharp drop in Be_{avg} from the predominance of thermal irreversibility to the predominance of frictional irreversibility for *Ha*>2. For example, 200% and 300% decrements in Be_{avg} are reported for *Re*=150 and 100, respectively within the considered values of *Ha*. As presented in Figure 4.22, the rate of energy transport enhances with an augment in *Re*. Therefore, this tends to make the temperature gradients more incremental within the fluid flow region and, as a result, causes a reduction in heat transfer irreversibility. Figure 4.32 (c) investigates the heat transfer performance of the considered channel by applying Equation 3.32, which represents the criterion of thermal performance. As the Reynolds number, *Re* increases, the magnitude of ξ reduces, showing an augment in the thermal performance of the channel. Therefore, for a given value of *Ha*, *Re*=150 always offers the best thermal performance corresponding to the lower value of ξ. For *Re*=20 and *Re*=50, the magnitude of the thermal criterion, ξ is unaffected by changing the intensity of the magnetic field, while a significant change in this criterion is indicated for *Re*=150 and *Re*=100. For example, about 8% and 7% increments in thermal criterion, ξ are detected for *Re*=150 and *Re*=100, respectively at Hartmann numbers between *Ha*=0 and *Ha*=22. The optimum thermal performance criterion, ξ according to the highest rate of thermal transmission and the lowest production of irreversibility, is discovered for *Re*=150 and *Ha*=0.

The findings of related parameters such as S_{ave}, Be_{avg} and ξ are illustrated in Figure 4.33 (a-c), respectively for the considered values of Hartman numbers, *Ha* and ferrofluid volume concentrations, Φ for *Re*=25. As shown in Figure 4.33 (a), increasing the concentration of Fe_3O_4 nanoparticles gives a reduction in the total average entropy production, S_{ave} for a given value of the Hartmann number, *Ha*. Note that these reductions are almost constant along the considered range of the magnetic field intensity. Figure 4.33 (b) demonstrates that the dominance of thermal irreversibility along the flow field boosts by increasing the concentration of ferro-nanoparticles, Φ that is added to the base fluid for all the values of the *Ha*. For $Ha<10$, the total average entropy production, S_{ave} shows a decreasing trend for all volume fraction, Φ values. Nevertheless, there is an opposite behavior of the total average entropy production, S_{ave} for $Ha>10$. Consequently, the total average entropy production, S_{ave} has the lowest value at $Ha=10$ for all the presented volume fractions, Φ, and this particular Hartmann number, *Ha* represents the optimal value from the thermodynamics perspective. As a result, the contribution of the volume fraction, Φ in raising *S* is related to the strength of the magnetic source. As indicated in Figure 4.33 (c), the thermal criterion, ξ has decreased markedly by increasing the concentration of ferro-nanoparticles, Φ for all Hartmann number, *Ha* values. Eventually, the optimal thermal performance criterion, ξ in relation to the appropriate concentration of nanoparticles mixed with pure fluid is found for $\Phi=4\%$ and $Ha=22$.

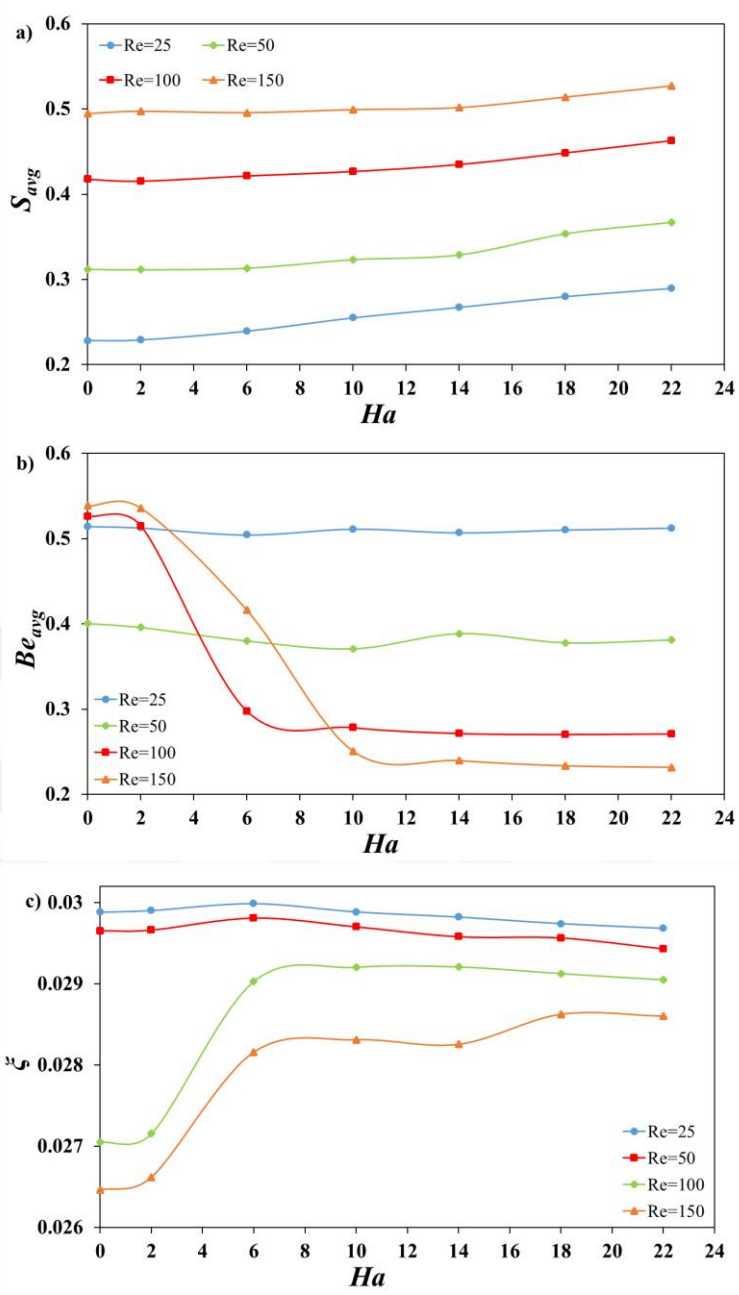

Figure 4.32. The non-uniform magnetic field influence on a) the total average entropy generation, S_{avg} b) the average Bejan number, Be_{avg} c) the thermal performance criterion, ξ at Re=25, 50, 100, 150 for Φ=0%

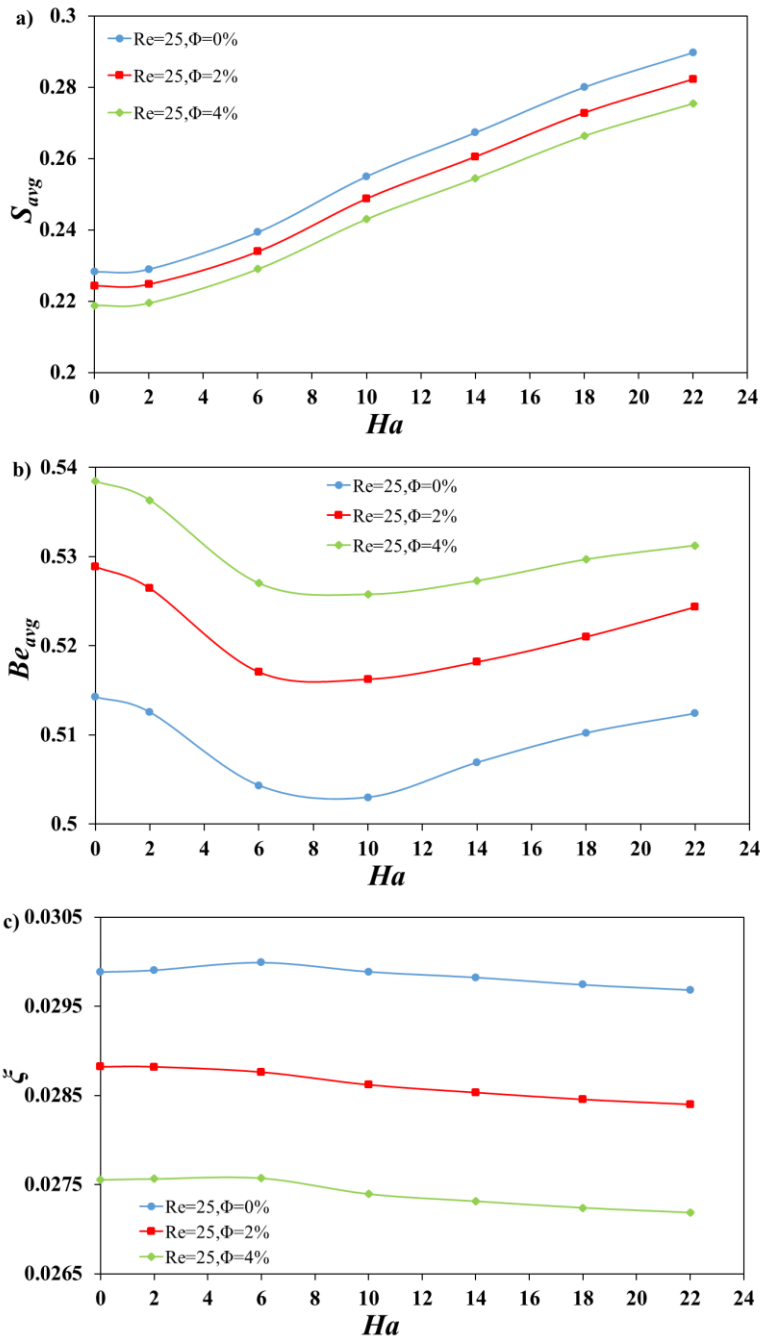

Figure 4.33. The impact of non-uniform magnetic field and the ferrofluid volume fraction, Φ on the a) S_{avg} b) Be_{avg} c) ξ at Re=25 for Φ=0, 2 and 4%

4.2. Effect of Uniform Magnetic Field on Hydrothermal and Entropy Generation Characteristics of Nanofluid Flow in a Rectangular Grooved Channel

4.2.1. Flow Pattern and Thermal Analysis

Figures 4.34-4.36 show the influence of the magnetic field on the time-averaged streamline patterns in the rectangular grooved channel at Re=250,750 and 1250, respectively for Φ=3%. Obtained results demonstrated that applying a uniform magnetic field with different intensities induces major changes in the streamline patterns. In Figure 4.34, it can be seen that when the

Hartmann number, *Ha* increases from *Ha*=0 towards *Ha*=24 progressively the extent of the recirculation region in the rectangular grooves diminishes. At *Re*=250, although the recirculation region is not completely suppressed, it is restricted to a very small region in rectangular grooves for *Ha*=16 and *Ha*=24. The separated flow region in the rectangular grooves is the smallest for *Ha*=24. According to Figure 4.34, the recirculation region does not cover the whole gap in rectangular grooves at *Re*=250 and *Ha*=0 since the Reynolds number, *Re* is not great enough and the low-pressure regions are small which causes the occurrence of small recirculation in rectangular grooves. But, in Figure 4.36, one can observe that the recirculation region occupies the whole gap in the rectangular groove, at *Re*=1250 and *Ha*=0 due to the increased inertia force at a higher Reynolds number, *Re*. Figure 4.36 depicts that when the Hartmann number, *Ha* enhances from *Ha*=0 to *Ha*=8, no considerable change is detected in the streamline patterns and the recirculation region covers the whole gap in the rectangular groove similar to the case of *Ha*=0 at *Re*=1250. But the further increment in Hartmann number to *Ha*=16 and then *Ha*=24 leads to the suppression of recirculation region in the grooves which let the flow penetrate the groove and leave the groove without rotation. It should be noted that the amount of flow penetrated the rectangular groove is higher at *Ha*=24 compared to *Ha*=16. So it is apparent that the flow rate will be increased near the corrugated walls with increasing Hartmann number, *Ha*. The one of main observations from Figures 4.34 and 4.36 is that the required Hartmann number for the beginning of recirculation region suppression increases with the rise in Reynolds number, *Re*. Because the extent of the recirculation region in the rectangular groove attenuates when the Hartmann number grows from *Ha*=0 to *Ha*=8 at *Re*=250 while there is almost no change in streamline pattern with increasing Hartmann number from *Ha*=0 to *Ha*=8 at *Re*=1250. At high Reynolds numbers, *Re* due to the strong inertia effect of main-stream flow, the uniform magnetic field has less influence on the flow characteristics in the rectangular grooved channel than at smaller Reynolds numbers, *Re*.

The uniform magnetic field in a nanofluid flow produces a resistive force which is described as a Lorentz force and this force is influential on a fluid carrying current density in a magnetic field. The Lorentz force slows down the movement of nanofluid flow and it is an opposite body force. The weakening of the recirculation zone in the rectangular grooves with a uniform magnetic field can be attributed to the magnetic field induced Lorentz force which leads to the suppression of nanofluid flow, supplies stability to the flow, and behaves like a damping force that diminishes instabilities in the flow domain. As a result, one way to weaken the recirculation zone in the rectangular grooved channel is to apply a uniform magnetic field. The suppression of the recirculation zone in the rectangular grooved channel is an effective situation in terms of heat transfer and flow characteristics since it increases heat transfer due to the penetrating more cold fluid in the groove which will be discussed in the following sections.

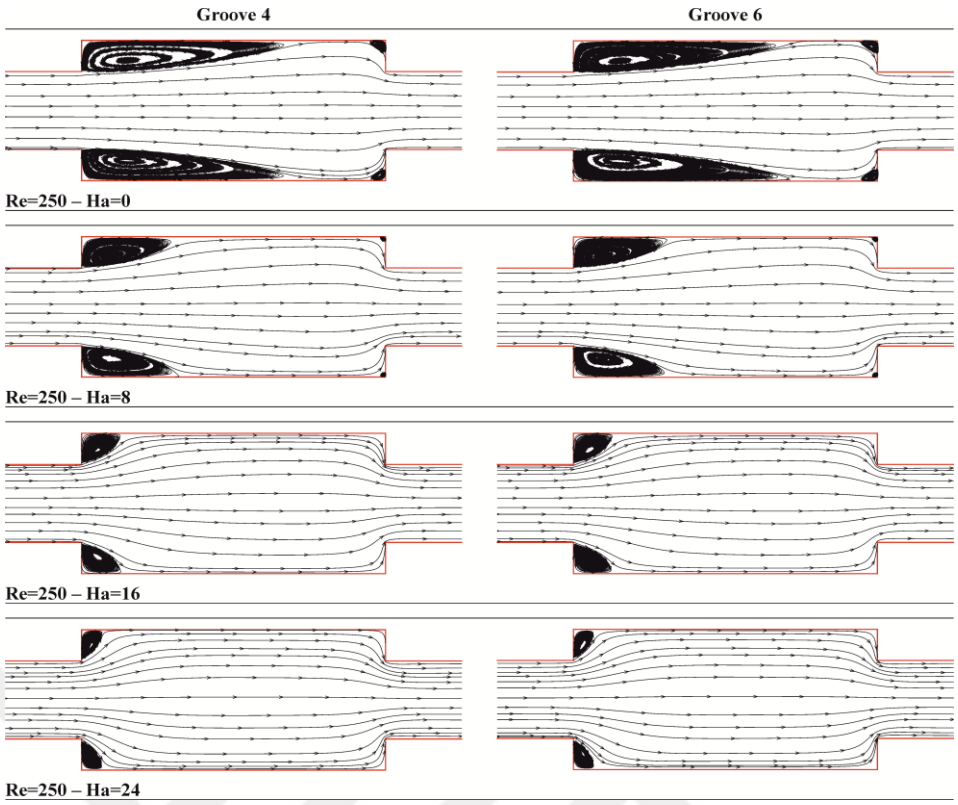

Figure 4.34. The effect of the magnetic field on the time-averaged streamline patterns in the rectangular grooved channel for Groove 4 and Groove 6 at *Re*=250 and *Φ*=3%

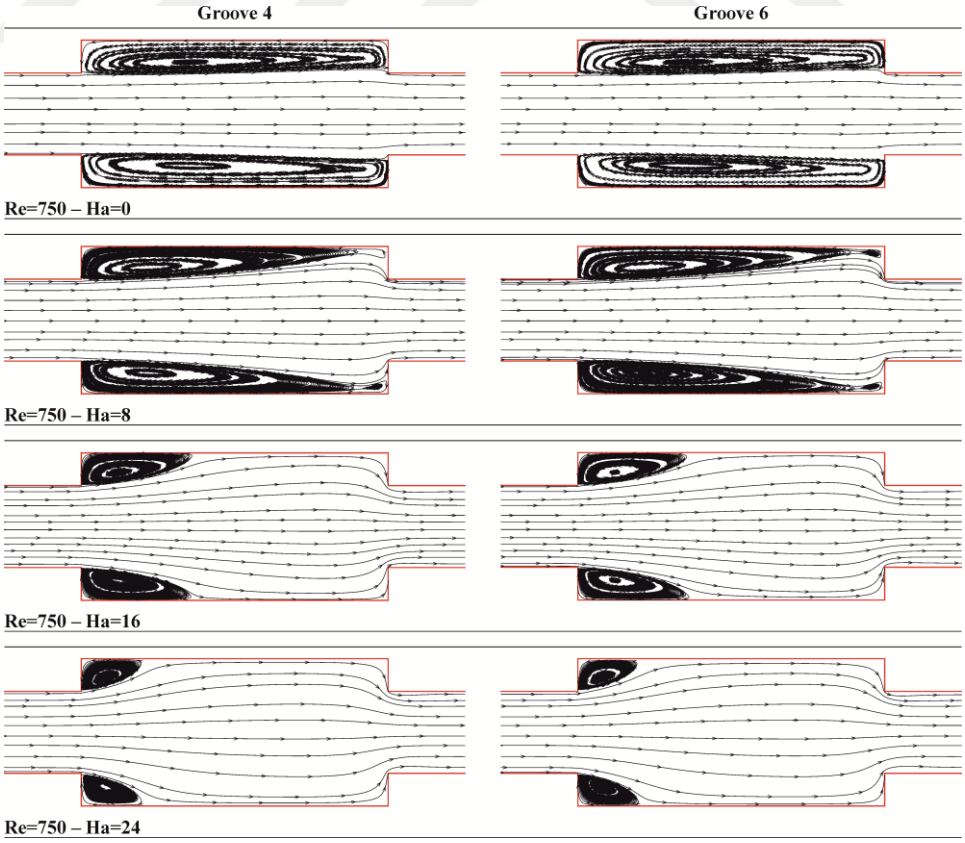

Figure 4.35. The effect of the magnetic field on the time-averaged streamline patterns in the rectangular grooved channel for Groove 4 and Groove 6 at *Re*=750 and *Φ*=3%

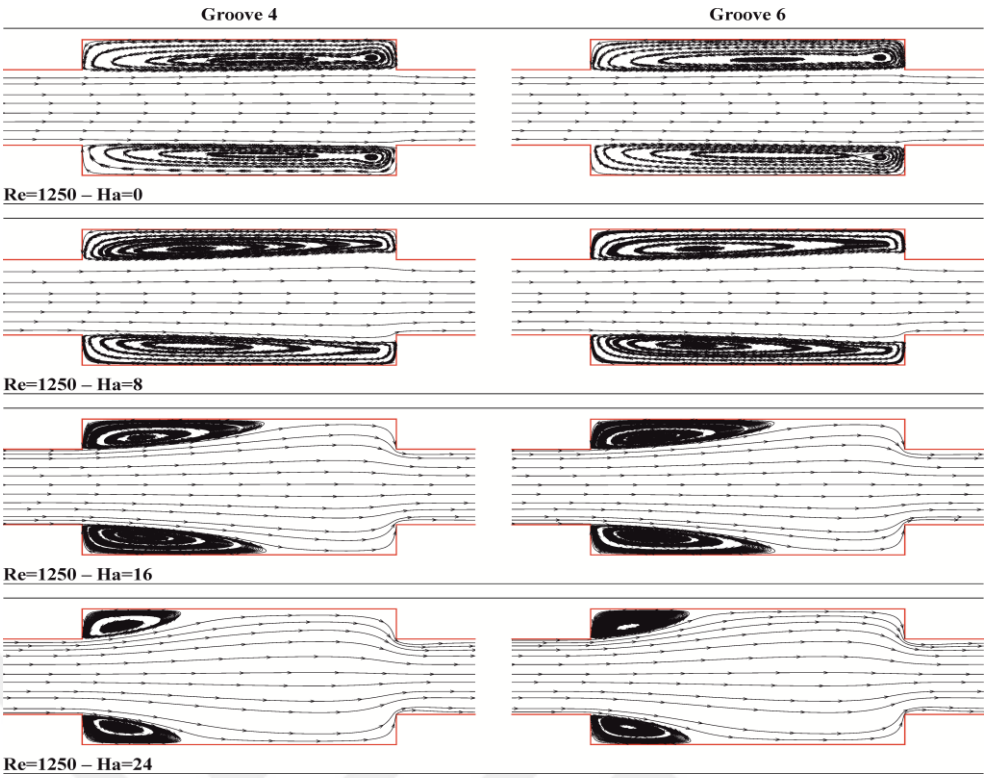

Figure 4.36. The effect of the magnetic field on the time-averaged streamline patterns in the rectangular grooved channel for Groove 4 and Groove 6 at *Re*=1250 and *Φ*=3%

Figures 4.37 and 4.39 show the influence of the uniform magnetic field on the variation of normalized streamwise velocity contours at *Re*=250, 750 and 1250, respectively for nanoparticle volume fraction, *Φ*=3%. The results demonstrated that the velocity gradient near walls gets higher by increasing the Hartmann number, *Ha* so the extent of vortices close to the walls diminishes at both Reynolds numbers, *Re*=250 and 1250. Because the Lorentz force resulting from the magnetic field reduces the flow velocity at the center of the channel and with regarding constant mass flow throughout the channel, the flow velocity substantially enhances near the hot walls. This situation grows the velocity gradient and temperature gradient near the hot walls and heat exchange between heated walls and nanofluid flow enhances. An increase in the Hartmann number, *Ha* augments the mass flow rate and velocity gradient in the vicinity of hot walls providing greater heat diffusion throughout the wall and lower wall temperature which enhances heat transfer rate and Nusselt number. Furthermore, it can be observed that the velocity profile becomes flatter by amplifying the magnetic field intensity at both Reynolds numbers, *Re*=250 and 1250. The extent of the separated flow region in rectangular grooves reduces when the Hartmann number progressively augments from *Ha*=0 towards *Ha*=24. However, as the magnetic field strength increases, the situation that the separated flow region occupies a smaller zone within rectangular grooves is more effective at *Re*=250 than *Re*=1250. Because, at *Re*=1250, the uniform magnetic field is less effective on the flow structure in rectangular grooves due to the vigorous inertia effect of nanofluid flow compared to the Reynolds number, *Re*=250.

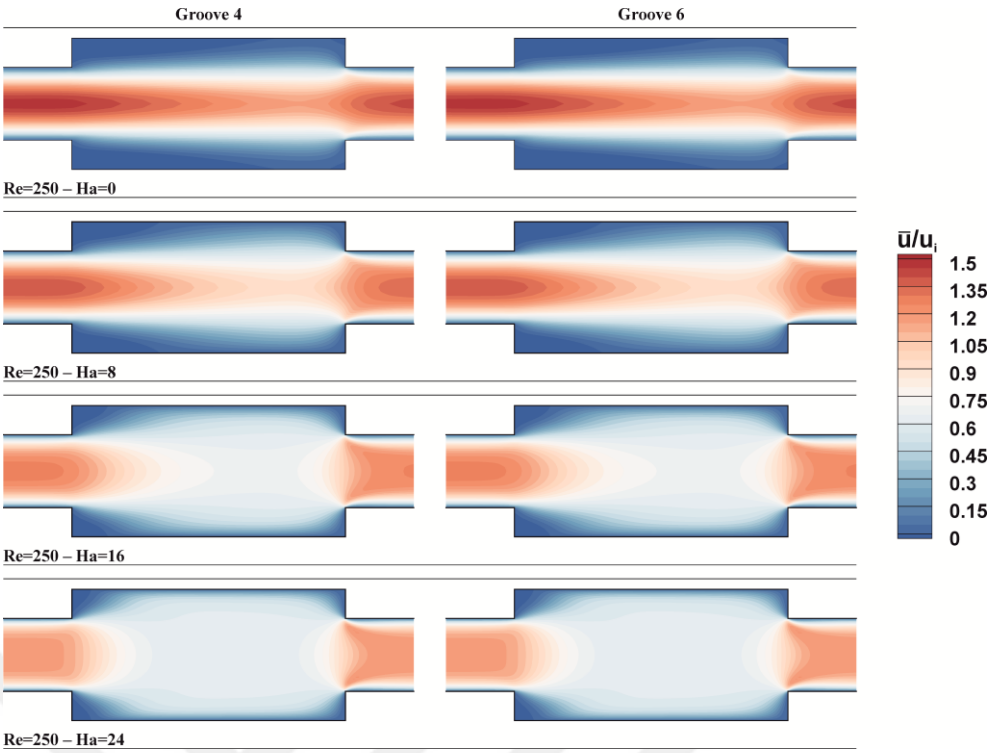

Figure 4.37. The influence of the magnetic field on the variation of normalized streamwise velocity contours in the rectangular grooved channel for Groove 4 and Groove 6 at *Re*=250 and *Φ*=3%

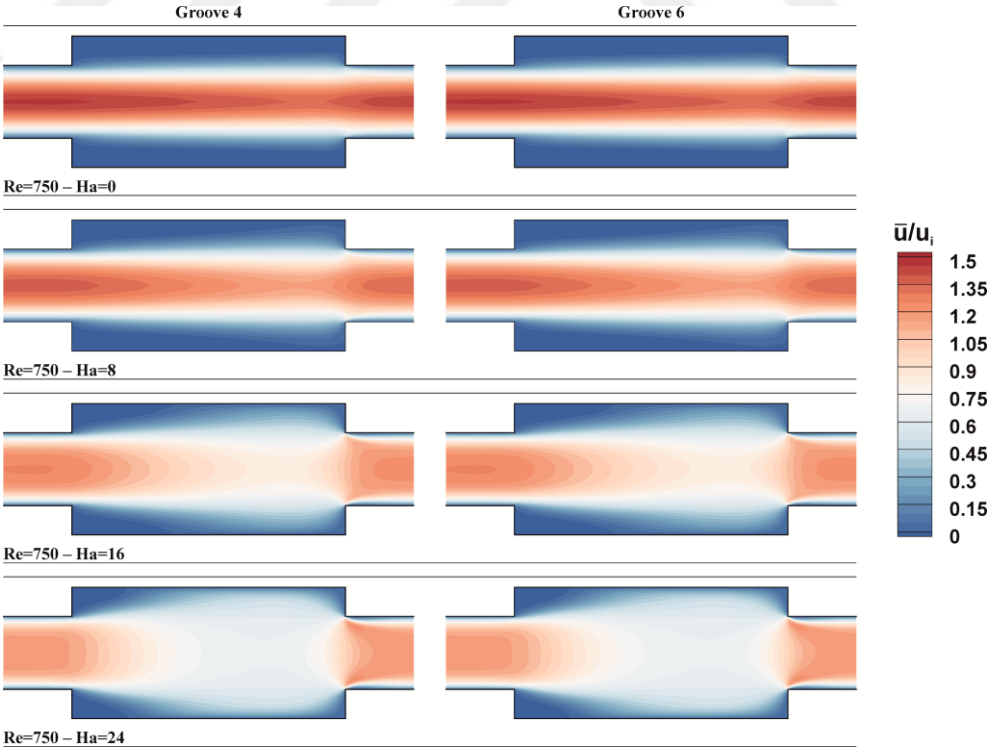

Figure 4.38. The influence of the magnetic field on the variation of normalized streamwise velocity contours in the rectangular grooved channel for Groove 4 and Groove 6 at *Re*=750 and *Φ*=3%

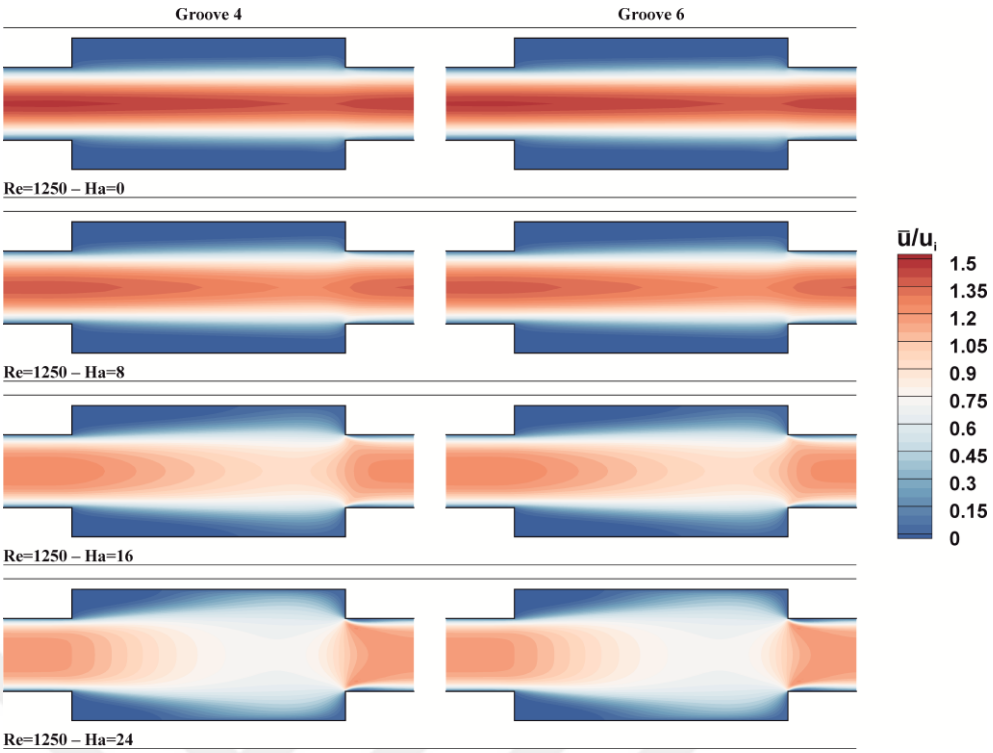

Figure 4.39. The influence of the magnetic field on the variation of normalized streamwise velocity contours in the rectangular grooved channel for Groove 4 and Groove 6 at *Re*=1250 and *Φ*=3%

The impact of the uniform magnetic field on the normalized temperature distribution, T/T_c in the rectangular grooved channel is demonstrated in Figures 4.40-4.42 at *Re*=250, 750 and 1250, respectively. These figures reveal that the applied uniform magnetic field in a transverse direction is very effective on the change of temperature distribution and isotherm lines in the rectangular grooved channel. It can be seen that when the Hartmann number progressively increases from *Ha*=0 towards *Ha*=24, the thermal boundary layer in the rectangular grooves gets thinner at both Reynolds numbers, *Re*=250 and 1250. Furthermore, the applied uniform magnetic field in a transverse direction makes the temperature gradient in the vicinity of heated walls to be increased. It is due to the direct contact of heated walls with the main cold flow which induces a high-temperature gradient near the heated walls. This situation also augments the heat transfer rate and Nusselt number, *Nu* in the rectangular grooved channel by the presence of the uniform magnetic field. For the absence of the uniform magnetic field, *Ha*=0 at both Reynolds numbers, *Re*=250 and 1250, the recirculation zone in the rectangular grooves obstructs the direct contact of the main cold with heated walls. The greater magnetic field strength is associated with smaller wall temperature because of the rise in mass flow rate and velocity gradient in close regions to the wall thus heat diffusion enhances in the vicinity of the heated wall. This observation (reduction in temperature of the wall) can be employed in the cooling of the industrial equipment and sensitive electronic components. As it is clear from Figures 4.40 and 4.42, when the Reynolds number is increased

from *Re*=250 to *Re*=1250, the thickness of the thermal boundary layer attenuates in the rectangular grooves for the same Hartmann numbers, *Ha* which points out increasing Nusselt number, *Nu* and heat transfer rate with increasing Reynolds number, *Re*. When these two figures are carefully examined, especially in Figure 4.42, one can say that the normalized temperature distribution, T/T_c in Groove 6 is higher than in Groove 4. Because the temperature of the nanofluid enhances after passing through each groove due to the direct contact of the nanofluid with the heated wall in each groove.

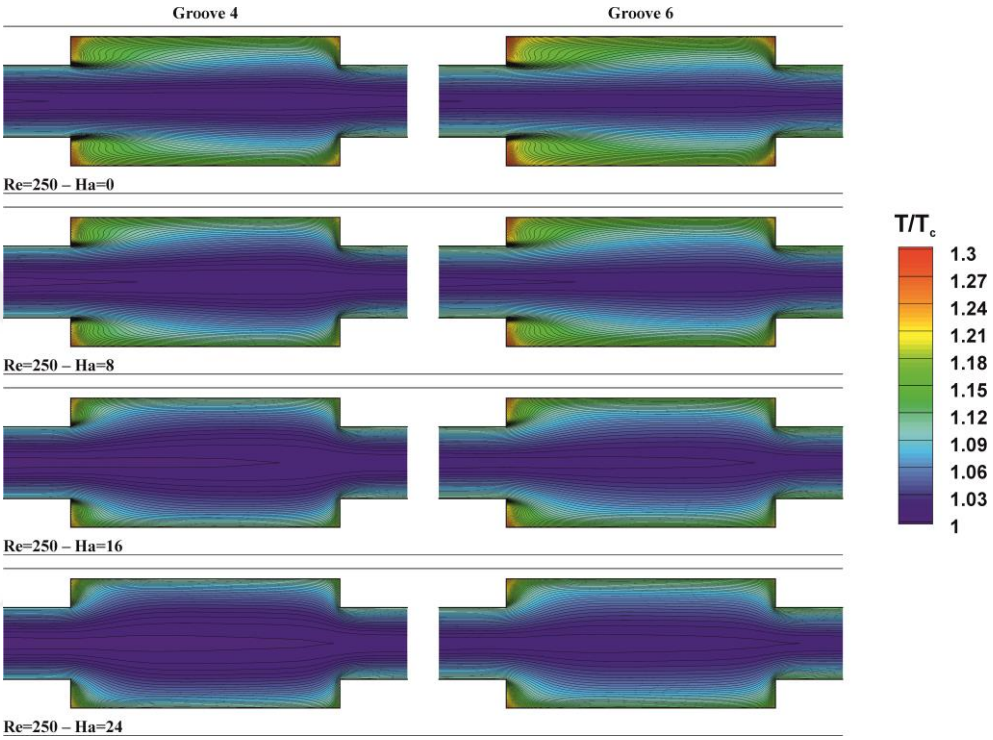

Figure 4.40. The impact of the magnetic field on the variation of normalized temperature contours and isotherm lines in the rectangular grooved channel for Groove 4 and Groove 6 at *Re*=250 and *Φ*=3%

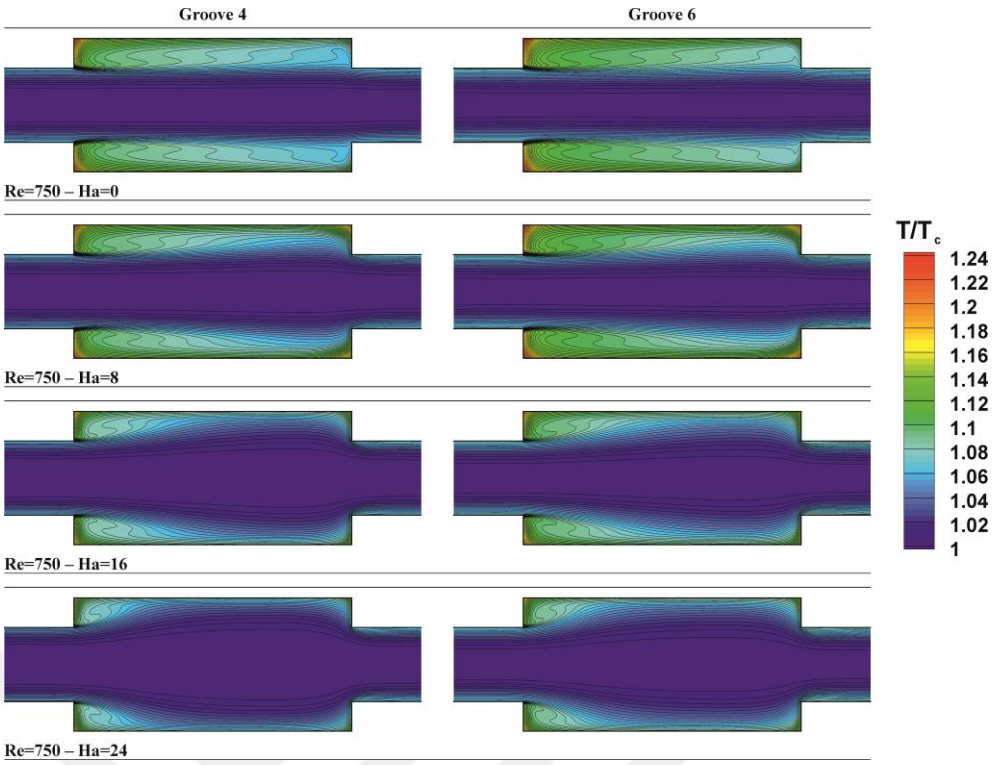

Figure 4.41. The impact of the magnetic field on the variation of normalized temperature contours and isotherm lines in the rectangular grooved channel for Groove 4 and Groove 6 at *Re*=750 and *Φ*=3%

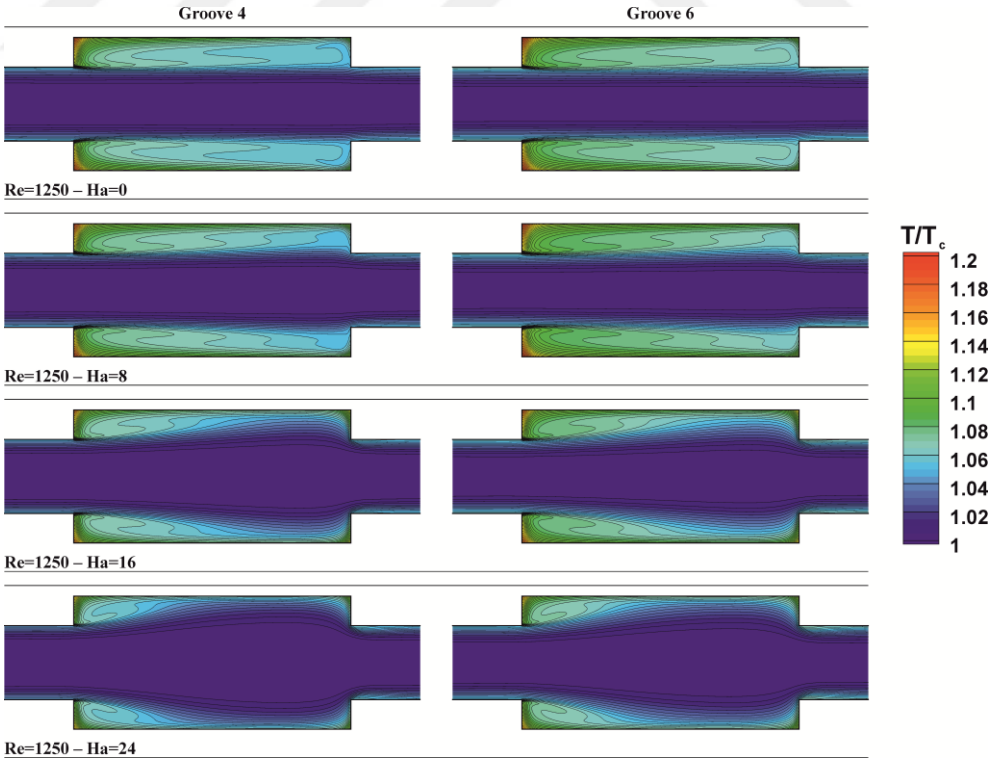

Figure 4.42. The impact of the magnetic field on the variation of normalized temperature contours and isotherm lines in the rectangular grooved channel for Groove 4 and Groove 6 at *Re*=1250 and *Φ*=3%

4.2.2. Heat Transfer Analysis

In Figure 4.43, the uniform magnetic field effect on the variation of the average Nusselt number, Nu_{avg} at Reynolds number, *Re* within the range of $250 \leq Re \leq 1250$ for Φ=3% is demonstrated. According to the results, the average Nusselt number, Nu_{avg} by increasing uniform magnetic field intensity. For example, whereas the average Nusselt number is observed as Nu_{avg}= 4.976 at *Ha*=0 it enhances to values of Nu_{avg}=5.428 and 6.49 for *Ha*=8 and 24, respectively at *Re*=250. On the other hand, when the average Nusselt number is detected as Nu_{avg}=9.328 for *Ha*=0, there is a slight augmentation in heat transfer rate by observing Nu_{avg}= 9.336 for *Ha*=8 and it remarkably increases to Nu_{avg}=11.3 for *Ha*=24 at *Re*=1250. Obtained results demonstrated that Nu_{avg} augmentation is in the vicinity of 9.08% for *Ha*=8 and 30.42% for *Ha*=24 at *Re*=250 and 0.087% for *Ha*=8 and 21.13% for *Ha*=24 at *Re*=1250 compared to the absence of uniform magnetic field application case, *Ha*=0. It can be said that in greater Reynolds number, *Re* because of the high inertia effect of the main flow, the uniform magnetic field has less influence on the average Nusselt number, Nu_{avg} since Nu_{avg} enhancement ratio due to the rise in the Hartmann number, *Ha* is higher at *Re*=250 compared to *Re*=1250. *Nuavg* augmentation with a uniform magnetic field can be attributed to the situation that applying a uniform magnetic field suppresses the recirculation zones in the rectangular grooves and thus main cold flow can penetrate the rectangular grooves. As a result, the velocity gradient and temperature gradient increase, and the thermal boundary layer gets thinner in the vicinity of heated walls in rectangular grooves which enhances heat transfer rate and average Nusselt number, Nu_{avg} by increasing Hartmann number, *Ha*. The other important observation from Figure 4.43 is that the average Nusselt number, Nu_{avg} augments when the Reynolds number, *Re* increases. For example, in Fig.7, the average Nusselt number is observed as Nu_{avg}=6.235 and 8.430 at Re=500 for *Ha*=0 and 24, respectively, on the other side, it is enhanced to the levels of Nu_{avg}=8.584 and 10.587 at *Re*=100 for *Ha*=0 and 24, respectively. Thus, the percentage enhancement of Nu_{avg} corresponds to 37.66% and 25.58% at *Ha*=0 and 24 respectively, as the Reynolds number gets higher from *Re*=500 to *Re*=100. The enhancement of Nu_{avg} because of the increment in *Re* can be attributed to the greater fluid velocity and convection heat transfer rate. The convective transport structure enhances for the greater nanofluid velocities. Additionally, as explained in Figures 4.40-4.42, the thermal boundary layer thickness decreases with an increment in *Re* which makes *Nuavg* to be enhanced.

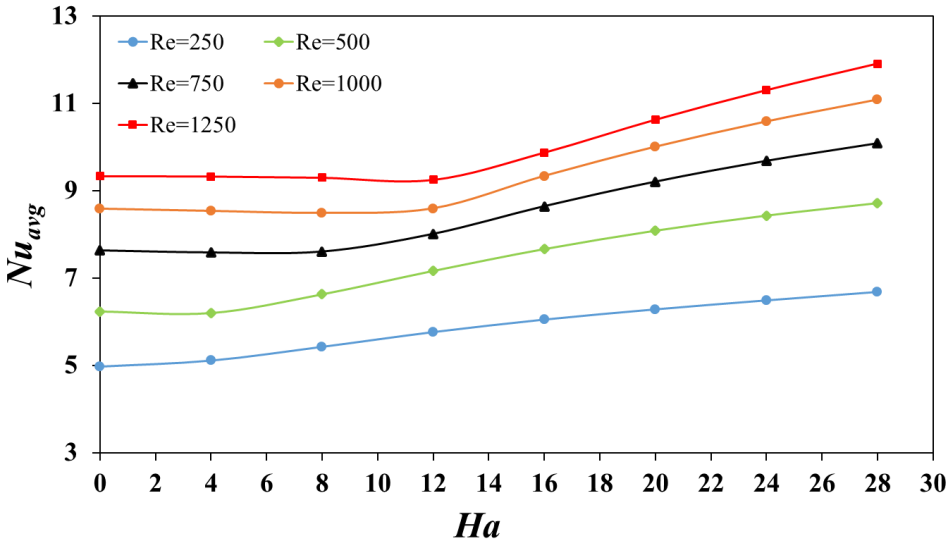

Figure 4.43. The magnetic field effect on the variation of the average Nusselt number, Nu_{avg} at Reynolds number in the range of $250 \leq Re \leq 1250$ for the volume fraction of nanoparticle, Φ=3%

In Figure 4.44, as expected, including CuO nanoparticles into the water with volume fractions, Φ=3%, and 5% makes the Nu_{avg} to be augmented for all examined Ha at Re=250. Obtained results demonstrated that in the absence of the magnetic field, Ha=0 increasing volume fraction of nanoparticles from Φ=0% to Φ=5% gives rise to 3.71% average Nusselt number, Nu_{avg} augmentation while this value is 3.13 %, 2.3% and 2.09% when the Hartmann number increases to Ha=8, 16 and 24, respectively. On the other hand, in Figure 4.46, there is an enhancement in Nu_{avg} with 3.48%, 3.01% and 2.1% for Ha=8, 16 and 24, respectively when the volume fraction of nanoparticles increases from Φ=0% to Φ=5% at Re=1250. The Nu_{avg} improvement with the increment in nanoparticle volume fraction, Φ can be attributed to the increasing thermal conductivity, k of the nanofluid and more intense Brownian motion of CuO nanoparticles compared to the pure water. The weakening thermal resistance induced by enhancing the volume fraction of nanoparticles (growing thermal conductivity) is useful for heat transfer and average Nusselt number, Nu_{avg} improvement. Furthermore, the Brownian motion of CuO solid particles can attenuate the thermal resistance of heat transfer between heated walls in the channel and water-CuO nanofluids which is effective in the Nu_{avg} improvement.

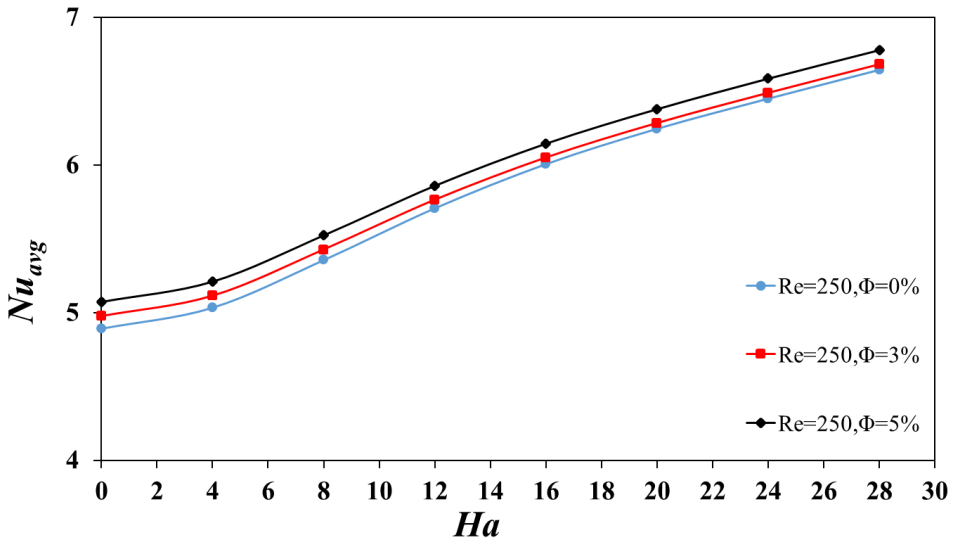

Figure 4.44. The influences of Hartmann number, *Ha* and nanoparticle volume fraction, *Φ* on average Nusselt number, Nu_{avg} at Reynolds numbers *Re*=250 for the nanoparticle volume fractions, *Φ*=0%, 3% and 5%

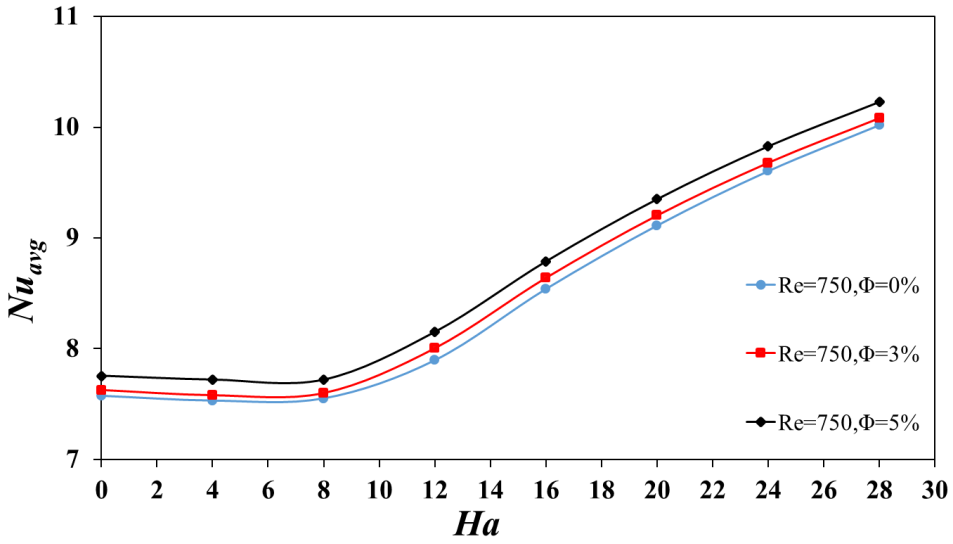

Figure 4.45. The influences of Hartmann number, *Ha* and nanoparticle volume fraction, *Φ* on average Nusselt number, Nu_{avg} at Reynolds numbers *Re*=750 for the nanoparticle volume fractions, *Φ*=0%, 3% and 5%

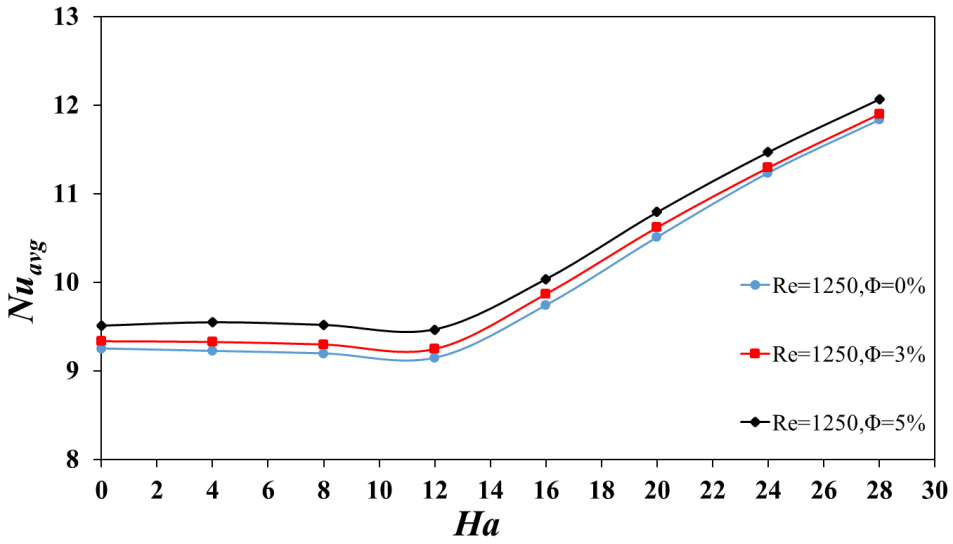

Figure 4.46. The influences of Hartmann number, *Ha* and nanoparticle volume fraction, Φ on average Nusselt number, Nu_{avg} at Reynolds numbers *Re*=1250 for the nanoparticle volume fractions, Φ=0%, 3% and 5%

Figures 4.47-4.49 depict the influence of the magnetic field on local Nusselt number, Nu_L for the ferrofluid volume fractions, Φ=3% in the rectangular grooved channel at *Re*=250, 750 and 1250, respectively. As it is apparent in the figures, the Nu_L is enhanced when the uniform magnetic field is applied and its intensity gets higher along the rectangular grooved channel at both Reynolds numbers, *Re*=250 and 1250. When the Hartmann number progressively increases from *Ha*=0 towards *Ha*=24, the Nu_L is distributed with greater values along the grooved channel. Furthermore, the value of Nu_L is always higher at *Re*=1250 compared to *Re*=250 for the same case of all examined Hartmann numbers, *Ha*. It should be noted that the value of Nu_L is greater on the straight section of the heated wall compared to the grooved section of the heated wall for all examined *Ha*. It occurs due to the direct contact of the straight section of the heated wall with the main cold flow which induces a higher temperature gradient thus heat transfer rate and Nusselt number. On the grooved section of the heated wall, the recirculation zone restrains the contact of the wall surfaces with the main cold flow. Furthermore, the Nu_L deteriorates in the downstream direction due to the increasing temperature of the main flow after passing each groove. Increasing the temperature of the main flow deteriorates the heat transfer rate since heated walls contact with high temperature main flow instead of a cold one. The findings show that the difference in the distribution of Nu_L between grooves in the flow direction diminishes due to the developing thermal boundary layer in the flow direction for all examined *Ha* and *Re*.

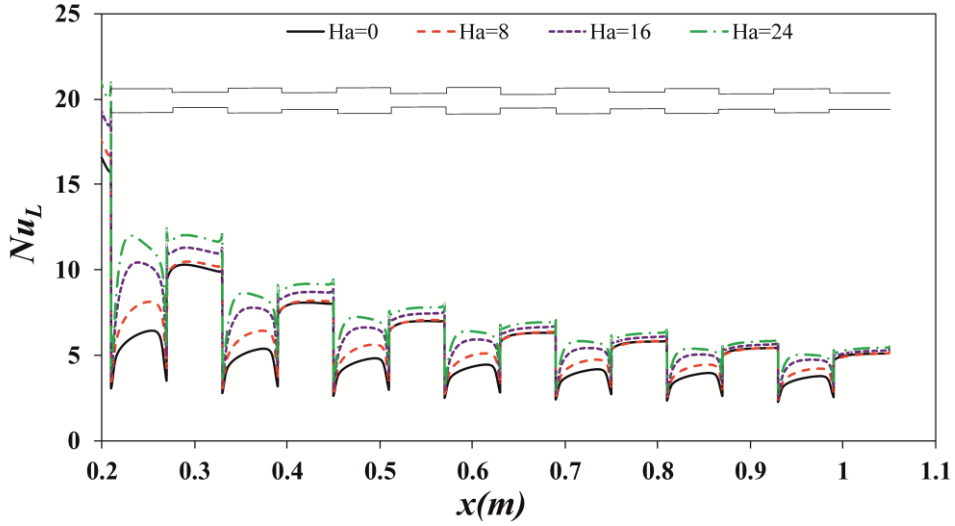

Figure 4.47. The influence of the magnetic field on local Nusselt number, Nu_L at Reynolds number, Re=250 for the nanoparticle volume fraction, Φ=3% in the rectangular grooved channel

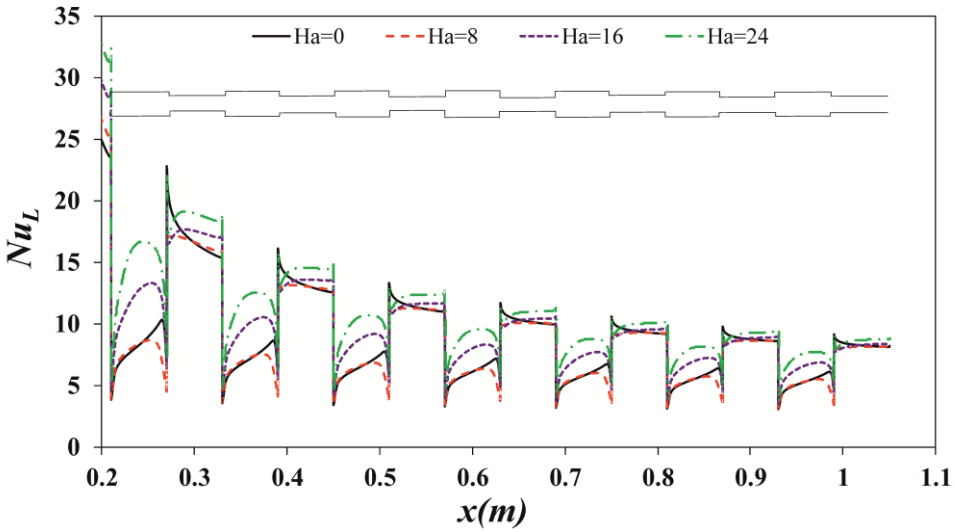

Figure 4.48. The influence of the magnetic field on local Nusselt number, Nu_L at Reynolds number, Re=750 for the nanoparticle volume fraction, Φ=3% in the rectangular grooved channel

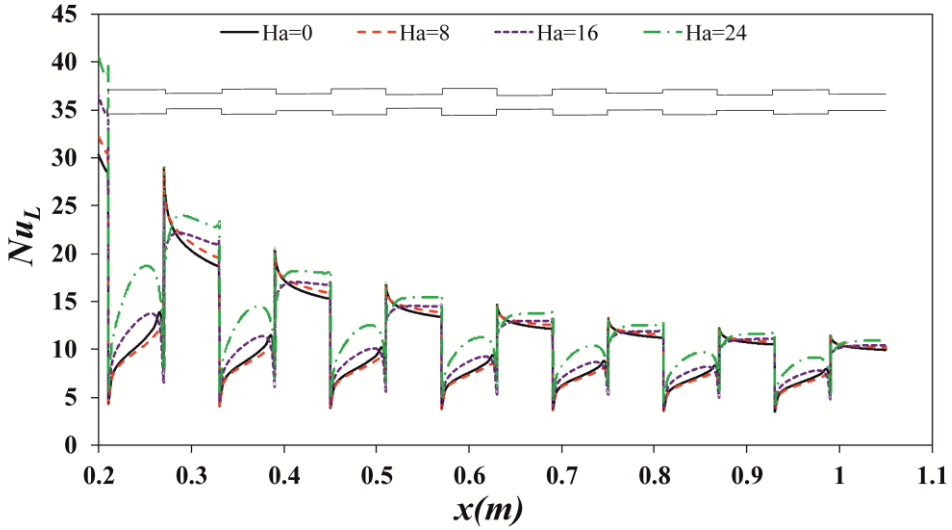

Figure 4.49. The influence of the magnetic field on local Nusselt number, Nu_L at Reynolds number, Re=1250 for the nanoparticle volume fraction, Φ=3% in the rectangular grooved channel

4.2.3. Entropy Analysis

As already mentioned, analytical quantification of entropy production determines irreversible processes. A reduction in entropy production corresponds to an increase in thermal performance. Therefore, the characterization of irreversible processes through the investigated channel points directly to a precise statement of hydrothermal performance.

Figures 4.50-4.52 display the impact of various intensities of magnetic field on the thermal entropy generation contour lines for the Groove 4 and Groove 6 of the considered channel at Re=250, 750 and 1250, respectively for nanoparticle volume fraction, Φ=3%. As can be seen from these contour lines, in all cases shown, the high level of thermal entropy production spreads along the solid walls of the channel. This is due to the high-temperature gradients in these regions, as demonstrated in Figures 4.40-4.42. It is noted that the entropy generation resulting from the heat transfer effect is almost non-existent along the center flow region of the channel. This is directly related to the uniform temperature distribution within this region, as presented in isothermal contours. Further, a low level of thermal entropy is shown in each rectangular groove along the corrugated channel. As portrayed in Figures 4.34-4.36, the flow recirculation zone is emerged within each groove. This flow recirculation precludes the connection between the cold fluid and the heated walls, thus reducing temperature gradients. Accordingly, the generation of thermal entropy drops significantly in these regions. Furthermore, the maximum amount of thermal entropy is generated near the left sharp edge of each groove. Regardless of the intensity of the applied magnetic field, it is clearly indicated that the regions of high thermal entropy generation levels shrink as the Reynolds number changes from Re=250 to Re=1250. As mentioned earlier, increasing the Reynolds number makes the temperature gradients more gradual and consequently, the entropy

generation due to the thermal impact decreases. For a given Reynolds number, *Re* the thermal entropy production inside the channel diminishes as the intensity of the uniform magnetic field increases (i.e., increases the Hartmann number, *Ha*). This implies that the applied magnetic source reduces the generation of thermal irreversibility in corrugated channels.

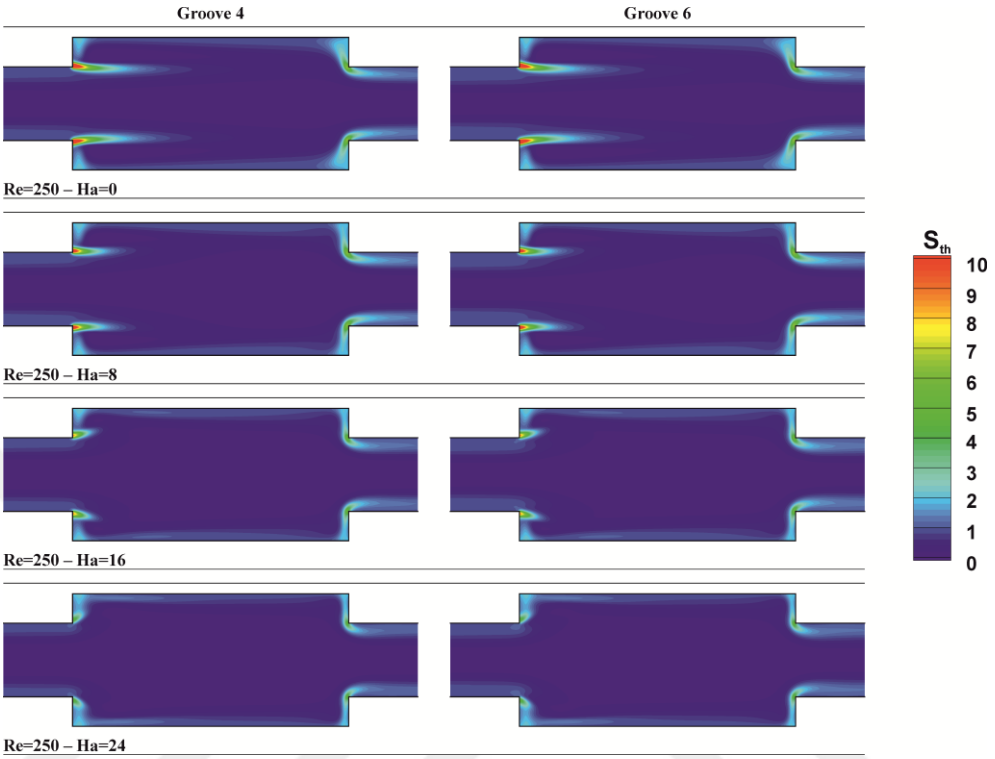

Figure 4.50. The effect of the magnetic field on the contour of the thermal entropy generation, S_{th} at Reynolds number, *Re*=250 for nanoparticles volume fraction, Φ=3%.

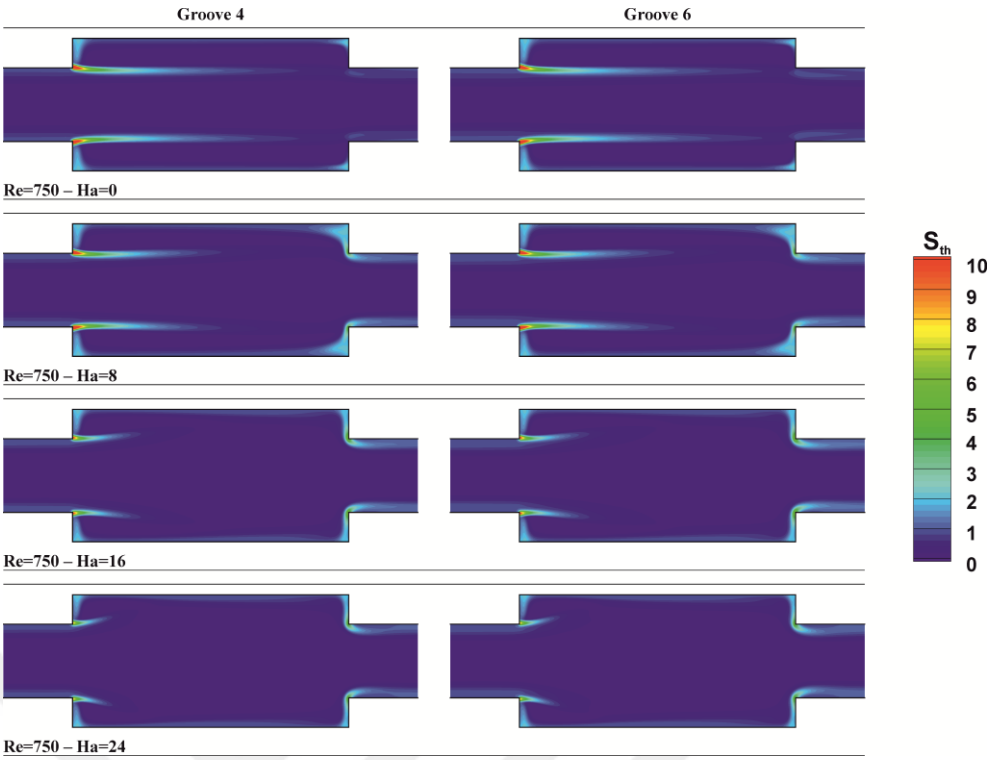

Figure 4.51. The effect of the magnetic field on the contour of the thermal entropy generation, S_{th} at Reynolds number, Re=750 for nanoparticles volume fraction, Φ=3%.

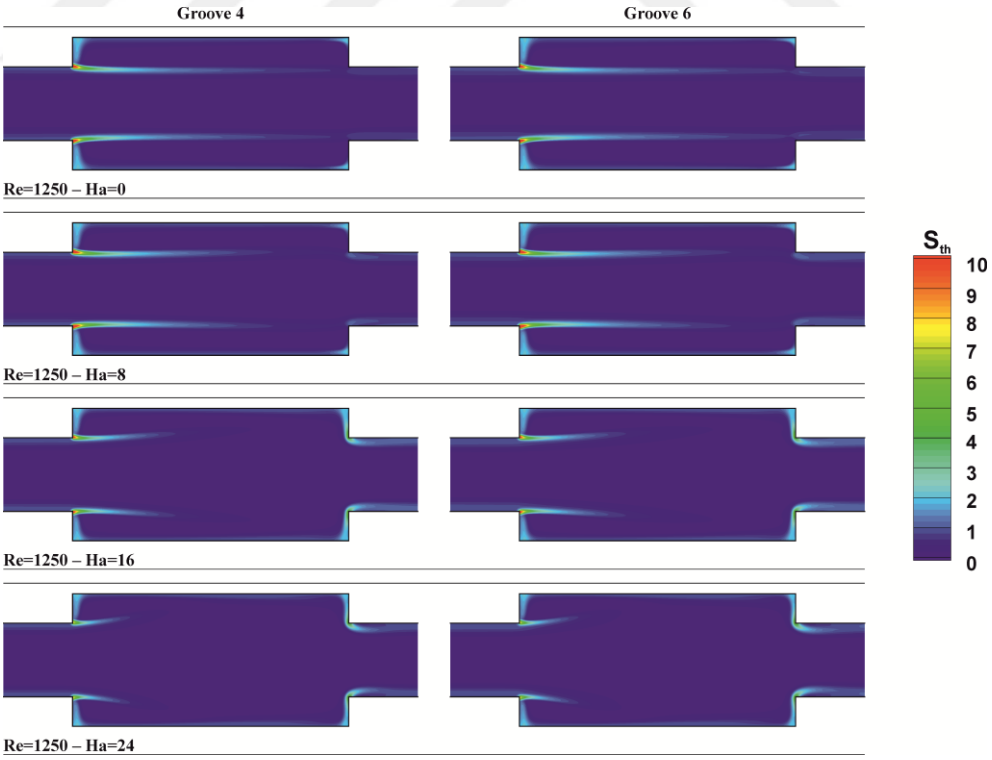

Figure 4. 52. The effect of the magnetic field on the contour of the thermal entropy generation, S_{th} at Reynolds number, Re=1250 for nanoparticle volume fraction, Φ=3%.

Figures 4.53-4.55 present the impact of various intensities of magnetic field on the variation of viscous entropy, S_{vis} generation contour lines for the Groove 4 and Groove 6 of the considered channel at *Re*=250, 750 and 1250, respectively for the nanoparticles volume fraction, Φ=3%. These contours clearly revealed that the high level of viscous entropy, S_{vis} generation extends alongside the straight walls of the convergent sections. This behavior is associated with high values of velocity gradients in these regions, as shown in Figures 4.37-4.39. In addition, it is worth noting that the entropy production due to the frictional effect of the working fluid flow is almost not generated within the remaining flow domain of the channel. This is directly related to the low-velocity gradients within these regions. As expected, the maximum level of viscous entropy, S_{vis} generation appears close to the right sharp angle of each groove of the tested channel, where the sudden contraction leads to the highest values of velocity gradients. As can be seen from the color bar values, regardless of the intensity of the applied magnetic field, it is found that viscous entropy values augment significantly with an augmentation in Reynolds number from *Re*=250 to *Re*=1250. This augment in the Reynolds number directly affects the flow velocity of nanofluid as explained in figures of velocity contours and thus leads to further production of frictional entropy. At a fixed value of Reynolds number, *Re* the production of viscous entropy, S_{vis} gradually increased with an increase in the intensity of a uniform magnetic field. For *Re* = 250, the high-level friction entropy distribution is more affected by changes in the magnetic field strength than for *Re* = 1250. As a result, it can be stated that applying a uniform magnetic field does not have much influence on the frictional irreversibility through the rectangular corrugated channel.

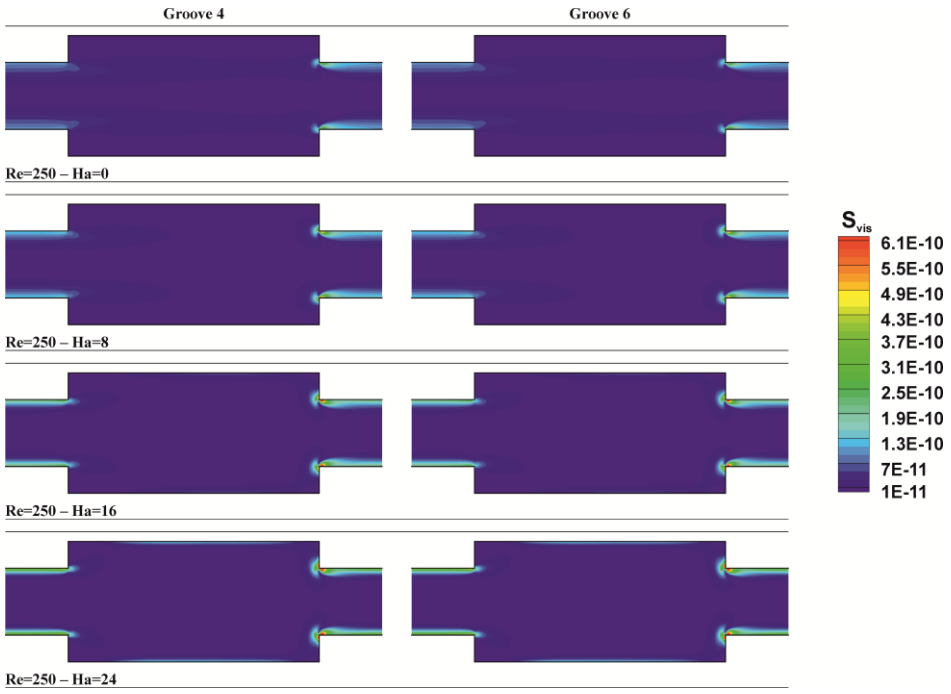

Figure 4.53. The effect of the magnetic field on the contour of the viscous entropy generation, S_{vis} at the Reynolds number, *Re*=250 for the nanoparticles volume fraction, Φ=3%

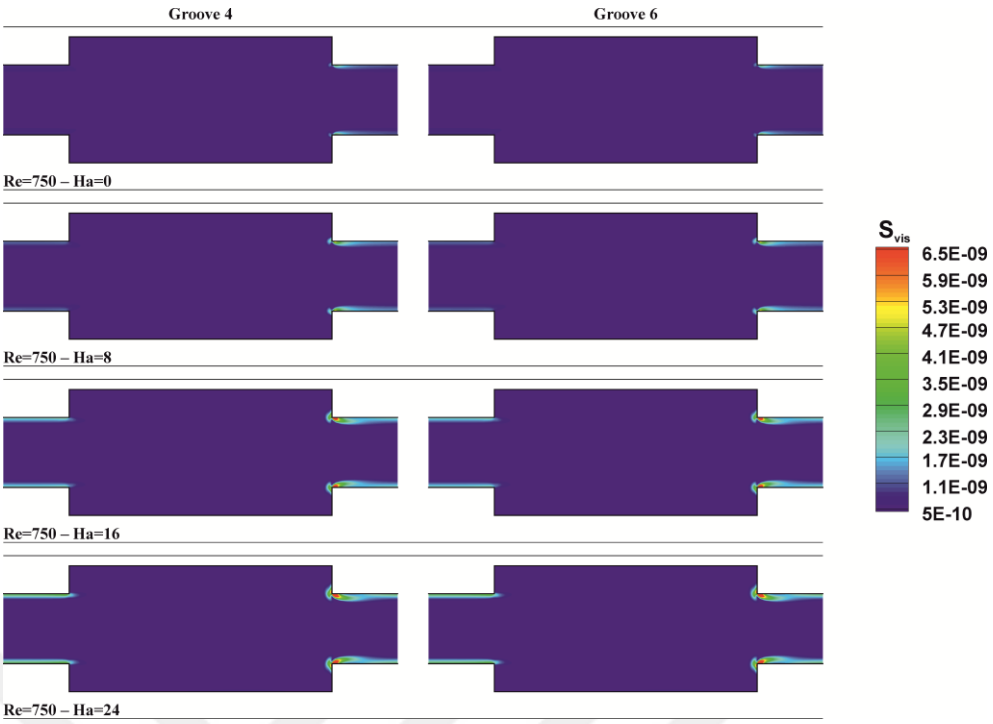

Figure 4.54. The effect of the magnetic field on the contour of the viscous entropy generation, S_{vis} at the Reynolds number, Re=750 for the nanoparticles volume fraction, Φ=3%

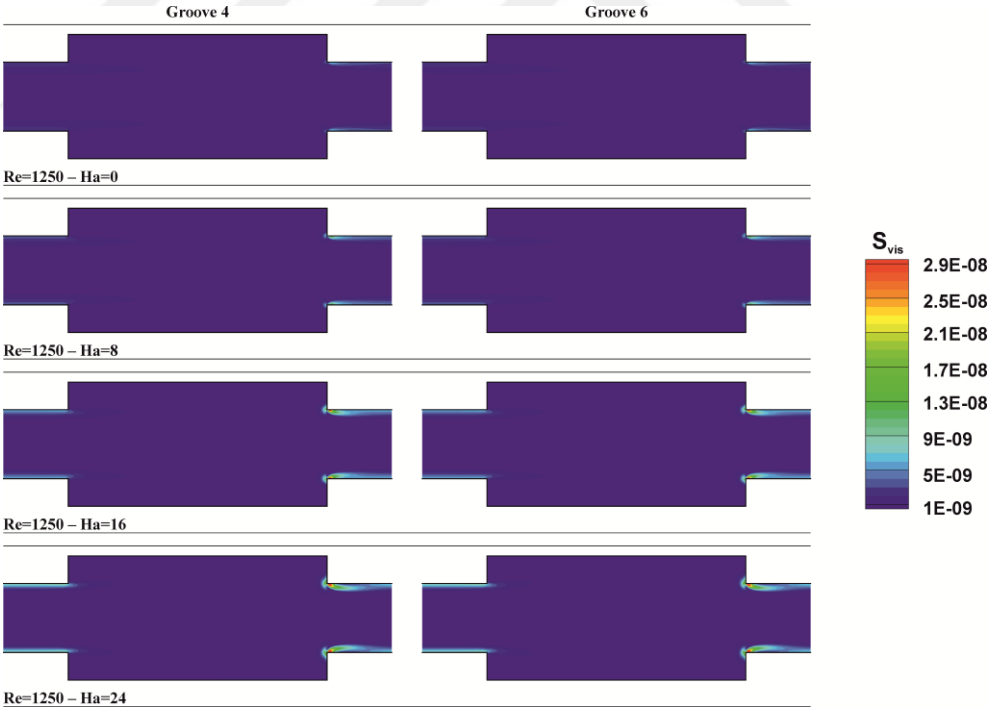

Figure 4.55. The effect of the magnetic field on the contour of the viscous entropy generation, S_{vis} at the Reynolds number, Re=1250 for the nanoparticles volume fraction, Φ=3%.

Figures 4.56-4.58 depict the effect of the uniform magnetic field on the change in the magnetic entropy, S_{mag} generation contours at Re=250 and 1250, respectively, for the nanoparticle volume fraction, Φ=3%. As written in the last term of the total entropy generation equation (Equation 3.51), the magnetic entropy is an increasing function of both the velocity magnitude and the Hartmann number, Ha. Therefore, for all the introduced cases, there is no entropy generation due to the magnetic impact adjacent to the solid walls of the channel where the no-slip boundary conditions are assumed for these walls. Moreover, the results revealed that the production of the entropy, S_{mag} due to the magnetic impact significantly increased by increasing the value of the Hartmann number, Ha for both Reynolds numbers. For Re= 250 and 1250 at Ha=8, the high-level zone of magnetic entropy, S_{mag} generation occurs within the core flow of the convergent and divergent sections. By increasing the Ha to the value of 16, the high level of magnetic entropy, S_{mag} spreads to half of the divergent grooves for Re=250, while remaining within the mainstream of divergent grooves for Re=1250. At the highest intensity of the applied magnetic field (Ha=24), this level of entropy extends to cover most regions of divergent grooves for Re=250 and almost half of the regions of divergent grooves for Re=1250. As already mentioned, this type of entropy is directly related to the velocity distribution of the flow region. Accordingly, these behaviors are consistent with those shown in the velocity contours in Figures 4.37-4.39. In addition, the magnitude of the magnetic entropy, S_{mag} increased with increasing the Reynolds number, Re as demonstrated in the color bar of these contours.

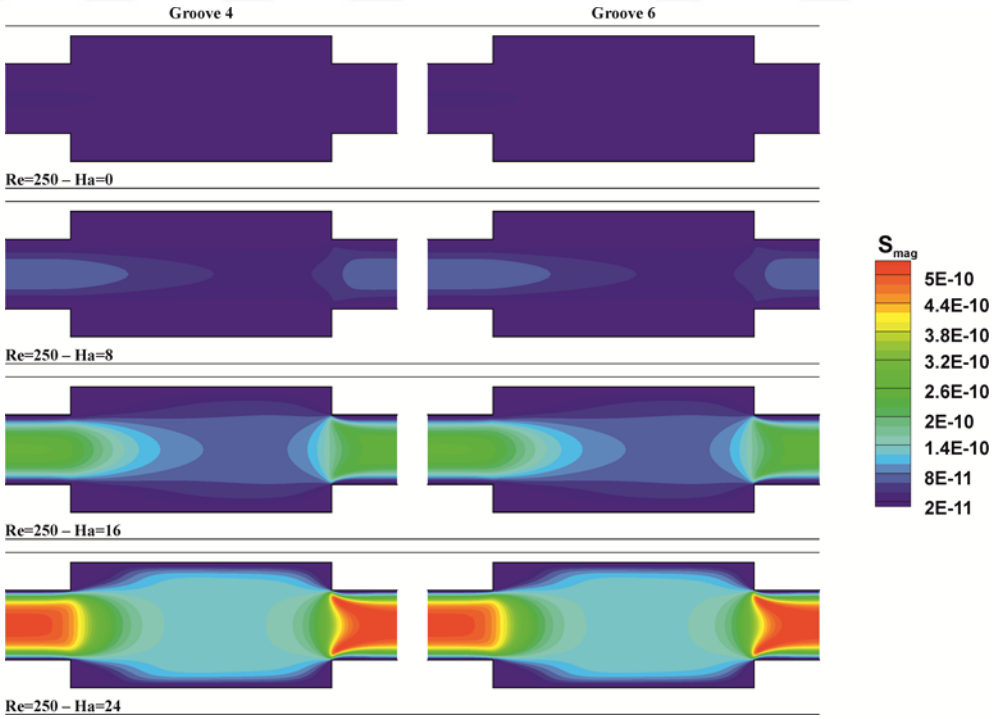

Figure 4.56. The effect of the magnetic field on the contour of the magnetic entropy generation, S_{mag} at the Reynolds number, Re=250 for the nanoparticles volume fraction, Φ=3%

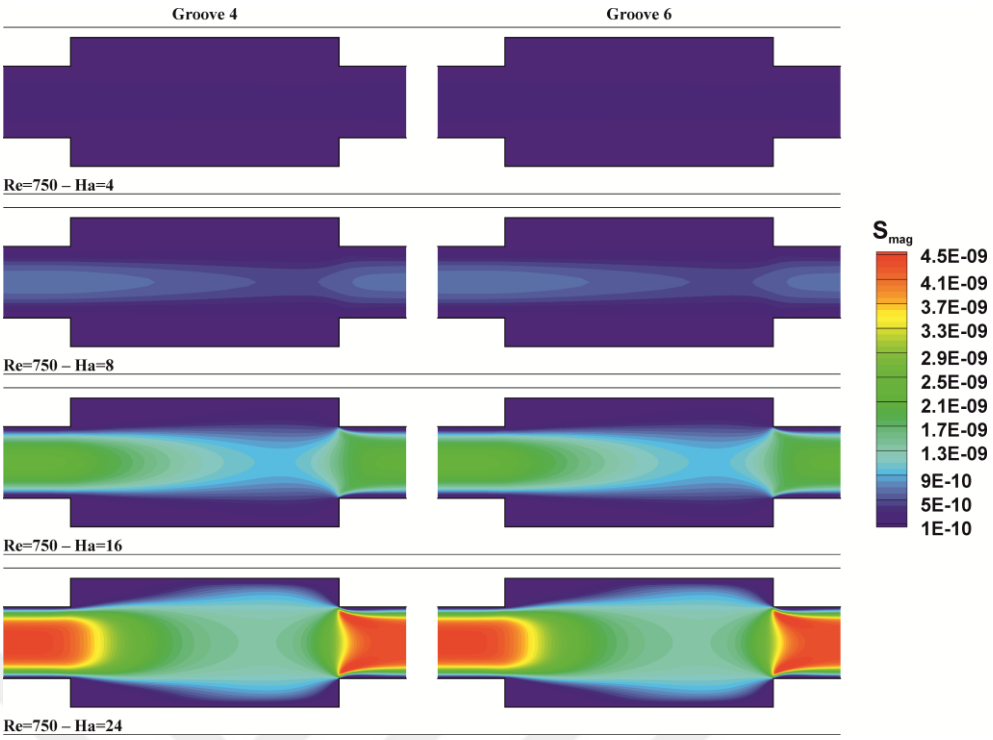

Figure 4.57. The effect of the magnetic field on the contour of magnetic entropy generation, S_{mag} at the Reynolds number, Re=750 for the nanoparticles volume fraction, Φ=3%.

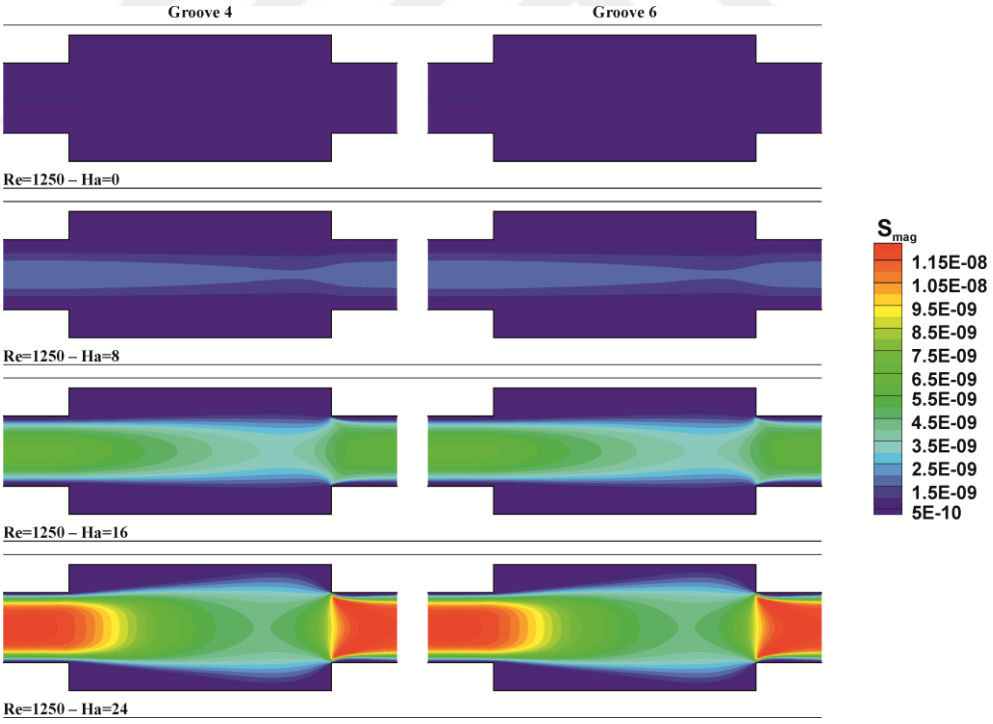

Figure 4.58. The effect of the magnetic field on the contour of magnetic entropy generation, S_{mag} at the Reynolds number, Re=1250 for the nanoparticles volume fraction, Φ=3%.

Figures 4.59-4.61 display the local production contours of the total entropy, S_L under different intensities of the uniform magnetic field at Re=250,750 and 1250, respectively, for the nanoparticles volume fraction, Φ=3%. For the current corrugated channel, the generation of entropy by the nanofluid flow happens mainly due to the effects of heat transfer, frictional flow, and magnetic source. Therefore, Figures 4.59-4.61 define the summation of thermal, S_{th} viscous, S_{vis} and magnetic entropy, S_{mag} generation contours for Re=250 and 1250, respectively. The patterns and values of the total entropy, S_L generation contours showed that there is a high degree of coincidence with the thermal entropy, S_{th} generation contours shown in Figures 4.50-4.52. This indicates that the total irreversible process through the considered channel is mainly due to thermal effects. In other words, the thermal entropy, S_{th} generation is dominant over the considered entropy, S_L generations.

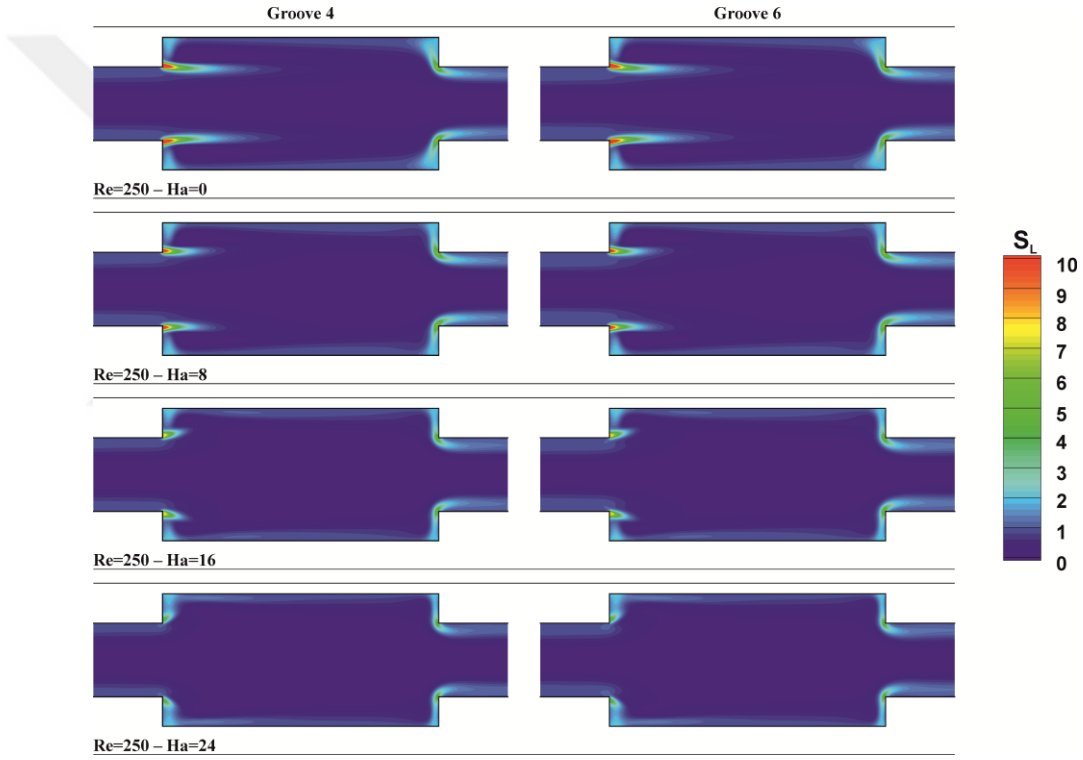

Figure 4.59. The effect of the magnetic field on the contour of the total entropy generation, S_L at the Reynolds number, Re=250 for the nanoparticles volume fraction, Φ=3%

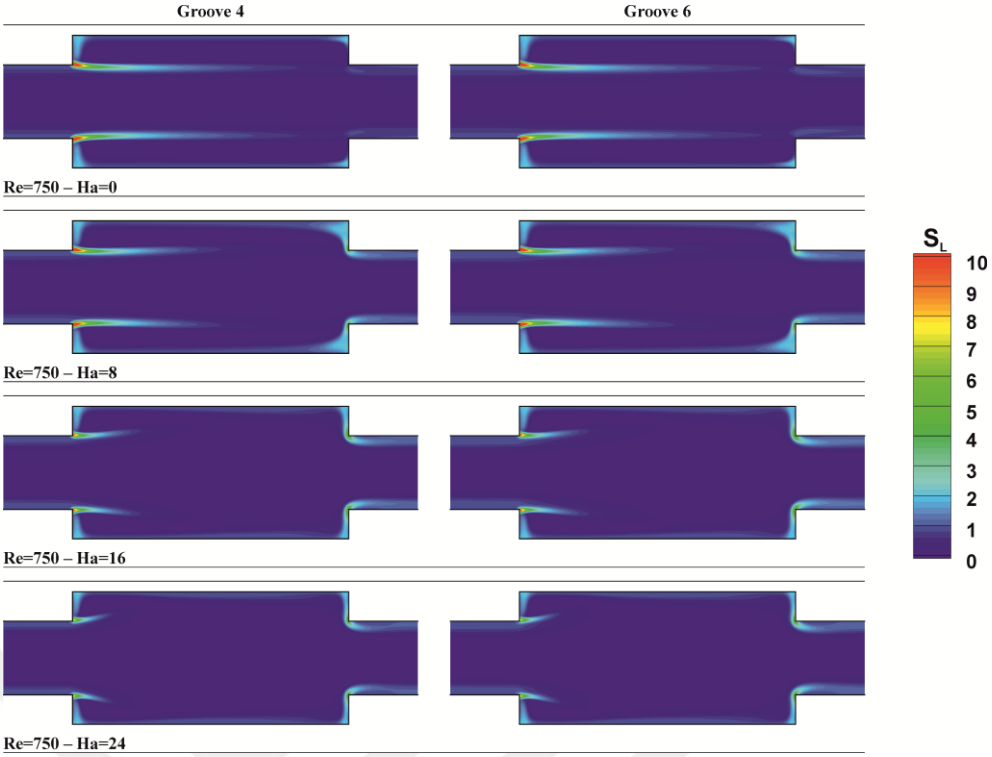

Figure 4.60. The effect of the magnetic field on the contour of the total entropy generation, S_L at the Reynolds number, Re=750 for the nanoparticles volume fraction, Φ=3%

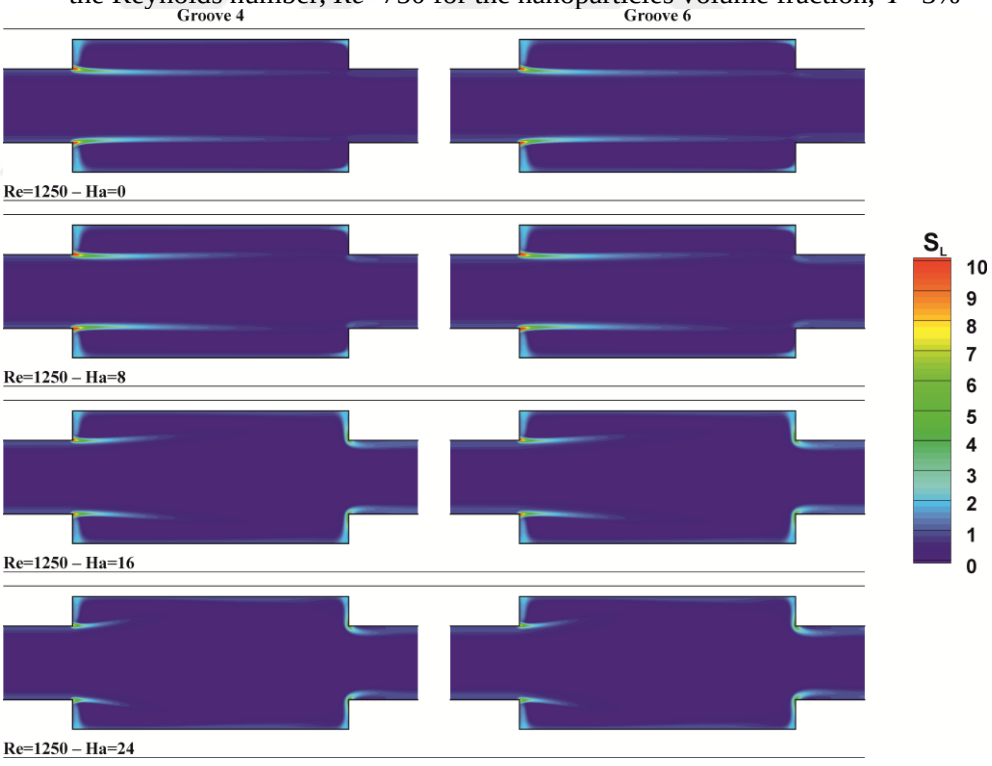

Figure 4.61. The effect of the magnetic field on the contour of the total entropy generation, S_L at the Reynolds number, Re=1250 for the nanoparticles volume fraction, Φ=3%

Figure 4.62 exhibits the influence of the magnetic field on the average thermal entropy generation, $<S_{th}>$ viscous entropy generation, $<S_{vis}>$ magnetic entropy generation, $<S_{mag}>$ and total

entropy generation, S_{avg} at Reynolds numbers, *Re*=250, 750 and 1250 for nanoparticles volume fraction, Φ=3% The results of this figure provide useful details for understanding the basic effects of fluid flow situations and magnetic fields on the overall entropy, S_{avg} production within rectangular corrugated channels. It can be clearly seen that the total entropy, S_{avg} increases as the Reynolds number, *Re* increases. For instance, in the absence of an applied magnetic field (i.e., *Ha*=0), the amount of total entropy, S_{avg} increases by about 31% by increasing the Reynolds number from *Re*=250 to *Re*=1250. In addition, this increment was found to be 103% when the uniform magnetic field has an intensity of *Ha*=8. This is owing to the fact that the increment in *Re* causes an increase in both velocity and temperature gradients through the flow field and, thus, leads to further generation of entropy. For a given value of *Re*, it can be seen that the total entropy, S_{avg} decreases sharply after *Ha*>8. This is due to the significant effect of high magnetic field intensity on both flow and thermal distributions.

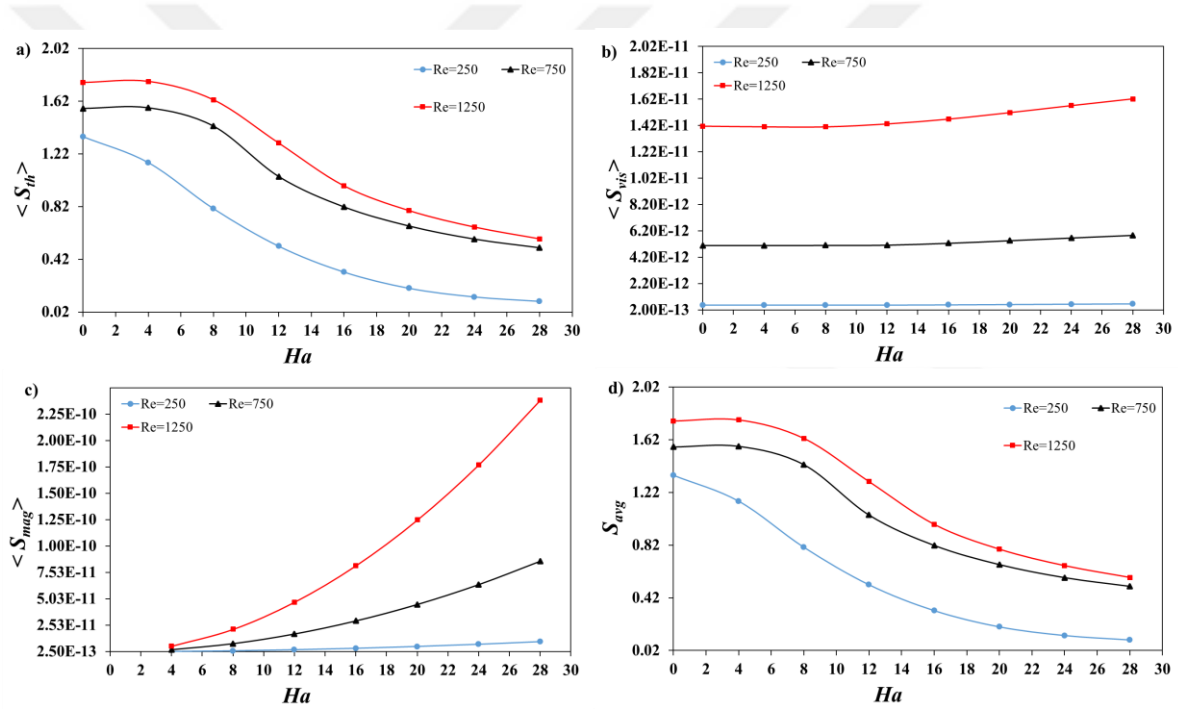

Figure 4.62. The influence of the magnetic field on the average a) thermal entropy generation, $<S_{th}>$ b) viscous entropy generation, $<S_{vis}>$ c) magnetic entropy generation, $<S_{mag}>$ d) total entropy generation, S_{avg} at Reynolds numbers, *Re*=250, 750 and 1250 for nanoparticles volume fraction, Φ=3%

Figures 4.63-4.65 demonstrate the effects of the magnetic field and volume fraction of the nanofluid, Φ on the average thermal entropy generation, $<S_{th}>$ viscous entropy generation, $<S_{vis}>$ magnetic entropy generation, $<S_{mag}>$ and total entropy generation, S_{avg} at Reynolds numbers, *Re*=250, 750 and 1250, respectively for nanoparticles volume fractions, Φ=0%, 3% and 5%. Numerous investigations have informed that there is little variation in the hydrothermal features between host fluids and nanofluids (Hamzah and Sahin, 2023). They attributed this to the

insignificant effect of changing thermophysical properties on hydrothermal behavior compared to changing operating and boundary conditions. Accordingly, this figure revealed that the average value of the total entropy, S_{avg} decreases slightly with increasing CuO concentration in the base liquid. In Figure 4.63 for Re=250, it is possible to detect a difference in S_{avg} value with a change in the CuO concentration, but this difference fades with an increase in the intensity of the magnetic field subjected to the channel. This is because increasing the strength of the magnetic field reduced the difference in temperature gradients, thereby reducing the influence of the thermal properties. In Figure 4.65 for Re=1250, no clear difference can be determined by changing the nanoparticles concentration. This is due to the dominance of a high Reynolds number on both velocity and temperature gradients rather than the change in thermophysical properties.

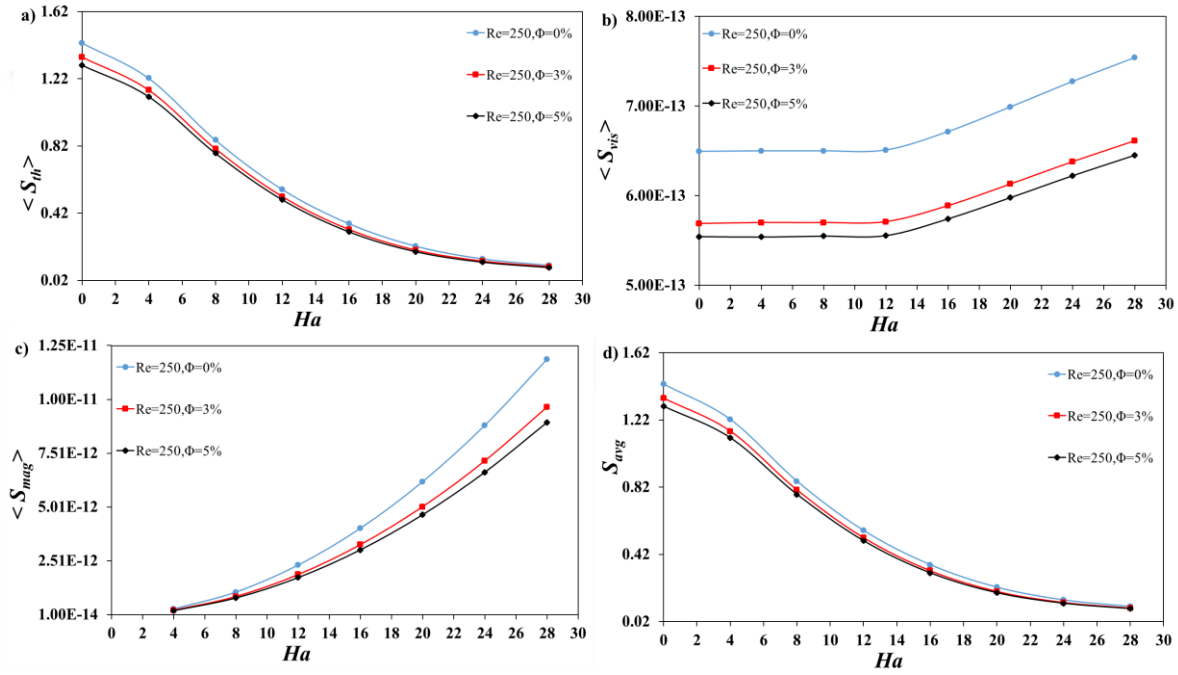

Figure 4.63. The impacts of the magnetic field and volume fraction of the nanofluid, Φ on the average a) thermal entropy generation, $<S_{th}>$ b) viscous entropy generation, $<S_{vis}>$ c) magnetic entropy generation, $<S_{mag}>$ d) total entropy generation, S_{avg} at Reynolds numbers, Re=250 for nanoparticles volume fractions, Φ=0%, 3% and 5%

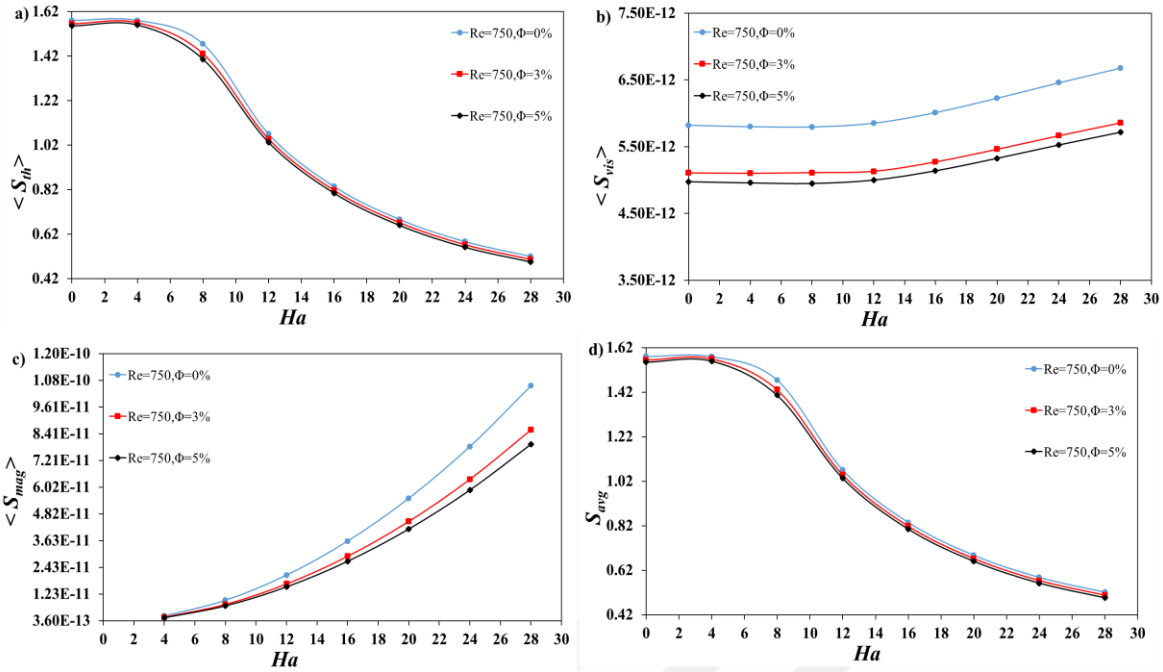

Figure 4.64. The impacts of the magnetic field and volume fraction of the nanofluid, Φ on the average a) thermal entropy generation, $<S_{th}>$ b) viscous entropy generation, $<S_{vis}>$ c) magnetic entropy generation, $<S_{mag}>$ d) total entropy generation, S_{avg} at Reynolds numbers, Re=750 for nanoparticles volume fractions, Φ=0%, 3% and 5%

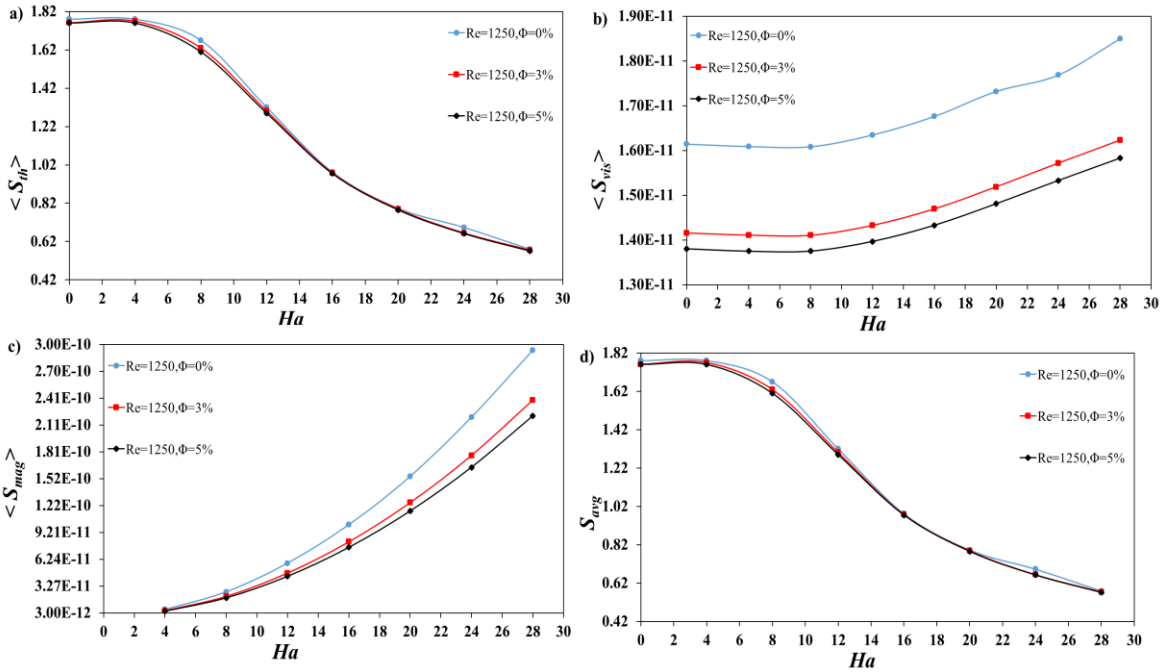

Figure 4.65. The impacts of the magnetic field and volume fraction of the nanofluid, Φ on the average a) thermal entropy generation, $<S_{th}>$ b) viscous entropy generation, $<S_{vis}>$ c) magnetic entropy generation, $<S_{mag}>$ d) total entropy generation, S_{avg} at Reynolds numbers, Re=1250 for nanoparticles volume fractions, Φ=0%, 3% and 5%

5. CONCLUSION

In the first part of the thesis, a numerical simulation has been performed to investigate the influences of the non-uniform magnetic field on the laminar forced convection heat transfer and flow characteristics of a ferrofluid (water and Fe_3O_4) inside a channel with a circular cylinder. In this investigation, the ANSYS Fluent software with a UDF module is employed to simulate MHD laminar forced convection heat transfer in a channel with ferrofluid with a circular cylinder under constant heat flux. The present study becomes the first report of the non-uniform magnetic field effect on the flow and thermal characteristics of a ferrofluid on the confined cylinder with comprehensive analysis including the effects of together with Reynolds numbers, *Re* ferrofluid volume fraction, Φ and magnetic field intensity, *Ha*. The most significant outcomes are highlighted as follows:

The non-uniform magnetic field lessens the recirculation bubble length and alters the flow structure from the unsteady state to the steady state since the magnetic field induced Lorentz forces have a tendency to suppress the vortex diffusion, therefore, the length of the recirculation bubble lowers, and the alternate vortex shedding diminishes.

The two symmetrical vorticity concentrations occur due to the applied non-uniform magnetic field in the channel close to the region where current-carrying wires are located. These vorticity bubbles improve the heat transfer mechanism.

It has been detected that the separation angle, φ of conducting fluid flow from the cylinder surface declines with increasing the *Ha*. For example, when the flow of conducting fluid separates from the cylinder surface at angles of φ= 45º and 56º at *Ha*=0 for *Re*=25 and 50, respectively, it takes place on the location of φ= 27.5º and 46º for *Ha*=6, φ= 2.5º and 23.75º for *Ha*=14 at *Re*=25 and 50, respectively.

The increasing trend of the total C_D with increasing *Ha* may be associated with an increased value of the Lorentz force which acts directly to suppress mainstream flow component and augmented variation between upstream and downstream pressures. At *Re*=50, the total C_D increases by almost 20% when *Ha* grows from *Ha*=0 to *Ha*=6 and subsequently increases by 61% at *Ha*=10.

Obtained results demonstrate that the thermal boundary layer thickness progressively decreases, and the temperature gradient gets higher as the *Ha* is gradually increased from *Ha*=0 to *Ha*=18 at *Re*=25 which means that the heat transfer rate around the cylinder is enhanced.

When the average Nusselt number is computed as Nu_{avg}= 7.637 for the case of no applied magnetic field, *Ha*=0 it enhances to the values of Nu_{avg}=8.532 and 9.414 for *Ha*=10 and 18, respectively at *Re*=25

While increasing the ferrofluid volume fraction, Φ improves the Nu_{avg} independent of the non-uniform magnetic field application, it has no substantial effect on patterns of streamlines and vorticity as well as the total C_D. According to outcomes of numerical simulation, there is an increase in Nu_{avg} with 3.98% and 3.88% for Ha=2 and 18 respectively when values of Φ increase from Φ=0% to Φ=4% at Re=25.

It can be deduced that within the considered range of Reynolds, Re and Hartmann numbers, Ha the Re has a greater influence on the generation of the total entropy.

The optimum thermal performance criterion, ξ according to the highest rate of heat transfer and the lowest production of irreversibility, is detected for Re=150, Ha=0 and Φ =4%.

In the second part of the thesis, a numerical study has been carried out to explore the impacts of the uniform magnetic field on the hydrothermal characteristics of a nanofluid (water and CuO) inside a rectangular grooved channel. In this work, the ANSYS Fluent software with UDF module is used to perform numerical simulation of MHD laminar forced convection heat transfer in the rectangular grooved channel filled with nanofluid. The current investigation becomes the first study related to the uniform magnetic field effect on the hydrothermal behaviors of a nanofluid in the rectangular grooved channel with extensive analysis comprising the influences of together Hartmann number, Ha, Reynolds number, Re and volume fraction of nanoparticles, Φ. The most important results are demonstrated as follows:

The size of the recirculation region in rectangular grooves diminishes with the application of a uniform magnetic field at both Re=250 and 1250. Furthermore, this uniform magnetic field is found to be more effective in the suppression of the recirculation zone in rectangular grooves at Re=250 compared to Re=1250.

The Lorentz force resulting from the uniform magnetic field enhances the velocity gradient and temperature gradient near the hot walls which makes Nu_{avg} to be augmented.

When the average Nusselt number is observed as Nu_{avg}= 4.976 at Ha=0 it enhances to values of Nu_{avg}=5.428 and 6.49 for Ha=8 and 24, respectively corresponding Nu_{avg} augmentation by 9.08% for Ha=8 and 30.42% for Ha=24 compared to the absence of magnetic field, Ha=0 at Re=250

The value of the local Nusselt number, Nu_L is greater on the straight section of the heated wall compared to the grooved section of the heated wall for all examined Ha due to the direct contact of the straight section of the heated wall with the main cold flow which induces a higher temperature gradient thus heat transfer rate. On the grooved section of the heated wall, the recirculation zone restrains the contact of the wall surfaces with the main cold flow.

In the absence of the magnetic field, Ha=0 increasing volume fraction of nanoparticles from Φ=0% to Φ=5% gives rise to 3.71% average Nusselt number, Nu_{avg} augmentation while this value is 3.13 %, 2.3% and 2.09% when the Hartmann number increases to Ha=8, 16 and 24, respectively at Re=250.

For a given Reynolds number, *Re* it can be observed that total entropy production reduces substantially after the Hartmann number, *Ha*>8 due to a significant influence of the high magnetic field intensity on the flow and thermal distributions together.

REFERENCES

Abu-Nada, E., Masoud, Z., Oztop, H. F., and Campo, A., 2010. Effect of nanofluid variable properties on natural convection in enclosures. International Journal of Thermal Sciences, 49(3): 479-491.

Albojamal, A., and Vafai, K., 2017. Analysis of single phase, discrete and mixture models, in predicting nanofluid transport. International Journal of Heat and Mass Transfer, 114: 225-237.

Albojamal, A., Hamzah, H., Haghighi, A., and Vafai, K., 2017. Analysis of nanofluid transport through a wavy channel. Numerical Heat Transfer, Part A: Applications, 72(12): 869-890.

Ali, F. H., Hamzah, H. K., Egab, K., Arıcı, M., and Shahsavar, A., 2020. Non-newtonian nanofluid natural convection in a U-shaped cavity under magnetic field. International Journal of Mechanical Sciences, 186: 105887.

Ali, M. M., Akhter, R., and Alim, M. A., 2020. MHD natural convection and entropy generation in a grooved enclosure filled with nanofluid using two-component non-homogeneous model. SN Applied Sciences, 2(4).

Al-Kouz, W., Alshare, A., Kiwan, S., Al-Muhtady, A., Alkhalidi, A., and Saadeh, H., 2018. Two-dimensional analysis of low-pressure flows in an inclined square cavity with two fins attached to the hot wall. International Journal of Thermal Sciences, 126: 181–193.

Aminfar, H., Mohammadpourfard, M., and Ahangar Zonouzi, S., 2013. Hydrothermal behavior of a ferrofluid in a corrugated channel in the presence of a magnetic field. Heat Transfer-Asian Research, 43(1): 80-92.

Aminfar, H., Mohammadpourfard, M., and Ahangar Zonouzi, S., 2013. Numerical Study of the ferrofluid flow and heat transfer through a rectangular duct in the presence of a non-uniform transverse magnetic field. Journal of Magnetism and Magnetic Materials, 327: 31-42.

Anagnostopoulos, P., Iliadis, G., and Richardson, S., 1996. Numerical Study of the blockage effects on viscous flow past a circular cylinder. International Journal for Numerical Methods in Fluids, 22(11): 1061-1074.

Arjun, K. S., and Rakesh, K., 2020. Heat transfer in magnetohydrodynamic nanofluid flow past a circular cylinder. Phys. Fluids. 32: 045112.

Asadi, A., Hossein Nezhad, A., Sarhaddi, F., and Keykha, T., 2019. Laminar ferrofluid heat transfer in presence of non-uniform magnetic field in a channel with sinusoidal wall: A numerical study. Journal of Magnetism and Magnetic Materials, 471: 56-63.

Ashorynejad, H. R., Mohamad, A. A., and Sheikholeslami, M., 2013. Magnetic field effects on natural convection flow of a nanofluid in a horizontal cylindrical annulus using lattice Boltzmann method. International Journal of Thermal Sciences, 64: 240-250.

Bahiraei, M., 2016. A numerical study of heat transfer characteristics of CuO-water nanofluid by Euler-Lagrange approach. Journal of Thermal Analysis and Calorimetry, 123(2): 1591–1599.

Bai, M., Xu, Z., and Lv, J., 2008. Application of nanofluids in engine cooling system. SAE Technical Paper Series.

Barzegar Gerdroodbary, M., Sheikholeslami, M., Mousavi, S. V., Anazadehsayed, A., and Moradi, R., 2018. The influence of non-uniform magnetic field on heat transfer intensification of ferrofluid inside a T-junction. Chemical Engineering and Processing - Process Intensification, 123: 58-66.

Behr, M., Hastreiter, D., Mittal, S., and Tezduyar, T., 1995. Incompressible flow past a circular cylinder: Dependence of the computed flow field on the location of the lateral boundaries. Computer Methods in Applied Mechanics and Engineering, 123(1-4): 309-316.

Bi, S., Shi, L., and Zhang, L., 2008. Application of nanoparticles in domestic refrigerators. Applied Thermal Engineering, 28(14-15): 1834-1843.

Blishchik, A., Van der Lans, M., and Kenjereš, S., 2021. An extensive numerical benchmark of the various magnetohydrodynamic flows. International Journal of Heat and Fluid Flow, 90: 108800.

Boungiorno, J., Hu, L. W., Kim, S. J., Hannink, R., Truong, B., and Forrest, E., 2008. Nanofluids for enhanced economics and safety of nuclear reactors: An evaluation of the potential features issues, and research gaps. Nuclear Technology, 162(1): 80–91.

Bovand, M., Rashidi, S., Dehghan, M., Esfahani, J., and Valipour, M., 2015. Control of Wake and vortex shedding behind a porous circular obstacle by exerting an external magnetic field. Journal of Magnetism and Magnetic Materials, 385: 198-206.

Bramley, J. S., 1975. Magnetohydrodynamic flow past a circular cylinder. II. Zeitschrift Für Angewandte Mathematik Und Physik ZAMP, 26(2): 203-209.

Chakraborty, J., Verma, N., and Chhabra, R., 2004. Wall effects in flow past a circular cylinder in a plane channel: A numerical study. Chemical Engineering and Processing: Process Intensification, 43(12): 1529-1537.

Chatterjee, D., Chatterjee, K., Mondal, B., and Hui, N. B., 2013. Wall-confined flow and heat transfer around a square cylinder at low Reynolds and hartmann numbers. Heat Transfer-Asian Research, 43(5): 459-475.

Chen, J., Pritchard, W. G., and Tavener, S. J., 1995. Bifurcation for flow past a cylinder between parallel planes. Journal of Fluid Mechanics, 284: 23-41.

Cliffe, K. A., and Tavener, S. J., 2004. The effect of cylinder rotation and blockage ratio on the onset of periodic flows. Journal of Fluid Mechanics, 501: 125-133.

Coutanceau, M., and Bouard, R., 1977. Experimental determination of the main features of the viscous flow in the wake of a circular cylinder in uniform translation. part 1. Steady Flow. Journal of Fluid Mechanics, 79(2): 231-256.

Cuevas, S., Smolentsev, S., and Abdou, M. A., 2006. On the flow past a magnetic obstacle. Journal of Fluid Mechanics, 553(-1): 227.

Darr, S., Hu, H., Glikin, N., Hartwig, J., Majumdar, A., Leclair, A., and Chung, J., 2016. An experimental study on terrestrial cryogenic tube Chilldown II. effect of flow direction with respect to gravity and new correlation set. International Journal of Heat and Mass Transfer, 103: 1243-1260.

Devendiran, D. K., and Amirtham, V. A., 2016. A review on preparation, characterization, properties and applications of nanofluids. Renewable and Sustainable Energy Reviews, 60: 21–40.

Dousset, V., and Pothérat, A., 2008. Numerical simulations of a cylinder wake under a strong axial magnetic field. Physics of Fluids, 20(1): 017104.

Fan, X., Chen, H., Ding, Y., Plucinski, P. K., and Lapkin, A. A., 2008. Potential of 'nanofluids' to further intensify microreactors. Green Chemistry, 10(6): 670.

Farahi, S., and Hossein, N., 2017. Investigation of magnetohydrodynamics flow and heat transfer in the presence of a confined square cylinder using SM82 equations. Thermal Science, 21(2): 889-899.

Feng, X., Liu, Q., and He, Y., 2020. Numerical simulations of convection heat transfer in porous media using a cascaded lattice Boltzmann method. International Journal of Heat and Mass Transfer, 151: 119410.

Frank, M., Barleon, L., and Müller, U., 2001. Visual analysis of two-dimensional magnetohydrodynamics. Physics of Fluids, 13(8): 2287-2295.

Ghasemi, B., Aminossadati, S. M., and Raisi, A., 2011. Magnetic Field Effect on natural convection in a nanofluid-filled square enclosure. International Journal of Thermal Sciences, 50: 1748-1756.

Ghasemian, M., Najafian Ashrafi, Z., Goharkhah, M., and Ashjaee, M., 2015. Heat transfer characteristics of Fe3O4 ferrofluid flowing in a mini channel under constant and alternating magnetic fields. Journal of Magnetism and Magnetic Materials, 381: 158-167.

Ghosh, S., Sarkar, S., Sivakumar, R., and Sekhar, T. V., 2018. Full magnetohydrodynamic flow past a circular cylinder considering the penetration of magnetic field. Physics of Fluids, 30(8): 087102.

Gibanov, N. S., Sheremet, M. A., Oztop, H. F., and Nusier, O. K., 2017. Convective heat transfer of ferrofluid in a lid-driven cavity with a heat-conducting solid backward step under the effect of a variable magnetic field. Numerical Heat Transfer, Part A: Applications, 72(1): 54-67.

Gnanadason, M., Kumar, P., Jemilda, G., and Jasper, S., 2012. Effect of nanofluids in a modified vacuum single basin solar still. Int J Sci Eng Res, January, 1–7.

Gosselin, L., and Da Silva, A. K., 2004. Combined “heat transfer and power dissipation” optimization of nanofluid flows. Applied Physics Letters, 85(18): 4160-4162.

Grigoriadis, D., Kassinos, S., and Votyakov, E., 2009. Immersed boundary method for the MHD flows of liquid metals. Journal of Computational Physics, 228(3): 903-920.

Grigoriadis, D., Sarris, I., and Kassinos, S., 2010. MHD flow past a circular cylinder using the immersed boundary method. Computers & Fluids, 39(2): 345-358.

Gürdal, M., Arslan, K., Gedik, E., and Minea, A. A., 2022. Effects of using nanofluid, applying a magnetic field, and placing turbulators in channels on the Convective Heat Transfer: A comprehensive review. Renewable and Sustainable Energy Reviews, 162: 112453.

Gürdal, M., Pazarlıoğlu, H. K., Tekir, M., Arslan, K., and Gedik, E., 2022. Numerical investigation on turbulent flow and heat transfer characteristics of Ferro-nanofluid flowing in dimpled tube under magnetic field effect. Applied Thermal Engineering, 200: 117655.

Hamzah, H., Albojamal, A., Sahin, B., and Vafai, K., 2020. Thermal management of transverse magnetic source effects on nanofluid natural convection in a wavy porous enclosure. Journal of Thermal Analysis and Calorimetry, 143(3): 2851-2865.

Hamzah, H., and Sahin, B., 2023. Analysis of SWCNT-water nanofluid flow in wavy channel under turbulent pulsating conditions: Investigation of homogeneous and discrete phase models. International Journal of Thermal Sciences, 184: 108011.

Hariri, S., Mokhtari, M., Gerdroodbary, M. B., and Fallah, K., 2017. Numerical investigation of the heat transfer of a ferrofluid inside a tube in the presence of a non-uniform magnetic field. The European Physical Journal Plus, 132(2).

Heidary, H., Kermani, M., and Dabir, B., 2017. Magnetic field effect on convective heat transfer in corrugated flow channel. Thermal Science, 21(5): 2105-2115.

Hu, P., and Li, Q., 2020. Effect of heat source on forced convection in a partially-filled porous channel under LTNE condition. International Communications in Heat and Mass Transfer, 114: 104578.

Hussain, S., Öztop, H. F., Qureshi, M. A., and Abu-Hamdeh, N., 2019. Magnetohydrodynamic flow and heat transfer of ferrofluid in a channel with non-symmetric cavities. Journal of Thermal Analysis and Calorimetry, 140(2): 811-823.

Hussam, W. K., and Sheard, G. J., 2013. Heat transfer in a high hartmann number MHD duct flow with a circular cylinder placed near the heated side-wall. International Journal of Heat and Mass Transfer, 67: 944-954.

Hussam, W. K., Thompson, M. C., and Sheard, G. J., 2011. Dynamics and heat transfer in a quasi-two-dimensional MHD flow past a circular cylinder in a duct at High Hartmann number. International Journal of Heat and Mass Transfer, 54(5-6): 1091-1100.

Hwang, Y., Park, H., Lee, J., and Jung, W., 2006. Thermal conductivity and lubrication characteristics of nanofluids. Current Applied Physics, 6.

International Energy Agency, 2020. World gross electricity production, by source, 2018,https://www.iea.org/data-and-statistics/charts/world-gross-electricityproduction- by-source-2018, (last accessed in October,2020).

Ishak, A., Nazar, R., and Pop, I., 2008. Magnetohydrodynamic (MHD) flow and heat transfer due to a stretching cylinder. Energy Conversion and Management, 49(11): 3265-3269.

Izadi, M., Maleki, N. M., Pop, I., and Mehryan, S., 2019. Natural convection of a hybrid nanofluid subjected to non-uniform magnetic field within porous medium including circular heater. International Journal of Numerical Methods for Heat and Fluid Flow, 29(4): 1211-1231.

Jafari, M., Farhadi, M., and Sedighi, K., 2017. An experimental study on the effects of a new swirl generator on thermal performance of a circular tube. International Communications in Heat and Mass Transfer, 87: 277–287.

Jalal, R., Goharshadi, E. K., Abareshi, M., Moosavi, M., Yousefi, A., and Nancarrow, P., 2010. ZnO nanofluids: Green synthesis, characterization, and antibacterial activity. Materials Chemistry and Physics, 121(1–2): 198–201.

Janssen, L. A. M., and Hoogendoorn, C. J., 1978. Laminar convective heat transfer in helical coiled tubes. International Journal of Heat and Mass Transfer, 21(9): 1197–1206.

Josserand, J., Marty, P., and Alemany, A., 1993. Pressure and drag measurements on a cylinder in a liquid metal flow with an aligned magnetic field. Fluid Dynamics Research, 11(3): 107-117.

Kanaris, N., Albets, X., Grigoriadis, D., and Kassinos, S., 2013. Three-dimensional numerical simulations of magnetohydrodynamic flow around a confined circular cylinder under low, moderate, and strong magnetic fields. Physics of Fluids, 25(7): 074102.

Kao, M., Lo, C., Tsung, T., Wu, Y., Jwo, C., and Lin, H., 2007. Copper-oxide brake nanofluid manufactured using ARC-submerged Nanoparticle Synthesis System. Journal of Alloys and Compounds, 434-435: 672-674.

Kefayati, G., 2016. Simulation of heat transfer and entropy generation of MHD natural convection of non-newtonian nanofluid in an enclosure. International Journal of Heat and Mass Transfer, 92: 1066-1089.

Khan, W. A., Culham, J. R., and Yovanovich, M. M., 2004. Fluid flow and heat transfer from a cylinder between parallel planes. Journal of Thermophysics and Heat Transfer, 18(3): 395-403.

Kim, S., and Lee, C. M., 2000. Investigation of the flow around a circular cylinder under the influence of an electromagnetic force. Experiments in Fluids, 28(3): 252-260.

Kim, Y. S., and Kim, Y. H., 2003. Application of ferro-cobalt magnetic fluid for oil sealing. Journal of Magnetism and Magnetic Materials, 267(1): 105–110.

Kolesnikov, Y. B., and Tsinober, A. B., 1976. Experimental investigation of two-dimensional turbulence behind a grid. Fluid Dynamics, 9(4): 621-624.

Kotcioğlu, İ., 1998. Heat Transfer and Flow Structure in a Rectangular Channel with Wing-Type Vortex Generator. Turkish Journal of Engineering and Environmental Sciences, 22 (3): 185-196.

Krasnov, D., Zikanov, O., and Boeck, T., 2012. Numerical study of magnetohydrodynamic duct flow at High Reynolds and Hartmann Numbers. Journal of Fluid Mechanics, 704: 421-446.

Kulkarni, D. P., Das, D. K., and Vajjha, R. S., 2009. Application of nanofluids in heating buildings and reducing pollution. Applied Energy, 86(12): 2566-2573.

Kurtulmuş, N., Zontul, H., and Sahin, B., 2020. Heat transfer and flow characteristics in a sinusoidally curved converging-diverging channel. International Journal of Thermal Sciences, 148: 106163.

Lahjomri, J., Capéran, P., and Alemany, A., 1993. The cylinder wake in a magnetic field aligned with the velocity. Journal of Fluid Mechanics, 253(-1): 421.

Larimi, M., Ghanaat, A., Ramiar, A., and Ranjbar, A., 2016. Forced convection heat transfer in a channel under the influence of various non-uniform transverse magnetic field arrangements. International Journal of Mechanical Sciences, 118: 101-112.

Lee, M., and Kim, Y., 2020. Effect of non-uniform magnetic fields on the characteristics of ferrofluid flow in a square enclosure. Journal of Magnetism and Magnetic Materials, 506: 166697.

Ma, Y., Mohebbi, R., Rashidi, M., and Yang, Z., 2019. MHD convective heat transfer of AG-mgo/water hybrid nanofluid in a channel with active heaters and Coolers. International Journal of Heat and Mass Transfer, 137: 714-726.

Malmir-Chegini, Y., and Amanifard, N., 2019. Heat transfer enhancement inside semi-insulated horizontal pipe by controlling the secondary flow of oil-based ferro-fluid in the presence of non-uniform magnetic field: A general correlation for the Nusselt number. Applied Thermal Engineering, 159: 113839.

Mehrez, Z., El Cafsi, A., Belghith, A., and Le Quéré, P., 2015. MHD effects on heat transfer and entropy generation of nanofluid flow in an open cavity. Journal of Magnetism and Magnetic Materials, 374: 214-224.

Mei, S., Qi, C., Luo, T., Zhai, X., and Yan, Y., 2019. Effects of magnetic field on thermo-hydraulic performance of Fe3O4-water nanofluids in a corrugated tube. International Journal of Heat and Mass Transfer, 128: 24-45.

Mettu, S., Verma, N., and Chhabra, R. P., 2006. Momentum and heat transfer from an asymmetrically confined circular cylinder in a plane channel. Heat and Mass Transfer, 42(11): 1037-1048.

Meyer, J., McKrell, T., and Grote, K., 2013. The influence of multi-walled carbon nanotubes on single-phase heat transfer and pressure drop characteristics in the transitional flow regime of smooth tubes. International Journal of Heat and Mass Transfer, 58(1-2): 597-609.

Midya, C., Layek, G. C., Gupta, A. S., and Mahapatra, T. R., 2003. Magnetohydrodynamic viscous flow separation in a channel with constrictions. Journal of Fluids Engineering, 125(6): 952-962.

Moreau, R. J., and Wright, A. F., 1990. Magnetohydrodynamics. Dordrecht: Kluwer academic.

Morley, N. B., Smolentsev, S., Barleon, L., Kirillov, I. R., and Takahashi, M., 2000. Liquid magnetohydrodynamics — recent progress and future directions for fusion. Fusion Engineering and Design, 51-52: 701-713.

Mousavi, S. M., Biglarian, M., Darzi, A. A., Farhadi, M., Afrouzi, H. H., and Toghraie, D., 2019. Heat transfer enhancement of ferrofluid flow within a wavy channel by applying a non-uniform magnetic field. Journal of Thermal Analysis and Calorimetry, 139(5): 3331-3343.

Mousavi, S. V., Sheikholeslami, M., Gorji bandpy, M., and Barzegar Gerdroodbary, M., 2016. The influence of magnetic field on heat transfer of magnetic nanofluid in a sinusoidal double pipe heat exchanger. Chemical Engineering Research and Design, 113: 112-124.

Mück, B., Günther, C., Müller, U., and Bühler, L., 2000. Three-dimensional MHD flows in rectangular ducts with internal obstacles. Journal of Fluid Mechanics, 418: 265-295.

Müller, U., and Bühler, L., 2001. Magnetohydrodynamics in channels and containers. Berlin: Springer.

Mutschke, G., Gerbeth, G., Shatrov, V., and Tomboulides, A., 1997. Two- and three-dimensional instabilities of the cylinder wake in an aligned magnetic field. Physics of Fluids, 9(11): 3114-3116.

Mutschke, G., Gerbeth, G., Shatrov, V., and Tomboulides, A., 2001. The scenario of three-dimensional instabilities of the cylinder wake in an external magnetic field: A Linear Stability Analysis. Physics of Fluids, 13(3): 723-734.

Mutschke, G., Shatrov, V., and Gerbeth, G., 1998. Cylinder wake control by magnetic fields in liquid metal flows. Experimental Thermal and Fluid Science, 16(1-2): 92-99.

Naphon, P., and Wongwises, S., 2006. A review of flow and heat transfer characteristics in curved tubes. Renewable and Sustainable Energy Reviews, 10(5): 463-490.

Nikelham, A., Enjilela, V., Vaziri, N., and Poolaei Moziraji, Z., 2022. The effects of magnetic-field direction and magnitude on forced convection of aluminum oxide–water nanofluid over a circular cylinder. International Journal of Thermal Sciences, 173: 107398.

O'Hanley, H., Buongiorno, J., McKrell, T., and Hu, L., 2011. Measurement and model correlation of specific heat capacity of water-based nanofluids with silica, alumina and copper oxide nanoparticles. Volume 10: Heat and Mass Transport Processes, Parts A and B.

Papailiou, D. D., 1985. Magneto-fluid-mechanic turbulent vortex streets. Single- and Multi-Phase Flows in an Electromagnetic Field: Energy, Metallurgical, and Solar Applications, 152-173.

Paramane, S. B., and Sharma, A., 2009. Numerical investigation of heat and fluid flow across a rotating circular cylinder maintained at constant temperature in 2-D laminar flow regime. International Journal of Heat and Mass Transfer, 52(13-14): 3205-3216.

Philip, J., Jaykumar, T., Kalyanasundaram, P., and Raj, B., 2003. A tunable optical filter. Measurement Science and Technology, 14(8): 1289–1294.

Popa, I., Gillies, G., Papastavrou, G., and Borkovec, M., 2010. Attractive and repulsive electrostatic forces between positively charged latex particles in the presence of anionic linear polyelectrolytes. Journal of Physical Chemistry B, 114(9): 3170–3177.

Prasad, K., Paramane, S. B., Agrawal, A., and Sharma, A., 2011. Effect of channel-confinement and rotation on the two-dimensional laminar flow and heat transfer across a cylinder. Numerical Heat Transfer, Part A: Applications, 60(8): 699-726.

Rashidi, M., Nasiri, M., Khezerloo, M., and Laraqi, N., 2016. Numerical investigation of magnetic field effect on mixed convection heat transfer of nanofluid in a channel with sinusoidal walls. Journal of Magnetism and Magnetic Materials, 401: 159-168.

Rashidi, S., and Esfahani, J., 2015. The effect of magnetic field on instabilities of heat transfer from an obstacle in a channel. Journal of Magnetism and Magnetic Materials, 391, 5-11.

Rashidi, S., Bovand, M., Esfahani, J. A., Öztop, H. F., and Masoodi, R., 2015. Control of wake structure behind a square cylinder by Magnetohydrodynamics. Journal of Fluids Engineering, 137(6).

Rashidi, S., Dehghan, M., Ellahi, R., Riaz, M., and Jamal-Abad, M., 2015. Study of stream wise transverse magnetic fluid flow with heat transfer around an obstacle embedded in a porous medium. Journal of Magnetism and Magnetic Materials, 378: 128-137.

Rezaie, M. R., and Norouzi, M., 2018. Numerical investigation of MHD flow of non-newtonian fluid over confined circular cylinder: A lattice Boltzmann approach. Journal of the Brazilian Society of Mechanical Sciences and Engineering, 40(4).

Sáchica, D., Treviño, C., and Martínez-Suástegui, L., 2020. Numerical study of magnetohydrodynamic mixed convection and entropy generation of Al2O3-water nanofluid in a channel with two facing cavities with discrete heating. International Journal of Heat and Fluid Flow, 86: 108713.

Saeedinia, M., Akhavan-Behabadi, M. A., and Razi, P., 2012. Thermal and rheological characteristics of CuO-Base oil nanofluid flow inside a circular tube. International Communications in Heat and Mass Transfer, 39(1): 152–159.

Sahin, M., and Owens, R. G., 2004. A numerical investigation of wall effects up to high blockage ratios on two-dimensional flow past a confined circular cylinder. Physics of Fluids, 16(5): 1305-1320.

Said, Z., El Haj Assad, M., Hachicha, A. A., Bellos, E., Abdelkareem, M. A., Alazaizeh, D. Z., and Yousef, B. A., 2019. Enhancing the performance of Automotive Radiators using nanofluids. Renewable and Sustainable Energy Reviews, 112: 183-194.

Saidur, R., Leong, K. Y., and Mohammed, H. A., 2011. A review on applications and challenges of nanofluids. Renewable and Sustainable Energy Reviews, 15(3): 1646–1668.

Sathiyamoorthy, M., and Chamkha, A., 2010. Effect of magnetic field on natural convection flow in a liquid gallium filled square cavity for linearly heated side wall(s). International Journal of Thermal Sciences, 49(9): 1856-1865.

Sekhar, T., Sivakumar, R., and Ravi Kumar, T., 2006. Flow around a circular cylinder in an external magnetic field at high Reynolds Numbers. International Journal of Numerical Methods for Heat & Fluid Flow, 16(6): 740-759.

Sekhar, T., Sivakumar, R., Kumar, H., and Ravi kumar, T., 2007. Effect of aligned magnetic field on the steady viscous flow past a circular cylinder. Applied Mathematical Modelling, 31(1): 130-139.

Sekhar, T., Sivakumar, R., Kumar, H., and Ravi kumar, T., 2007. Effect of aligned magnetic field on the steady viscous flow past a circular cylinder. Applied Mathematical Modelling, 31(1): 130-139.

Selimefendigil, F., and Öztop, H. F., 2015. Influence of inclination angle of magnetic field on mixed convection of nanofluid flow over a backward facing step and entropy generation. Advanced Powder Technology, 26(6): 1663-1675.

Selimefendigil, F., and Öztop, H. F., 2018. Magnetic field effects on the forced convection of CuO-water nanofluid flow in a channel with circular cylinders and thermal predictions using ANFIS. International Journal of Mechanical Sciences, 146-147: 9-24.

Selimefendigil, F., and Öztop, H. F., 2019. MHD pulsating forced convection of nanofluid over parallel plates with blocks in a channel. International Journal of Mechanical Sciences, 157-158: 726-740.

Selimefendigil, F., and Öztop, H. F., 2020. Control of natural convection in a CNT-water nanofluid filled 3D cavity by using an inner T-shaped obstacle and thermoelectric cooler. International Journal of Mechanical Sciences, 169: 105104.

Shaker, H., Abbasalizadeh, M., Khalilarya, S., and Motlagh, S. Y., 2021. Two-phase modeling of the effect of non-uniform magnetic field on mixed convection of magnetic nanofluid inside an open cavity. International Journal of Mechanical Sciences, 207: 106666.

Sheikholeslami, M., and Vajravelu, K., 2017. Nanofluid flow and heat transfer in a cavity with variable magnetic field. Applied Mathematics and Computation, 298: 272-282.

Sheikholeslami, M., Gorji-Bandpy, M., and Ganji, D. D., 2014. Investigation of nanofluid flow and heat transfer in presence of magnetic field using KKL model. Arabian Journal for Science and Engineering, 39(6): 5007-5016.

Sheikholeslami, M., Rashidi, M., and Ganji, D., 2015. Effect of non-uniform magnetic field on forced convection heat transfer of Fe3O4–water nanofluid. Computer Methods in Applied Mechanics and Engineering, 294: 299-312.

Shen, B., Shih, A. J., and Tung, S. C., 2008. Application of nanofluids in minimum quantity lubrication grinding. Tribology Transactions, 51(6): 730–737.

Siavashi, M., Yousofvand, R., and Rezanejad, S., 2018. Nanofluid and porous fins effect on natural convection and entropy generation of flow inside a cavity. Advanced Powder Technology, 29(1): 142-156.

Singha, S., and Sinhamahapatra, K., 2011. Control of vortex shedding from a circular cylinder using imposed transverse magnetic field. International Journal of Numerical Methods for Heat and Fluid Flow, 21(1): 32-45.

Singha, S., Sinhamahapatra, K. P., and Mukherjea, S. K., 2006. Control of vortex shedding from a bluff body using imposed magnetic field. Journal of Fluids Engineering, 129(5): 517-523.

Sivakumar, A., Alagumurthi, N., and Senthilvelan, T., 2015. Experimental investigation of forced convective heat transfer performance in nanofluids of Al2O3/water and CuO/water in a serpentine shaped micro channel heat sink. Heat and Mass Transfer, 52(7): 1265-1274.

Sivakumar, R., Vimala, S., and Sekhar, T. V., 2015. Influence of induced magnetic field on thermal MHD flow. Numerical Heat Transfer, Part A: Applications, 68(7): 797-811.

Sommeria, J., and Moreau, R., 1982. Why, how, and when, MHD turbulence becomes two-dimensional. Journal of Fluid Mechanics, 118: 507-518.

Syam Sundar, L., Naik, M., Sharma, K., Singh, M., and Siva Reddy, T., 2012. Experimental investigation of forced convection heat transfer and friction factor in a tube with Fe3O4 magnetic nanofluid. Experimental Thermal and Fluid Science, 37: 65-71.

Tassone, A., Nobili, M., and Caruso, G., 2018. Numerical Study of the MHD flow around a bounded heating cylinder: Heat transfer and pressure drops. International Communications in Heat and Mass Transfer, 91: 165-175.

Taylor, R. A., Phelan, P. E., Otanicar, T. P., Walker, C. A., Nguyen, M., Trimble, S., and Prasher, R., 2011. Applicability of nanofluids in high flux solar collectors. Journal of Renewable and Sustainable Energy, 3(2): 023104.

Teamah, M. A., 2008. Numerical simulation of double diffusive natural convection in rectangular enclosure in the presences of magnetic field and heat source. International Journal of Thermal Sciences, 47(3): 237-248.

Thirugnanasambandam, M., Iniyan, S., and Goic, R., 2010. A review of solar thermal technologies. Renewable and Sustainable Energy Reviews, 14(1): 312–322.

Tokgoz, N., Aksoy, M., and Sahin, B., 2017. Investigation of flow characteristics and heat transfer enhancement of corrugated duct geometries. Applied Thermal Engineering, 118: 518-530.

Tsai, C. Y., Chien, H. T., Ding, P. P., Chan, B., Luh, T. Y., and Chen, P. H., 2004. Effect of structural character of gold nanoparticles in nanofluid on heat pipe thermal performance. Materials Letters, 58(9): 1461–1465.

Tzeng, S. C., Lin, C. W., and Huang, K. D., 2005. Heat transfer enhancement of nanofluids in rotary blade coupling of four-wheel-drive vehicles. Acta Mechanica, 179(1–2): 11–23.

U.S. Energy Information Administration 2020. International Energy Outlook 2019 with projections to 2050,https://www.eia.gov/outlooks/ieo/pdf/ieo2019.pdf, (lastaccessed in April,2020).

Uda, N., Miyazawa, A., Inoue, S., Yamaoka, N., Horiike, H., and Miyazaki, K., 2001. Forced convection heat transfer and temperature fluctuations of lithium under transverse magnetic fields. Journal of Nuclear Science and Technology, 38(11): 936-943.

Udhayakumar, S., Abin Rejeesh, A. D., Sekhar, T. V., and Sivakumar, R., 2016. Numerical investigation of magnetohydrodynamic mixed convection over an isothermal circular cylinder in presence of an aligned magnetic field. International Journal of Heat and Mass Transfer, 95: 379-392.

Udhayakumar, S., Rajeesh, A.D.A., Sekhar, T. V. S., and Sivakumar R., 2016 Study of directional control of heat transfer and flow control in the magnetohydrodynamic flow in cylindrical geometry. Int. J. Heat Fluid Flow, 61:482–498.

Valiallah Mousavi, S., Barzegar Gerdroodbary, M., Sheikholeslami, M., and Ganji, D. D., 2016. The influence of a magnetic field on the heat transfer of a magnetic nanofluid in a sinusoidal channel. The European Physical Journal Plus, 131(9).

Vimala, S., Damodaran, S., Sivakumar, R., and Sekhar, T., 2016. The role of Magnetic Reynolds number in MHD forced convection heat transfer. Applied Mathematical Modelling, 40(13-14): 6737-6753.

Wang, B. X., Zhou, L. P., and Peng, X. F., 2006. Surface and size effects on the specific heat capacity of nanoparticles. International Journal of Thermophysics, 27(1): 139–151.

Wang, C. C., and Chen, C. K., 2002. Forced convection in a wavy-wall channel. International Journal of Heat and Mass Transfer, 45: 2587–2595.

Williamson, C. H., 1996. Vortex Dynamics in the cylinder wake. Annual Review of Fluid Mechanics, 28(1): 477-539.

Ying, F., and Hulin, H., 2007. Simulation of free surface MHD-flow and heat transfer around a cylinder. Heat Transfer—Asian Research, 37(1): 11-19.

Yoon, H., Chun, H., Ha, M., and Lee, H., 2004. A numerical study on the fluid flow and heat transfer around a circular cylinder in an aligned magnetic field. International Journal of Heat and Mass Transfer, 47(19-20): 4075-4087.

Yu, P., Qiu, J., Qin, Q., and Tian, Z. F., 2013. Numerical investigation of natural convection in a rectangular cavity under different directions of uniform magnetic field. International Journal of Heat and Mass Transfer, 67: 1131-1144.

Zdravkovich, M. M., 2009. Flow around circular cylinders: A comprehensive guide through flow phenomena, experiments, applications, mathematical models, and computer simulations. Oxford: Oxford Univ. Press.

Zhou, J., Wu, Z., Zhang, Z., Liu, W., and Xue, Q., 2000. Tribological behavior and lubricating mechanism of Cu nanoparticles in oil. Tribology Letters, 8(4): 213–218.

Zontul, H., Hamzah, H., Kurtulmuş, N., and Şahin, B., 2021. Investigation of convective heat transfer and flow hydrodynamics in rectangular grooved channels. International Communications in Heat and Mass Transfer, 126: 105366.

Zovatto, L., and Pedrizzetti, G., 2001. Flow about a circular cylinder between parallel walls. Journal of Fluid Mechanics, 440: 1-25.

CURRICULUM VITAE

Sergen TÜMSE, graduated from Toki Şehit Ozan Onur İlgen high school in Adana in 2012. He enrolled to Mechanical Engineering Department of Çukurova University in 2012. He graduated from the department of Mechanical Engineering and Automotive Engineering in 2017 and began his Master of Science in 2017 in Mechanical Engineering Department. Then he started his PhD in 2019. After completing his undergraduate studies, he worked as a Research Assistant at Mechanical Engineering Department in Çukurova University in 2018. He is currently working as a Research Assistant in the same department. His research areas are energy, heat transfer, applied fluid mechanics, aerodynamics and machine learning.